DISSECTING THE MYSTERY BEHIND RPG5 MEDIATED PUCCINIA GRAMINIS RESISTANCE IN BARLEY USING GENETICS, MOLECULAR AND BIOINFORMATICS APPROACHES

A Dissertation
Submitted to the Graduate Faculty
of the
North Dakota State University
of Agriculture and Applied Science

By

Shyam Solanki

In Partial Fulfillment of the Requirements
for the Degree of
DOCTOR OF PHILOSOPHY

Major Department:
Plant Pathology

December 2017

Fargo, North Dakota

North Dakota State University
Graduate School

Title

DISSECTING THE MYSTERY BEHIND RPG5 MEDIATED PUCCINIA GRAMINIS RESISTANCE IN BARLEY USING GENETICS, MOLECULAR AND BIOINFORMATICS APPROACHES

By

Shyam Solanki

The Supervisory Committee certifies that this ***disquisition*** complies with North Dakota State University's regulations and meets the accepted standards for the degree of

DOCTOR OF PHILOSOPHY

SUPERVISORY COMMITTEE:

Dr. Robert Brueggeman
Chair

Dr. Timothy Friesen

Dr. Zhaohui Liu

Dr. Stuart Haring

Approved:

December 04, 2017
Date

Dr. Jack Rasmussen
Department Chair

ABSTRACT

Barley *rpg4*/*Rpg5* locus harbors three tightly linked genes, two NLRs *Rpg5* and *HvRga1,* and *HvAdf3,* togather providing resistance against *Puccinia graminis f. sp. tritici*, causal agent of wheat stem rust including race TTKSK, considered a threat to global food security. The integrated decoy hypothesis proposes role for head-to-head genome architecture present in the dual plant NLR immunity receptors, where one NLR partner contains an integrated sensory domain (ISD). The ISDs represent mimics of virulence effector targets translocated to the immunity receptors and act as baits to recognize virulent effectors to initiate defense responses. Alleles of *Rpg5* contain two diverse C-terminal, the *Rpg5* resistance allele has a serine threonine protein kinase (*STPK*) ISD whereas the major class of *rpg5* susceptible alleles contain a protein phosphatase 2C (*PP2C*) ISD. Genetic and functional analysis shows that in the heterozygous state *rpg5-PP2C* allele acts as a dominant susceptibility factor suppressing *Rpg5-STPK* mediated *Pgt* resistance. This is the first integrated decoy NLR gene identified that contains two distinct ISDs. Liabrary scale Y2H screeing using Rpg5-STPK as bait identified HvVoz1. HvVoz1 was also interacts with the HvRga1, Rpg5-LRR, and rpg5-PP2C domains suggesting that it may act as a scaffold to hold the R-protein complex together until effector manipulation. We identified *Rpg5-STPK* ISD progenitor *HvGak1*, ortholog of the *Arabidopsis* guard cell *AT5G15080* and *AtAPK1b*, shown to function in stomatal aperture opening in response to light. We hypothesize that several *forma specialis* of *P. graminis* contain virulence effector/s, that manipulate *HvGak1,* mimicking the presence of light to open the stomates, allowing the pathogen to gain entry in to the plant during dark period that *P. graminis* spores evolved to germinate. We identified dark period pathogen penteration through stomata by deveoping a novel staining method and using confocal microscopy. To further characterize the *Rpg5* immunity pathway fast-neutron

irradiation was utilized to generate *rpr9* mutant, compromised for *rpg4/Rpg5*-mediated resistance. Utilizing genetic mapping and exom capture we identified candidate genes for *rpr9* mutants. Based on our understanding of this resistance mechanism it would be a good candidate system for generating synthetic resistances utilizing different ISD baits fused to the Rpg5 NLR.

ACKNOWLEDGEMENTS

Ph.D. research at North Dakota State University has been a passage of rigorous learning, transforming my scientific and personal perspective. I would like to reflect on the people who have immensely supported and helped me in each step throughout this journey.

Foremost, I would like to express my sincere gratitude towards my major adviser Dr. Robert Saxon Brueggeman, to nurture and polish me as a young scientist. His continuous encouragement, support, and experienced professional guidance shaped my scientific enthusiasm into a well-organized scientific approach. There were many methodological failures and moment of hopelessness during my research undertaking, yet his selfless time and attention were sometimes all that kept me going. His humor and care created an amicable umbrella in the lab under which creative thinking fluorished and enthusiastic environment was built for all the graduate students including me.

My research work is supported by National Science Foundation (NSF) early career award granted to Dr. Brueggeman, and I cannot imagine carrying out such an outstanding research without NSF funding support.

I would also like to thank members of my Ph.D. supervisory committee, Dr. Timothy Friesen, Dr. Zhaohui Liu, and Dr. Stuart Haring for their constructive suggestions and support during my research work.

A big thanks to our greenhouse research technician Patrick Gross for maintaining plant materials, field, and green house trials, and carefully making plant genotype crossing experiments fullfiling needs of my research projects. Not to forget, Thomas Gross, our laboratory technician who helped me in lab whenever I needed. I would also like to acknowledge the contribution of all the present and former students and visiting scientists in our lab.

During this scientific journey, my wife, Gazala Ameen who is fortunately my lab partner walked along me shoulder to shoulder. She has always been supportive, motivating and pushing me to propel myself towards academic and scientific excellence. I would like to thank her for countless thoughtful discussions, constructive criticisms, and her immense support during my Ph.D. work.

My father Piyush Solanki and mother Asha Solanki always believed in me and encouraged me to go for the higher studies. I cannot describe and acknowledge their contributions in few words here and only can convey my heartfelt regards in small token of words. I would also like to thank my brother Manish and Praveen Solanki for taking care of my patents and always being very supportive.

There are many names of friends and family which I have not mentioned here but without them I could not complete my Ph.D. A big thanks to all of them.

Finally, I would like to thank my new born son Amaan Solanki who allowed me to work on my dissertation and did not cried a lot.

DEDICATION

I dedicate my disquisition to my parents Asha and Piyush Solanki.

TABLE OF CONTENTS

LIST OF TABLES

LIST OF FIGURES

LIST OF ABBREVIATIONS

FF.....Farmers Fixative

aa.....Amino Acid

LCM.....LASER Capture Microdissection

NBS.....Nucleotide Binding Site

LRR.....Leucine Rich Repeats

STPK.....Serine/Threonine Protein Kinase

PP2C.....Protein Phosphatase 2C

ISD.....Integrated Sensory Domain

NLR.....Nucleotide Binding Leucine Rich Repeat

ID.....Integrated Domain

RMRL.....*Rpg4*/*5* Mediated Resistance Locus

Rpr9.....Required for *P. Graminis* Resistance 9

TTSS.....Type Three Secretion System

HR.....Hypersensitive Response

FN.....Fast Neutron

CNL.....Coiled Coil Nucleotide Binding Leucine Rich Repeat

TNL.....Toll Interleukin Nucleotide Binding Leucine Rich Repeat

cv.....Cultivar

LIST OF APPENDIX TABLES

CHAPTER 1. LITERATURE REVIEW

1.1. Introduction

1.1.1. Barley: History of domestication and utilization

Barley (*Hordeum vulgare* L.) was one of the first cereal crops domesticated during the Neolithic era and its wide adoption for cultivation and dry storage along with wheat sparked the rise of civilization in the Fertile Crescent region. Similar effect were also seen in other regions of the world where the dry storage grains rice, sorghum and maize were domesticated (Pankin and Korff, 2016). Historical evidence of crop domestication was first found in fossil form from storage and waste remnants at various archeological excavations dating back 12000-9500 years ago, indicating the transition from hunter-gatherers to one of agriculture and settlements. The technological advancement of crop domestication gave rise to early agricultural communities, increasing populations, and eventually civilization (Tanno and Willcox, 2006; Zohary et al., 2012). The diagnostic morphological trait that differentiates wild barley (*Hordeum spontaneum* C. Koch) from domesticated barley (*H. vulgare* L.) is brittle rachis or spike. Two tightly linked genes, *Btr1* and *Btr2,* at chromosome 3H are responsible for thin cell walls at the rachis nodes, resulting in the morphological trait known as brittle rachis in wild barley at maturity. Domesticated barley lines contain mutated *Btr1* or *Btr2* genes with primary gene sequences that give rise to nonfunctional proteins resulting in the non-brittle rachis phenotype (Pourkheirandish et al., 2015; Civáň and Brown, 2017). Although wild-type brittle rachis barley spikes were excavated and dated to ~23 thousand years ago (Weiss et al., 2008), the first non-brittle spikes similar to domesticated barley was excavated in the Fertile Crescent (Fig. 1.1.) dating back to ~10 thousand years ago, possibly representing the era of crop domestication. In fact, recent sequencing and reconstruction of barley genomic sequences from 6000 year old barley seeds

excavated from the Judean Desert in Israel marked barley as the crop plant with the most ancient genome sequence to date (Mascher et al., 2016).

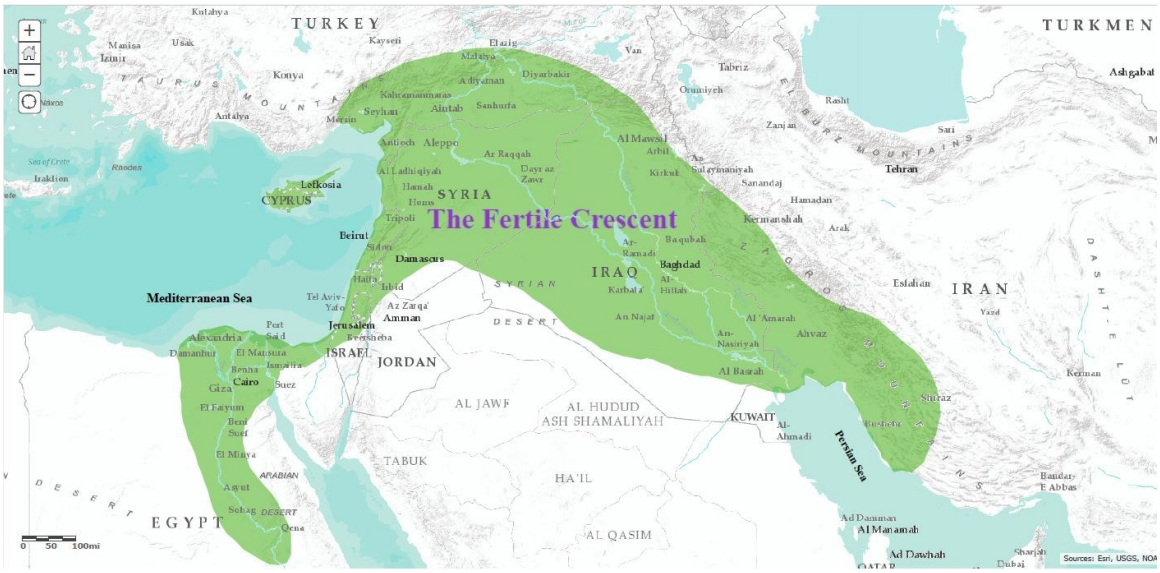

Fig. 1.1. The Fertile Crescent represented by green shadow over the present day partial continental map. It is a hypothetically drawn crescent shaped green area encompassing relatively moist and fertile region of the arid and semi-arid regions of western Asia, eastern Africa, and Europe. (Map was generated on ArcGIS).

The prehistoric barley genotype that was recently sequenced has considerable genetic overlap with present day barley cultivated in Israel, Palestine, and Jordan. On the other hand the genetic variability between the excavated barley grains and wild forms of barley and landraces in the region is vast (Mascher et al., 2016), thus, supporting the hypothesis of very early domestication of barley in the Fertile Crescent which is known as the cradle of civilization. Due to the range of human migration and barley's wide adaptability and ability to thrive on marginal lands, we observe it grown under a wide range of environmental conditions (Russell et al., 2016). The use of barley for food and beverage was found in many civilizations dating back to 5700-3000 BC in diverse cultures including the famous Indus valley civilization. In Greek and Roman culture, barley was an important food source for athletes to give strength and stamina. In popular

Roman culture gladiators were sometimes referred to as *hordearii*, "barley eaters" (Lösch et al., 2014), since barley was a major part of their dietary supplement.

The necessity to feed rapidly growing urban populations spurred the art and science of plant breeding which over generations required the conscious selection of desired cultivable traits such as higher yield, biotic and abiotic resistance. However, this selection came at the cost of reducing genetic variability, but a shift in modern crop breeding is the necessity to increase genetic diversity in breeding programs to introduce novel genes from the primary gene pools for traits including biotic and abiotic resistance. Presently, with the availability of state-of-the-art crop genome modification methods such as genetic engineering a new vista has opened for fast paced genome editing allowing for the precise integration of desirable traits.

1.1.2. Black rust: A threat for small grain crops

Although barley is a hardy crop, adapted for a wide range of climatic conditions, it is still vulnerable to many biotic and abiotic stresses. The obligate biotrophic fungal pathogen *Puccinia graminis* (*P. graminis*) is a notorious pathogen of barley and wheat and has historically caused devastating rust epidemics to cereal crops. Many host-specific "f. sp. (*forma specialis),* plural *ff. spp.,(formae speciales*)" of *P. graminis* were described that include but are not limited to wheat stem rust cause by, *Puccinia graminis* f. sp. *tritici* (*Pgt*) infecting wheat and barley; rye stem rust, *P. graminis* f. sp. *secalis* (*Pgs*), which infects rye and barley; and oat stem rust cause by *P. graminis* f. sp. *avenae* (*Pga*) of oats (Eriksson and Henning, 1984). Further subdivision in different pathogen "races" is common based on virulence on their respective cereal host or hosts.

1.1.2.1. Stem rust: Biology, life cycle and infection mechanism

P. graminis requires warm (27-30°C) and moist conditions allowing for ample dew formation on the host surface for optimal infection (Roelfs, 1985b). Stem rust is heterocious,

producing five different types of spores to complete its lifecycle. The primary host barberry or *Mahonia spp.* shelters pycniospores and aeciospore whereas the secondary hosts (wheat, barley, rye, oat, other grass species) shelters urediniospores, teliospores and basidiospores (Aurthur, 1934).

The repeating asexual spores, dikaryotic urediniospores (n+n), are the primary source of inoculum in cereal fields. Urediniospores are produced in large quantities and can travel across very long distances on wind currents exemplified by the annual phenomenon across the North America Great Plains popularly known as the "Puccinia Pathway" and also from Australia to New Zealand (Luig, 1985).

P. graminis infection on primary hosts requires the landing of urediniospores on leaf surfaces followed by spore germination and extension of germ tubes within 3-5 hours after contacting the leaf surface during the night when high humidity allows for dew formation on the stem and leaf sheath. Germ tubes grow perpendicular to leaf veins until they encounter stomata. The topology of host guard cells plays an important role in stomata identification and formation of appressorium from viable spore during initial 04-16 hour of infection. Appressoria forms a substomatal tube between two guard cells and initiate substomatal growth, followed by formation of primary infection hyphae and differentiation and formation of haustorial mother cells and invagination and formation of haustoria upon contacting the host plant mesophyll cells. However requirement of light after initial 10-18 hour of dark moist period of germination is considered to be required for pathogen penetration by sub-stomatal vesicle through stomatal pore (Yirgou and Caldwell, 1963; Figueroa et al., 2016).

The haustoria acts as a feeding structure and facilitates pathogen manipulation of the host as the pathogen hijacks host cell physiology by utilizing an effector repertoire that establishes an

artificial nutrient sink which leads to pathogen feeding and profuse growth. Eventually a life cycle shift results in the formation of Uredinium and millions of Urediniospores erupting from the epidermis of the stem and leaf surface in ~10-14 days after infection fulfilling the pathogen's main goal of reproduction (Leonard and Szabo, 2005). Urediniospores act as primary inoculum causing polycyclic disease if congenial environmental conditions and suitable hosts are available. Pathogen signs occur primarily on the stem and leaf sheaths but may also be found on leaves and glumes. Typical signs of *Pgt* are characterized by small chlorotic flecks which occurs in 4-5 days after inoculation, progressing into round to elongated diamond shaped brick red lesions on its cereal host in ~8-10 days post inoculation (Roelfs, 1985a; Roelfs and Bushnell, 1985). Severe disease results in heavy yield penalty due to reduction in photosynthetic area, loss of water through epidermal rupture at the point of pathogen spore production, and channeling of plant nutrients towards the pathogen infection sight, thus, resulting in overall reduction of plant vigor and stem breakage that ultimately leads to plant lodging (Roelfs and Bushnell, 1985; Leonard and Szabo, 2005). This severe damage to host causes enormous yield loss in cereal production posing a threat to world food security (Saari and Prescott, 1985; Singh et al., 2008; Bhattacharya, 2017).

1.1.2.2. Stem rust: A reemerging threat for world cereal basket

A severe stem rust epidemic occurred across the Northern Great Plains in 1916 (Steffenson, 1992a) warranting extensive research and breeding efforts to identify and deploy durable sources of resistance in both barley and wheat. These efforts intensified with recurrent epidemics in the following decades (Steffenson, 1992a; Steffenson et al., 2016). Serious epidemics were effectively managed, by pyramiding several resistance genes (R-genes) in wheat (Ayliffe et al., 2008; Singh et al., 2009; Haile and Rouml, 2013; Niu et al., 2011) and the single

remarkably durable resistance gene, *Rpg1,* in barley (Brueggeman et al., 2002). The effectiveness of stem rust resistance genes for the past seventy-five years had forged a complacent attitude towards stem rust as if we had defeated this once devastating disease. However, the sudden emergence of a new hypervirulent race of wheat stem rust in Uganda Africa in 1998, *Pgt* race TTKSK popularly known as Ug99, that was virulent on the majority of current wheat and barley cultivars including those with the widely deployed wheat stem rust resistance gene *Sr31*, resurrected the threat that stem rust poses to cereal production. Since the identification of *Pgt* race TTKSK in Uganda in 1998 and its characterization in 1999 it has spread with alarming speed to several countries with the most recent reports in Egypt (Pretorius et al., 2000; Singh, 2006; Singh et al., 2011). Since the initial emergence and characterization of *Pgt* race TTKSK it has evolved in a stepwise manner to change its virulence structure. Interestingly, a single step mutation has been determined to be responsible for the virulence shift on wheat containing the stem rust resistance gene *Sr31* to virulence on wheat lines containing other known sets of SR genes of wheat of alien origin (Bhardwaj et al., 2014). At present, there are thirteen established variants of the TTKSK lineage (Fig. 1.2.)

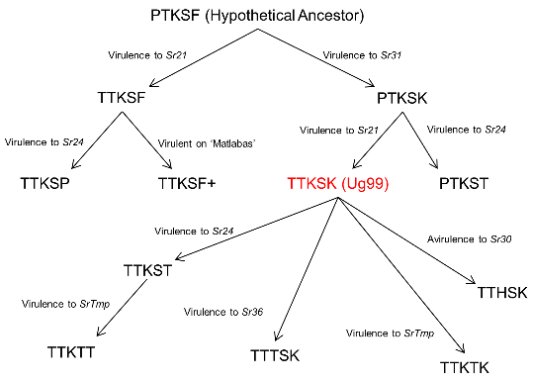

Fig. 1.2. Proposed race evolution of the TTKSK-lineage. TTKSK-lineage evolution are single step mutation events that apparently resulted in race differentiation against known sets of resistance genes of wheat including SR genes from alien introgressions. Modified from Singh et al. 2015 (Singh et al., 2015). (Length of arrows are for schematic purposes and does not represents evolutionary scale).

Per the February-2016 global wheat rust monitoring system reports (Hodson et al., 2012; BGRI), the TTKSK race group is present in thirteen countries covering 11 East-African countries and 2 Middle East countries in Asia. Furthermore, there is a recent report of a new highly virulent race TTTTF infecting both bread and durum wheat grown on the island of Sicily, Italy (Bhattacharya, 2017).

1.1.3. Plant defense mechanism to combat infections

1.1.3.1. Armory against the enemy

Plants continuously encounter diverse microbes, but the vast majority of them are non-pathogenic. Although plants are non-hosts to majority of potential phytopathogenic microbes, a small proportion of microbes have evolved to be specialized pathogens causing disease on their respective host/s which represents a major challenge to agricultural production. Plant pathogens are broadly classified as either: (a) biotrophic pathogens that require living host cells to acquire nutrients and complete their lifecycle, and (b) necrotrophic pathogens that require dead or dying host tissue to feed and complete their lifecycle. To combat these microbes, plants evolved a multiple layered defense system to identify and respond to the challenge, which involves different levels of spatio-temporal activation of innate immunity receptors representing molecular switches. Microbe Associated Molecular Patterns, (MAMPs) are conserved motifs associated with an entire class of microbes that are essential for their fitness, thus, cannot be eliminated or diversified to a great degree. The host plants evolved to recognize these microbial patterns via Pattern-Recognition Receptors (PRRs) that are present on plant cell surfaces with extracellular receptor domains that can recognize MAMPs early in the host-parasite interaction to initiate the first layer of inducible defense responses. This early identification of microbes at the cell periphery results in physiological reprogramming of energy from normal cellular

function towards rapid defense responses that include but are not limited to cell wall reorganization, pathogen defense response gene activation, PR protein mobilization, oxidative burst, and may involve a localized programmed cell death response, collectively known as Pattern-Triggered Immunity (PTI) (Jones and Dangl, 2006).

It is a well-accepted hypothesis that microbes have evolved a repertoire of effectors and a effector delivery system to manipulate host cell physiology in order to become specialized pathogens. A well-characterized central target of these virulence effectors are to suppress the early PTI resistance responses which typically involves manipulation of PTI pathways (Couto and Zipfel, 2016) at the receptor (Göhre et al., 2008), signaling pathways (Zhang et al., 2007; He et al., 2006), or transcriptional activation levels (Boch et al., 2014; Read et al., 2016; Moscou and Bogdanove, 2009). To combat specialized pathogenic microbes, adapted to inhibit the PTI responses by the secretion and delivery of effectors by direct penetration strategies such as Type 3 Secretion System (T3SS) (Salmond and Reeves, 1993) in bacteria and by haustorial secretion strategies in fungi, plants evolved a second layer of predominantly intracellular receptors known as resistance (R) proteins. Majority of R proteins are containing the Nucleotide Binding-Leucine Rich Repeat (NLR) protein domain architecture that recognizes the pathogen virulence effectors and elicits Effector Triggered Immunity (ETI) (Win et al., 2012; Dodds and Rathjen, 2010).

1.1.3.2. Dissecting the working components of a typical NLR

The majority of *R*-genes known to operate in the plant resistance pathway belongs to the intracellular NLR class, having an N-terminal domain, a conserved central Nucleotide Binding site shared by human Apoptosis protease-activating factor-1, plant R proteins involve in resistance responses and *Caenorhabditis elegans* Cell death protein-4 (NB-ARC) domain and C-terminal Leucine-Rich Repeat (LRR) domain (van der Biezen and Jones, 1998; Kobe and

Deisenhofer, 1995; Takken et al., 2006). The diverse N-terminal domain can show resemblance to the protein interacting domain homologous to the Toll-Interleukin Receptor (TIR) domain shared with Toll Receptors in *Drosophila* and Interleukin-1 Receptor in humans, or the Coiled-Coil (CC) domain class found in many monocot and dicot plant R-proteins. Thus, providing the basis for broad classification of plant NLRs into TIR-NB-LRR (TNL) or CC-NB-LRR (CNL) R protein classes (Meyers et al., 1999; Jones and Dangl, 2006; Maekawa et al., 2011b). Plant *R*-genes were shown to provide disease resistance against taxonomically diverse class of plant pathogens including bacteria, viruses, oomycetes, fungi, nematodes and insects (Wanderley-Nogueira et al., 2016; Jones et al., 2014; Jupe et al., 2013; Chisholm et al., 2006) and largely rely on pathogen specific sensing and defense signal activation.

1.1.3.2.1. Role of N-terminal effector domain in defense function

The N-terminal TIR or CC domain (Table -1) of NLRs play an important role in plant defense signal activation. In fact, these modular domains from *Arabidopsis*, flax, wheat, and barley NLRs were shown to induce spontaneous effector independent cell death in transient overexpression studies *in planta* for both TIRs (RPP1, RPS4, L6, L10) and CCs (MLA, ADR1, Sr33 and Sr50) (Krasileva et al., 2010; Bernoux et al., 2016; Cesari et al., 2016; Maekawa et al., 2011a). Protein oligomerization in the forms of homo or hetero dimer formation upon pathogen perception were shown to play a key role in NLR signaling in plants (Swiderski et al., 2009; Collier et al., 2011). These N terminal TIR and CC domains are known to provide the protein domain interaction platform for the homodimerization (L6, Prf, RPS5, N, MLA, Sr33, and Sr50) (Cesari et al., 2016; Maekawa et al., 2011a; Qi et al., 2012; Bernoux et al., 2011) or heterodimerization (RPS4/RRS1, RGA4/RGA5) (Césari et al., 2014; Williams et al., 2014) of NLR immunity receptors, thus, form the basis for these NLR immunity receptor complexes.

1.1.3.2.1.1. TIR domain in NLR: Role in interaction and defense signaling

The first crystal structure of TIR was determined in the *Arabidopsis thaliana* AtTIR protein, which is a TIR only protein (Chan et al., 2010). The first crystal structure for a TIR domain in a TNL was determined for Flax L6, which provides resistance against flax rust *Melampsora lini* (Bernoux et al., 2011; Ve et al., 2011) and was shown to self-interact in Y2H. It has been reported that truncated TIR portions of many TNLs notably Flax L6 or *Arabidopsis* RPS4 are auto active, working as minimal functional unit to induce cell death when overexpressed ectopically in the absence of cognate elicitors (Bernoux et al., 2011; Swiderski et al., 2009). Recent functional characterization of the *Pseudomonas syringae* HopBA1 effector and its cognate TIR-only pathogen sensor, RBA1, whose interaction mediates expression dependent cell death opens a new paradigm for NLR function (Nishimura et al., 2017). This interaction further supports the importance of the specific modular domains present within R proteins especially the TIR domain such is in the case for the tobacco TNL N gene requiring a truncated TIR-NB splice variant for its full function (Dinesh-Kumar and Baker, 2000).

1.1.3.2.1.2. Coiled-Coil domain in NLR: Role in interaction and defense signaling

The first crystal structure of the plant Coiled-Coil (CC) modular domain was resolved from barley MLA10, a CC-NLR protein providing resistance against powdery mildew. The crystal structure for MLA-CC was resolved for residues 6-120, using single-wavelength anomalous diffraction (SAD) at a resolution of 2.0 Å (Maekawa et al., 2011a). The monomeric structure of the barley MLA-CC is mainly α helical consisting of three helices, in which two long antiparallel α helices are connected by a short loop taking a helix-loop-helix (HLH) structure. As a crystallized protein, the MLA-CC domain dimerized symmetrically with a helical bundle at each end in a rod-shaped structure. Transient expression assays with Agrobacteria infiltrated leaf

discs showed that the dimerization of MLA10-CC is essential for cell death, thus serving as a minimal functional unit to initiate cell death response (Rairdan et al., 2008; Bai et al., 2012) resulting in resistance against the biotrophic pathogen. MLA-CC dimer formation was further confirmed using LexA based yeast-two-hybrid (Y2H) and *in planta* assays, although the dimerization of the CC domain was not shown to be the consequence of Avr recognition nor was the dimer complex disrupted upon perception of the cognate avirulence effector. The CC domains of many NLRs contain a short 5 amino acid consensus "EDVID" motif except for the RRS1, RPS5, RPS2 and DM3 NLRs (Rairdan et al., 2008), which were shown to fall into a different evolutionary clade (Meyers et al., 1999). Structure-function analysis of the potato CNL, *Rx* gene, conferring resistance to Potato Virus X show that the EDVID motif is involved in CC mediate interactions with intra-domain NB-LRR moieties. Furthermore, the NB domain of Rx was shown to be sufficient to induce HR but not its CC domain (Rairdan et al., 2008). These results are in line with *Arabidopsis* CNL RPS5 where overexpression of RPS5-CC-NB domain did not induce cell death (Qi et al., 2012). The crystal structure of the potato CNL Rx CC domain complexed with the WPP domain of its cofactor RanGAP2 was resolved at 2.1 Å, showing the role of heterodimeric pairs regulating the defense responses (Hao et al., 2013). Although host parasite interactions that evolved separately have distinctions in their defense mechanisms (i.e. MLA10 and Rx comparison), it appears that the same structural configuration of EDVID motif side chains indicate its key role in CC mediated interactions (Rairdan et al., 2008). However, race-specific physical interactions have also been shown between the CC domains of the rice NLR, Pik, and corresponding Avr-Pik effectors from the fungus *Magnaporthe oryzae* (Ortiz et al., 2017; Césari et al., 2014).

1.1.3.2.2. NB-ARC domain

The NB-ARC domains represents blocks of conserved motifs in plant and animal NLR proteins which is the most conserved domain in NLRs (van der Biezen and Jones, 1998; Meyers et al., 2003; Yue et al., 2012; Meyers et al., 1999). These motifs take part in NTP-binding and hydrolysis, thus evoke conformational modulation in protein structure. Such modulation can change the equilibrium between the on-and-off state, playing a major role in intramolecular interactions between different NLR domains or intermolecular interaction between different proteins and the subsequent elicitation of defense responses (Mo and Duncan, 2013). In NB-ARC domains the Walker A (P-loop) motif is represented by consensus sequence "GxxxxGKS/T" (G represents glycine, x represents any amino acid residue, K represents Lysine, S represents Serine and T represents Threonine), where the K amino acid binds to the β- and γ-phosphates of ADP/ATP and S and T residues are crucial for coordinating Mg^{2+} ions. The walker B motif in NB-ARC domains is represented by "hhhhDD/E" (h represent hydrophobic residues Ds represent Aspartic Acid and E represents Glutamic Acid) and is crucial for NB-ARC domain function. Many important motifs are present as blocks in NB-ARC domains such as RNBS-A, RNBS-C, GLPL, RNBS-D and MHD and are also required for its function. Aberrations in these NLR motifs via mutations were shown to cause autoactivation or loss-of-function (Takken et al., 2006; van Ooijen et al., 2008)

1.1.3.2.3. Role of LRR domain in immunity

Identification of foreign molecules is a key function of plant and animal immune receptors to regulate defense responses. The LRR domain is a structural motif present in both plant and animal receptors that is involved in ligand perception, protein-protein interaction, signal transduction and other important NLR functions. The LRR domain has an important

structural motif consist of two or more tandem repeats with the consensus core pattern of 11 residues "LxxLxLxxNxL or the 12 residue motif "LxxLxLxxCxxL" (L represents Valine/Leucine/Isoleucine residue, x represents any residue, N is either Threonine, Serine, Cysteine or Aspartic acid and C represents Cysteine or Serine) (Enkhbayar et al., 2004; Bella et al., 2008). LRR domains form a curved solenoid structure resembling a horse shoe shape that provides a broad interaction surface which can resist high level of variability (Padmanabhan et al., 2009). The LRRs are rifted by a sequence of 30-70 residues known as the Island Domains (IDs) (Song et al., 2014). Crystal structure of the *Arabidopsis* BRI1 (She et al., 2011; Hothorn et al., 2011) and RPK2 containing two IDs (Song et al., 2014) was reported recently, although the crystal structure of an LRR belonging to a NLR protein has yet to be determined. Interestingly, intracellular LRR (iLRR) domains have been suggested to be distinct from extracellular LRR (eLRR) domains in plant NB-LRRs and receptor like kinases (RLKs) or receptor like proteins (RLPs). The majority of TNL and CNL contain a conserved "VLDL" motif in the third LRR. This motif was first elucidated in the *Arabidopsis* CNL RPS5 where an induced mutation in adjacent amino acids abolish the resistance function (Warren et al., 1998). Contrastingly, in the potato NLR Rx, VLDL to VLEL mutation results in constitutive activation of defense signaling (Bendahmane et al., 2002). Thus, manipulation in VLDL motif in LRR can leads to either abolishment or auto activation of defense response depending on type of R protein indicating this motif seems to be biologically relevant yet function may be discordant

Many studies have shown the role of LRR domains in the recognition specificity of R proteins (Wulff et al., 2001; Dodds et al., 2001; Hwang and Williamson, 2003; Moffett et al., 2002) while maintaining a high degree of plasticity. The high degree of duplication that occurs at NLR loci and the LRR domains ability to diversify within regions that code for surface exposed

aa acid residues outside the structural motifs, facilitates the diversification that accounts for NLR islands evolving faster than other regions of the plant genome which gives rise to novel interaction specificities and diversity within the plant immune system (Ellis et al., 2000; DeYoung and Innes, 2006; Ng and Xavier, 2011; Padmanabhan et al., 2009).

1.1.3.3. Pathogen sensing: A crucial step for NLR activation

1.1.3.3.1. Direct interaction provides diversifying advantages

Resistance responses initiated by plants are evoked upon recognition and the signal perception of a potential pathogens arrival and challenge, which leads to the activation of the molecular switch from homeostasis at the "off" state to the alarm "on" state, resulting in massive physiological reprogramming and activation of defense mechanisms. The intracellular NLR class of R proteins make up the main class of terminal weaponry utilized by plants to mount defenses against pathogenic microbes. The firing of R induced molecular defenses depends on direct or indirect recognition of the pathogen intracellular footprints. Direct physical interaction between specific NLRs and their cognate pathogen elicitors have been observed for relatively few host pathogen interactions characterized. The first direct NLR-elicitor interaction was shown between the rice blast fungus *Magnaporthe grisea* effector Avr-Pita and rice resistance CNL protein Pi-ta using Y2H and *in vitro* far-western protein binding assays (Jia et al., 2000). Another well studied example is the direct interaction between the *Arabidopsis* TNL RRS1-R and its corresponding Avr $PopP_2$ effector from *Ralstonia solanacearum,* the causal organism of bacterial wilt (Deslandes et al., 2003). Such direct interactions can play an important role in the diversifying selection of the cognate Avr protein and corresponding NLR. The selection pressure from the resistant host evolves the pathogen towards Avr effector diversification to lose the host-pathogen interaction and gain susceptibility and on the other hand, the evolved virulence effectors from the

pathogen provide selection pressure on the host to regain recognition and resistance. Recognition of flax rust AvrL567 variants with the flax TNL L5, L6 and L7 suggests polymorphisms present at NLR loci lead to quantitative resistance responses based on the efficiency of recognition (Dodds et al., 2006). Thus, the molecular arms race between host and pathogen on one hand provides diversifying variation in the elicitor virulence motifs of the pathogen recognized by host R proteins to avoid recognition without introducing substantial fitness penalty such as the loss of virulence effector function in conserved virulence motif. Whereas on other hand host evolution leads to acquiring new identification specificities suggesting a very active co-evolutionary arms race where the host and pathogen are constantly evolving to get the upper hand. Protein moieties involved in effector recognition by a NLR are usually different than the moieties required for its function, thus any mutation accumulation disrupting only the recognition will provide benefit to pathogen without a fitness penalty.

1.1.3.3.2. Indirect interactions

Examples for direct interactions between NLRs and their cognate pathogen elicitors are few, thus other mechanistic models for indirect recognition were proposed for NLR function. NLRs must function as tightly regulated sensors for any modifications induced during pathogen arrival and subsequent effector manipulation of host proteins that facilitate colonization. This pathogen manipulation typically disrupts the equilibrium state of the plant host's molecular environment as the pathogen needs to tailor this environment to its own requirements. Indirect recognition of pathogen challenge relies on a third intermediate component in the interaction complex. Thus, these pathogen elicitor targets, shown to be virulence targets, have been designated as guards or decoys, which the NLR R-protein surveils and upon recognition of

pathogen virulence effector manipulation triggers the molecular switch to the "on" state mediating defense signal activation (Collier and Moffett, 2009).

1.1.3.3.2.1. Guards, an evolutionary dilemma for its own existence

The guard model was proposed to explain these indirect interactions where pathogen effectors mediate manipulation of host proteins involved in PTI immune pathway are detected by R proteins causing release of their inhibitory regulation and activation of the higher amplitude ETI HR response (Van der Biezen and Jones, 1998; Jones and Dangl, 2006; Spoel and Dong, 2012). In the *Arabidopsis* model system, RIN4 is a well characterized guardee targeted by four known *Pseudomonas* secreted effectors, AvrRpm1, AvrB, AvrRpt2 (Mackey et al., 2002; Kim et al., 2005; Wilton et al., 2010) and HopF2 (Pto) (Wilton et al., 2010). Guardee manipulator is monitored by two known guards, CNLs RPM1 and RPS2, and both are negatively regulated by RIN4. RIN4 phosphorylation in presence of AvrRpm1 and AvrB leads to RPM1 activation (Mackey et al., 2002) whereas AvrRpt2 a cysteine protease causes RIN4 proteolysis and RPS2 activation (Mackey et al., 2003; Coaker et al., 2005). Both events lead to protein modification of guard NLRs, release of inhibition and leading to activation of plant defense signaling. Thus, effector manipulation of host proteins known as the guardee are essential for pathogen virulence in the absence of the cognate guard R protein yet indispensable for early PTI mediated resistance function when the functional R protein is not present. This contrasting situation for the pathogen poses a dilemma as the natural selection force on guardee's binding site interacting with its cognate effector to select "for and against" binding depending on R protein availability thus presents an evolutionary unstable situation (van der Hoorn and Kamoun, 2008).

1.1.3.3.2.2. Plant ruse the pathogen, decoys acting as molecular bait for pathogen identification

The decoy model was proposed to accommodate the observations that few of guardee proteins do not contain their original biological function yet were mimics of the ancestral virulence effector targets. This provided the perspective of evolutionary constraints on guardee and the speculation that some guarded host proteins are not the pathogen's virulence target but rather function as an effector bait and are mimic of the host protein that is specifically manipulated by a pathogen. Thus, decoys are hypothesized to lose their original functionality (given enough evolutionary time to evolve as decoys) and present no benefit to pathogen upon interaction or modification (van der Hoorn and Kamoun, 2008; Block and Alfano, 2011). Indirect recognition of unrelated *Pseudomonas syringe* effectors AvrPto and AvrPtoB by the tomato CNL transduction module Prf is mediated by the Pto kinase which is proposed to act as a decoy and interacts with the pathogen Avr (Wu et al., 2004; Tang et al., 1996) (Mucyn et al., 2006). Bacterial cell surface immunity receptor FLS2 is an operative virulence target for AvrPto to suppress the PTI (Xing et al., 2007). Pto, not the Prf is shown to physically interact with the AvrPto and AvrB in Y2H studies (Kim et al., 2002; Tang et al., 1996; Mucyn et al., 2006)

Another well documented example is activation of *Arabidopsis* CNL RPS5 upon recognition of *P. syringae* effector AvrPphB. AvrPphB cleaves BIK1 kinase to suppress the FLS2 mediated PTI but also trips the wire via cleaving PBS1 (Zhang et al., 2010), a guarded kinase decoy whose perturbation is monitored by RPS5 to activate defense signaling (Chinchilla et al., 2007; Couto and Zipfel, 2016). Although it was suggested that during initial PTI activation phosphorylation of an actin depolymerization factor AtAdf4 results in early pathogen sensing and priming of RPS5 for later robust ETI response (Porter et al., 2012). Thus, actin

depolymerization factors not only play a role in cytoskeleton rearrangement (Tian et al., 2009; Henty-Ridilla et al., 2014) during initial PTI but also have important link in ETI signaling (Brueggeman et al., 2009).

1.1.3.3.2.3. Consummation of host virulence targets with NLR, integrated baits

The presence of additional unusual non-NLR domains integrated into standard functional NLR protein domain architectures were puzzling until recent genome analyses coupled with effector functional analyses provided a clue to their biological functions. Many NLR have been identified with these unusual domains typically attached at the C or N terminal of NLRs or less commonly are sandwiched within the typical NLR domains. Interestingly, these domains have been shown to be important for the *R*-gene's resistance function (Eitas and Dangl, 2010). The importance of the paired NLRs in defense signaling first came from the *Arabidopsis* RPP_2B and RPP_2A TNLs that were shown to be required together for resistance against *Hyalopernospora arabidopsidis,* an oomycete pathogen (Sinapidou et al., 2004). Later several heterodimeric NLR pair in other pathosystems were identified including; (i.) the TNLs RPS4 and RRS1 from *Arabidopsis* that recognize the diverse elicitors, AvrRps4 from *P. syringae*, $PopP_2$ secreted by *Ralstonia solanacearum* and a yet to be identified effector from *Colletotrichum higginsianum* (Gassmann et al., 1999; Deslandes et al., 2003; Narusaka et al., 2009; Sarris et al., 2015; Le Roux et al., 2015); (ii.) the barley CNLs *HvRga1* and *Rpg5* mediate the perception of a yet to be characterized effectors from diverse forma specialis of the stem rust pathogen *Puccinia graminis* including *Puccinia graminis* f. sp. *tritici, Puccinia graminis* f. sp. *secalis* and *Puccina graminis* f. sp. *avenae* (Brueggeman et al., 2008; Wang et al., 2013; Arora et al., 2013); (iii.) the rice CNLs RGA4 and RGA5 that recognize the *Magnaporthae oryzae* effectors Avr-Pia and Avr-CO39 (Césari et al., 2014); and (iv.) the wheat Lr10 and RGA2 pair providing resistance against

Puccinia triticina (Loutre et al., 2009). Several other NLR pairs were found to function together to confer resistance and we can expect that their interactions will be further characterized in the near future. Thus, heterodimeric pairing of these dual NLR is probably required for their function, as has been determined in some of the better characterized mechanisms like RPS4/RRS1 (Narusaka et al., 2009) and RGA4/RGA5 (Césari et al., 2014). An important twist to this story is the presence of additional domain/s in one of the NLR partner, shown to be required for the activation of pathogen induced defense signaling. This has been shown by the presence of the WRKY domain in RRS1 (Sarris et al., 2015), a putative functional kinase domain in *Rpg5* (Brueggeman et al., 2008) and a heavy metal associated RATX1 domain in RGA5 (Ortiz et al., 2017), that are indispensable for pathogen induced HR response for RPS4/RRS1 and RGA4/RGA5, an HR independent resistance response for HvRga1 and Rpg5 (dissertation chapter 2). Thus, the " Integrated decoy model" was proposed to assign a possible role of additional domains present in one of the NLR partners in these paired NLR as an extension to the guard/decoy models (Cesari et al., 2014). Later, it was suggested that until the function of these accessory domains can be elucidated they should be referred to as "Integrated Sensory Domains" (ISDs) (Wu et al., 2015) or "Integrated Domains" (IDs) because the accessory domains acting as NLR baits are possibly functional mimics of the host effector target proteins, meaning they retained their original biological function. Further, NLR-IDs can expand the NLR functional diversity due to the integration of different ISDs to perceive diverse pathogens, initiating defense response through a common conserved NLR pair. Also, if a virulence hub is integrated in an NLR, which is targeted by several pathogens to cause disease (i.e. RIN4), then a single NLR pair can confer resistance to a large diverse set of plant pathogens. This concept has been the focus of

several ideas for engineering broad resistances (McDowell and Woffenden, 2003; Römer et al., 2009).

Recent comparative analysis in diverse plant genomes revealed that the NLR pairs with additional ISD domains are common in diverse plant genomes and usually have a genome architecture where the two NLRs are present in a head-to-head genome architecture. An average of 10% of all known NLRs in plant species are identified to contain the exogenous ISDs which were preciously overlooked due to incomplete annotation. Further evolutionary analysis on grass genomes suggest that such integrations are not random and are uniform across the NLR phylogeny but favored in certain NLR taxon in cereals. NLRs with the head-to-head configuration are evolutionary hot spots where NLR-ID integration and diversification Fluorish (Bailey et al., 2017a). Linkage of NLR pairs with diverse ISDs gives these immunity receptors advantage of genetic co-segregation and co-evolution with an adaptive pathogen. ISDs may represent an ancient form of adaptive immunity receptor targeted by adapted pathogen and acting as susceptibility hubs. High degree of diversifying pressure on these susceptibility hubs to undergo adaptive evolution and avoid detection leads to integration of these susceptibility targets to a NLRs. This integration allows evolution of these susceptibility hubs as ISDs, functioning in pathogen identification and rapid activation of NLR signaling required for plant defense activation.

1.1.3.4. NLR distribution and diversity

The presence of hundreds of NLR genes were shown in many land plants using genome-wide studies in *Arabidopsis*, rice, barley, wheat, tomato, poplar and other species, thus, underlining their important role in the physiology of plant disease resistance. Interestingly, *R* genes were found to be clustered in the genome (Kang et al., 2012) and a single cluster can take

parts in resistance response to a diverse pathogen group (Eckardt, 2007). Polymorphism in the domain architecture of NLR repertoire of members of a species, determines their ability to recognize a specific set of attacking pathogen elicitors and the plants ability to invoke a defense response. Polymorphic molecular markers not only helped in the introgression and pyramiding of *R* genes in crops but also proved to be an essential tool for map based cloning (Kage et al., 2016; Huang et al., 2003). With the recent advent of Next-Generation-Sequencing (NGS) technology and the comparatively lowered cost of genome sequencing we are witnessing a rapid acceleration in the identification and annotation of plant *R* genes which mainly fall within the NLR superfamily of genes. However, the repetitive nature of NLR families made sequence assembly difficult to identify NLR with mutations or novel domain combination as highly homologous NLRs are present at different positions of sequenced genome making it difficult to assemble and annotate. However, the recent RenSeq (Resistance-Gene-Enrichment-Sequencing) technology coupled with SMART (Pacific Biosciences Single-Molecule Real Time) sequencing reduces the genome complexity by targeted enrichment of NB-LRR portion thus increasing read depth for each NLR. These new technologies coupled with the new long read sequencing techniques like PacBio and MinION are providing new tools for NLR gene family discovery and re-annotation from sequenced plant genomes (Jupe et al., 2013; Witek et al., 2016) which is allowing researchers to have a better look at PANgenomes and the NLR complements across species. Also, worth noting is that changes in spatio-temporal gene expression of non-polymorphic *R* genes can also contribute to phenotypic changes, thus phenotypic polymorphism can be generated without polymorphism in the primary gene sequence, making it essential for the characterization of promoter regions (Carrol 2000, Wray 2007).

1.1.4. Molecular mechanism for stem rust resistance in barley

1.1.4.1. Rpg1 mediated resistance

Genetic resistance is one of the most effective strategies to control rust diseases including stem rust. In barley the single R gene *Rpg1* effectively managed stem rust in the upper Great Plains of the United States and Western Canadian Prairies since 1942 (Steffenson, 1992b). This effectiveness for 70 years upon *Rpg1* deployment, is remarkable durability for a rust resistance gene. Identification of *Rpg1* via a positional cloning strategy identified an atypical resistance gene (Brueggeman et al., 2002) that does not belong to the general NLR class of resistance genes and encodes a tandem serine threonine protein kinase (STPK) having two kinase moieties (Brueggeman et al., 2002; Nirmala et al., 2006). The majority of RPG1 protein was shown to be localized in the cytosol, though low amounts were also found to be present in membrane fractions (Nirmala et al., 2006). The *Rpg1* transcripts were also shown to be present in significantly higher amount in epidermal cells than other leaf cell layers (Rostoks et al., 2004), suggesting its possible role and site in early pathogen detection at the leaf surface. Functional characterization of RPG1 protein kinase domains show only one being an active kinase (PK2) whereas the other domain acts as a pseudokinase (PK1), although the resistance response requires presence of both domains (Nirmala et al., 2006). The stem rust resistance mechanism does not depend on alteration of *Rpg1* expression since its presence is constitutive and pathogen independent. The resistance responses against avirulent stem rust races mediated by *Rpg1* depends on an early RPG1 phosphorylation event within five minutes of the avirulent spores landing on leaf surfaces. This response is followed by the degradation of phosphorylated RPG1 protein via the ubiquitin pathway occurring 20-24 hours post inoculation leading to undetectable protein levels (Nirmala et al., 2010, 2006, 2007). The pathogen avirulence proteins involved in

RPG1 interaction, phosphorylation and degradation were found to be large proteins, the VPS9 and RGD-domain binding proteins, present in viable spores. These dual large molecular weight proteins required for avirulent interactions are in contrast with typical avirulence effectors as they usually encode small secreted pathogen effectors with unknown functional domains (Nirmala et al., 2011). Thus, it is hypothesized that the spore localized RGD-binding protein and VPS9 elicit an early recognition by the plant by a yet to be discovered extracellular/cell surface localized receptor. This detection results in rapid RPG1 phosphorylation and the subsequent degradation primes the defense mechanism for a later stronger ETI response. It could be further hypothesized that RPG1 is a suppressor of defense responses and its degradation allows for the activation of other defense related genes once the pathogen is able to secret additional effectors through intercellular haustoria. Thus, it is more appropriate to view this early interaction as a non-host resistance although not initiated by the virulent pathogenic races. RPG1 was shown to interact with a fragment of HvRIN4, but not the full length protein in a Y2H cDNA library screening suggesting that it may be a RIN4 signaling component which is a central hub of virulence effectors from a wide spectrum of pathogens as RIN4 has been shown to be involved in defense responses in *Arabidopsis* (Belkhadir et al., 2004) and is an ISD of dual NLR mechanisms (Baggs et al., 2017; Bailey et al., 2017b, 2017a). RNAi experiments to validate the direct role of HvRIN4 in the RPG1 mediated stem rust resistance were inconclusive (Gill et al., 2012) suggesting the need of a more sensitive method compared to the traditional BSMV induced gene silencing. Interestingly, RPG1 degradation was shown to be delayed in highly resistant barley cultivars like Q21861 and in a single copy transgenic line GP/rpg1T1, although it was explained pointing at much higher level of *Rpg1* expression in these barley cultivars. Rapid phosphorylation and degradation of RPG1 is required but not sufficient to provide the resistance.

Since nonfunctional RPG1 containing altered pseudokinase domain for specific residues do get rapidly phosphorylated and degrades later but fails to provide resistance (Nirmala et al., 2010). Later, fast neutron mutagenesis approaches identified *rpr1* a gene which possibly function downstream to *Rpg1* for resistance signaling (Zhang et al., 2006).

RPG1 mediated resistance being primed at very early stage of pathogen landing, its phosphorylation and protein degradation required for resistance response can be considered as atypical resistance mechanism suggesting plant defenses should not be considered mere a straightforward Avr-R detection resulting in defense signaling. Defense signaling is complex, involving many polymorphic and conserved proteins in the signaling hub. Alteration in plant system homeostasis due to pathogen and disturbance of resistance hub equilibria leading to defense activation may be involving mutable specific upstream signaling but may coalesce to a single pathway for final signaling.

1.1.4.2. rpg4/Rpg5 locus mediated resistance

The remarkable durability of *Rpg1* under the constant selection pressure from evolutionary dynamic broad spectrum of stem rust pathogen population was reported to be finally broken in 1989, by the new stem rust race QCCJB that was virulent on *Rpg1* containing barley lines. Race QCCJ caused mini epidemic and yield loss in the northern great plains until the QCCJ susceptible wheat cultivar TAM 105 was removed from production in the lower great plains (Eversmeyer and Kramer, 2000) Further, the emergence of the hypervirulent TTKSK race group of stem rust which was shown to be virulent on 80-95% of cultivated wheat varieties worldwide and more than 95% of the barley accessions assayed, including lines carrying *Rpg1* (Steffenson et al., 2013), warranted the need to find new sources of resistance. This search of over 18,000 world barley lines culminated in the identification of the QCCJ and TTKSK

resistant barley line Q21861 harboring the *rpg4/Rpg5* temperature sensitive and recessive resistance locus at the telomeric region of chromosome 5HL (Steffenson et al., 2009; Brueggeman et al., 2008; Wang et al., 2013). The original *rpg4* nomenclature has proven to be confusing because the three genes present at the locus could not be genetically separated or eliminate by recombination after screening over 5,000 recombinant gametes and in two mapping populations, the same interval containing the dominant rye stem rust resistance gene *Rpg5* also harbors the recessive *rpg4*-mediated resistance against wheat stem rust (Brueggeman et al., 2008; Wang et al., 2013; Arora et al., 2013). The *rpg4/Rpg5* resistance locus designated *rpg4*/*Rpg5*-mediated resistance locus (*RMRL*) harbors three tightly linked genes *(Rpg5*, *HvRga1* and *HvAdf3*) and provides resistance against a broad spectrum of stem rust races including TTKSK also known as Ug99 (Brueggeman et al., 2008). This locus was also shown to provide dominant resistance for races of rye stem rust caused by *Puccinia graminis* f. sp. *secalis* (Steffenson et al., 1995) and oat stem rust caused by *Puccinia graminis* f. sp. *avenae* (Dracatos et al., 2015). Interestingly, a study of 73 landraces collected from the mountainous region of Switzerland screened with *P. graminis* f. sp. *tritici* race TTKSK to find new sources of resistance resulted in an unexpectedly high frequency of TTKSK and its surrogate race QCCJB resistance (>43%) (Steffenson et al., 2016) and the major contributor was *RMRL*. Though under the fact that resistance provided by the locus for wheat stem rust is recessive whereas for rye stem rust is dominant the nomenclature should be understood rpg4 as a phenotype.

The *Rpg5* and *Rga1* genes are NLR proteins, whereas *HvAdf3* encodes a putative actin depolymerization/modifier protein. Polymorphism in *HvRga1* and *HvAdf3* are minimal and do not correlate with compatible or incompatible interactions, and both were shown to be expressed in resistant and susceptible lines using qPCR, thus, appear to not contain primary sequence or

transcriptional polymorphism that can explain resistance function (Wang et al., 2013; Arora et al., 2013; Brueggeman et al., 2008). The predicted translation of *Rpg5* alleles are functionally polymorphic due to single base pair substitutions and insertion/deletion events that perfectly correlate with compatibility (susceptibility) and incompatibility (resistance). Two distinct diverse C-terminal integrated sensory domain (ISDs) are fused to the NLR of *Rpg5*, a serine threonine protein kinase domain in resistance *Rpg5-PK* alleles or a protein phosphatase 2C domain in the susceptibility *rpg5-PP2C* alleles representing two functionally antagonistic ISDs attached to the same NLR. Thus, making *Rpg5* the first characterized R-protein reported with the CC, NB-ARC, LRR and S/TPK domains that were previously reported in different R protein classes as discussed previously in literature. Using three different susceptible parents (Steptoe, Harrington and MD2) and the single resistant parent (Q21861) to develop three separate mapping populations to resolve further genetically *RMRL* via recombination was not fruitful because even after characterizing more than 5000 recombinant gametes, the *RMRL* remained a recombination quiescent region showing that the block of genes co-segregated in a tight linkage block passed on to progeny as a single package. It was later shown that all three genes are required together for resistance via BSMV-RNAi experiment that determined silencing of any one of the genes compromised the resistance response for *Pgt* race QCCJ (Wang et al., 2013). Interestingly, the presence of two head-to-head oriented NLRs, *Rpg5* and *HvRga1*, suggested the possibility of both following the most recent "Integrated decoy" model. The molecular mechanisms underlying in the resistance provided by these three genes is investigated in the presented research studies in my dissertation.

1.1.4.3. Technological advances to achieve new horizons

The pressing need to improve agricultural production is a key goal for crop-scientists to provide a sustainable and continuous food supply for a burgeoning world population which is estimated to exceed 9 billion by the year 2050. Scientific advances and massive breeding efforts to harness genetic diversity already present in gene pool brought tremendous changes in agricultural practices world-wide and is famously known as the Green Revolution. The Green Revolution starting in the 1960s and was led by Dr. Norman Borlaug who largely contributed to the movement by the incorporation of dwarfing genes into wheat and using agrochemicals to improve production. These practices allowed us to increase production by enhancing fertilization and reducing the disease pressure using agrochemicals to keep pace with the population explosion, yet concerns of chemical pollution via pesticide and fertilizer runoff are a real concern. Although in the present scenario of a global demand of increased crop productivity there is a need to adopt technologies and production practices to further improve crop production to keep pace with global demands. Genetic engineering offers a great tool to capture diversity not present in primary germplasm pool, though strict regulatory policies and poor consumer acceptance due to misleading information and misconceptions in the public for GMO products is a major obstacle. Chemical and radiation induced mutagenesis provides a cheap and less technical know-how requiring option for genetic diversity creation. This can also reduce the linkage drag associated when introducing diversity from wild progenitor species or non-adapted germplasm. The mutagenesis approach is immensely helpful to identify conserved non-polymorphic genes participating in the signaling pathway under study. For example NDR1(Non-race specific Disease Resistance1) an integrin like plasma membrane localized protein was identified using mutagenesis and positional cloning (Century et al., 1997, 1995) and has been

shown to cause susceptibility to bacterial and fungal pathogen if compromised. NDR1 was shown to interact with RIN4 (RPM1 Interacting Protein4) (Day et al., 2006; Knepper et al., 2011) a molecular switch participating in many host-pathogen interactions as a negative regulator of many NLR proteins (Jones and Dangl, 2006). Interestingly, the barley Rpg1 protein was shown to interact with the C-terminal fragment of HvRIN4 in a Y2H screen (Gill et al., 2012), presumably indirectly indicating a role of the barley homolog HvNDR1 in the stem rust PAMP detection at the host plasma membrane. A Fast Neutron (FN) mutagenesis approach was used to identify the signaling partners working in the *Rpg1* resistance pathway resulted in the identification of the *rpr1* mutation, a suppressor of *Rpg1* resistant pathway. Attempts have been made to identify the *Rpr1* gene using genetic mapping and transcript based cloning (Zhang et al., 2006; Mitra et al., 2004). In another study gamma irradiation was utilized to identify six non allelic mutants *rpr2, rpr3, rpr4, rpr5, rpr6* and *rpr7* containing a functional *Rpg1* yet failed to provide *Rpg1* mediated resistance (Gill et al., 2016). The *rpr1* gene was mapped to the barley chromosome 4H and *rpr2* on 6H thus representing non-allelic mutations, however, the rpr1 mutant has not been tested with other *rpr* mutants to rule out the possibility of allelism. Thus, these few examples indicate how mutagenesis approaches could be a valuable tool to identify gene function and interactions to decipher their interactions at molecular level.

1.1.5. Barley as a model crop to understand disease resistance

After the successful Human Genome Project (HGP), increasing efforts are made to understand the genome structure of important species on earth eventually leading to sequence "all life on Earth" under the Earth BioGenome Project (EBP) (Pennisi, 2017). First steps are taken towards important species, including important grass species in *Poaceae* family which originated 120 million years ago and is the source of major cereals for human food (Prasad et al.,

2005). Barley, Rice and Brachypodium are few species in *Poaceae* family completely sequenced, assembled and genome information is publicly available. Parallel efforts are ongoing to construct the whole genome assembly of Wheat and Maize, yet the large size of the grass genomes, low gene density and abundance of repetitive and silent genomic region poses a constant hurdle for genome assembly, and gene annotation. Sequenced genomes are the essential first ingredients to study and analyze the structure, evolution and diversification for genetic components. Barley being a diploid cereal crop species with a moderate genome size of ~5.6 Gbp (Giga base pair) comparing to the large genome size of hexaploid wheat (~17Gbp) and small genomes of Rice (~430 Mbp) and *Brachypodium* (~270 Mbp) provide an excellent platform for functional genomics studies. Understanding of host pathogen interaction during powdery mildew disease caused by *Blumeria graminis* f. sp. *hordei* was first studied in barley to identify pathogen recognition (Schulze-Lefert and Panstruga, 2003), activation of plant susceptibility or resistance response and downstream signaling cascade, paving the way for further studies and translated into other plant species including the universally accepted model plant *Arabidopsis thaliana* (genome size of ~135 Mbp). The stem rust-barley interactions were thoroughly investigated in many studies (Brueggeman et al., 2002, 2008; Horvath et al., 2003; Nirmala et al., 2006, 2007, 2010, 2011; Wang et al., 2013; Solanki et al., 2016). Currently, barley is being used as a model system to study many host-pathogen interactions including stem rust, yield parameters and malting qualities at molecular level. These studies will be a valuable source to improve our understanding and to fill knowledge gaps about biotic and abiotic stress resistance mechanisms, yield and quality in a cereal crop very closely related to wheat. Many studies have indicated the role of moisture, light-dark cycle, and stomatal opening in *Puccinia graminis* virulence on its host wheat and barley, yet a clear mechanism is not established. Since

Rpg1 and *Rpg5* stem rust resistance genes are already cloned and functionally validated in barley a further investigation to understand the signaling pathway would strengthen barley as a model system.

1.2. Literature cited

Arora, D., Gross, T., and Brueggeman, R. (2013). Allele characterization of genes required for rpg4-mediated wheat stem rust resistance identifies Rpg5 as the R gene. *Phytopathology* 103, 1153–1161. doi:10.1094/PHYTO-01-13-0030-R.

Aurthur, J. C. (1934). *Manual of Rusts in the United States and Canada*. Lancaster, PA, USA: The science press printing co.

Ayliffe, M., Singh, R., and Lagudah, E. (2008). Durable resistance to wheat stem rust needed. *Curr Opin Plant Biol* 11, 187–192. doi:10.1016/j.pbi.2008.02.001.

Baggs, E., Dagdas, G., and Krasileva, K. V. (2017). NLR diversity, helpers and integrated domains: making sense of the NLR IDentity. *Curr Opin Plant Biol* 38, 59–67. doi:10.1016/j.pbi.2017.04.012.

Bai, S., Liu, J., Chang, C., Zhang, L., Maekawa, T., Wang, Q., Xiao, W., Liu, Y., Chai, J., Takken, F. L. W., et al. (2012). Structure-function analysis of barley NLR immune receptor MLA10 reveals its cell compartment specific activity in cell death and disease resistance. *PLoS Pathog* 8, e1002752. doi:10.1371/journal.ppat.1002752.

Bailey, P. C., Dagdas, G., Baggs, E., Haerty, W., and V. Krasileva, K. (2017a). Immune receptors with exogenous domain fusions form evolutionary hotspots in grass genomes. *bioRxiv preprint*.

Bailey, P. C., Schudoma, C., Jackson, W., Baggs, E., Dagdas, G., Haerty, W., Moscou, M., and Krasileva, K. V. (2017b). Dominant integration locus drives continuous diversification of plant immune receptors with exogenous domain fusions. *BioRxiv*. doi:10.1101/100834.

Belkhadir, Y., Nimchuk, Z., Hubert, D. A., Mackey, D., and Dangl, J. L. (2004). *Arabidopsis* RIN4 negatively regulates disease resistance mediated by RPS2 and RPM1 downstream or independent of the NDR1 signal modulator and is not required for the virulence functions of bacterial type III effectors AvrRpt2 or AvrRpm1. *Plant Cell* 16, 2822–2835. doi:10.1105/tpc.104.024117.

Bella, J., Hindle, K. L., McEwan, P. A., and Lovell, S. C. (2008). The leucine-rich repeat structure. *Cell Mol Life Sci* 65, 2307–2333. doi:10.1007/s00018-008-8019-0.

Bendahmane, A., Farnham, G., Moffett, P., and Baulcombe, D. C. (2002). Constitutive gain-of-function mutants in a nucleotide binding site-leucine rich repeat protein encoded at the Rx locus of potato. *Plant J* 32, 195–204.

Bernoux, M., Burdett, H., Williams, S. J., Zhang, X., Chen, C., Newell, K., Lawrence, G. J., Kobe, B., Ellis, J. G., Anderson, P. A., et al. (2016). Comparative Analysis of the Flax Immune Receptors L6 and L7 Suggests an Equilibrium-Based Switch Activation Model. *Plant Cell* 28, 146–159. doi:10.1105/tpc.15.00303.

Bernoux, M., Ve, T., Williams, S., Warren, C., Hatters, D., Valkov, E., Zhang, X., Ellis, J. G., Kobe, B., and Dodds, P. N. (2011). Structural and functional analysis of a plant resistance protein TIR domain reveals interfaces for self-association, signaling, and autoregulation. *Cell Host Microbe* 9, 200–211. doi:10.1016/j.chom.2011.02.009.

BGRI RustTracker.org. Available at: http://rusttracker.cimmyt.org/ [Accessed April 9, 2017].

Bhattacharya, S. (2017). Deadly new wheat disease threatens Europe's crops. *Nature* 542, 145–146. doi:10.1038/nature.2017.21424.

Van der Biezen, E. A., and Jones, J. D. (1998). Plant disease-resistance proteins and the gene-for-gene concept. *Trends Biochem Sci* 23, 454–456. doi:10.1016/S0968-0004(98)01311-5.

Van der Biezen, E. A., and Jones, J. D. (1998). The NB-ARC domain: a novel signalling motif shared by plant resistance gene products and regulators of cell death in animals. *Curr Biol* 8, R226–7.

Block, A., and Alfano, J. R. (2011). Plant targets for Pseudomonas syringae type III effectors: virulence targets or guarded decoys? *Curr Opin Microbiol* 14, 39–46. doi:10.1016/j.mib.2010.12.011.

Boch, J., Bonas, U., and Lahaye, T. (2014). TAL effectors--pathogen strategies and plant resistance engineering. *New Phytol* 204, 823–832. doi:10.1111/nph.13015.

Brueggeman, R., Druka, A., Nirmala, J., Cavileer, T., Drader, T., Rostoks, N., Mirlohi, A., Bennypaul, H., Gill, U., Kudrna, D., et al. (2008). The stem rust resistance gene Rpg5 encodes a protein with nucleotide-binding-site, leucine-rich, and protein kinase domains. *Proc Natl Acad Sci U S A* 105, 14970–14975. doi:10.1073/pnas.0807270105.

Brueggeman, R., Rostoks, N., Kudrna, D., Kilian, A., Han, F., Chen, J., Druka, A., Steffenson, B., and Kleinhofs, A. (2002). The barley stem rust-resistance gene Rpg1 is a novel disease-resistance gene with homology to receptor kinases. *Proc Natl Acad Sci U S A* 99, 9328–9333. doi:10.1073/pnas.142284999.

Brueggeman, R., Steffenson, B. J., and Kleinhofs, A. (2009). The rpg4/Rpg5 stem rust resistance locus in barley: resistance genes and cytoskeleton dynamics. *Cell Cycle* 8, 977–981. doi:10.4161/cc.8.7.8079.

Century, K. S., Holub, E. B., and Staskawicz, B. J. (1995). NDR1, a locus of *Arabidopsis* thaliana that is required for disease resistance to both a bacterial and a fungal pathogen. *Proc Natl Acad Sci U S A* 92, 6597–6601.

Century, K. S., Shapiro, A. D., Repetti, P. P., Dahlbeck, D., Holub, E., and Staskawicz, B. J. (1997). NDR1, a pathogen-induced component required for *Arabidopsis* disease resistance. *Science* 278, 1963–1965.

Cesari, S., Bernoux, M., Moncuquet, P., Kroj, T., and Dodds, P. N. (2014). A novel conserved mechanism for plant NLR protein pairs: the "integrated decoy" hypothesis. *Front Plant Sci* 5, 606. doi:10.3389/fpls.2014.00606.

Césari, S., Kanzaki, H., Fujiwara, T., Bernoux, M., Chalvon, V., Kawano, Y., Shimamoto, K., Dodds, P., Terauchi, R., and Kroj, T. (2014). The NB-LRR proteins RGA4 and RGA5 interact functionally and physically to confer disease resistance. *EMBO J* 33, 1941–1959. doi:10.15252/embj.201487923.

Cesari, S., Moore, J., Chen, C., Webb, D., Periyannan, S., Mago, R., Bernoux, M., Lagudah, E. S., and Dodds, P. N. (2016). Cytosolic activation of cell death and stem rust resistance by cereal MLA-family CC-NLR proteins. *Proc Natl Acad Sci U S A* 113, 10204–10209. doi:10.1073/pnas.1605483113.

Chan, S. L., Mukasa, T., Santelli, E., Low, L. Y., and Pascual, J. (2010). The crystal structure of a TIR domain from *Arabidopsis* thaliana reveals a conserved helical region unique to plants. *Protein Sci* 19, 155–161. doi:10.1002/pro.275.

Chinchilla, D., Zipfel, C., Robatzek, S., Kemmerling, B., Nürnberger, T., Jones, J. D. G., Felix, G., and Boller, T. (2007). A flagellin-induced complex of the receptor FLS2 and BAK1 initiates plant defence. *Nature* 448, 497–500. doi:10.1038/nature05999.

Chisholm, S. T., Coaker, G., Day, B., and Staskawicz, B. J. (2006). Host-microbe interactions: shaping the evolution of the plant immune response. *Cell* 124, 803–814. doi:10.1016/j.cell.2006.02.008.

Civáň, P., and Brown, T. A. (2017). A novel mutation conferring the nonbrittle phenotype of cultivated barley. *New Phytol* 214, 468–472. doi:10.1111/nph.14377.

Coaker, G., Falick, A., and Staskawicz, B. (2005). Activation of a phytopathogenic bacterial effector protein by a eukaryotic cyclophilin. *Science* 308, 548–550. doi:10.1126/science.1108633.

Collier, S. M., Hamel, L.-P., and Moffett, P. (2011). Cell death mediated by the N-terminal domains of a unique and highly conserved class of NB-LRR protein. *Mol Plant Microbe Interact* 24, 918–931. doi:10.1094/MPMI-03-11-0050.

Collier, S. M., and Moffett, P. (2009). NB-LRRs work a "bait and switch" on pathogens. *Trends Plant Sci* 14, 521–529. doi:10.1016/j.tplants.2009.08.001.

Couto, D., and Zipfel, C. (2016). Regulation of pattern recognition receptor signalling in plants. *Nat Rev Immunol* 16, 537–552. doi:10.1038/nri.2016.77.

Day, B., Dahlbeck, D., and Staskawicz, B. J. (2006). NDR1 interaction with RIN4 mediates the differential activation of multiple disease resistance pathways in *Arabidopsis*. *Plant Cell* 18, 2782–2791. doi:10.1105/tpc.106.044693.

Deslandes, L., Olivier, J., Peeters, N., Feng, D. X., Khounlotham, M., Boucher, C., Somssich, I., Genin, S., and Marco, Y. (2003). Physical interaction between RRS1-R, a protein conferring resistance to bacterial wilt, and PopP2, a type III effector targeted to the plant nucleus. *Proc Natl Acad Sci U S A* 100, 8024–8029. doi:10.1073/pnas.1230660100.

DeYoung, B. J., and Innes, R. W. (2006). Plant NBS-LRR proteins in pathogen sensing and host defense. *Nat Immunol* 7, 1243–1249. doi:10.1038/ni1410.

Dinesh-Kumar, S. P., and Baker, B. J. (2000). Alternatively spliced N resistance gene transcripts: their possible role in tobacco mosaic virus resistance. *Proc Natl Acad Sci U S A* 97, 1908–1913. doi:10.1073/pnas.020367497.

Dodds, P. N., Lawrence, G. J., Catanzariti, A.-M., Teh, T., Wang, C.-I. A., Ayliffe, M. A., Kobe, B., and Ellis, J. G. (2006). Direct protein interaction underlies gene-for-gene specificity and coevolution of the flax resistance genes and flax rust avirulence genes. *Proc Natl Acad Sci U S A* 103, 8888–8893. doi:10.1073/pnas.0602577103.

Dodds, P. N., Lawrence, G. J., and Ellis, J. G. (2001). Six amino acid changes confined to the leucine-rich repeat beta-strand/beta-turn motif determine the difference between the P and P2 rust resistance specificities in flax. *Plant Cell* 13, 163–178.

Dodds, P. N., and Rathjen, J. P. (2010). Plant immunity: towards an integrated view of plant-pathogen interactions. *Nat Rev Genet* 11, 539–548. doi:10.1038/nrg2812.

Dracatos, P., Singh, D., Fetch, T., and Park, R. (2015). Resistance to Puccinia graminis f. sp. avenae in Barley Is Associated with the Rpg5 Locus. *Phytopathology* 105, 490–494. doi:10.1094/PHYTO-08-14-0224-R.

Eckardt, N. A. (2007). Positive and negative feedback coordinate regulation of disease resistance gene expression. *THE PLANT CELL ONLINE* 19, 2700–2702. doi:10.1105/tpc.107.056226.

Eitas, T. K., and Dangl, J. L. (2010). NB-LRR proteins: pairs, pieces, perception, partners, and pathways. *Curr Opin Plant Biol* 13, 472–477. doi:10.1016/j.pbi.2010.04.007.

Ellis, J., Dodds, P., and Pryor, T. (2000). The generation of plant disease resistance gene specificities. *Trends Plant Sci* 5, 373–379.

Enkhbayar, P., Kamiya, M., Osaki, M., Matsumoto, T., and Matsushima, N. (2004). Structural principles of leucine-rich repeat (LRR) proteins. *Proteins* 54, 394–403. doi:10.1002/prot.10605.

Eriksson, J., and Henning, E. (1984). Die Hauptresultate einer neuen Untersuchung über die Getreidesorte. *Z. Pflanzenkr* 4, 66–73, 140–142, 197–203, 257–262.

Eversmeyer, M. G., and Kramer, C. L. (2000). Epidemiology of wheat leaf and stem rust in the central great plains of the usa. *Annu Rev Phytopathol* 38, 491–513. doi:10.1146/annurev.phyto.38.1.491.

Garnica, D. P., Nemri, A., Upadhyaya, N. M., Rathjen, J. P., and Dodds, P. N. (2014). The ins and outs of rust haustoria. *PLoS Pathog* 10, e1004329. doi:10.1371/journal.ppat.1004329.

Gassmann, W., Hinsch, M. E., and Staskawicz, B. J. (1999). The *Arabidopsis* RPS4 bacterial-resistance gene is a member of the TIR-NBS-LRR family of disease-resistance genes. *Plant J* 20, 265–277.

Gill, U., Brueggeman, R., Nirmala, J., Chai, Y., Steffenson, B., and Kleinhofs, A. (2016). Molecular and genetic characterization of barley mutants and genetic mapping of mutant rpr2 required for Rpg1-mediated resistance against stem rust. *Theor Appl Genet* 129, 1519–1529. doi:10.1007/s00122-016-2721-3.

Gill, U., Nirmala, J., Brueggeman, R., and Kleinhofs, A. (2012). Identification, characterization and putative function of HvRin4, a barley homolog of *Arabidopsis* Rin4. *Physiological and Molecular Plant Pathology* 80, 41–49. doi:10.1016/j.pmpp.2012.08.002.

Göhre, V., Spallek, T., Häweker, H., Mersmann, S., Mentzel, T., Boller, T., de Torres, M., Mansfield, J. W., and Robatzek, S. (2008). Plant pattern-recognition receptor FLS2 is directed for degradation by the bacterial ubiquitin ligase AvrPtoB. *Curr Biol* 18, 1824–1832. doi:10.1016/j.cub.2008.10.063.

Haile, J., and Rouml, M. (2013). Status of genetic research for resistance to Ug99 race of Puccinia graminis f. sp. tritici: A review of current research and implications. *African Journal of Agricultural Research* 8, 6670–6680. Available at: http://www.academicjournals.org/journal/AJAR/article-abstract/2113F3842429.

Hao, W., Collier, S. M., Moffett, P., and Chai, J. (2013). Structural basis for the interaction between the potato virus X resistance protein (Rx) and its cofactor Ran GTPase-activating protein 2 (RanGAP2). *J Biol Chem* 288, 35868–35876. doi:10.1074/jbc.M113.517417.

He, P., Shan, L., Lin, N.-C., Martin, G. B., Kemmerling, B., Nürnberger, T., and Sheen, J. (2006). Specific bacterial suppressors of MAMP signaling upstream of MAPKKK in *Arabidopsis* innate immunity. *Cell* 125, 563–575. doi:10.1016/j.cell.2006.02.047.

Henty-Ridilla, J. L., Li, J., Day, B., and Staiger, C. J. (2014). ACTIN DEPOLYMERIZING FACTOR4 regulates actin dynamics during innate immune signaling in *Arabidopsis*. *Plant Cell* 26, 340–352. doi:10.1105/tpc.113.122499.

Hodson, D., Grønbech-Hansen, J., Lassen, P., Alemayehu, Y., Arista, J., Sonder, K., Kosina, P., Moncada, P., Nazari, K., Park, R., et al. (2012). Tracking the wheat rust pathogens. in *Proceedings Borlaug Global Rust Initiative 2012 Technical Workshop, China, pp11-22*.

Van der Hoorn, R. A. L., and Kamoun, S. (2008). From Guard to Decoy: a new model for perception of plant pathogen effectors. *Plant Cell* 20, 2009–2017. doi:10.1105/tpc.108.060194.

Horvath, H., Rostoks, N., Brueggeman, R., Steffenson, B., von Wettstein, D., and Kleinhofs, A. (2003). Genetically engineered stem rust resistance in barley using the Rpg1 gene. *Proc Natl Acad Sci U S A* 100, 364–369. doi:10.1073/pnas.0136911100.

Hothorn, M., Belkhadir, Y., Dreux, M., Dabi, T., Noel, J. P., Wilson, I. A., and Chory, J. (2011). Structural basis of steroid hormone perception by the receptor kinase BRI1. *Nature* 474, 467–471. doi:10.1038/nature10153.

Huang, L., Brooks, S. A., Li, W., Fellers, J. P., Trick, H. N., and Gill, B. S. (2003). Map-based cloning of leaf rust resistance gene Lr21 from the large and polyploid genome of bread wheat. *Genetics* 164, 655–664.

Hwang, C.-F., and Williamson, V. M. (2003). Leucine-rich repeat-mediated intramolecular interactions in nematode recognition and cell death signaling by the tomato resistance protein Mi. *Plant J* 34, 585–593.

Jia, Y., McAdams, S. A., Bryan, G. T., Hershey, H. P., and Valent, B. (2000). Direct interaction of resistance gene and avirulence gene products confers rice blast resistance. *EMBO J* 19, 4004–4014. doi:10.1093/emboj/19.15.4004.

Jones, J. D. G., and Dangl, J. L. (2006). The plant immune system. *Nature* 444, 323–329. doi:10.1038/nature05286.

Jones, J. D. G., Witek, K., Verweij, W., Jupe, F., Cooke, D., Dorling, S., Tomlinson, L., Smoker, M., Perkins, S., and Foster, S. (2014). Elevating crop disease resistance with cloned genes. *Philos Trans R Soc Lond, B, Biol Sci* 369, 20130087. doi:10.1098/rstb.2013.0087.

Jupe, F., Witek, K., Verweij, W., Sliwka, J., Pritchard, L., Etherington, G. J., Maclean, D., Cock, P. J., Leggett, R. M., Bryan, G. J., et al. (2013). Resistance gene enrichment sequencing (RenSeq) enables reannotation of the NB-LRR gene family from sequenced plant genomes and rapid mapping of resistance loci in segregating populations. *Plant J* 76, 530–544. doi:10.1111/tpj.12307.

Kage, U., Kumar, A., Dhokane, D., Karre, S., and Kushalappa, A. C. (2016). Functional molecular markers for crop improvement. *Crit Rev Biotechnol* 36, 917–930. doi:10.3109/07388551.2015.1062743.

Kang, Y. J., Kim, K. H., Shim, S., Yoon, M. Y., Sun, S., Kim, M. Y., Van, K., and Lee, S.-H. (2012). Genome-wide mapping of NBS-LRR genes and their association with disease resistance in soybean. *BMC Plant Biol* 12, 139. doi:10.1186/1471-2229-12-139.

Kim, H.-S., Desveaux, D., Singer, A. U., Patel, P., Sondek, J., and Dangl, J. L. (2005). The Pseudomonas syringae effector AvrRpt2 cleaves its C-terminally acylated target, RIN4, from *Arabidopsis* membranes to block RPM1 activation. *Proc Natl Acad Sci U S A* 102, 6496–6501. doi:10.1073/pnas.0500792102.

Kim, Y. J., Lin, N. C., and Martin, G. B. (2002). Two distinct Pseudomonas effector proteins interact with the Pto kinase and activate plant immunity. *Cell* 109, 589–598.

Knepper, C., Savory, E. A., and Day, B. (2011). *Arabidopsis* NDR1 is an integrin-like protein with a role in fluid loss and plasma membrane-cell wall adhesion. *Plant Physiol* 156, 286–300. doi:10.1104/pp.110.169656.

Kobe, B., and Deisenhofer, J. (1995). A structural basis of the interactions between leucine-rich repeats and protein ligands. *Nature* 374, 183–186. doi:10.1038/374183a0.

Krasileva, K. V., Dahlbeck, D., and Staskawicz, B. J. (2010). Activation of an *Arabidopsis* resistance protein is specified by the in planta association of its leucine-rich repeat domain with the cognate oomycete effector. *Plant Cell* 22, 2444–2458. doi:10.1105/tpc.110.075358.

Leonard, K. J., and Szabo, L. J. (2005). Stem rust of small grains and grasses caused by Puccinia graminis. *Mol Plant Pathol* 6, 99–111. doi:10.1111/j.1364-3703.2005.00273.x.

Lösch, S., Moghaddam, N., Grossschmidt, K., Risser, D. U., and Kanz, F. (2014). Stable isotope and trace element studies on gladiators and contemporary Romans from Ephesus (Turkey, 2nd and 3rd Ct. AD)--mplications for differences in diet. *PLoS ONE* 9, e110489. doi:10.1371/journal.pone.0110489.

Loutre, C., Wicker, T., Travella, S., Galli, P., Scofield, S., Fahima, T., Feuillet, C., and Keller, B. (2009). Two different CC-NBS-LRR genes are required for Lr10-mediated leaf rust resistance in tetraploid and hexaploid wheat. *Plant J* 60, 1043–1054. doi:10.1111/j.1365-313X.2009.04024.x.

Luig, N. H. (1985). “Epidemiology in Australia and New Zealand,” in *Diseases, Distribution, Epidemiology, and Control*, eds. A. P. Roelfs and W. R. Bushnell (Orlando, Academic Press,), 301–328. doi:10.1016/B978-0-12-148402-6.50018-3.

Mackey, D., Belkhadir, Y., Alonso, J. M., Ecker, J. R., and Dangl, J. L. (2003). *Arabidopsis* RIN4 is a target of the type III virulence effector AvrRpt2 and modulates RPS2-mediated resistance. *Cell* 112, 379–389.

Mackey, D., Holt, B. F., Wiig, A., and Dangl, J. L. (2002). RIN4 interacts with Pseudomonas syringae type III effector molecules and is required for RPM1-mediated resistance in *Arabidopsis*. *Cell* 108, 743–754. doi:10.1016/S0092-8674(02)00661-X.

Maekawa, T., Cheng, W., Spiridon, L. N., Töller, A., Lukasik, E., Saijo, Y., Liu, P., Shen, Q.-H., Micluta, M. A., Somssich, I. E., et al. (2011a). Coiled-coil domain-dependent homodimerization of intracellular barley immune receptors defines a minimal functional module for triggering cell death. *Cell Host Microbe* 9, 187–199. doi:10.1016/j.chom.2011.02.008.

Maekawa, T., Kufer, T. A., and Schulze-Lefert, P. (2011b). NLR functions in plant and animal immune systems: so far and yet so close. *Nat Immunol* 12, 817–826. doi:10.1038/ni.2083.

Mascher, M., Schuenemann, V. J., Davidovich, U., Marom, N., Himmelbach, A., Hübner, S., Korol, A., David, M., Reiter, E., Riehl, S., et al. (2016). Genomic analysis of 6,000-year-old cultivated grain illuminates the domestication history of barley. *Nat Genet* 48, 1089–1093. doi:10.1038/ng.3611.

McDowell, J. M., and Woffenden, B. J. (2003). Plant disease resistance genes: recent insights and potential applications. *Trends Biotechnol* 21, 178–183. doi:10.1016/S0167-7799(03)00053-2.

Meyers, B. C., Dickerman, A. W., Michelmore, R. W., Sivaramakrishnan, S., Sobral, B. W., and Young, N. D. (1999). Plant disease resistance genes encode members of an ancient and diverse protein family within the nucleotide-binding superfamily. *Plant J* 20, 317–332. doi:10.1046/j.1365-313X.1999.00606.x.

Meyers, B. C., Kozik, A., Griego, A., Kuang, H., and Michelmore, R. W. (2003). Genome-wide analysis of NBS-LRR-encoding genes in *Arabidopsis*. *Plant Cell* 15, 809–834.

Mitra, R. M., Gleason, C. A., Edwards, A., Hadfield, J., Downie, J. A., Oldroyd, G. E. D., and Long, S. R. (2004). A Ca2+/calmodulin-dependent protein kinase required for symbiotic nodule development: Gene identification by transcript-based cloning. *Proc Natl Acad Sci U S A* 101, 4701–4705. doi:10.1073/pnas.0400595101.

Mo, J., and Duncan, J. A. (2013). Assessing ATP binding and hydrolysis by NLR proteins. *Methods Mol Biol* 1040, 153–168. doi:10.1007/978-1-62703-523-1_12.

Moffett, P., Farnham, G., Peart, J., and Baulcombe, D. C. (2002). Interaction between domains of a plant NBS-LRR protein in disease resistance-related cell death. *EMBO J* 21, 4511–4519.

Moscou, M. J., and Bogdanove, A. J. (2009). A simple cipher governs DNA recognition by TAL effectors. *Science* 326, 1501. doi:10.1126/science.1178817.

Mucyn, T. S., Clemente, A., Andriotis, V. M. E., Balmuth, A. L., Oldroyd, G. E. D., Staskawicz, B. J., and Rathjen, J. P. (2006). The tomato NBARC-LRR protein Prf interacts with Pto kinase in vivo to regulate specific plant immunity. *Plant Cell* 18, 2792–2806. doi:10.1105/tpc.106.044016.

Narusaka, M., Shirasu, K., Noutoshi, Y., Kubo, Y., Shiraishi, T., Iwabuchi, M., and Narusaka, Y. (2009). RRS1 and RPS4 provide a dual Resistance-gene system against fungal and bacterial pathogens. *Plant J* 60, 218–226. doi:10.1111/j.1365-313X.2009.03949.x.

Ng, A., and Xavier, R. J. (2011). Leucine-rich repeat (LRR) proteins: integrators of pattern recognition and signaling in immunity. *Autophagy* 7, 1082–1084.

Nirmala, J., Brueggeman, R., Maier, C., Clay, C., Rostoks, N., Kannangara, C. G., von Wettstein, D., Steffenson, B. J., and Kleinhofs, A. (2006). Subcellular localization and functions of the barley stem rust resistance receptor-like serine/threonine-specific protein kinase Rpg1. *Proc Natl Acad Sci U S A* 103, 7518–7523. doi:10.1073/pnas.0602379103.

Nirmala, J., Dahl, S., Steffenson, B. J., Kannangara, C. G., von Wettstein, D., Chen, X., and Kleinhofs, A. (2007). Proteolysis of the barley receptor-like protein kinase RPG1 by a proteasome pathway is correlated with Rpg1-mediated stem rust resistance. *Proc Natl Acad Sci U S A* 104, 10276–10281. doi:10.1073/pnas.0703758104.

Nirmala, J., Drader, T., Chen, X., Steffenson, B., and Kleinhofs, A. (2010). Stem rust spores elicit rapid RPG1 phosphorylation. *Mol Plant Microbe Interact* 23, 1635–1642. doi:10.1094/MPMI-06-10-0136.

Nirmala, J., Drader, T., Lawrence, P. K., Yin, C., Hulbert, S., Steber, C. M., Steffenson, B. J., Szabo, L. J., von Wettstein, D., and Kleinhofs, A. (2011). Concerted action of two avirulent spore effectors activates Reaction to Puccinia graminis 1 (Rpg1)-mediated cereal stem rust resistance. *Proc Natl Acad Sci U S A* 108, 14676–14681. doi:10.1073/pnas.1111771108.

Nishimura, M. T., Anderson, R. G., Cherkis, K. A., Law, T. F., Liu, Q. L., Machius, M., Nimchuk, Z. L., Yang, L., Chung, E.-H., El Kasmi, F., et al. (2017). TIR-only protein RBA1 recognizes a pathogen effector to regulate cell death in *Arabidopsis*. *Proc Natl Acad Sci U S A* 114. doi:10.1073/pnas.1620973114.

Niu, Z., Klindworth, D., Friesen, T., Chao, S., Jin, Y., Cai, X., and Xu, S. (2011). Targeted introgression of a wheat stem rust resistance gene by DNA marker-assisted chromosome engineering. *Genetics* 187, 1011–1021. Available at: http://www.genetics.org/content/187/4/1011.full-text.pdf+html.

Van Ooijen, G., Mayr, G., Kasiem, M. M. A., Albrecht, M., Cornelissen, B. J. C., and Takken, F. L. W. (2008). Structure-function analysis of the NB-ARC domain of plant disease resistance proteins. *J Exp Bot* 59, 1383–1397. doi:10.1093/jxb/ern045.

Ortiz, D., de Guillen, K., Cesari, S., Chalvon, V., Gracy, J., Padilla, A., and Kroj, T. (2017). Recognition of the Magnaporthe oryzae Effector AVR-Pia by the Decoy Domain of the Rice NLR Immune Receptor RGA5. *Plant Cell* 29, 156–168. doi:10.1105/tpc.16.00435.

Padmanabhan, M., Cournoyer, P., and Dinesh-Kumar, S. P. (2009). The leucine-rich repeat domain in plant innate immunity: a wealth of possibilities. *Cell Microbiol* 11, 191–198. doi:10.1111/j.1462-5822.2008.01260.x.

Pankin, A., and von Korff, M. (2017). Co-evolution of methods and thoughts in cereal domestication studies: a tale of barley (Hordeum vulgare). *Curr Opin Plant Biol* 36, 15–21. doi:10.1016/j.pbi.2016.12.001.

Pennisi, E. (2017). Biologists propose to sequence the DNA of all life on Earth. *Science*. Available at: http://www.sciencemag.org/news/2017/02/biologists-propose-sequence-dna-all-life-earth [Accessed April 4, 2017].

Porter, K., Shimono, M., Tian, M., and Day, B. (2012). *Arabidopsis* Actin-Depolymerizing Factor-4 links pathogen perception, defense activation and transcription to cytoskeletal dynamics. *PLoS Pathog* 8, e1003006. doi:10.1371/journal.ppat.1003006.

Pourkheirandish, M., Hensel, G., Kilian, B., Senthil, N., Chen, G., Sameri, M., Azhaguvel, P., Sakuma, S., Dhanagond, S., Sharma, R., et al. (2015). Evolution of the grain dispersal system in barley. *Cell* 162, 527–539. doi:10.1016/j.cell.2015.07.002.

Prasad, V., Strömberg, C. A. E., Alimohammadian, H., and Sahni, A. (2005). Dinosaur coprolites and the early evolution of grasses and grazers. *Science* 310, 1177–1180. doi:10.1126/science.1118806.

Pretorius, Z., Singh, R., Wagoire, W., and Payne, T. (2000). Detection of virulence to wheat stem rust resistance gene Sr31 in Puccinia graminis. f. sp. tritici in Uganda. *Plant Disease* 84, 203–203. Available at: http://apsjournals.apsnet.org/doi/abs/10.1094/pdis.2000.84.2.203b.

Qi, D., DeYoung, B. J., and Innes, R. W. (2012). Structure-function analysis of the coiled-coil and leucine-rich repeat domains of the RPS5 disease resistance protein. *Plant Physiol* 158, 1819–1832. doi:10.1104/pp.112.194035.

Rairdan, G. J., Collier, S. M., Sacco, M. A., Baldwin, T. T., Boettrich, T., and Moffett, P. (2008). The coiled-coil and nucleotide binding domains of the Potato Rx disease resistance protein function in pathogen recognition and signaling. *Plant Cell* 20, 739–751. doi:10.1105/tpc.107.056036.

Razzaq, A. (2016). Rust of Wheat. Available at: http://istudy.pk/rust-of-wheat/ [Accessed April 30, 2017].

Read, A. C., Rinaldi, F. C., Hutin, M., He, Y.-Q., Triplett, L. R., and Bogdanove, A. J. (2016). Suppression of Xo1-Mediated Disease Resistance in Rice by a Truncated, Non-DNA-Binding TAL Effector of Xanthomonas oryzae. *Front Plant Sci* 7, 1516. doi:10.3389/fpls.2016.01516.

Roelfs, A. (1985a). Epidemiology in North America. *The cereal rusts* 2, 403–434. Available at: http://www.globalrust.org/sites/default/files/cereal-rusts/volume2.pdf#page=395.

Roelfs, A., and Bushnell, W. (1985). The Cereal Rusts. Vol. 2. Diseases, Distribution. *Epidemiology, and Control. Academic Press, Orlando*.

Roelfs, A. P. (1985b). "Wheat and rye stem rust," in *The Cereal Rusts*, eds. A. P. Roelfs and W. R. Bushnell, 3–27.

Römer, P., Recht, S., and Lahaye, T. (2009). A single plant resistance gene promoter engineered to recognize multiple TAL effectors from disparate pathogens. *Proc Natl Acad Sci U S A* 106, 20526–20531. doi:10.1073/pnas.0908812106.

Rostoks, N., Steffenson, B. J., and Kleinhofs, A. (2004). Structure and expression of the barley stem rust resistance gene Rpg1 messenger RNA. *Physiological and Molecular Plant Pathology* 64, 91–101. doi:10.1016/j.pmpp.2004.05.006.

Le Roux, C., Huet, G., Jauneau, A., Camborde, L., Trémousaygue, D., Kraut, A., Zhou, B., Levaillant, M., Adachi, H., Yoshioka, H., et al. (2015). A receptor pair with an integrated decoy converts pathogen disabling of transcription factors to immunity. *Cell* 161, 1074–1088. doi:10.1016/j.cell.2015.04.025.

Russell, J., Mascher, M., Dawson, I. K., Kyriakidis, S., Calixto, C., Freund, F., Bayer, M., Milne, I., Marshall-Griffiths, T., Heinen, S., et al. (2016). Exome sequencing of geographically diverse barley landraces and wild relatives gives insights into environmental adaptation. *Nat Genet* 48, 1024–1030. doi:10.1038/ng.3612.

Saari, E., and Prescott, J. (1985). World distribution in relation to economic losses. *The cereal rusts* 2, 259–298. Available at: https://www.ars.usda.gov/ARSUserFiles/50620500/Publications/CerealRusts/The%20Cereal%20Rusts_VOLUME%20II.pdf#page=257.

Salmond, G. P., and Reeves, P. J. (1993). Membrane traffic wardens and protein secretion in gram-negative bacteria. *Trends Biochem Sci* 18, 7–12.

Sarris, P. F., Duxbury, Z., Huh, S. U., Ma, Y., Segonzac, C., Sklenar, J., Derbyshire, P., Cevik, V., Rallapalli, G., Saucet, S. B., et al. (2015). A Plant Immune Receptor Detects Pathogen Effectors that Target WRKY Transcription Factors. *Cell* 161, 1089–1100. doi:10.1016/j.cell.2015.04.024.

Schulze-Lefert, P., and Panstruga, R. (2003). Establishment of biotrophy by parasitic fungi and reprogramming of host cells for disease resistance. *Annu Rev Phytopathol* 41, 641–667. doi:10.1146/annurev.phyto.41.061002.083300.

She, J., Han, Z., Kim, T.-W., Wang, J., Cheng, W., Chang, J., Shi, S., Wang, J., Yang, M., Wang, Z.-Y., et al. (2011). Structural insight into brassinosteroid perception by BRI1. *Nature* 474, 472–476. doi:10.1038/nature10178.

Sinapidou, E., Williams, K., Nott, L., Bahkt, S., Tör, M., Crute, I., Bittner-Eddy, P., and Beynon, J. (2004). Two TIR:NB:LRR genes are required to specify resistance to Peronospora parasitica isolate Cala2 in *Arabidopsis*. *Plant J* 38, 898–909. doi:10.1111/j.1365-313X.2004.02099.x.

Singh, R. (2006). Current status, likely migration and strategies to mitigate the threat to wheat production from race Ug99 (TTKS) of stem rust pathogen. *CAB Reviews: Perspectives in Agriculture, Veterinary Science, Nutrition and Natural Resources* 1. doi:10.1079/PAVSNNR20061054.

Singh, R., Hodson, D., Huerta-Espino, J., Jin, Y., Njau, P., Wanyera, R., Herrera-Foessel, S., and Ward, R. (2008). Will stem rust destroy the world's wheat crop?. *Advances in agronomy* 98, 271–309. Available at: http://www.sciencedirect.com/science/article/pii/S0065211308002058.

Singh, R., Huerta-Espino, J., Bhavani, S., Singh, D., Singh, P., Herrera-Foessel, S., Njau, P., Wanyera, R., and Jin, Y. (2009). Breeding for minor gene-based adult plant resistance to stem rust in wheat. *Proceedings, oral papers and posters, 2009 Technical Workshop, Borlaug Global Rust Initiative, Cd. Obregón, Sonora, Mexico, 17-20 March, 2009*. Available at: https://www.cabdirect.org/cabdirect/abstract/20103156332.

Singh, R. P., Hodson, D. P., Huerta-Espino, J., Jin, Y., Bhavani, S., Njau, P., Herrera-Foessel, S., Singh, P. K., Singh, S., and Govindan, V. (2011). The emergence of Ug99 races of the stem rust fungus is a threat to world wheat production. *Annu Rev Phytopathol* 49, 465–481. doi:10.1146/annurev-phyto-072910-095423.

Solanki, S., Ameen, G., Richards, J., and S. Brueggeman, R. (2016). Modulation of integrated decoy R-genes/transcription factor assembly elicits wheat stem rust resistance responses in barley: rpg4/Rpg5-mediated Ug99 resistance. in *International Barley Genetics Symposium* Biotic Stresses., eds. K. Smith and R. Dill-Macky (Minneapolis-St. Paul, Minnesota, USA: IBGS). Available at: http://ibgs2016.org/.

Song, W., Han, Z., Sun, Y., and Chai, J. (2014). Crystal structure of a plant leucine rich repeat protein with two island domains. *Sci China Life Sci* 57, 137–144. doi:10.1007/s11427-013-4586-x.

Spoel, S. H., and Dong, X. (2012). How do plants achieve immunity? Defence without specialized immune cells. *Nat Rev Immunol* 12, 89–100. doi:10.1038/nri3141.

Steffenson, B. (1992a). Analysis of durable resistance to stem rust in barley. *Breeding for Disease Resistance*, 153–167. Available at: http://link.springer.com/chapter/10.1007/978-94-017-0954-5_13.

Steffenson, B. J. (1992b). Analysis of durable resistance to stem rust in barley. *Euphytica* 63, 153–167. doi:10.1007/BF00023920.

Steffenson, B. J., Jin, Y., Brueggeman, R. S., Kleinhofs, A., and Sun, Y. (2009). Resistance to stem rust race TTKSK maps to the rpg4/Rpg5 complex of chromosome 5H of barley. *Phytopathology* 99, 1135–1141. doi:10.1094/PHYTO-99-10-1135.

Steffenson, B. J., Jin, Y., Rossnagel, B. G., Rasmussen, J. B., and Kao, K. (1995). Genetics of multiple disease resistance in a doubled-haploid population of barley. *Plant Breeding* 114, 50–54. doi:10.1111/j.1439-0523.1995.tb00758.x.

Steffenson, B. J., Solanki, S., and Brueggeman, R. S. (2016). Landraces from mountainous regions of Switzerland are sources of important genes for stem rust resistance in barley. *Alpine botany* 126, 23–33. doi:10.1007/s00035-015-0161-3.

Steffenson, B. J., Zhou, H., Chai, Y., and Grando, S. (2013). "Vulnerability of cultivated and wild barley to african stem rust race TTKSK," in *Advance in barley sciences*, eds. G. Zhang, C. Li, and X. Liu (Dordrecht: Springer Netherlands), 243–255. doi:10.1007/978-94-007-4682-4_21.

Swiderski, M. R., Birker, D., and Jones, J. D. G. (2009). The TIR domain of TIR-NB-LRR resistance proteins is a signaling domain involved in cell death induction. *Mol Plant Microbe Interact* 22, 157–165. doi:10.1094/MPMI-22-2-0157.

Takken, F. L., Albrecht, M., and Tameling, W. I. (2006). Resistance proteins: molecular switches of plant defence. *Curr Opin Plant Biol* 9, 383–390. doi:10.1016/j.pbi.2006.05.009.

Tang, Frederick, Zhou, Halterman, Jia, and Martin (1996). Initiation of plant disease resistance by physical interaction of avrpto and pto kinase. *Science* 274, 2060–2063.

Tanno, K.-I., and Willcox, G. (2006). How fast was wild wheat domesticated? *Science* 311, 1886. doi:10.1126/science.1124635.

Tian, M., Chaudhry, F., Ruzicka, D. R., Meagher, R. B., Staiger, C. J., and Day, B. (2009). *Arabidopsis* actin-depolymerizing factor AtADF4 mediates defense signal transduction triggered by the Pseudomonas syringae effector AvrPphB. *Plant Physiol* 150, 815–824. doi:10.1104/pp.109.137604.

Ve, T., Williams, S., Valkov, E., Ellis, J. G., Dodds, P. N., and Kobe, B. (2011). Crystallization, X-ray diffraction analysis and preliminary structure determination of the TIR domain from the flax resistance protein L6. *Acta Crystallogr Sect F Struct Biol Cryst Commun* 67, 237–240. doi:10.1107/S1744309110051006.

Wanderley-Nogueira, A. C., Bezerra-Neto, J. P., Kido, E. A., de Araújo, F. T., Amorim, L. L. B., Crovella, S., and Benko-Iseppon, A. M. (2016). Plant Elite Squad: First Defense Line and Resistance Genes - Identification, Diversity and Functional Roles. *Curr Protein Pept Sci* 18, 294–310. doi:10.2174/1389203717666160724193045.

Wang, X., Richards, J., Gross, T., Druka, A., Kleinhofs, A., Steffenson, B., Acevedo, M., and Brueggeman, R. (2013). The rpg4-mediated resistance to wheat stem rust (Puccinia graminis) in barley (Hordeum vulgare) requires Rpg5, a second NBS-LRR gene, and an actin depolymerization factor. *Mol Plant Microbe Interact* 26, 407–418. doi:10.1094/MPMI-06-12-0146-R.

Warren, R. F., Henk, A., Mowery, P., Holub, E., and Innes, R. W. (1998). A mutation within the leucine-rich repeat domain of the *Arabidopsis* disease resistance gene RPS5 partially suppresses multiple bacterial and downy mildew resistance genes. *Plant Cell* 10, 1439–1452.

Weiss, E., Kislev, M. E., Simchoni, O., Nadel, D., and Tschauner, H. (2008). Plant-food preparation area on an Upper Paleolithic brush hut floor at Ohalo II, Israel. *J Archaeol Sci* 35, 2400–2414. doi:10.1016/j.jas.2008.03.012.

Williams, S. J., Sohn, K. H., Wan, L., Bernoux, M., Sarris, P. F., Segonzac, C., Ve, T., Ma, Y., Saucet, S. B., Ericsson, D. J., et al. (2014). Structural basis for assembly and function of a heterodimeric plant immune receptor. *Science* 344, 299–303. doi:10.1126/science.1247357.

Wilton, M., Subramaniam, R., Elmore, J., Felsensteiner, C., Coaker, G., and Desveaux, D. (2010). The type III effector HopF2Pto targets *Arabidopsis* RIN4 protein to promote Pseudomonas syringae virulence. *Proc Natl Acad Sci U S A* 107, 2349–2354. doi:10.1073/pnas.0904739107.

Win, J., Chaparro-Garcia, A., Belhaj, K., Saunders, D. G. O., Yoshida, K., Dong, S., Schornack, S., Zipfel, C., Robatzek, S., Hogenhout, S. A., et al. (2012). Effector biology of plant-associated organisms: concepts and perspectives. *Cold Spring Harb Symp Quant Biol* 77, 235–247. doi:10.1101/sqb.2012.77.015933.

Witek, K., Jupe, F., Witek, A. I., Baker, D., Clark, M. D., and Jones, J. D. G. (2016). Accelerated cloning of a potato late blight-resistance gene using RenSeq and SMRT sequencing. *Nat Biotechnol* 34, 656–660. doi:10.1038/nbt.3540.

Wu, A.-J., Andriotis, V. M. E., Durrant, M. C., and Rathjen, J. P. (2004). A patch of surface-exposed residues mediates negative regulation of immune signaling by tomato Pto kinase. *Plant Cell* 16, 2809–2821. doi:10.1105/tpc.104.024141.

Wu, C.-H., Krasileva, K. V., Banfield, M. J., Terauchi, R., and Kamoun, S. (2015). The “sensor domains” of plant NLR proteins: more than decoys? *Front Plant Sci* 6, 134. doi:10.3389/fpls.2015.00134.

Wulff, B. B., Thomas, C. M., Smoker, M., Grant, M., and Jones, J. D. (2001). Domain swapping and gene shuffling identify sequences required for induction of an Avr-dependent hypersensitive response by the tomato Cf-4 and Cf-9 proteins. *Plant Cell* 13, 255–272.

Xing, W., Zou, Y., Liu, Q., Liu, J., Luo, X., Huang, Q., Chen, S., Zhu, L., Bi, R., Hao, Q., et al. (2007). The structural basis for activation of plant immunity by bacterial effector protein AvrPto. *Nature* 449, 243–247. doi:10.1038/nature06109.

Yue, J.-X., Meyers, B. C., Chen, J.-Q., Tian, D., and Yang, S. (2012). Tracing the origin and evolutionary history of plant nucleotide-binding site-leucine-rich repeat (NBS-LRR) genes. *New Phytol* 193, 1049–1063. doi:10.1111/j.1469-8137.2011.04006.x.

Zhang, J., Li, W., Xiang, T., Liu, Z., Laluk, K., Ding, X., Zou, Y., Gao, M., Zhang, X., Chen, S., et al. (2010). Receptor-like cytoplasmic kinases integrate signaling from multiple plant immune receptors and are targeted by a Pseudomonas syringae effector. *Cell Host Microbe* 7, 290–301. doi:10.1016/j.chom.2010.03.007.

Zhang, J., Shao, F., Li, Y., Cui, H., Chen, L., Li, H., Zou, Y., Long, C., Lan, L., Chai, J., et al. (2007). A Pseudomonas syringae effector inactivates MAPKs to suppress PAMP-induced immunity in plants. *Cell Host Microbe* 1, 175–185. doi:10.1016/j.chom.2007.03.006.

Zhang, L., Fetch, T., Nirmala, J., Schmierer, D., Brueggeman, R., Steffenson, B., and Kleinhofs, A. (2006). Rpr1, a gene required for Rpg1-dependent resistance to stem rust in barley. *Theor Appl Genet* 113, 847–855. doi:10.1007/s00122-006-0342-y.

Zohary, D., Hopf, M., and Weiss, E. (2012). *Domestication of Plants in the Old World: The origin and spread of domesticated plants in Southwest Asia, Europe, and the Mediterranean Basin*. Oxford University Press on Demand.

CHAPTER 2. RPG5-MEDIATED STEM RUST RESISTANCE IN BARLEY: STOMATAL MANIPULATION LEADS TO COUNTER EVOLUTION OF AN INTEGRATED DECOY JANUS IMMUNE RECEPTOR

2.1. Abstract

The barley *rpg4/Rpg5*-Mediated Resistance Locus (*RMRL*) is effective against broad *P. graminis* f. sp. *tritici* (*Pgt*) races including TTKSK (Ug99), with resistance also extending across forma specialis including *P. graminis* f. sp. *secalis* (rye stem rust) and *avenae* (oat stem rust). The *RMRL* contains two Nucleotide binding Leucine rich Repeat (NLR) immunity receptor genes required for resistance, *Rpg5* and *HvRga1*, with typical head-to-head genome architecture characteristic of "integrated decoy" resistance loci. The recessive *rpg4*-mediated resistance is conferred by the dominant *Rpg5* gene yet distinct allelic C-terminal integrated domains (IDs), a predicted functional protein kinase (PK) in resistant lines or protein phosphatase 2C (PP2C) in susceptible lines, represent unprecedented allelic diversity of a single NLR-ID resistance gene. Exploring the new "integrated decoy" hypothesis of plant innate immunity using the *rpg4/Rpg5*-mediated stem rust resistance model in barley uncovered this mechanism representing the first NLR with two independent, functionally antagonistic integrated domains in one species. The presented researchwork shows that when the dominant rye stem rust *R*-gene, *Rpg5-PK* is present with *rpg5-PP2C* alleles in a heterozygous state *RMRL* behaves as a recessive gene, thus, the *rpg5-PP2C* allele has dominant suppressive action. The progenitor of the *Rpg5-PK* ID, *Gak1*, is the *Arabidopsis AtAPK1b* orthologue, that is localized to and involved in stomata opening. The *Gak1* is also highly expressed in barley stomata, thus, we hypothesize that *P. graminis* contains virulence effector/s that manipulate *Gak1,* to facilitate stomata opening for pathogen entry. Genome analysis data suggests that *Brachypodium* and barley, counter evolved distinct *Gak1*

Rpg5 orthologous NLR-ID fusions independently that could serve as a pathogen "baits", conferring resistance against *P. graminis* before the divergence of wheat, rye, and oat *forma specialis*.

2.2. Introduction

As in mammals, detection of invading pathogens by the immune system is essential in plants to ensure survival in hostile environment, rich with opportunistic microbial pathogens. But due to the lack of a circulatory immune system plant defenses rely on innate immunity conferred by diverse receptors expressed in each individual cell. Thus, every cell has the ability to induce defense responses to protect the rest of the plant. These receptors are present in complexes held in an inactive state, analogous to "molecular switches", waiting to be activated by the recognition of pathogen elicitors (Takken et al., 2006; Zhang and Zhou, 2010).

Early host-parasite interactions resulting in the plant's perception of a potential invader occurs through detection of Microbe Associated Molecular Patterns (MAMPs) which are motifs present on or released from the microbe that are highly conserved within the class of microbes (Zipfel, 2008). The MAMP elicitors are detected via plant cell surface receptors, known as Pattern-Recognition Receptors (PRR's) and upon recognition, a rapid low magnitude defense response is elicited to stop or impede the initial colonization processes. In diverse pathosystems including bacterial and fungal pathogens, these responses involve stomata closure and lock-shut (Mur et al., 2013), such responses amongst several others is collectively referred to as Pattern-Triggered Immunity (PTI), which has been reviewed by others in depth (Ausubel, 2005; Boller and Felix, 2009; Monaghan and Zipfel, 2012; Macho and Zipfel, 2014). This first layer of defense, considered a form of non-host resistance effectively suppresses colonization until a pathogen evolves effectors to evade PTI, either through suppression of immunity signaling,

including stomata closure, or disguising its MAMPs. This evolutionary step allows the microbe to become a specialized pathogen on the host.

To combat adapted pathogens plants evolved a second layer of predominantly cytoplasmic localized resistance proteins, typically containing the Nucleotide Binding-Leucine Rich Repeat (NLR) domains that recognize the pathogen virulence effectors. The perception of these virulence effectors initiates the second layer of defense responses known as Effector Triggered Immunity (ETI), which is characterized by the programmed cell death response known as the Hypersensitive Response (HR). The HR evolved to stop the colonization of biotrophic pathogens that require living cells to feed, by sequestering them in the HR lesions. Thus, through the evolution of host resistance genes (*R*-genes) the pathogen virulence effectors effectively become biotrophic avirulence genes in the presence of the cognate host NLR immunity receptors, following H.H. Flor's gene-for-gene model (Flor, 1971). Identification of pathogen avirulence effectors through NLR's can be direct (Dodds and Rathjen, 2010) as in the case of the Flax L6 NLR and flax rust AvrL567 (Dodds et al., 2006). However, NLR's commonly act as "the guards" perceiving pathogen effectors indirectly through their manipulation of intermediate virulence target proteins, "the guardees"(Dangl and Jones, 2001). The indirect interactions have been described by the "guard model"(Van der Biezen and Jones, 1998; Dangl and Jones, 2001), which was proposed based on the data showing that NLRs surveil the host virulence targets and upon detection of effector manipulation trigger defense responses (Mackey et al., 2002; Kim et al., 2005; Ntoukakis et al., 2014; Khan et al., 2016). More recently "the decoy model" (van der Hoorn and Kamoun, 2008) was proposed, which is similar to the guard model except that the guardee is a duplicated version of the actual virulence target, thus, the redundancy provides plasticity to lose its original biological activity. This may also provide the decoy with greater

flexibility to evolve stronger binding affinity between the avirulence proteins than the original virulence target (van der Hoorn and Kamoun, 2008; Ortiz et al., 2017). A recent fundamental paradigm shift in the mechanisms of plant innate immunity and a twist on the gene-for-gene model, is the hypothesis that plants evolve to integrate pathogen virulence effector targets with NLR resistance proteins, known as "integrated decoys"(Cesari et al., 2014; Kroj et al., 2016; Wu et al., 2015).

Pathogens evolve to subvert host physiology to suppress basal defense mechanisms, acquire nutrients, and complete their lifecycle in a tailored host environment, which is essential for their success. The specialized pathogens accomplished this through the evolution of virulence effectors that target weak links in the host's defense, cell cycle, and nutrient transport signaling mechanisms (Abramovitch and Martin, 2004; Spanò et al., 2016; Ford et al., 2016; Ye and Ma, 2016; Streubel et al., 2013). Plants counter evolved different means to detect this manipulation, explained by the "guard", "decoy", and "integrated decoy" models (Wu et al., 2015; van der Hoorn and Kamoun, 2008; Cesari et al., 2014), which includes direct and indirect perception of effectors as discussed earlier (Ellis, 2016; Khan et al., 2016; Moffett, 2016). Interestingly, the most recent paradigm shift arose from the knowledge that gene translocation events attach a copy of key susceptibility targets, "susceptibility hubs", to NLR immunity receptors, now referred to as integrated domains (IDs), that serve as effective pathogen receptors or "baits"(Sarris et al., 2016; Kroj et al., 2016). As the pathogen hijacks the susceptibility hub to tailor its environment it consequently triggers the plants defense responses as the virulence function betrays the pathogen by alerting the plant to its presence. The genome reorganization leading to the NLR-IDs may occur via random intrachromosomal or interchromosomal translocation events, but the relocalization of these susceptibility hubs to the NLR immunity proteins may also be directed by

a currently unknown mechanism, but till now this is speculation. However, recent genome wide analysis and phylogenetic analysis of NLR proteins show that certain clades of NLRs represent recombination/translocation hotspots that preferentially give rise to NLR-IDs (Bailey et al., 2017) further supporting the hypothesis that the fusion of NLRs and virulence hub proteins could be directed by specific genome architecture.

The NLR-ID immunity mechanisms typically require unrelated dual NLR genes, one having the typical NLR gene architecture and the second containing the variable ID. These variable IDs are diverse but predominantly include protein kinases, WRKY transcription factors, and heavy metal binding domains (Sarris et al., 2016; Kroj et al., 2016; Sarris et al., 2015). There is also evidence of significant overlaps between the ID proteins and known effector targets in *Arabidopsis* (Sarris et al., 2016). Thus, NLR IDs may represent effective "baits" that lure diverse pathogens into their NLR-ID traps. These non-canonical IDs fused to NLRs enable rapid pathogen sensing and evolutionary benefits to the host during the co-evolutionary arms race. Thus, in short, the IDs represent integrated functional mimic of actual pathogen targets, "integrated decoys", that serve as pathogen sensors or functionally as receptor domains that provide direct interaction between the NLR immunity receptor and the pathogen avirulence protein.

For the integrated decoy model it has been determined that one of the NLRs acts as a pathogen signal sensor, the switch in the resistance complex, and the other NLR acts as the plant defense signal transducer (Le Roux et al., 2015; Cesari et al., 2014; Duxbury et al., 2016). A limited number of examples have been functionally characterized providing support to this model, yet have been elucidated in two diverse pathosystems. Supporting models include the rice NLR pair RGA4/RGA5 (Cesari et al., 2013; Hutin et al., 2016; Ortiz et al., 2017) and Pikp-

1/Pikp-2 (Okuyama et al., 2011) that confer resistance against *Magnaporthae oryzae* carrying the AvCO-39/Avr-pia and AVR-PikD, respectively. Another *Arabidopsis* NLR pair RRS1/RPS4 (Saucet et al., 2015) confer resistance to the bacterial and fungal pathogens *Pseudomonas syringae* and *Ralstonia solenacearum* (Narusaka et al., 2014; Le Roux et al., 2015). Although in the RRS1/RPS4 NLR pair, it was shown that the RRS1 NLR integrated WRKY transcription factor domain actively takes part in defense response generation upon binding with PopP2, a YopJ family acetyltransferase effector (Le Roux et al., 2015; Sarris et al., 2015). PopP2 acetylates and reduces the DNA binding activity of the integrated WRKY domain to activate defense responses (Sarris et al., 2015). Thus, NLR non-canonical domains can be "decoys" or "active domains", and it has been suggested that the variable domains should be referred to as "integrated sensory domains" instead of integrated decoys (Wu et al., 2015).

The *rpg4/Rpg5* locus in barley (*Hordeum vulgare*) provides recessive and temperature sensitive resistance against several wheat stem rust races (*Puccinia graminis* f. sp. *tritici*) including the highly virulent race TTKSK (Ug99) and its lineage (Jin, 1994). This broad resistance also extends across several *Puccinia graminis forma specialis* including *P. graminis* f. sp. *tritici, secalis* (Brueggeman et al., 2008; Arora et al., 2013; Solanki et al., 2016; Steffenson et al., 2016) and *avenae* (Dracatos et al., 2015). High-resolution mapping and post transcriptional gene silencing previously identified three genes required for wheat stem rust resistance, *Rpg5*, *Hv*Rga1, and *Hv*Adf3, at the ~ 70 kbp *RMRL* (Brueggeman et al., 2008; Wang et al., 2013). The dominant rye stem rust resistance gene *Rpg5* is predicted to have the typical NLR R-protein domains including the NBS and LRR, yet, encodes a C-terminal serine/threonine protein kinase (STPK) domain (Brueggeman et al., 2008). *Rpg5* is the gene conditioning compatible or incompatible interactions with the wheat stem rust races because it is the only polymorphic gene

correlating with resistance and susceptibility in the delimited *RMRL* but requires its NLR partner *HvRga1* for resistance (Wang et al., 2013; Arora et al., 2013).

Sequencing *rpg5* susceptible alleles showed that they fall into four subgroups yet the major difference between resistant and susceptible alleles is the integration of two different variable IDs. The susceptible alleles fall into two major groups with the group 1 susceptible lines containing an insertion/deletion with a predicted C-terminal functional protein phosphatase 2C ID (*Hv*PP2C) in place of the *Rpg5* STPK domain. The group 2 susceptible lines have the STPK ID but have a single cytosine insertion causing a frame shift mutation resulting in a premature stop codon at amino acid (aa) position 219 (Arora et al., 2013). These two classes of IDs present on the same NLR indicate that an important mechanism of signal transduction activation and deactivation may be hijacked by the pathogen in the barley-*Puccinia graminis* pathosystem. Genome sequence information has determined that PP2Cs are a major class of serine/threonine phosphatases in plants and the recurrent theme is that this superfamily of plant PP2Cs negatively-regulate protein kinase phosphorylation signaling pathways by their dephosphorylation function. Although there is little information on their specific substrates the large number of PP2Cs in plant genomes suggest that individual PP2Cs may have tight specificity in substrate binding.

We have studied the *RMRL* Ug99 resistance locus in barley with the aim of testing the hypothesis that *Rpg5* alleles conferring resistance or susceptibility contain two integrated sensory domains (ISDs) with antagonistic function, a protein kinase domain or a protein phosphatase domain, that result in the recessive nature of *RMRL*–mediated wheat stem rust resistance in barley. We also determine that the Rpg5 STPK ISD ancestral protein is encoded by the guard cell associated kinase 1 (*Gak1*) gene, which we hypothesize to have undergone duplication and

translocation to the dual kinase *RMRL* Rpg5 NLR receptor, following the "integrated decoy" or "integrated sensory domain" hypothesis model. The Rpg5-STPK domain and Gak1 share 85.5 % aa identity and 88.2 % aa similarity (EMBOSS Water). Under this model we posit that the HvGAK1 protein is the target of a *Pgt* virulence effector that evolved to open stomates early in the infection process. Two independent full-scale Y2H infection libraries constructed utilizing different resistant and susceptible barley genotypes identified the barley ortholog of the *Arabidopsis* VOZ1 protein, designated HvVoz1 as an Rpg5-STPK protein kinase domain interactor. The *Arabidopsis* VOZ1 interacts with PhyB and is involved in stomate opening in response to far red light. Our experiments show that contrary to previous reports *Pgt* is able to penetrate through the stomates during the dark cycle (dissertation chapter 4) and thus may produce an early effector that targets Gak1 to hijack the far-red light stomatal opening response to open the stomates during the night, the period in which *Puccinia graminis* evolved to germinate. Thus, this effector possibly evolved for the effective *incognito* entry into the host. However, following the integrated sensory domain model of host-parasite evolution barley counter evolved to utilize this interaction to bait the pathogen into an NLR integrated sensory domain trap that suppresses and sequesters the pathogen's growth providing effective immunity.

2.3. Material and methods

2.3.1. Rust genotype and plant material

The highly resistant barley line Q21861, the original line from which the rye stem rust resistance gene *Rpg5* was cloned (Brueggeman et al., 2008), carries the functional *Rpg5* allele providing resistant to a wide spectra of *Pgt* races (Steffenson et al., 2016) including *Pgt* race TTKSK. The line Q21861 was used as the resistant parent in the crosses developed for genetic analyses of the dominant or recessive nature of resistance inheritance. The barley lines

Harrington, Steptoe, and Sm89010 containing non-functional *rpg5* alleles (Brueggeman et al., 2008) previously classified as the group 2 and group 3 susceptible alleles (Arora et al., 2013) have the PP2C domain in place of the *Rpg5* kinase domain. The susceptible barley lines Golden Promise and MD2 as well as the wild barley (*Hordeum sponteneum*) accession OSU6 harbor nonfunctional *rpg5* alleles (Brueggeman et al., 2008) yet were previously classified as containing the group 1 susceptible alleles (Arora et al., 2013) that still have the Q21861-like protein kinase domain intact yet a single nucleotide insertion in exon 1 results in a predicted 217 aa truncated nonfunctional protein. Utilizing the Q21861 x Harrington cross, and a recurrent backcrossing scheme and marker assisted selection for the Q21861 *RMRL*, two independent *RMRL* near isogenic lines (NILs) in the cv. Harrington background designated HQ1 and HQ18 were developed. Approximately 15 $BC_{1\text{-}3}F_2$ individuals at each generation were genotyped to identify homozygous Q21861 *Rpg5-STPK* individuals via PCR, utilizing the dominant STS markers *Rpg5-STPK* allele specific Rpg5-LRK-F1/R1 primer pair and the *rpg5-PP2C* allele specific Rpg5-LRK-F1 and PP2C-R1 primer pair (Appendix table A1). The HQ1 and HQ18 NILs were also phenotyped and shown to have *Pgt* race QCCJ resistance in growth chamber seedling resistance assays performed as previously described in Mirlohi et al. (Mirlohi et al., 2008) as well as were assayed in Njoro Kenya, at the adult plant stage as previously described by Zurn et al. (Zurn et al., 2014). Thus, the HQ1 and HQ18 NILs represent Harrington genotype with the Q21861 *RMRL* integration carrying *Rpg5-PK* and the other two genes, *HvRga1* and *HvAdf3*, at the locus required for resistance and were utilized in the genetic analysis.

2.3.2. Plant maintenance and stem rust inoculation

The barley genetic stocks, germplasm and recombinant populations were tested with *P. graminis* f. sp. *tritici* races "QCCJ" and "HKHJ" (wheat stem rust races) in controlled

environment growth chambers. One seed of each genotype was planted in cones filled with Metromix, and fertilized with Osmocote Pro (17-N+11-P+10-K+2MgO+trace elements). Plants were grown in growth chamber set at 20/21°C day/night temperature with a 16/8-hour day/night cycle with 60 W fluorescent tubes (Steffenson et al., 2009). Seven to ten-day old seedlings were used for rust urediniospore inoculation when the majority of plants had fully expanded primary leaves as described in Steffenson et al. (2009) with a slight modification in spore concentration (10mg/ml in 700 µl soltrol oil per rack containing 96 cones). Infection types (ITs) were assayed 13 to 14 days after inoculation using a modified 0-to-4 scale as described by Stakeman et al. (Stakman et al., 1962) in order of their prevalence on leaf. Two or more ITs were frequently observed on each phenotyped leaf giving a mesothetic disease reaction. The mesothetic categorical disease IT scores were converted to numerical values for the BSMV-VIGS experiments by as described in Zhou et al. (Zhou et al., 2014) (Appendix Table A2).

2.3.3. RNA isolation and qRT PCR

Primary seedling leaf tissues (~30 mg) were collected from the barley lines Q21861 (*rpg4/Rpg5* +) and Steptoe (*Rpg4/rpg5*-) from soltrol rust non-inoculated (control), and *Pgt* race QCCJ inoculated (treatment) 10-day old seedlings at 6, 12, 24, 48, and 72-hour post inoculation (HPI). Three biological replicates were collected at each time point and total RNA was isolated from each sample using the Qiagen RNeasy Mini Kit (QIAGEN) following the manufacturer's standard protocol. RNA samples were visualized on 0.8% agarose gels stained with gel red (Biotium) to confirm the integrity of samples. RNA samples containing four sharp ribosomal RNA (rRNA) bands at the molecular weights of ~ 3.4, 1.8, 1.5, and 1.1 kb that correspond to the nuclear 28S and 18S rRNA and the 23S and 16S plastid rRNA, respectively, without high molecular weight gDNA contamination were considered as quality RNA. The samples were

quantified using the RNA broad range fluorescence based detection Qubit RNA broad range kit (ThermoFisher Scientific) on a Qubit 2.0 instrument (ThermoFisher Scientific). Total RNA (~250 ng) was used to synthesize cDNA in 20 µl reactions using oligo-dT primers provided in the GoScript Reverse transcription system (Promega) according to the manufacturers protocol followed by a 1:5 dilution with ultrapure water (Ambion). The diluted cDNA was tested for GAPDH amplification via RT-PCR to validate the integrity and uniformity of cDNA synthesis. 20 µl qPCR reactions containing 500 nM of each forward and reverse primers designed to specifically amplify the *Rpg5-STPK allele, rpg5-PP2C* allele*, HvRga1,* and *GAPDH* (Appendix Table A1) were performed using the BIO-RAD SsoFast Evagreen supermix following the manufacturer's standard protocol on a CFX-96 Real Time PCR detection system (BIO-RAD) using signal acquisition parameters described in Appendix Table A1. Three technical replicates were performed for each of the three biological replicates. The barley *GAPDH* gene was used as a reference gene to normalize expression levels across samples. Non-inoculated time point 0-HPI samples were used as controls for relative expression analysis. Soltrol oil inoculated samples were used as controls at each time point to identify any differential gene expression occurring in response to the inoculation procedure and to determine expression variation. To determine PCR efficiencies standard curves were generated for each target gene using 500 ng initial template across eight 10-fold dilutions. Three technical replicates from each of three biological replicates per treatment were analyzed using the BIORAD CFX Manager software using the delta delta CT (Livak and Schmittgen, 2001; Schmittgen and Livak, 2008) method. Differential regulation was determined using t-test statistics at $P<0.05$ using SEM (Standard Error of Mean) ±1.

2.3.4. Functional characterization of *rpg5-PP2C* using BSMV-VIGS post transcriptional gene silencing

For functional characterization of the *rpg5-PP2C* allele we utilized barley stripe mosaic virus-virus induced gene silencing (BSMV-VIGS) to post transcriptionally silence the *rpg5-PP2C* allele in F_2 individuals generated from a Q21861 x Steptoe cross. The homozygous or heterozygous state of the *Rpg5-STPK* and *rpg5-PP2C* alleles, which have a single gene segregation ratio of 1:2:1, was checked by PCR utilizing Rpg5-LRK-F1/R1 primer and Rpg5-LRK-F1 and PP2C-R1 primers (Appendix Table A1). The *Rpg5-STPK* and *rpg5-PP2C* heterozygous plants were used for the BSMV-VIGS silencing experiments. To silence the *rpg5-PP2C* allele in the heterozygous F_2 seedlings a specific 150 base pair (bp) region of the mRNA encoding the *PP2C* domain was identified using the IPK-BLASTn barley database (http://webblast.ipk-gatersleben.de/barley_ibsc/). This unique sequence was utilized to design forward and reverse primers with 5'-*Not*I/3'-*Pac*I and 3'-*Not*I/5'-*Pac*I restriction site adapters and the two sets of primers were utilized in separate reactions to amplify the *rpg5-PP2C* fragment from Steptoe cDNA, which contains the group 2 *rpg5* susceptible allele. The *rpg5-PP2C* knock down amplicons (1 µg each) were double digested overnight at 37℃ in 30 µl reactions using 1 unit of *Not*I and *Pac*I (NEB) enzyme to create 5' and 3' compatible cohesive ends along with the infectious ϒ strand clone pSL38.1-MCS. To generate directional clones with both sense and antisense oriented *rpg5-PP2C* fragments ligation reactions were performed with 2 units of ligase (Promega) using a vector to insert molar end ratio of 1:3 in a standard 10 µl ligation reaction following the manufacturers standard procedure with ~ 100 ng of total amount of DNA. The ligation reactions were incubated for 24 hours at 4 °C. Upon completion of ligation incubation period transformations were carried out with chemically competent Top10 *E. coli*

cells (Thermo Fisher Scientific) using 10 µl of the ligation reaction and 50 µl of competent cells following the manufacturer's standard protocol. 50 µl Transformation mixture was plated on LB agar plates amended with selection antibiotic ampicillin (100 µg/ml) and incubated overnight at 37 °C. Next day 5 colonies were picked and inoculated into 4 ml of LB liquid media with 100µg/ml of ampicillin and incubated at 37 °C for 16 hours in an orbital shaker incubator (VWR) set at 250 rpm. 3 ml *E. coli* cells were pelleted by centrifugation at 11000 rcf for 5 min and the plasmid DNA was isolated using the PureYield plasmid Miniprep kit (Promega). Plasmids were also extracted from infectious α and β strand clones required for full assembly of BSMV virus. Confirmations of positive clones containing the *rpg5-PP2C* amplicons was accomplished by digesting ~20 µg of each plasmids using SpeI (β) and MluI (α, β, ϒ-MCS control, ϒ-pSL38.1-PP2C) restriction enzymes (NEB) at recommended temperatures for 4 hours and the enzymes were heat inactivated by incubation at 70 ℃ for 20 minutes. Detection of the expected insert sizes was confirmed by running the 1 µg restriction digestion products on a 1% agarose gel supplemented with GelRed DNA staining dye (Biotium). The constructs containing the expected insert sizes were further validated by DNA sequencing. ϒ BSMV-PP2C sense and PP2C antisense infectious clone constructs were utilized for in vitro transcription. *In vitro* transcription was carried out for RNA synthesis for the α, β and ϒ BSMV sub genomic RNAs to produce the full complement of the BSMV tripartite genome from linearized and purified infectious clone plasmid DNA using the m-MESSAGE mMACHINE T7 Transcription kit (Ambion) using manufacturer's standard protocol. FES buffer was made to inoculate infectious RNA mixture of RNA on plants. To make 500 ml of FES, we mixed 100 ml of GP buffer (1.9 g glycine, 2.6 g K_2HPO_4 dibasic dissolved in ddH_2O to make 100 ml volume) with 5.0 g of tetrasodium pyrophosphate, 5.0 g bentonite, 5.0 g celite in a volume of 500 ml with ddH_2O. 2.5

µl of in vitro transcribed sub genomic RNA from either ϒ insert plasmids, pSL38.1 or MCS-insert, along with the α and β sub-genomic RNAs were mixed with 45 µl FES buffer, this mixture can be used to inoculate five plants using ten µl mix on each, thus this reaction was scaled up to adjust with number of plants to be inoculated. Using the target specific sense and antisense ϒ subgenomic RNAs allowed for the formation of double stranded RNA specific to the target gene during virus replication and more efficient formation of gene specific siRNAs which has been shown to provide higher efficiency of RNAi induced post transcriptional gene silencing. The amount of in-vitro transcribed BSMV-VIGS inoculum scaled according to the number of plants to be inoculated. Barley seedling secondary leaves were rub inoculated with 10 µl inoculum placed between the thumb and finger and leaf pulled with slight pressure until the entire leaf was rubbed twice. The rub inoculated leaf was misted, and plants were placed in a humidity chamber for 18 hours at 100% humidity. Visible virus symptoms, yellow streaking and mottling on the newly emerging tertiary leaves, begin to appear ~ 5-8 days post inoculation. At ~13 days post BSMV inoculation, *Pgt* race QCCJ inoculations were carried out on the 4th leaf. At 14-16 days post *Pgt* inoculation *the BSMV-PP2C, BSMV-MCS* controls and non-virus infected seedlings were phenotyped using the 0-4 stem rust seedling rating scale.

2.3.5. Stomatal microdissection and low sample RNA isolation

We developed a rapid LASER Capture Microdissection (LCM) based stomatal tissue isolation method for barley (Solanki et al, Unpublished). In brief, 1cm^2 primary leaf samples were collected and transferred into 40 ml of ice cold 100% acetone in a 50-ml falcon tube. Vacuum was applied using syringe for one minute, 3 times, and then samples were gently swirled on a rotator at 20 rpm/4°C for 1 hour. The samples were then transferred into 40 ml of fresh 100% acetone and vacuum was applied twice for 30 seconds and again rotated for 3-4

hours and stored in -20°C until stomata collection within 5-8 days of sample preparation. Prior to stomata collection samples were washed briefly in 10 ml PBS (Phosphate Buffer Saline) prepared in RNase free water. The leaf samples were oriented abaxial side up on PEN membrane glass slides (Zeiss) and a mist of Zeiss RNA stabilizer was sprayed over the leaf samples. 35 stomata were dissected and collected in 500 µl adhesive cap tubes (Zeiss), using 40 Mw LASER strength with aperture size 1 and speed of 5 ms on a Zeiss 700 microscope. RNA was extracted from the stomata capture cells using the Arcturus pico pure kit (ThermoFisher Scientific) following the manufacturers standard procedure. RNA quantity and quality were estimated using a pico RNA chip on the Agilent bioanalyzer (Agilent). The GoScript™ Reverse Transcription kit (Promega) was used to synthesize cDNA with oligo-dT primers and 4 µl of RNA, following the manufacturer's standard protocol. A 20 µl qPCR reaction consisting of 5x SsoAdvance Universal SYBR Green Supermix (BioRad) and 500 nM of each SS_GAK1_qF1 and SS_GAK1_qR1 primers (Appendix Table A1) and 5 µl cDNA was analyzed with the BioRad CFX-96 system. The efficiency of amplification and data analyses were carried out as described in the qPCR method for the *Rpg5-STPK allele, rpg5-PP2C* allele*, HvRga1,* and *GAPDH* genes.

2.3.6. DAB and WGA-Alexa Fluor-488 staining for microscopic observation

Two primary leaf samples from *Pgt* race QCCJ inoculated barley lines Q21861 and Steptoe, ~3 cm in length, were collected at 0, 12, 24, 30, 36, 48 and 72 HPI and immediately transferred to 10 ml of freshly prepared 1mg/ml DAB (Sigma Aldrich) solution (pH 3.6) in 15 ml conical tubes. Plastic mesh was inserted in the top of the tubes to ensure the proper submersion of leaf the leaf samples in the DAB solution. Samples were DAB stained for 6 hours on an orbital shaker (VWR) set for 120 rpm at room temperature. The DAB solution was poured off and samples were washed twice with anhydrous Farmer's fixative (3-ethanol:1- glacial acetic

acid) then transferred to 50 ml tubes and cleared and fixed simultaneously in 30 ml of Farmers fixative (FF) for 12 hours. The FF was changed after the 12 hours and samples were cleared for an additional 3 hours. Cleared samples were stored in fresh 45 ml FF solution in the same 50 ml tube in the dark until processed for microscopy. To visualize the germination and growth of stem rust spores and their association with DAB staining we stained DAB processed samples with WGA conjugate-Alexa Fluor 488 according to Solanki et al. (dissertation chapter 3). Slides were mounted and visualized on an epifluorescent Zeiss Axio Imager M2 microscope (Zeiss) at 200x total magnification to visualize individual spores. The 10x magnification objective lens was used for leaf surface scanning to identify and count the total number of germinated spores, appressoria formed and DAB stained regions.

2.3.7. Cloning of candidate genes and their modular domains for Forward Yeast two hybrid assay and Y2H cDNA library screening

The full length and modular domains of *Rpg5, HvRga1, rpg5-PP2C* and *HvAdf3* were amplified via PCR for the development of Yeast two hybrid (Y2H) "bait" and "prey" constructs utilizing the primers and PCR parameters described in Appendix Table A1. Each PCR amplicon was initially visualized on agarose gels stained with Biotium GelRed Nucleic acid gel stain (Biotium). The amplicons of the expected size were sent for sequencing confirmation (Genscript, Piscataway, NJ). The confirmed gene specific PCR amplicons were cloned into the pENTR/D/TOPO vector (ThermoFisher Scientific) and subsequently transferred into gateway pDEST32-bait and pDEST22-prey vectors via LR transfer reactions as suggested in the manufacturers protocol (ThermoFisher Scientific). MaV203 competent yeast cells were made using the S.c. EasyComp Transformation Kit (ThermoFisher Scientific) and Forward Yeast 2 Hybrid (FY2H) interactions were performed by co-transformation with both the bait and prey

vectors together and subsequent selection according to Proquest Y2H kit protocol (ThermoFisher Scientific). To construct a full-scale yeast-two-hybrid prey library ~ 30 µg of total RNA was extracted from the barley line Q21861 primary seedling leaves harvested 48 HPI with *Pgt* race QCCJ. A nano-quantity library was created using the CloneMiner II cDNA library construction kit (ThermoFisher Scientific) according to manufacturer's instructions. Approximately 2.4×10^6 primary entry clones were obtained which were further transferred into gateway pDEST22 prey plasmid using a LR recombination reaction. Library scale chemically competent *Saccharomyces cerevisiae* MaV203 cells (ThermoFisher Scientific) were used to co-transform with bait plasmids and the prey library and plated on SC-Leu-Trp-His+30 mM 3AT auxotrophic selection plate following the ProQuest Y2H protocol (ThermoFisher Scientific). For the library screening the *Pgt* race QCCJ and TTKSK resistant line Q21861 *Rpg5* protein kinase domain (PK) and the full length *Rga1* NLR as well as the variety Steptoe r*pg5* protein phosphatase 2C domain cloned into the pDEST32 vector were used as baits. For selection, a 30mM 3AT concentration was determined to reduce false positives on histidine selection plates. Candidates colonies were picked and transferred to a master plate and tested with X Gal assay as described in manufacturer protocol. Later retransformation assay was performed to check specificity of interactions.

2.3.8. Bioinformatics via BLAST analysis

To identify orthologs and paralogs of the *Rpg5* C-terminal STPK and PP2C IDs nucleotide and protein BLAST searches were conducted using the IPK barley genome browser (webblast.ipk-gatersleben.de/barley/) and NCBI database (https://blast.ncbi.nlm.nih.gov/Blast.cgi), respectively. A minimum of 70 % sequence coverage with 80% identity was used as a cutoff for sequence similarity determination. EggNOG-mapper

(Huerta-Cepas et al., 2017) was also used parallelly to find the homologs in a genome wide search using HMM model.

2.4. Results

2.4.1. Genetic analysis of *Rpg5* alleles with variable IDs

The F_1 and F_2 progeny from five crosses between the resistant parent Q21861 and six susceptible *H. vulgare* cultivars (cvs) Harrington, Steptoe, and Sm89010 containing two different stem rust susceptible *rpg5-PP2C* alleles as well as cv Golden Promise and the *H. sponteneum* line OSU6 containing nonfunctional *rpg5-STPK* alleles were phenotyped. The F_1 and F_2 phenotyping was to test the hypothesis that the *RMRL* locus originating from the resistant line Q21861 (*rpg4*/*Rpg5*-mediated resistance locus) behaves differentially, showing a dominant resistance or recessive resistance nature, in the heterozygous state with the susceptible *rpg5-STPK* and *rpg5-PP2C* alleles, respectively. The heterozygous F_1 progeny from all three crosses containing a copy of the Q21861 group 1 resistance (G1R) *Rpg5-STPK* allele and a copy of the group 2 susceptible (G2S) or group 3 susceptible (G3S) (G2S = Steptoe and SM89010, and G3S = Harrington) *rpg5-PP2C* allele were inoculated with *Pgt* race QCCJ which served as a surrogate isolate for TTKSK as all the high resolution *RMRL* recombinants representing >5000 gametes from three different crosses behaved similarly to both *Pgt* race QCCJ and TTKSK (Brueggeman et al., 2008). Independent experiments resulted in 100% susceptible infection type (IT) scores similar to the susceptible parent of each cross for the Q21861 x Steptoe, SM89010 and Harrington crosses. The F_2 progeny from the crosses also segregated in a 1 resistant to 3 susceptible ratio showing that in the presence of these PP2C containing *rpg5-PP2C* alleles there is a recessive resistance segregation. Conversely, the F_1 progeny from the two crosses between the susceptible cultivar Golden Promise and the *Hordeum sponteneum* line OSU6, which

contained non-functional *rpg5-STPK* alleles, with an intact protein kinase domain similar to Q21861, yet nonfunctional due to a single nucleotide insertion which caused a frame shift mutation resulting in a predicted truncated protein resulted in resistant ITs similar to those of the resistant parent Q21861. The F_2 progeny from these crosses segregated in a 3 resistant to 1 susceptible ratio showing that in the presence of these STPK containing *rpg5-STPK* alleles there is a dominant resistance gene segregation (Fig. 2.1).

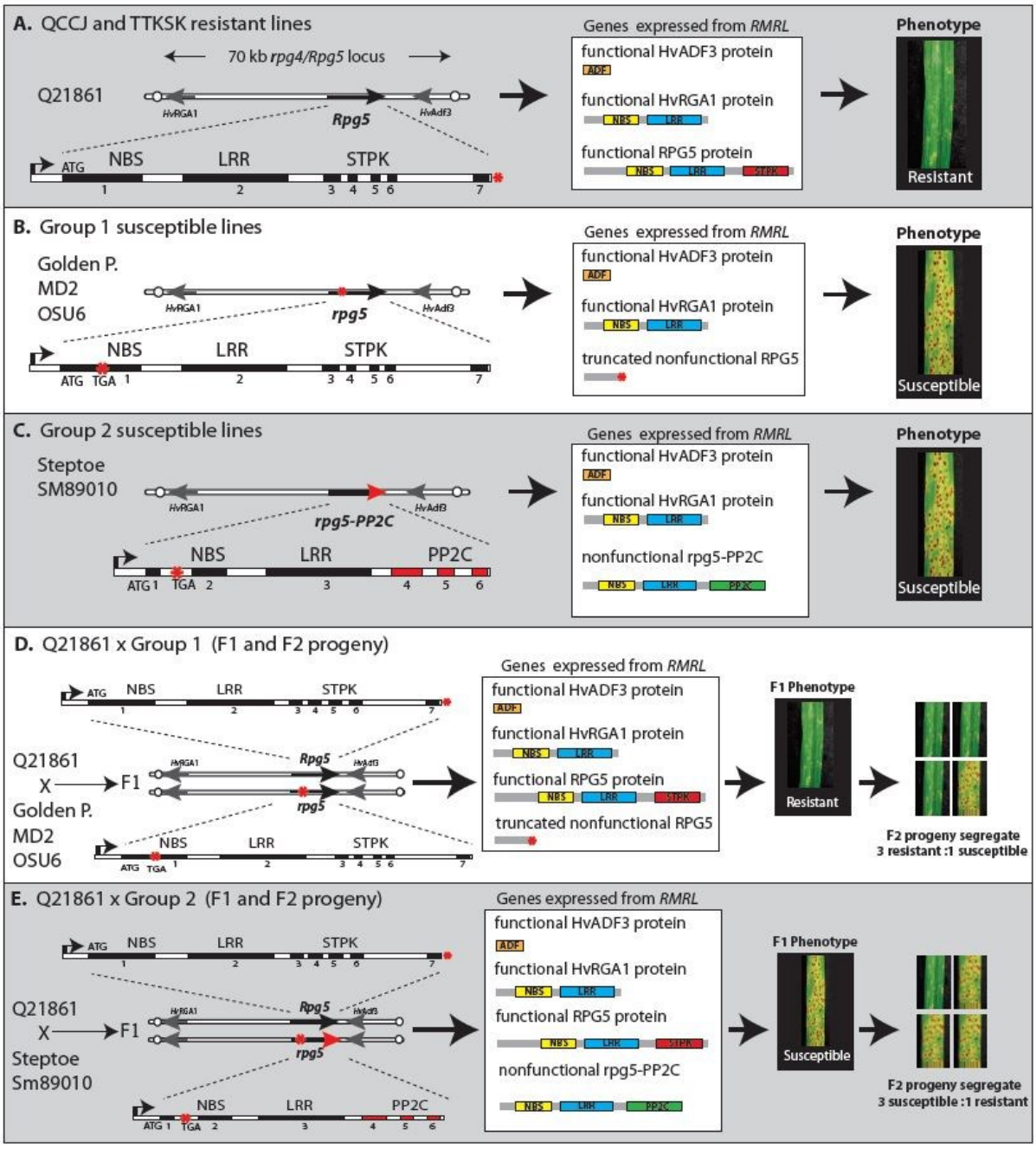

Fig. 2.1. The *rpg4/Rpg5*-mediated resistance locus (*RMRL*) haplotypes from resistant and susceptible barley lines with allele analysis, predicted proteins, and the F1 and F2 phenotypic segregation ratios on primary leaf of barley. HvRga1 and HvAdf3 protein sequences are similar in resistance and susceptible barley genotypes, however Rpg5 is polymorphic thus designated as R protein. Rpg5 encodes for a NBS LRR protein with diverse c-terminal domain. HvAdf3 encodes for an actin depolymerization factor whereas HvRga1 encode for a NLR protein. *Rpg5* and *Rga1* are head to head oriented NBS LRR genes. (2.1.A.) Stem rust QCCJ and TTKSK resistant barley line Q21861 with resistance allele of *Rpg5-STPK*. (2.1.B., 2.1.C.) Stem rust QCCJ and TTKSK susceptible barley lines with absence of resistance allele of *Rpg5*.

Group 1 susceptibles have a truncated *rpg5* allele whereas Group 2 barley lines have truncation in NBS region along with a PP2C domain insertion in C-terminal instead of a kinase domain, thus making a *rpg5-PP2C* susceptibility allele. (2.1.D., 2.1.E.) Genetic characterization of dominant nature of *rpg5-PP2C* and recessive nature of *Rpg5* mediated stem rust resistance. For stem rust phenotyping with race QCCJ, *Rpg5-STPK*/*rpg5*-truncated heterozygous F_1 plants are resistant and segregate in 3:1 ratio for resistance to susceptibility in F_2 generation whereas *Rpg5-STPK*/*rpg5-PP2C* heterozygous F_1 plants are susceptible and segregate in 3:1 ratio for susceptibility to resistance in F_2 generation.
Legends - NBS- Nucleotide Binding Site, LRR- Leucine Rich Repeats, STPK- Serine/Threonine Protein Kinase, PP2C – Protein Phosphatase 2C. For each panel (A-E) the white vertical bars represent the ~70kb RMRL genomic sequences delimited by the markers ARD5112 (left) and Rsnp.1 (right) shown as white circles (Wang et al., 2014). The black arrows present on the line represent the orientation and approximate size of the *HvRga1*, *Rpg5* and *rpg5* alleles, and *HvAdf3* genes present in barley line. The intron (white bars) and exon (black bars) structures for the *Rpg5*/*rpg5* alleles are shown above or below with promoter region shown as a black arrow, ATG as start codon, and stop codons as red asterisks.

2.4.2. Functional characterization of *rpg5-PP2C* using BSMV-VIGS

For the functional characterization of the *rpg5-PP2C* alleles BSMV-VIGS post transcriptional gene silencing was carried out on the F_2 individuals from a Q21861 x Steptoe cross. Heterozygous plants were identified and used for the BSMV-VIGS characterization as described in the material and methods. Non-virus inoculated controls Q21861 x Steptoe (G2S) F_2 seedlings were phenotyped after inoculation with *Pgt* race QCCJ showed that the homozygous individuals containing functional *Rpg5-STPK* resistant allele had disease rating scores ranging from 0.35-3.0 with a median of 1.42 and a mean of 1.57, whereas the F_2 individuals with homozygous susceptible *rpg5-PP2C* alleles had scores ranging from 3.37-4.12, with a median of 3.87 and a mean of 3.81. However, heterozygous F_2 individuals containing both *Rpg5-STPK* and *rpg5-PP2C* alleles showed disease rating scores ranging from 3.0-4.13 with a median of 3.5 and a mean of 3.56 (Fig. 2.2; Table 2.1). Thus, these data further support the hypothesis that the *rpg5-PP2C* allele may functions as a dominant susceptibility factor suppressing the *Rpg5-STPK* allele resulting in susceptible heterozygous F_2 individuals (Fig. 2.2.A). After BSMV-VIGS mediated silencing of the *rpg5-PP2C* allele in the heterozygous F_2 individuals the phenotyping

data showed disease rating scores ranging from 0.12-3.74 with a median of 1.42 and a mean of 1.38 (Fig. 2.2.B; Table 2.1). The BSMV-MCS control virus inoculated heterozygous F_2 individuals showed disease rating scores ranging from 0.75-3.88 with a median of 2.75 and a mean of 2.31 (Fig. 2.2.A; Table 2.1). Also, the homozygous *Rpg5*-STPK showed similar phenotypes for resistance or susceptibility, respectively, as the non BSMV-PP2C inoculated plants (Fig. 2.2.A) and were not different after BSMV knockdown (Fig. 2.2.B). Thus, the *rpg4*/*Rpg5*-mediated resistance resumes functionally validating our hypothesis based on genetic analyses that the *rpg5-PP2C* functions as a dominant susceptibility factor for wheat stem rust resistance.

Table 2.1. Mean, median, standard deviation (std dev) and standard error (std err) values for Q21861xSteptoe F_2 segregating population for *Rpg5* alleles inoculated with BSMV-QCCJ and QCCJ only treatments at third leaf stage.

Genotype (Treatment)	MEAN	MEDIAN	std dev	std err
Rpg5_STPK+/rpg5_PP2C- (KD-QCCJ)	1.15	1.20	0.78	0.25
Rpg5_STPK+/rpg5_PP2C+ (KD-QCCJ)	1.38	1.43	1.00	0.23
Rpg5_STPK-/rpg5_PP2C+ (KD-QCCJ)	2.64	3.13	1.53	0.44
Rpg5_STPK+/rpg5_PP2C+ (MCS-QCCJ)	2.31	2.75	1.52	0.51
Rpg5_STPK+/rpg5_PP2C- (MCS-QCCJ)	2.25	2.25	0.00	0.00
Rpg5_STPK+/rpg5_PP2C- (QCCJ)	1.57	1.43	0.85	0.30
Rpg5_STPK+/rpg5_PP2C+ (QCCJ)	3.56	3.50	0.33	0.11
Rpg5_STPK-/rpg5_PP2C+ (QCCJ)	3.81	3.88	0.22	0.08

BSMV treatment was given with rpg5-PP2C knock down (KD) and MCS control at secondary leaf stage. *Pgt* race QCCJ was inoculated at tertiary leaf stage in BSMV and non-BSMV seedlings. Eleven *Rpg5-STPK* homozygous, twelve *rpg5*-PP2C heterozygous and twenty heterozygous ((*Rpg5_STPK+/rpg5_PP2C+*) F_2 plants were used for BSMV *rpg5*-PP2C KD experiment. One *Rpg5*-STPK homozygous and nine heterozygous F_2s were used for BSMV-MCS control experiment. Eight *Rpg5*-STPK homozygous, eight *rpg5*-PP2C homozygous and ten heterozygous (*Rpg5_STPK+/rpg5_PP2C+*) F_2s barley plants were inoculated with QCCJ only for disease assessment on non-BSMV plants. Thus, fifty-five BSMV and twenty-six non BSMV treated Q21861xSteptoe F_2 segregating population was assessed for QCCJ disease phenotype.

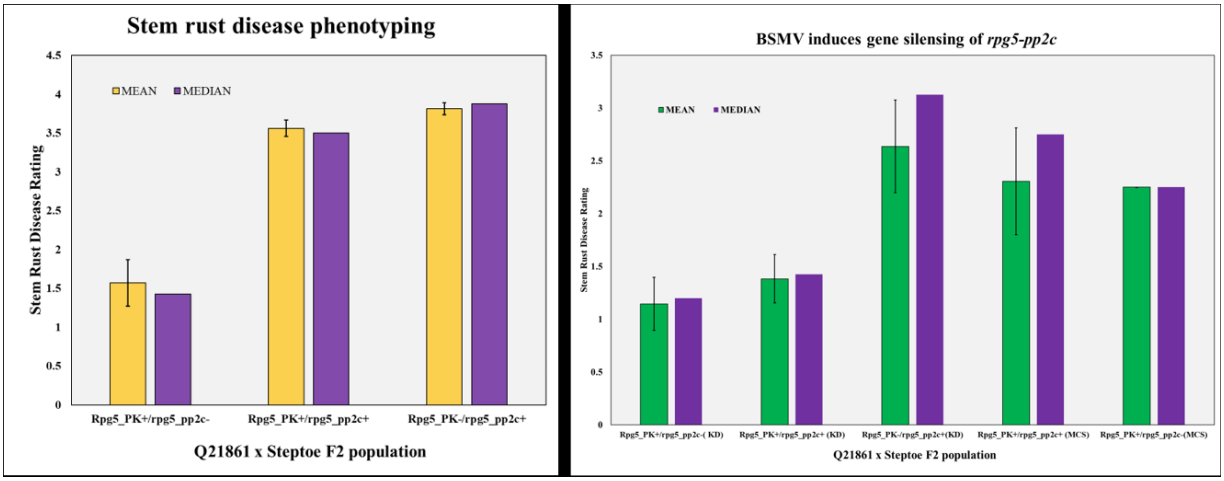

Fig. 2.A Fig. 2.B

Fig. 2.2. Utilization of BSMV-VIGS for the validation of the *rpg5-PP2C* allele as a dominant susceptibility factor. For the functional validation of *rpg5-PP2C* as a dominant susceptibility gene that suppressed Rpg5-*STPK*-mediated wheat stem rust resistance, F_2 population of Q21861 x Steptoe F_2 individuals were analyzed after BSMV-VIGS-mediated post transcriptional gene silencing of the *rpg5-PP2C* allele. Graphs show disease phenotyping data using a 0-4 infection type rating scale converted to numerical values (y-axis). The x-axis shows the genotype of the F_2 individuals as determined by genotyping with co-dominant STS markers that distinguished between the *Rpg5-STPK* functional allele and the *rpg5-PP2C* nonfunctional alleles. The average disease rating values were calculated with standard error of mean ±1. **(A)** Average disease rating scores on primary leaves of eight *Rpg5-STPK* homozygous, eight *rpg5-PP2C* homozygous and ten heterozygous barley plants inoculated with *Pgt* race QCCJ with error bars shown. **(B)** Disease ratings on tertiary leaves of Q21861 x Steptoe F_2 individuals after inoculation with BSMV *rpg5-PP2C* and the BSMV-MCS virus control.

2.4.3. Identification of integrated domain paralogs

To identify orthologs/paralogs and functional domains of the *Rpg5-STPK* and *rpg5-PP2C* alleles, nucleotide and protein BLAST searches were conducted using the IPK barley genome browser (http://webblast.ipk-gatersleben.de/barley/) and NCBI databases (https://blast.ncbi.nlm.nih.gov/Blast.cgi) using the full length $Rpg5_{1\text{-}4137}$ CDS sequence (EU883792.1) and the $Rpg5_{1\text{-}1378}$ protein sequence (ACG68417.1). BLAST searches of the IPK barley genome browser using the barley cv Q21861 Rpg5 aa sequence as the query identified a predicted gene, HORVU5Hr1G056920.1 at a chromosome 5H position of 446,194,774 – 446,200,757 bp with high homology, 89% nucleic acid identity with 85.5% amino acid identity

with the C-terminus of the Rpg5 protein which covers the STPK domain. This locus corresponds to the gene model MLOC_66562.1 (morex_contig_51755 CAJW010051755), located on chromosome 5HL at POPseq position 47.22 cM. Utilizing RT-PCR we amplified and sequenced the entire MLOC_66562.1 gene and determined that the gene annotation in the IPK database for the HORVU5Hr1G056920.1 CDS is incorrect, as determined by our cDNA amplification, and here we performed the analyses with the corrected exon and intron boundaries and functional CDS annotation. To our interest, the exon-intron boundaries for Rpg5-STPK amino acids 3172-4137 and HORVU5Hr1G056920.1 amino acids 1-1491were found to be perfectly conserved across the entire protein kinase domain supporting the hypothesis of a recent gene duplication followed by translocation event and the integration of the STPK domain onto the Rpg5 ancestral NLR. However, there are *Rpg5-STPK* alleles (G3R) (Arora et al., 2014) identified from *H. sponteneum* and Swiss landraces that contain a kinase domain that is more closely related to MLOC_66562.1. These Rpg5 STPK domains are lacking a 10-aa deletion (SSSYLYQTM) present in the Q21861-like *Rpg5* GR1 and GR2 allele predicted translated proteins that are missing from MLOC_66562.1. The kinase domain of G3R *Rpg5* allele shares 87% aa identity and 89 % aa similarity with the MLOC_66562.1 predicted protein suggesting that these alleles have not undergone as much divergence since the translocation and fusion event of the protein kinase domain. Thus, again strengthen the possible evolution of progenitor protein to adept more efficiently to function as a bait and trap the pathogen effectors evolve to interact with its ancient gene paralog.

BLASTP searches with the predicted amino acid (aa) sequence of the HORVU5Hr1G056920.1 protein aligns with the *Arabidopsis* AT5G15080.1 (94% aa identity; 96% aa positives) as well as orthologous genes from a wide diversity of monocot and dicot

plants suggesting a highly conserved protein across plant genera, indicating a conserved/important function. AT5G15080.1 is predicted to be a guard cell kinase thus we named HORVU5Hr1G056920.1 as *Gak1* (Guard cell Associated Kinase 1). HORVU5Hr1G056920.1 also showed the highest homology (72% aa identity and 81% aa positives) to the *Arabidopsis* annotated protein AT2G28930.1 (AtApk1B).

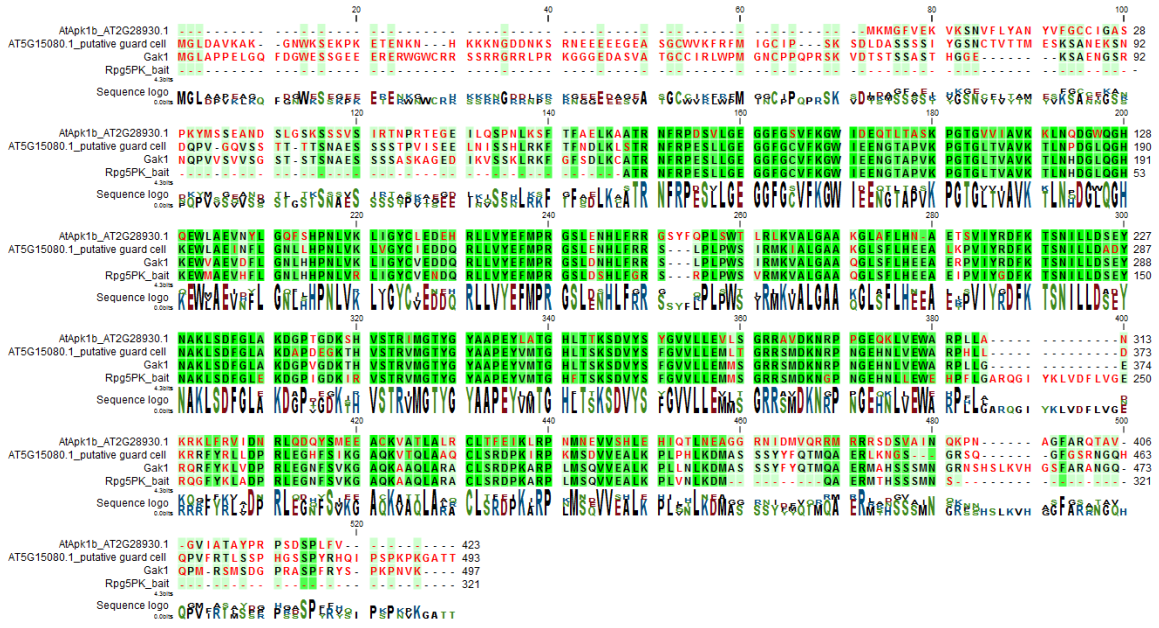

Fig. 2.3. Protein homology between the Rpg5 protein kinase domain (aa 1058-1378), HvGak1, ATG15080.1 and AtApk1b. The aa with the green background represent high sequence similarity among all aligned protein sequences. Red lettering represents diverged aa acids and dashes represent insertion/deletions. Letter height of consensus sequence depicts level of conservation at each aa residue.

The *AT2G28930.1* encodes the *Arabidopsis APK1b* gene that has been shown to be specifically expressed in the stomata compare to the whole leaf fractions and functions in stomatal opening in response to daylight (Elhaddad et al., 2014). *AT5G15080.1* is also annotated as a guard cell specific protein and active kinase (Benschop et al., 2007) in *Arabidopsis* and is highly homologous to *AtAPK1b* suggesting that they may share similar or redundant function. AtApk1b, AT2G28930.1, Gak1 and Rpg5 PK domain shows a high protein sequence similarity

(Fig. 2.3). Thus, these results indicate a possible role of Gak1 as a barley stomatal protein that also may play a role in stomata opening in response to light.

The BLAST searches of the IPK barley genome browser and NCBI databases with the PP2C aa sequences yielded no significant hits within the *Hordeum vulgare* sequence repositories. However, searches of the non-redundant protein database determined that the orthologs of the *rpg5*-PP2C domain are conserved across plant species with the best hit being the *Triticum aestivum* unnamed protein CDM81310.1 (87% query coverage with 66% identity, E value 3e-154). These findings suggest that the progenitor of the Rpg5-PP2C is missing from the cultivated barley lines that have been used for sequencing.

2.4.4. Possible role of Rpg5 C-terminal kinase acting as an integrated decoy

A simple genetic test to explore the possibility of NLR integrated domains acting as decoys or sensory domains was suggested by Wu et al., 2015 (Wu et al., 2015). We conducted an experiment to determine if the Rpg5 STPK domain acts as an ID. Upon inoculation with *Pgt* race HKHJ virulent on *rpg4/Rpg5* containing barley, we found no significant difference for disease levels in Harrington or the NILs HQ18 or HQ1 (Fig. 2.4 and Fig. 2.5).

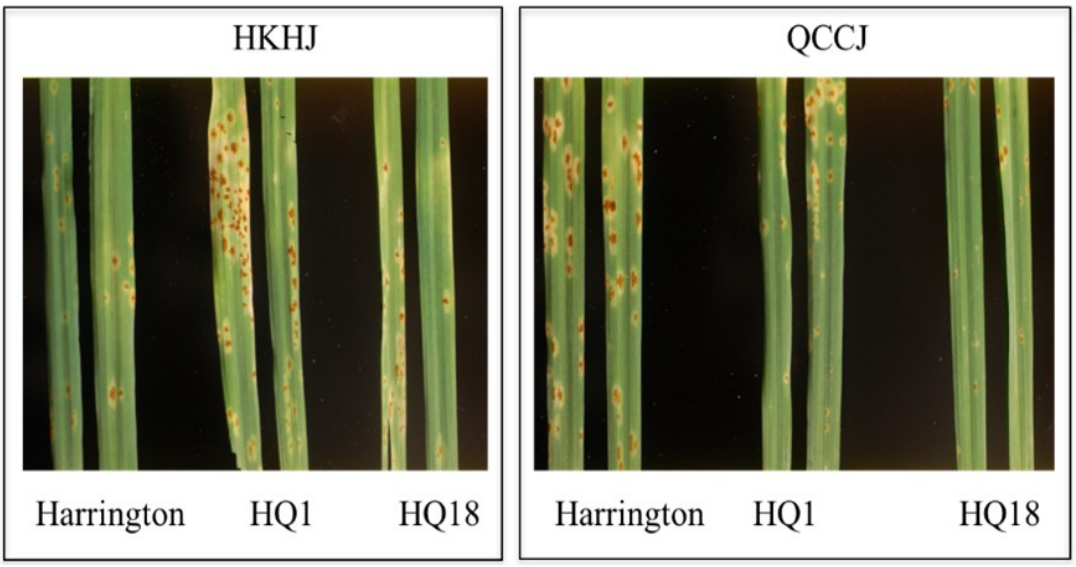

Fig. 2.4. Disease severity on barley line Harrington, and the near isogenic line HQ1 and HQ18, inoculated with two different rust races HKHJ and QCCJ respectively. Primary leaves after 14 days of *Pgt* inoculations are shown.

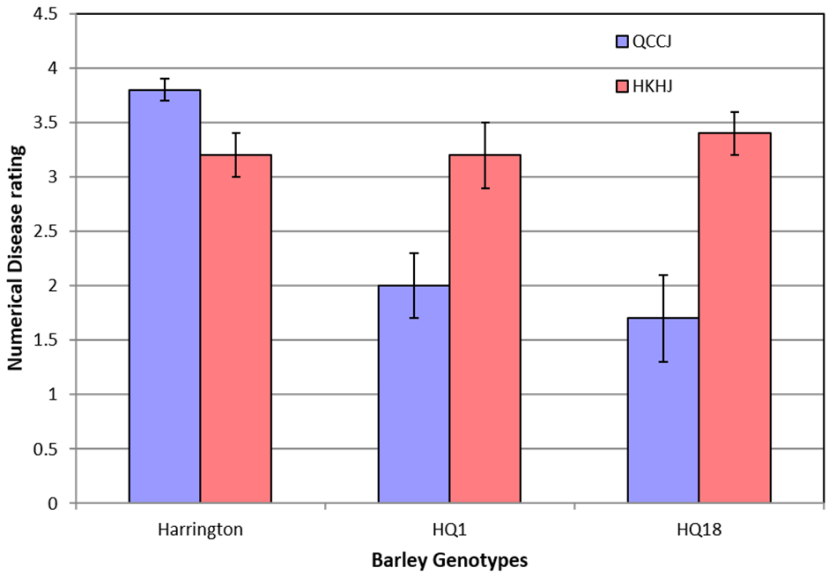

Fig. 2.5. Graphical representation of disease severity on primary leaves of barley line Harrington, near isogenic line HQ1 and HQ18, inoculated with two different rust races HKHJ and QCCJ respectively. Harrington HQ1, and HQ18 were susceptible for HKHJ (disease rating ~3.25) whereas QQCJ was virulent only on Harrington (3.75).

HQ18, HQ1 and Q21861 barley lines show resistance responses against *Pgt* race QCCJ, indicating that the *Rpg5* R-gene is required for the resistance reaction and is sufficient in a

Harrington background to provide QCCJ resistance. These results present compelling genetic evidence that the Rpg5 kinase domain is the sensory domain or has a role in general physiological function in plant rather than basal immunity and provides no additional immune function for avirulent effector present in QCCJ although it not shows any additional function if present in a NIL. Thus, null decoy hypothesis for Rpg5 integrated kinase domain cannot be rejected (Wu et al., 2015).

An interesting question arise here is what if these integrated domains are mimic of pathogen target proteins in plant involve in conserved physiological process rather than in basal immunity pathway. In such condition, it would be impossible to test decoy hypothesis with such simple genetic test.

2.4.5. Rpg5, HvRga1, and rpg5-PP2C NLR transcripts analysis

Our qPCR analysis of candidate NLR's suggested that they are expressed at low basal level in leaf tissues. Upon inoculation of resistant barley line Q21861 with *Pgt* race QCCJ containing Avr 4/5 *HvRga1* and the *Rpg5-STPK* and *rpg5-PP2C* allele transcript levels did not change significantly taking account of soltrol mock control at the early time points 6 to 12 HPI, but were down regulated ~2-fold at 24 HPI (Fig. 2.6 and Fig. 2.7). At the later time points tested (48 and 72 HPI) no differential regulation was observed. These results indicate the co transcriptional regulation of the dual NLR's present in *RMRL* during pathogen challenge corroborating with the common theme of integrated decoy hypothesis and the dual head-to-head NLR architecture at these loci under co-regulatory elements.

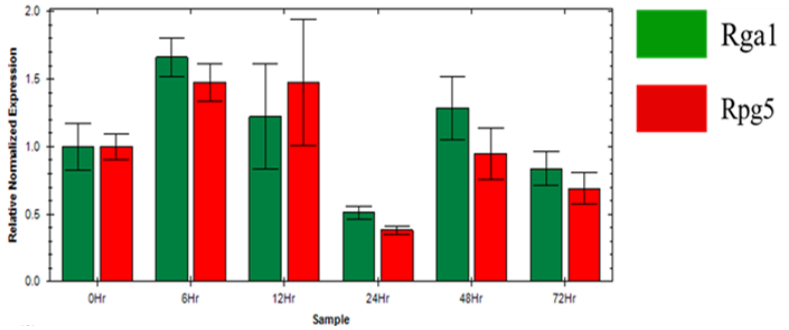

Fig. 2.6.A

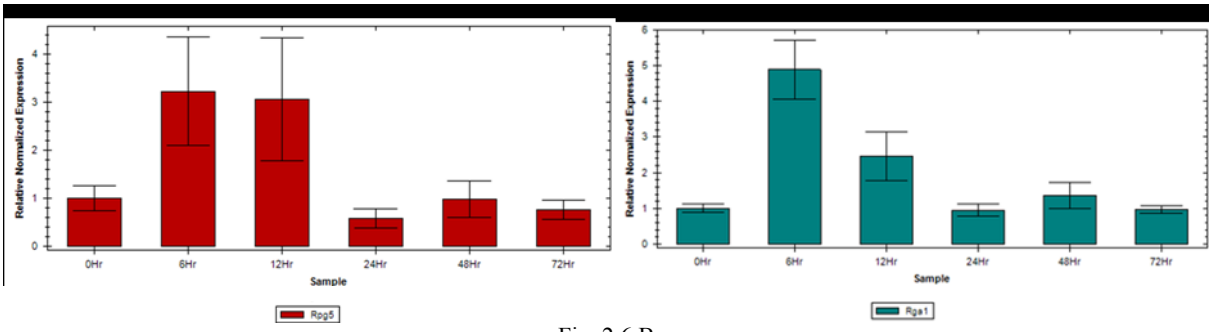

Fig. 2.6.B

Fig. 2.6. Time course qRT-PCR transcript analysis of the dual NLRs *HvRga1* and *Rpg5* required for *rpg4/Rpg5*-mediated wheat stem rust resistance in the line Q21861 when inoculated with the **(A)** Wheat stem rust race QCCJ (surrogate race for TTKSK) and **(B)** Soltrol oil control. The data was normalized to *HvGAPDH* expression at each time point (X-axis). Error bars depict SEM±1(n=3). Time point 0 HPI (non-inoculated) was used as control sample for relative expression analysis (Y-axis).

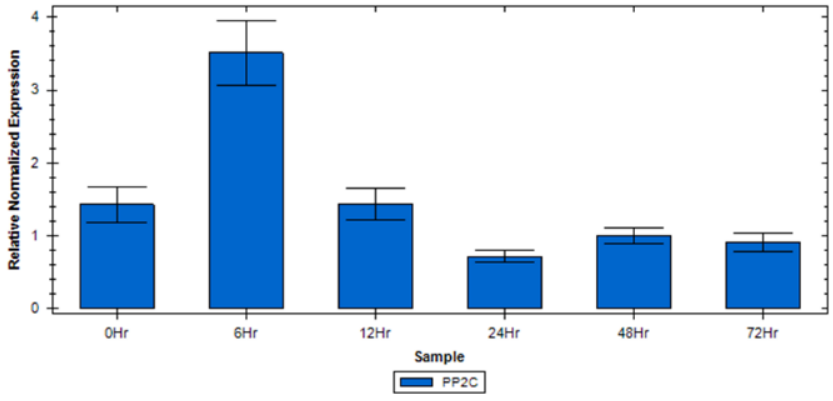

Fig. 2.7. Time course qRT-PCR transcript analysis *rpg5-PP2C* in susceptible Steptoe inoculated with stem rust race QCCJ. Data was normalized to *HvGAPDH* expression at each time point (X-axis). Error bar depict SEM±1(n=3). Time point 0HPI (non-inoculated) was used as control sample for relative expression (Y-axis).

2.4.6. DAB staining to determine timing of resistance response

To determine the timing of the resistance responses elicited by the *Rpg5-STPK* allele we conducted histochemical DAB staining on the resistant barley Q21861 and susceptible barley cultivar Steptoe. Leaf samples were DAB stained every 6 hours post inoculation with *Pgt* race QCCJ up to 72 hours (Fig. 2.8).

We observed that for the inoculated susceptible barley cultivar Steptoe there was very less DAB staining near to the germinated rust spores and formed appressoria at all time points except time point 24 hours. At 18 HPI a small number of appressoria formed over the stomata were associated with DAB. Interestingly, in the resistant barley Q21861 we were not able to detect any DAB staining correlated with fungal structures including appressoria at any time points tested up to 72 HPI, a deviation from common R gene mediated HR (Hypersensitive Response) and cell death.

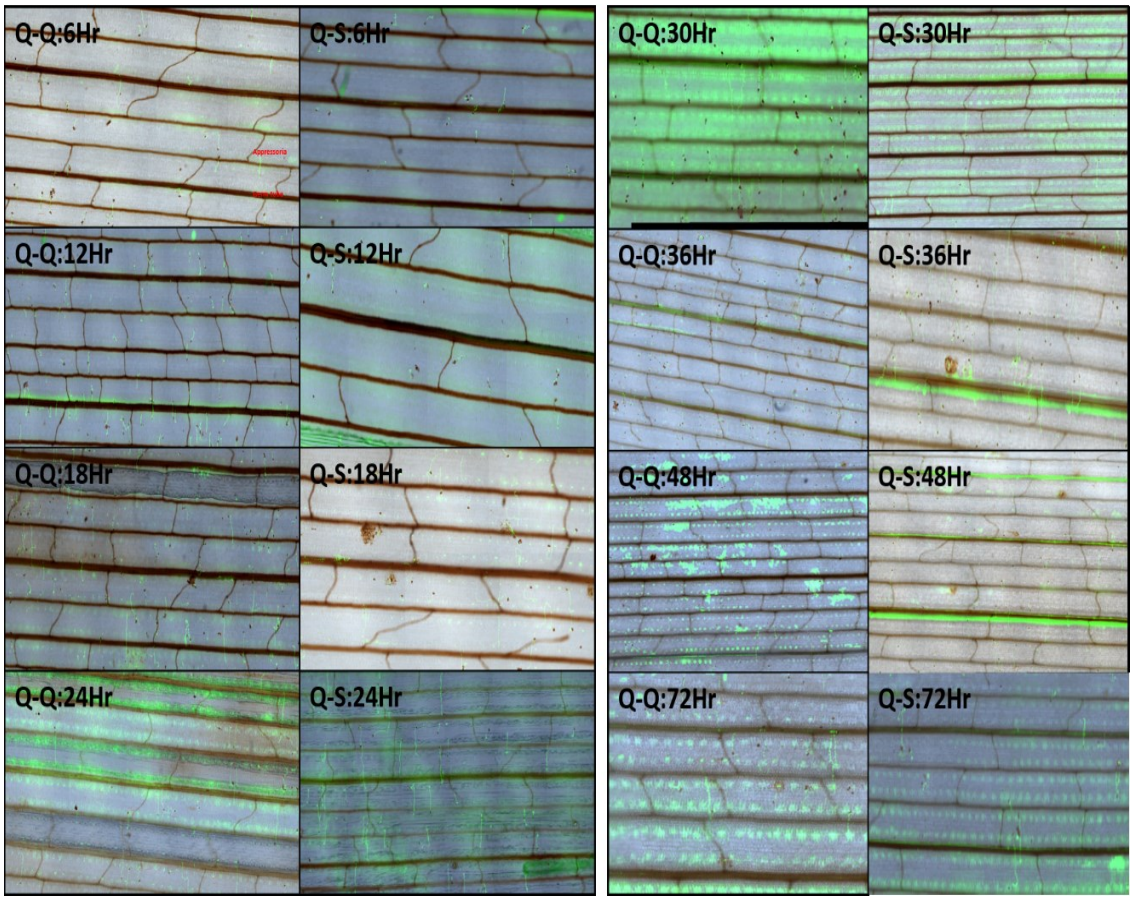

Fig. 2.8. DAB staining coupled with WGA-AF-488 fluorescent stain to characterize the *Pgt* race QCCJ infection timeline, and HR responses in the barley line Q21861 (*Rpg5-STPK+*) and cultivar Steptoe (*rpg5-PP2C+).* The panels show Pgt race QCCJ infection on Q21861 (labeled Q-Q:time) and on Steptoe (labeled Q-S:time) from 6 to 72 hours post inoculation.

2.4.7. Gak1 expression analysis

Previous studies using the *Arabidopsis* model system were demonstrated that the *AtApk1b* promoter drives specific GUS gene expression in the stomatal guard cells and that the expression level of *AtApk1b* was higher in stomatal guard cells compare to mesophyll tissue samples (Elhaddad et al., 2014). Since barley Gak1 has high aa similarity with AtApk1b and the *Arabidopsis* guard cell associated kinase AT5G15080.1, we explored the possibility of *Gak1* having high expression in barley stomata. We isolated the stomatal cells from the abaxial surface of 8-day old Q21861 primary seedling leaves using LASER microdissection and RNA was

isolated using single cell RNA isolation method form 75 collected stomata. The qPCR data show that *Gak1* transcription in the stomata is 600-800-fold higher than the whole leaf tissue samples (Fig. 2.9.). Thus, indicating that the tissue specific expression of *Gak1* in barley stomata could play a possible role in guard cell function. However, these results need to be repeated prior to making specific conclusion, since microdissection can cause degradation in RNA quality.

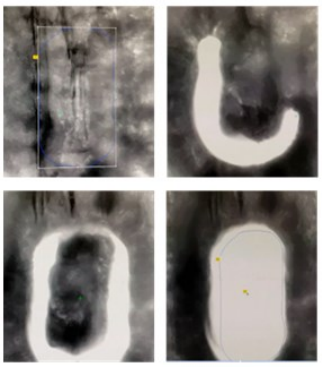

Fig. 2.9.A

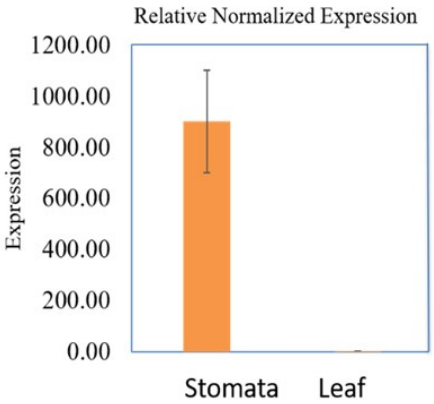

Fig. 2.9.B

Fig. 2.9. LASER microdissection of stomata from barley line Q21861 primary seedling leaves and qPCR expression analysis of *Gak1* in stomata comparing to the whole leaf tissue. (A) Different stages of stomatal laser capture microdissection (B) The qPCR analysis showing > 800-fold higher expression of *Gak1* in stomata compared to whole leaf fraction. N=3, SEM ±1.

2.4.8. Yeast two hybrid assay to determine the physical interaction between the candidate genes and their modular domains

A forward Y2H interaction screen using HvRga1, the Rpg5-STPK, HvAdf3, rpg5-PP2C proteins and the modular domains of each predicted protein (Fig. 2.10.A) as bait or prey did not result in any detectable direct interactions in yeast (Fig. 2.10.B). These preliminary interaction assays suggested that these proteins probably do not directly interact with each other during defense responses or to form homo or heterodimeric resistance complexes without intermediate interacting components.

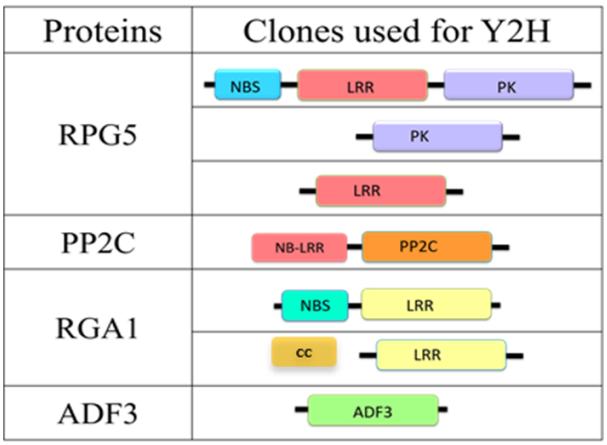

Fig. 2.10.A

Bait / Prey	Rpg5-FL	HvRga1-FL	HvAdf3-FL	Rpg5-LRR	Rpg5-PK	HvRga1-LRR	HvRga1-CC	rpg5-PP2C
Rpg5-FL	No	No	No	Na	Na	Na	Na	Na
HvRga1-FL	No	No	No	Na	Na	Na	Na	Na
HvAdf3-FL	No	No	No	No	No	Na	Na	Na
Rpg5-LRR	Na	Na	No	No	Na	No	Na	Na
Rpg5-PK	Na	Na	No	Na	Na	Na	Na	No
HvRga1LRR	Na	Na	Na	No	Na	No	Na	Na
HvRga1-CC	Na	Na	Na	Na	Na	Na	No	Na
Rpg5-PP2C	No	Na	Na	Na	No	Na	Na	No

Fig. 2.10.B

Fig. 2.10. Negative results of Y2H interactions tested with candidate *Rpg5*, *rpg5-PP2C*, *HvRga1*, *HvAdf3* and their modular domains. **(A)** Domains utilized in the Y2H interactions. **(B)** Interactions of full length (FL), leucine rich repeat (LRR), protein kinase (PK), coiled coil domain (CC) and protein phosphatase 2C (PP2C) domain YTH interactions in tabular form. No with red background indicates no detectable interaction and Na indicates interaction not tested.

PCR based detection using bait and prey specific primers (Appendix Table A1) confirmed the presence of target genes in the double transformed Mav203. Further western blotting confirmed the protein expression of candidate genes cloned in the prey vector (Fig. 2.11)

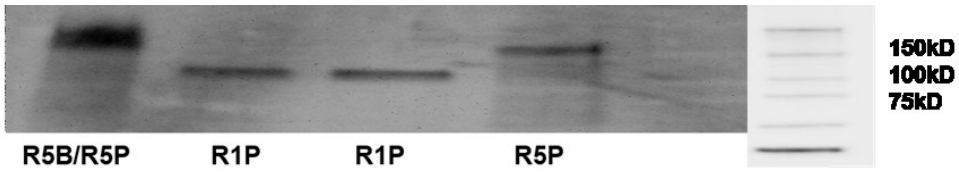

Fig. 2.11. Confirmation of protein expression in double transformed yeast colonies for protein expression using prey activation domain specific antibodies. Lane 1- Rpg5 prey (~160kD) with Rpg5 bait interaction, Lane 2- HvRga1 prey (~100kD) with HvAdf3 bait interaction, Lane 3- HvRga1prey (~100kD) with Rpg5 bait interaction, lane 4- Rpg5 prey (~160kD) with HvRga1 bait interaction, lane 5- empty, and Lane 6 – BioRad precision plus protein ladder with annotated bands for protein weight.

A full-scale barley line Q21861 cDNA prey library synthesized from *Pgt* race QCCJ infected leaf tissues and screened on SC-LTH-30mM selection plates resulted in the identification of 4 putative interactions, rapid growing large colonies for the Rpg5 protein kinase

domain utilized as the bait and 8 colonies for the *rpg5* PP2C domain as bait. Interestingly, further screening to validate true interacting proteins identified the HvVoz1 candidate protein as interacting independently with the Rpg5-PK (STPK) and rpg5 PP2C domains as bait. Further testing of HvVoz1 prey in a forward yeast-two-hybrid test with the HvRga1-LRR, Rpg5-LRR and HvAdf3 baits resulted identification of interactions with all but HvAdf3 bait. These interactions were tested along with Y2H control interactions i.e. with the strong interactor mouse protein RalGDS-wt (the Ral guanine nucleotide dissociator stimulator protein) as a prey and Krev1 (or Rap1A; a member of the Ras family of GTP binding proteins) as a bait, a moderated interactor mutant RalGDS-m1-prey and Krev1-bait and very weak interactor mutant RalGDS-m2-prey and Krev1-bait (Fig. 2.12). To test the transcription activation ability of the candidate genes alone without an interacting partner control with empty prey and target gene-baits were used.

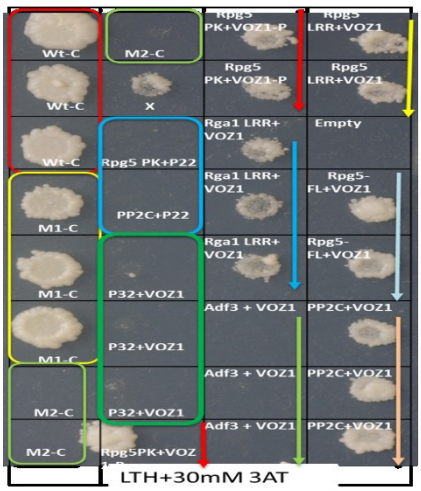

Fig. 2.12.A

Bait / Prey	Rpg5-FL	HvRga1-FL	HvAdf3-FL	Rpg5-LRR	Rpg5-PK	HvRga1-LRR	HvRga1-CC	rpg5-PP2C
Rpg5-FL	No	No	No	Na	Na	Na	Na	Na
HvRga1-FL	No	No	No	Na	Na	Na	Na	Na
HvAdf3-FL	No	No	No	No	No	Na	Na	Na
Rpg5-LRR	Na	Na	No	No	Na	No	Na	Na
Rpg5-PK	Na	Na	No	Na	Na	Na	Na	No
HvRga1LRR	Na	Na	Na	No	Na	No	Na	Na
HvRga1-CC	Na	Na	Na	Na	Na	Na	No	Na
Rpg5-PP2C	No	Na	Na	Na	No	Na	Na	No
Hv-Voz1	Yes	Na	No	Yes	Yes	Yes	Na	Yes

Fig. 2.12.B

Fig. 2.12. Y2H interactions tested with the HvVoz1 prey and the full-length Rpg5, Rpg5 LRR and STPK domains, rpg5 PP2C domain, HvRga1 LRR and full-length HvAdf3 as baits. **A.** Interactions tested on LTH+30mM 3AT selection plates showing Wt (strong), M1(moderate) and M2 (low) interaction controls along with the Rpg5 bait only and Voz1 prey only controls. Colony growth represents putative interactions. X and Empty depicts experimental false or non-inoculated slots, respectively. **B.** Results for all the interactions tested in tabular form. Yes, with green background means a positive interaction detected and No with a red background represents no interaction detected.

2.5. Discussion and conclusions

A recent fundamental change in the understanding of plant innate immunity stems from the hypothesis built upon solid genomic and functional data showing that plants evolve to integrate pathogen virulence effector targets with NLR immunity receptors to “bait” the intruder into “NLR traps”(Sarris et al., 2016), known as the “integrated decoy model”(Cesari et al., 2014). The primary weapons of the pathogen that they evolved to become specialized pathogens and further evolved during the host-pathogen molecular arms race are the virulence effectors. These effectors predominantly manipulate host target proteins providing a means to evade defense responses or acquire nutrient during the colonization and reproductive processes within the host environment. Based on studies performed in model pathosystems it is becoming clear that many effector targets are components of signaling pathways underlying receptors that sense

environmental cues, including the pathogen challenge. Thus, these signaling pathways represent weak links or "susceptibility hubs" that diverse pathogens have evolved to manipulate on different hosts. To protect these weak links in their physiology, plants counter or co-evolved different means to detect this perturbation, with the most recent integrated decoy model (Cesari et al., 2014; Wu et al., 2015) suggesting that genome translocations result in genome reshuffling events that attach susceptibility targets to NLR immunity receptors as R-protein receptors or "baits" (Kroj et al., 2016; Sarris et al., 2016; Bailey et al., 2017). These genome-shuffling events probably occur via intrachromosomal or interchromosomal translocation events but characterizing these events is difficult without the known paralog or progenitor of the ID that is the original virulence target of the pathogen, its putative biological function, and the genome sequence surrounding the ID progenitor locus and the NLR-ID locus. Even more rare would be to have all this information as well as a NLR-ID locus with two independent translocated IDs at the same NLR locus. In barley, we have identified an important NLR-ID locus *rpg4*/*Rpg5*-mediated resistance locus (*RMRL*), where we have generated this before mentioned information (Fig. 2.13), which provides an unprecedented opportunity to investigate the mechanisms in plant genomes that possibly integrate these susceptibility hubs to the dual NLR resistance loci.

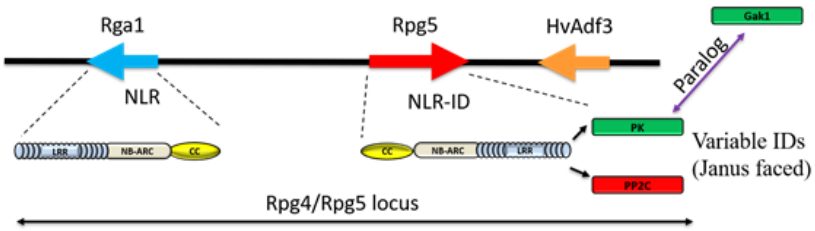

Fig. 2.13. Dual NLR genome architecture at *rpg4*/*Rpg5* mediated resistance locus (*RMRL*) at the subtelomeric region of barley chromosome 5H. The black line top represents the genome sequence of the ~70kb *RMRL* showing the three genes required for resistance as colored arrows. The HvRga1 NLR (blue arrow) is situated in head-to-head orientation with the Rpg5 NLR that contains either the protein kinase integrated sensory domain (ISD; PK green bar) or the protein phosphatase 2C ISD (PP2C red bar). Thus, the Rpg5 NLR can have an integration of a PK (Rpg5-STPK) or PP2C (rpg5-PP2C) integrated sensory domain. The PK integrated domain is very similar to the serine threonine protein kinase provisionally given the nomenclature Guard Cell Associated Kinase 1 (*Gak1*) with conserved intron/exon boundaries and highly conserved aa sequence (85.5% aa identity and 88.2% aa similarity (pairwise local alignment for 330 amino acids).

It is certainly remarkable that many diverse pathosystems show convergent evolution patterns where these loci contain very similar genomic architecture including the duel unrelated NLRs tightly linked in a head-to-head orientation with one of the NLRs containing a variable domain with a biological function typically targeted by known pathogen effectors. Thus, the similar resistance loci configuration involving many unrelated NLRs and diverse host-parasite genetic interactions and co-evolutionary pressures suggests that a selective advantage of this resistance locus configuration arose through convergent evolution giving rise to this common dual NLR integrated sensory domain architecture in diverse pathosystems (Fig. 2.14). It may be a bold statement that plant genomes have evolved a directed mechanism to produce immunity locus architecture, but it is an intriguing hypothesis and is increasingly questionable that these convergent architectures occurring in plants dating back to the mosses and as late as the divergence of wheat and barley is occurring via completely random translocation events.

The barley *rpg4/Rpg5*-mediated resistance locus on chromosome 5H is effective against broad wheat stem rust races including *Puccinia graminis* f. sp. *tritici* race TTKSK (A.K.A. Ug99) and its lineage that are considered a threat to world food security. The *RMRL* contains two tightly linked NLR genes, *Rpg5* and *HvRga1,* found with the typical head-to-head genome architecture of a dual NLR integrated decoy resistance mechanism. Intriguingly, the Rpg5 NLR has two different IDs, a STPK and PP2C, thus, the *Rpg5* alleles represent the only NLR R-gene with independent IDs, which we hypothesize to have occurred via intrachromosomal translocation events. The duality and antagonistic function of the ISDs present on the barley *Rpg5* alleles coupled with the well characterized genome region surrounding the translocated regions provided needed knowledge about the translocation events giving rise to the two NLR-ISD alleles.

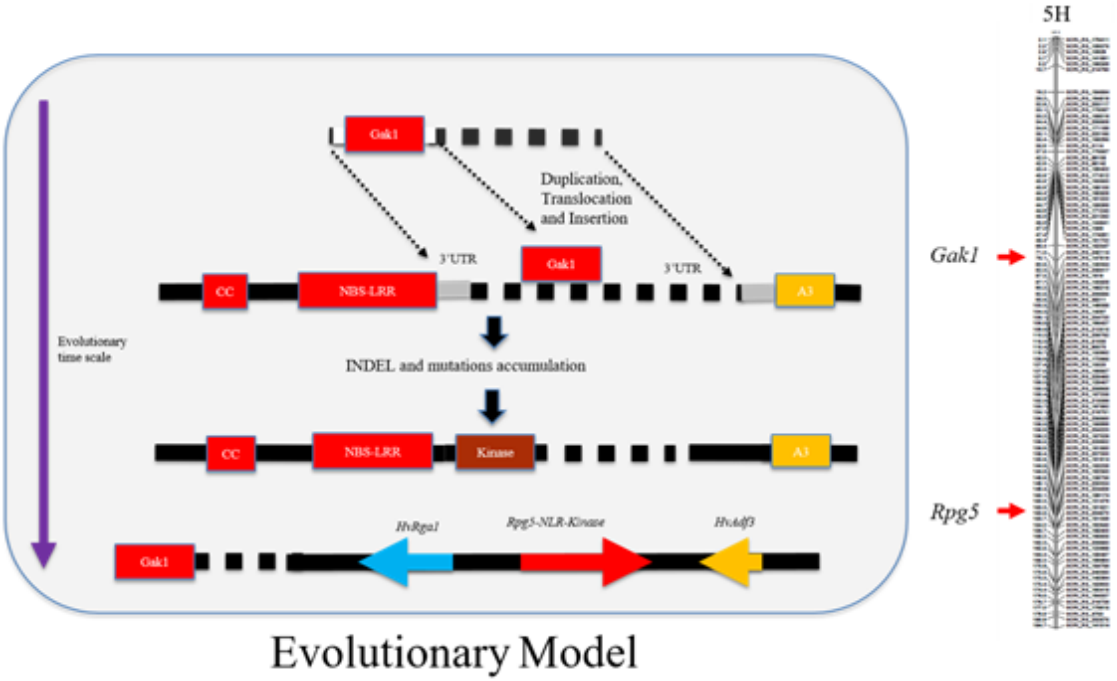

Fig. 2.14. Schematic representation of possible direct evolution of *Rpg5-STPK* NLR.

We hypothesize that duplication and translocation of *Gak1* resulted in the integration of a second copy of the gene into the 3' UTR (UnTranscribed Region) between ancient *rpg5* NLR (nonfunctional for stem rust resistance) and *HvAdf3* at *rpg4/Rpg5* locus on barley chromosome 5H. This event was possibly directed due to the evolutionary pressure on the barley to mount a counter attack mechanism for NLR diversification and identification of the pathogen targeting the Gak1 and utilizing it for the entry and establishment in the barley upon stomatal manipulation during initial dark period. Insertion of *Gak1* in the *rpg5* NLR and evolution of an adapted integrated Gak1 paralog resulted in the *Rpg5-STPK* functional NLR-ID acting as a bait pathogen sensor to activate NLR sensor.

The two NLRs, *Rpg5* and *HvRga1*, required for *rpg4/Rpg5*-mediated resistance raised the intriguing question of why the NLR-STPK domain resistance gene that behave as a dominant *R*-gene against *P. graminis* f. sp. *secalis* isolates including 92-MN-90 behaves as a recessive *R*-gene against broad *P. graminis* f. sp. *tritici* races including races QCCJ and TTKSK. The requirement of two NLR R-proteins that typically provide dominant resistance against biotrophic pathogens prompted the evaluation of crosses between the resistant line Q21861 and five susceptible parents. Of primary interest were the susceptible parental lines containing non-functional *rpg5* alleles with different insertion event leading to the presence of the *STPK* or *PP2C* ISD. Traditionally recessive resistance is considered the result of a non-functional allele or a dominant functional susceptibility factor. Analysis of the region determined that most of the susceptible barley varieties contain the insertion event which evolutionarily appears to predate the insertion deletion event which replaced the *PP2C* domain of *Rpg5* and replaced it with a predicted functional *STPK* domain (Arora et al. 2013), whose progenitor appears to be the *Gak1* gene. We hypothesized that the functional *PP2C* domain that is not present in the resistant alleles

could potentially function as a dominant susceptibility factor, conferring susceptibility when present as a single copy in the F_1 generation and would segregate 1:3 for resistance and susceptibility in the F_2 generations. We tested this hypothesis and three crosses with susceptible parents containing the *rpg5-PP2C* allele behaved as predicted. Previous F_2 phenotype analysis of one of the populations we tested and two different populations made with susceptible parents containing an intact *rpg5-PP2C* allele (Morex, Steptoe, and Robust x Q21861) revealed 1:3 segregation for resistance:susceptibility, further demonstrating the recessive nature of *rpg4*-mediated resistance in the presence of the *rpg5-PP2C* allele. Two susceptible barley lines, Golden Promise and OSU6, contain a non-functional *Rpg5* allele due to a nucleotide insertion resulting in a frame shift mutation and a truncated *Rpg5* protein. However, these non-functional alleles still have the STPK domain intact without the PP2C domain. Golden Promise and OSU6 were crossed with Q21861 and the F_1 progeny from these crosses were assayed for reaction type to *Pgt* race QCCJ. The F_1 progeny of the two crosses were resistant to *Pgt* race QCCJ suggesting that the *rpg5-PP2C* allele dominant susceptibility factor hypothesis may be correct. We also tested the F_2 progeny from the Golden Promise x Q21861 population and determined that the resistance:susceptibility segregated 3:1 as a single dominant resistance gene determined to be the *rpg4*/*Rpg5* locus (Fig. 2.1). This preliminary data suggests that the *rpg5-PP2C* may act as a dominant susceptibility factor that represses the resistance reaction triggered by the *Rpg5* and *Hv*Rga1 R-genes. These genetic analyses show that the *Rpg5-STPK/HvRga1*-mediated resistance behaves as a dominant in the absence of *rpg5-PP2C* allele when assayed with *P. graminis* race QCCJ. These two groups of susceptible parents both contain a predicted non-functional *Rpg5* allele with the insertion/deletion events that putatively replaced the apparently more ancient PP2C ISD with the STPK ISD. Analysis of F_2 progeny from crosses between Q21861 and group

1 and 2 susceptible lines segregated in 1: 3 ratio (resistant:susceptible) when the *rpg5-PP2C* allele is present but in a 3:1 ratio (resistant:susceptible) when the *rpg5-PP2C* allele is absent and a nonfunctional *rpg5-STPK* allele is present (Fig. 2.1). Thus, it appears that the *Rpg5* gene previously identified as the dominant rye stem rust resistance gene also imparts *rpg4*-mediated wheat stem rust resistance and behaves as a dominant gene in the absence of the *rpg5-PP2C* allele. These data indicated that the *Rpg5-STPK*-mediated resistance was recessive in nature when combined with a single copy of the *rpg5-PP2C* allele (Fig. 2.1) possibly due to its function being suppressed by the presence of the PP2C protein and results in a recessive segregation at the locus. The data suggests that the *rpg4* and *Rpg5* R-gene component may not be distinct genes and the difference in the dominant or recessive nature of resistance is due to the *rpg5-PP2C* allele acting as a dominant susceptibility factor that suppresses *Rpg5*-mediated resistance against the wheat stem rust races including Ug99.

Using a population derived by crossing the resistant line Q21861 and susceptible cultivar Steptoe for BSMV-VIGS of *rpg5-PP2C* silencing conclusively suggested that the *rpg5-PP2C* is a dominant susceptibility factor. Post transcriptional gene silencing of the *rpg5-PP2C* allele in heterozygous F_2 individuals (*Rpg5-STPK/rpg5-PP2C*) shifted the response to *Pgt* race QCCJ from susceptibility towards resistance. Thus, the presence of two diverse and known antagonistic functional domains, i.e. the STPK and PP2C, fused to a single NLR indicates two different selection pressures across a wide evolutionary time scale driving the insertion and evolution of a Janus faced NLR with diverse and functionally antagonistic ISDs (Fig. 2.13). Based on the evolution driving the "integrated decoy" or "integrated sensory domain" model we hypothesize that these ISDs are mimics of ancestral pathogen target proteins (Baggs et al., 2017; Sarris et al., 2016) acting as pathogen baits. A scan of the recently revised barley genome sequence to find

paralogs representing the ancestral progenitor effector targets for the *rpg5-PP2C* or *Rpg5-STPK* ISDs lead to the identification of the *Rpg5-STPK* ID progenitor*, Gak1*, which is the *Arabidopsis AT2G15080* (a putative guard cell kinase) and *AtAPK1b* ortholog, which is involved in stomate opening in response to light. The *AtAPK1b* promoter drives *GUS* gene expression in the guard cells in transgenic *Arabidopsis* with a AtApk1b_promoter-GUS cassette (Elhaddad et al., 2014).

With this knowledge in hand and using the ISD evolutionary model we further hypothesize that several of *P. graminis* (*Pg*) *forma specialis* contain an unknown elicitor that manipulates the barley Gak1 protein localized in the stomates to mimic the presence of light and induce stomatal aperture opening by untimely activation of signal transduction pathway that are otherwise reserved for the perception of light and subsequent induction of stomata aperture opening. Thus, this manipulation may provide the pathogen with unchallenged entry through the natural openings into the plant during the dark, the period that *P. graminis* spores evolved to germinate in order to avoid desiccation during the hat of the day. This hypothesis presents an interesting shift from our present knowledge which suggests light dependent stomatal opening is required for *Pg* penetration through stomatal apertures (Yirgou and Caldwell, 1963; Figueroa et al., 2016). A possible explanation for the *Gak1* integration into Rpg5-NLR is that to combat this broad virulence effector activity the progenitor of barley and wheat, counter evolved by duplicating and translocating the *Gak1* targeted protein to be expressed as an NLR fusion, serving as a pathogen "bait", which when manipulated elicits a resistance response. Thus, the pathogen's deceptive mimicking of light to facilitate colonization alerts the innate immunity responses resulting in avirulence. However, based on the allele diversity and divergence present in the natural wild barley and wheat populations examined the common barley and wheat progenitor had in its evolutionary history integrated a *PP2C* ID at the same position as the *STPK*

ID, which appears to negatively regulate stem rust resistance signaling activated by the Rpg5-STPK. However, the paralog for this domain was not found in the barley genome and the higher level of divergence in the *rpg5-PP2C* alleles suggests that this was a more ancient ISD introgression than the *STPK* ISD which gave rise to broad *Puccinia graminis* resistance as the *Rpg5* locus has been shown to provide resistance to broad *forma specialis* of *Puccinia graminis* including *P. graminis* f. sp. *secalis* the rye stem rust (Brueggeman et al., 2008; Wang et al., 2013; Arora et al., 2013) and *P. graminis* f. sp. *avenea* the oat stem rust (Dracatos et al., 2015). Presence of the *rpg5-PP2C* allele determines the recessive nature of what used to be termed *rpg4*-mediated wheat stem rust resistance in barley.

Interestingly it has been concluded that the head-to-head genome architecture of dual NLR resistances somehow facilitate this ISD evolution and that these dual NLRs are typically under coregulation by common transcriptional regulation cis elements. Transcript analysis of *Rpg5/ rpg5-PP2C* and *Hv*Rga1 NLRs determined that transcription of these NLR pair is also coregulated and not significantly changed upon pathogen challenge as shown for other integrated decoy systems such as the rice *RGA4/RGA5* ((Cesari et al., 2013, 2014)). Interestingly qPCR to evaluate the transcript abundance of *Gak1* in guard cells and whole leaf using laser micro dissected barley stomatal tissues showed a ~800-fold expression difference between the stomata specific expression and whole leaf expression, suggesting a specific functional role in guard cells probably related to guard cell physiology.

A key question still remains unanswered regarding the functional activity of these integrated domains in the absence of the cognate avirulence factors that elicit the NLR activation of immunity responses. An interesting yet simple genetic test was proposed by Wu et al., 2015 to test if integrated domains are “decoys” or represent “integrated sensory domains” that have

retained their ancestral protein function which was initially targeted and hijacked by the pathogen virulence effector. Thus, the role of such proteins in the absence of the gene-for-gene components that elicit and to provide disease resistance must be understood in order to achieve the goal of synthesizing global pathogen sensors for synthetic R-gene development and deployment in crop species (Dangel 2016) that are effective to a broad spectra of plant pathogens.

A simple genetic test proposed by Wu et al., that as far as we know has not been conducted for any dual NLR-ISD systems to date. Wu et al. (Wu et al., 2015) proposed that if there is no observe difference for disease severity and incidence detected between a NIL with the dual NLR-ISD locus and the background genotype control without the NLR-ISD when inoculated with a pathogen isolate lacking the cognate avirulence gene, it would indicate that the null "decoy hypothesis" cannot be rejected. This is inferred because either the integrated domain is an actual decoy without a function or plays no role in resistance phenotype. It may play a role in other biochemical pathway like development or housekeeping. However, if reduced disease in the NIL is observe then the integrated domain has retained ancestral basal immunity function and the "decoy hypothesis" can be rejected and the integrated domain has retained some function and is not an integrated decoy. A third possible scenario is if the NIL with integrated domain becomes more susceptible possibly indicating that it is targeted by an unknown effector (Table 2.2).

Table 2.2. Schematic representation for the genetic test and its various outcomes to determine if the integrated domains are sensory domains or decoys, using near isogenic lines (NIL) with and without the dual NLR-ISD locus. (Adapted from Wu et al, 2015)

HKHK (avr) response	Plant Genotype		Interpretation
	Harrington (NIL-SD)	HQ (NIL+SD)	
1.	-	-	Decoy hypothesis can't be rejected
2.	-	+	SD has retained ancestral ET biohchemical activity
3.	-	---	SD act as susceptibility factor, uncharacterized effector target

In our genetic test with the HQ18 NIL and Harrington both genotypes were susceptible when challenged by the virulent *Pgt* race HKHJ showing no significant difference between the disease scores, we can conclude that either the Rpg5 integrated STPK domain is not providing a significant level of basal immunity advantage upon integration in the susceptible Harrington background suggesting that it possibly functions as an "integrated decoy" or bait. However, Rpg5 STPK domain could maintain a redundant role in the general physiological function in the plant similar to its ancestral paralog, yet the integration into the NLR also trips the resistance response upon recognition of the virulence effector, which under this test assumes would be present in *Pgt* race QCCJ and absent from *Pgt* race HKHJ. This genetic test requires a pathogen race lacking the cognate avirulence effector a condition that may not be conclusively met in this pathosystem or interaction if our Gak1 hijacking hypothesis is correct. If, the broad *forma specialis* of *Puccinia graminis* including both virulent and avirulent isolates on *RMRL* containing barley (i.e. HKHJ and QCCJ, respectively) harbor a conserved effector required for the pathogen to open stomata during the night, which we found is race independent as both HKHJ and QCCJ were found to enter the stomates during the night (dissertation chapter 3), then the avirulent gene

requirement can't be met for this genetic test to be valid in our system. However, it is also possible that the pathogen arsenal for stomatal manipulation is diverse and redundant, and different effectors allow for the effective penetration of stomata.

Interestingly, the DAB and pathogen histology data show that this dual NLR integrated decoy defense mechanism provides effective resistance, which does not follow the typical HR mechanisms shown for other characterized dual NLR integrated decoy defense mechanisms (Cesari et al., 2014, 2013). These findings present a stark difference from the typical NLR R-gene mediated resistance mechanisms and indicate an inhibition of pathogen growth in the barley lines containing *RMRL*. This inhibition of the pathogen growth suggests the NLR mediated non-HR defense responses similar to that observed for incomplete resistance or slow rusting resistances which are typical of non-race specific resistance. The *RMRL* is in fact a very broad resistance mechanism and appears to slow the pathogen growth, and not kill it in a strong HR response as the resistance response will typically produce infection types of 1 which have a small amount of sporulation. Thus, *RMRL* inhibits the pathogen growth by a non-HR mechanism.

Our finding of HvVOZ1 as an interactive partner of Rpg5-STPK, rpg5-PP2C and HvRga1 modular domains in Y2H library screening experiments suggests that it could be acting as a scaffold protein, holding the resistance complex together, regulating the immune response until effector manipulation of the STPK integrated decoy domain triggers the immunity. *voz1voz2* mutants in *Arabidopsis* are shown to have a closed stomatal aperture upon temperature and drought stress and exhibits increased drought tolerance. Interestingly, *Arabidopsis voz* mutants have been shown to have increased resistance to the fungal pathogens *Collectrotrichum higginsianum* and the bacterial pathogen *Pseudomonas syringae*, yet are compromised for many abiotic stresses (Nakai et al., 2013b), indicating a positive role of the Voz proteins in biotic-stress

resistance. Overexpression, of Voz further reciprocated the similar results to strengthen the idea (Nakai et al., 2013a). Alternately *Xanthomonas oryzae* pv. *oryzae* (*Xoo*) T3 virulence effector $XopN_{KX085}$ was shown to directly interact with rice OsVOZ2 in Y2H studies. The *Xoo* strain KX085 failed to infect *OsVOz2* mutant rice, thus, implicating *OsVOz2's* role to inhibit the establishment of the pathogen and its virulence (Cheong et al., 2013; Verdier et al., 2012). It has been shown that AtVoz proteins interacts with Phytochrome B and are involved in photomorphogenesis and accelerate flowering (Yasui et al., 2012). PhyB and Voz primarily resides in the cytosol and upon red light induction their phosphorylation and nuclear localization is responsible for light induced flowering response (Yasui et al., 2012; Lazaro et al., 2015). In separate studies PhyB were shown to be responsive to the blue light spectrum and responsible for stomatal opening by inhibiting COP1, an inhibitor of stomatal opening (Kang et al., 2009). Thus, it is possible that the molecular orchestra involving Gak1-HvVoz interaction is responsible for stomatal aperture control and stem rust pathogen manipulation disrupts the balance for stomatal opening in the dark. Although, further investigations are required before making direct conclusion this information has been utilized to develop our model from which our hypothesis driven research efforts are being driven. The translocation of two different integrated domains, the STPK and PP2C, onto the single *Rpg5* NLR provides an excellent opportunity to investigate the mechanism behind the integration of functionally diverse IDs and will provide important information about the evolution of these very interesting immunity receptors in plants.

2.6. Literature cited

Abramovitch, R. B., and Martin, G. B. (2004). Strategies used by bacterial pathogens to suppress plant defenses. *Curr Opin Plant Biol* 7, 356–364. doi:10.1016/j.pbi.2004.05.002.

Arora, D., Gross, T., and Brueggeman, R. (2013). Allele characterization of genes required for rpg4-mediated wheat stem rust resistance identifies Rpg5 as the R gene. *Phytopathology* 103, 1153–1161. doi:10.1094/PHYTO-01-13-0030-R.

Ausubel, F. M. (2005). Are innate immune signaling pathways in plants and animals conserved? *Nat Immunol* 6, 973–979. doi:10.1038/ni1253.

Baggs, E., Dagdas, G., and Krasileva, K. V. (2017). NLR diversity, helpers and integrated domains: making sense of the NLR IDentity. *Curr Opin Plant Biol* 38, 59–67. doi:10.1016/j.pbi.2017.04.012.

Bailey, P. C., Schudoma, C., Jackson, W., Baggs, E., Dagdas, G., Haerty, W., Moscou, M., and Krasileva, K. V. (2017). Dominant integration locus drives continuous diversification of plant immune receptors with exogenous domain fusions. *BioRxiv*. doi:10.1101/100834.

Van der Biezen, E. A., and Jones, J. D. (1998). Plant disease-resistance proteins and the gene-for-gene concept. *Trends Biochem Sci* 23, 454–456. doi:10.1016/S0968-0004(98)01311-5.

Boller, T., and Felix, G. (2009). A renaissance of elicitors: perception of microbe-associated molecular patterns and danger signals by pattern-recognition receptors. *Annu Rev Plant Biol* 60, 379–406. doi:10.1146/annurev.arplant.57.032905.105346.

Brueggeman, R., Druka, A., Nirmala, J., Cavileer, T., Drader, T., Rostoks, N., Mirlohi, A., Bennypaul, H., Gill, U., Kudrna, D., et al. (2008). The stem rust resistance gene Rpg5 encodes a protein with nucleotide-binding-site, leucine-rich, and protein kinase domains. *Proc Natl Acad Sci U S A* 105, 14970–14975. doi:10.1073/pnas.0807270105.

Cesari, S., Bernoux, M., Moncuquet, P., Kroj, T., and Dodds, P. N. (2014). A novel conserved mechanism for plant NLR protein pairs: the “integrated decoy” hypothesis. *Front Plant Sci* 5, 606. doi:10.3389/fpls.2014.00606.

Cesari, S., Thilliez, G., Ribot, C., Chalvon, V., Michel, C., Jauneau, A., Rivas, S., Alaux, L., Kanzaki, H., Okuyama, Y., et al. (2013). The rice resistance protein pair RGA4/RGA5 recognizes the Magnaporthe oryzae effectors AVR-Pia and AVR1-CO39 by direct binding. *Plant Cell* 25, 1463–1481. doi:10.1105/tpc.112.107201.

Cheong, H., Kim, C.-Y., Jeon, J.-S., Lee, B.-M., Sun Moon, J., and Hwang, I. (2013). Xanthomonas oryzae pv. oryzae type III effector XopN targets OsVOZ2 and a putative thiamine synthase as a virulence factor in rice. *PLoS ONE* 8, e73346. doi:10.1371/journal.pone.0073346.

Dangl, J. L., and Jones, J. D. (2001). Plant pathogens and integrated defence responses to infection. *Nature* 411, 826–833. doi:10.1038/35081161.

Dodds, P. N., Lawrence, G. J., Catanzariti, A.-M., Teh, T., Wang, C.-I. A., Ayliffe, M. A., Kobe, B., and Ellis, J. G. (2006). Direct protein interaction underlies gene-for-gene specificity and coevolution of the flax resistance genes and flax rust avirulence genes. *Proc Natl Acad Sci U S A* 103, 8888–8893. doi:10.1073/pnas.0602577103.

Dodds, P. N., and Rathjen, J. P. (2010). Plant immunity: towards an integrated view of plant-pathogen interactions. *Nat Rev Genet* 11, 539–548. doi:10.1038/nrg2812.

Dracatos, P., Singh, D., Fetch, T., and Park, R. (2015). Resistance to Puccinia graminis f. sp. avenae in Barley Is Associated with the Rpg5 Locus. *Phytopathology* 105, 490–494. doi:10.1094/PHYTO-08-14-0224-R.

Duxbury, Z., Ma, Y., Furzer, O. J., Huh, S. U., Cevik, V., Jones, J. D. G., and Sarris, P. F. (2016). Pathogen perception by NLRs in plants and animals: Parallel worlds. *Bioessays* 38, 769–781. doi:10.1002/bies.201600046.

Elhaddad, N. S., Hunt, L., Sloan, J., and Gray, J. E. (2014). Light-induced stomatal opening is affected by the guard cell protein kinase APK1b. *PLoS ONE* 9, e97161. doi:10.1371/journal.pone.0097161.

Ellis, J. G. (2016). Integrated decoys and effector traps: how to catch a plant pathogen. *BMC Biol* 14, 13. doi:10.1186/s12915-016-0235-8.

Figueroa, M., Upadhyaya, N. M., Sperschneider, J., Park, R. F., Szabo, L. J., Steffenson, B., Ellis, J. G., and Dodds, P. N. (2016). Changing the Game: Using Integrative Genomics to Probe Virulence Mechanisms of the Stem Rust Pathogen Puccinia graminis f. sp. tritici. *Front Plant Sci* 7, 205. doi:10.3389/fpls.2016.00205.

Ford, S. A., Kao, D., Williams, D., and King, K. C. (2016). Microbe-mediated host defence drives the evolution of reduced pathogen virulence. *Nat Commun* 7, 13430. doi:10.1038/ncomms13430.

van der Hoorn, R. A. L., and Kamoun, S. (2008). From Guard to Decoy: a new model for perception of plant pathogen effectors. *Plant Cell* 20, 2009–2017. doi:10.1105/tpc.108.060194.

Hutin, M., Césari, S., Chalvon, V., Michel, C., Tran, T. T., Boch, J., Koebnik, R., Szurek, B., and Kroj, T. (2016). Ectopic activation of the rice NLR heteropair RGA4/RGA5 confers resistance to bacterial blight and bacterial leaf streak diseases. *Plant J* 88, 43–55. doi:10.1111/tpj.13231.

Jin, Y. (1994). Inheritance of Resistance to Pathotypes QCC and MCC of*Puccinia graminis* f. sp.*tritici* in Barley Line Q21861 and Temperature Effects on the Expression of Resistance. *Phytopathology* 84, 452. doi:10.1094/Phyto-84-452.

Kang, C.-Y., Lian, H.-L., Wang, F.-F., Huang, J.-R., and Yang, H.-Q. (2009). Cryptochromes, phytochromes, and COP1 regulate light-controlled stomatal development in *Arabidopsis*. *Plant Cell* 21, 2624–2641. doi:10.1105/tpc.109.069765.

Khan, M., Subramaniam, R., and Desveaux, D. (2016). Of guards, decoys, baits and traps: pathogen perception in plants by type III effector sensors. *Curr Opin Microbiol* 29, 49–55. doi:10.1016/j.mib.2015.10.006.

Kim, H.-S., Desveaux, D., Singer, A. U., Patel, P., Sondek, J., and Dangl, J. L. (2005). The Pseudomonas syringae effector AvrRpt2 cleaves its C-terminally acylated target, RIN4, from *Arabidopsis* membranes to block RPM1 activation. *Proc Natl Acad Sci U S A* 102, 6496–6501. doi:10.1073/pnas.0500792102.

Kroj, T., Chanclud, E., Michel-Romiti, C., Grand, X., and Morel, J.-B. (2016). Integration of decoy domains derived from protein targets of pathogen effectors into plant immune receptors is widespread. *New Phytol* 210, 618–626. doi:10.1111/nph.13869.

Lazaro, A., Mouriz, A., Piñeiro, M., and Jarillo, J. A. (2015). Red Light-Mediated Degradation of CONSTANS by the E3 Ubiquitin Ligase HOS1 Regulates Photoperiodic Flowering in *Arabidopsis*. *Plant Cell* 27, 2437–2454. doi:10.1105/tpc.15.00529.

Macho, A. P., and Zipfel, C. (2014). Plant PRRs and the activation of innate immune signaling. *Mol Cell* 54, 263–272. doi:10.1016/j.molcel.2014.03.028.

Mackey, D., Holt, B. F., Wiig, A., and Dangl, J. L. (2002). RIN4 interacts with Pseudomonas syringae type III effector molecules and is required for RPM1-mediated resistance in *Arabidopsis*. *Cell* 108, 743–754. doi:10.1016/S0092-8674(02)00661-X.

Mirlohi, A., Brueggeman, R., Drader, T., Nirmala, J., Steffenson, B. J., and Kleinhofs, A. (2008). Allele sequencing of the barley stem rust resistance gene Rpg1 identifies regions relevant to disease resistance. *Phytopathology* 98, 910–918. doi:10.1094/PHYTO-98-8-0910.

Moffett, P. (2016). Using decoys to detect pathogens: an integrated approach. *Trends Plant Sci* 21, 369–370. doi:10.1016/j.tplants.2016.04.002.

Monaghan, J., and Zipfel, C. (2012). Plant pattern recognition receptor complexes at the plasma membrane. *Curr Opin Plant Biol* 15, 349–357. doi:10.1016/j.pbi.2012.05.006.

Nakai, Y., Fujiwara, S., Kubo, Y., and Sato, M. H. (2013a). Overexpression of VOZ2 confers biotic stress tolerance but decreases abiotic stress resistance in *Arabidopsis*. *Plant Signal Behav* 8, e23358. doi:10.4161/psb.23358.

Nakai, Y., Nakahira, Y., Sumida, H., Takebayashi, K., Nagasawa, Y., Yamasaki, K., Akiyama, M., Ohme-Takagi, M., Fujiwara, S., Shiina, T., et al. (2013b). Vascular plant one-zinc-finger protein 1/2 transcription factors regulate abiotic and biotic stress responses in *Arabidopsis*. *Plant J* 73, 761–775. doi:10.1111/tpj.12069.

Narusaka, M., Hatakeyama, K., Shirasu, K., and Narusaka, Y. (2014). *Arabidopsis* dual resistance proteins, both RPS4 and RRS1, are required for resistance to bacterial wilt in transgenic Brassica crops. *Plant Signal Behav* 9.

Ntoukakis, V., Saur, I. M. L., Conlan, B., and Rathjen, J. P. (2014). The changing of the guard: the Pto/Prf receptor complex of tomato and pathogen recognition. *Curr Opin Plant Biol* 20, 69–74. doi:10.1016/j.pbi.2014.04.002.

Okuyama, Y., Kanzaki, H., Abe, A., Yoshida, K., Tamiru, M., Saitoh, H., Fujibe, T., Matsumura, H., Shenton, M., Galam, D. C., et al. (2011). A multifaceted genomics approach allows the isolation of the rice Pia-blast resistance gene consisting of two adjacent NBS-LRR protein genes. *Plant J* 66, 467–479. doi:10.1111/j.1365-313X.2011.04502.x.

Ortiz, D., de Guillen, K., Cesari, S., Chalvon, V., Gracy, J., Padilla, A., and Kroj, T. (2017). Recognition of the Magnaporthe oryzae Effector AVR-Pia by the Decoy Domain of the Rice NLR Immune Receptor RGA5. *Plant Cell* 29, 156–168. doi:10.1105/tpc.16.00435.

Le Roux, C., Huet, G., Jauneau, A., Camborde, L., Trémousaygue, D., Kraut, A., Zhou, B., Levaillant, M., Adachi, H., Yoshioka, H., et al. (2015). A receptor pair with an integrated decoy converts pathogen disabling of transcription factors to immunity. *Cell* 161, 1074–1088. doi:10.1016/j.cell.2015.04.025.

Sarris, P. F., Cevik, V., Dagdas, G., Jones, J. D. G., and Krasileva, K. V. (2016). Comparative analysis of plant immune receptor architectures uncovers host proteins likely targeted by pathogens. *BMC Biol* 14, 8. doi:10.1186/s12915-016-0228-7.

Sarris, P. F., Duxbury, Z., Huh, S. U., Ma, Y., Segonzac, C., Sklenar, J., Derbyshire, P., Cevik, V., Rallapalli, G., Saucet, S. B., et al. (2015). A Plant Immune Receptor Detects Pathogen Effectors that Target WRKY Transcription Factors. *Cell* 161, 1089–1100. doi:10.1016/j.cell.2015.04.024.

Saucet, S. B., Ma, Y., Sarris, P. F., Furzer, O. J., Sohn, K. H., and Jones, J. D. G. (2015). Two linked pairs of *Arabidopsis* TNL resistance genes independently confer recognition of bacterial effector AvrRps4. *Nat Commun* 6, 6338. doi:10.1038/ncomms7338.

Solanki, S., Ameen, G., Richards, J., and S. Brueggeman, R. (2016). Modulation of integrated decoy R-genes/transcription factor assembly elicits wheat stem rust resistance responses in barley: rpg4/Rpg5-mediated Ug99 resistance. in *International Barley Genetics Symposium* Biotic Stresses., eds. K. Smith and R. Dill-Macky (Minneapolis-St. Paul, Minnesota, USA: IBGS). Available at: http://ibgs2016.org/.

Spanò, S., Gao, X., Hannemann, S., Lara-Tejero, M., and Galán, J. E. (2016). A Bacterial Pathogen Targets a Host Rab-Family GTPase Defense Pathway with a GAP. *Cell Host Microbe* 19, 216–226. doi:10.1016/j.chom.2016.01.004.

Steffenson, B. J., Solanki, S., and Brueggeman, R. S. (2016). Landraces from mountainous regions of Switzerland are sources of important genes for stem rust resistance in barley. *Alp Bot* 126, 23–33. doi:10.1007/s00035-015-0161-3.

Streubel, J., Pesce, C., Hutin, M., Koebnik, R., Boch, J., and Szurek, B. (2013). Five phylogenetically close rice SWEET genes confer TAL effector-mediated susceptibility to Xanthomonas oryzae pv. oryzae. *New Phytol* 200, 808–819. doi:10.1111/nph.12411.

Takken, F. L., Albrecht, M., and Tameling, W. I. (2006). Resistance proteins: molecular switches of plant defence. *Curr Opin Plant Biol* 9, 383–390. doi:10.1016/j.pbi.2006.05.009.

Verdier, V., Triplett, L. R., Hummel, A. W., Corral, R., Cernadas, R. A., Schmidt, C. L., Bogdanove, A. J., and Leach, J. E. (2012). Transcription activator-like (TAL) effectors targeting OsSWEET genes enhance virulence on diverse rice (Oryza sativa) varieties when expressed individually in a TAL effector-deficient strain of Xanthomonas oryzae. *New Phytol* 196, 1197–1207. doi:10.1111/j.1469-8137.2012.04367.x.

Wang, X., Richards, J., Gross, T., Druka, A., Kleinhofs, A., Steffenson, B., Acevedo, M., and Brueggeman, R. (2013). The rpg4-mediated resistance to wheat stem rust (Puccinia graminis) in barley (Hordeum vulgare) requires Rpg5, a second NBS-LRR gene, and an actin depolymerization factor. *Mol Plant Microbe Interact* 26, 407–418. doi:10.1094/MPMI-06-12-0146-R.

Wu, C.-H., Krasileva, K. V., Banfield, M. J., Terauchi, R., and Kamoun, S. (2015). The "sensor domains" of plant NLR proteins: more than decoys? *Front Plant Sci* 6, 134. doi:10.3389/fpls.2015.00134.

Yasui, Y., Mukougawa, K., Uemoto, M., Yokofuji, A., Suzuri, R., Nishitani, A., and Kohchi, T. (2012). The phytochrome-interacting vascular plant one-zinc finger1 and VOZ2 redundantly regulate flowering in *Arabidopsis*. *Plant Cell* 24, 3248–3263. doi:10.1105/tpc.112.101915.

Ye, W., and Ma, W. (2016). Filamentous pathogen effectors interfering with small RNA silencing in plant hosts. *Curr Opin Microbiol* 32, 1–6. doi:10.1016/j.mib.2016.04.003.

Yirgou, D., and Caldwell, R. M. (1963). Stomatal penetration of wheat seedlings by stem and leaf rust: effect of light and carbon dioxide. *Science* 141, 272–273. doi:10.1126/science.141.3577.272.

Zhang, J., and Zhou, J.-M. (2010). Plant immunity triggered by microbial molecular signatures. *Mol Plant* 3, 783–793. doi:10.1093/mp/ssq035.

Zipfel, C. (2008). Pattern-recognition receptors in plant innate immunity. *Curr Opin Immunol* 20, 10–16. doi:10.1016/j.coi.2007.11.003.

CHAPTER 3. VISUALIZATION AND BIOVOLUME ANALYSIS OF DIVERSE PLANT PATHOGENIC FUNGI IN PLANTA

3.1. Abstract

Assessment of pathogen colonization processes, spatially and temporally, within a host can provide a robust metric to determine compatible or incompatible interactions in a pathosystem, as well as provide needed information about the host-pathogen interactions and the colonization processes. Fluorescent tags and dyes are widely used molecular tools to understand the growth dynamics of a pathogen *in planta* through time, although barriers due to a pathogen's lifestyle or plant surface physiology can be problematic mainly due to recalcitrant pathogen transformation or suboptimal penetration of histochemical dyes. Obligate biotrophic fungal pathogens require suitable living host cells at all stages of their life cycles, thus, transformation for the generation of tagged proteins for visualization purposes using fluorescence is difficult, time consuming, and impossible for some pathogens with the current technologies. Use of histochemical dyes that specifically bind to fungal cell wall components represent a suitable method to overcome the fungal pathogen transformation barrier. Wheat Germ Agglutinin (WGA) conjugated dyes (Kobae and Ohtomo, 2016) are the most widely used probes for *in planta* histology studies of fungal pathogen growth (Meyberg, 1988; Deshmukh et al., 2006) due to specific binding of sialic acid and N-acetylglucosaminyl residues, of which the latter is a major component of fungal cell walls. Imaging fungal growth *in planta* with these dyes is still difficult, due in part to surface wax layers on the leaf that suppress dye penetration, which is especially problematic in the cereal grasses, barley and wheat. Boiling samples in basic solutions was utilized in previously published protocols for visualization of internal fungal structures including intercellular hyphae and haustoria, yet fragility of samples after boiling poses a major obstacle to

preparing representative sample slides for proper visualization of fungal structures. Here we describe a WGA conjugated fluorescent staining protocol to overcome the above described difficulties for fungal staining and visualization using confocal microscopy. Further, the method was amendable for volume analysis using Imaris software algorithms providing an excellent tool for fungal total volume quantification and surface creation for complete fungal structure visualization, even in the deepest host leaf cell layers.

3.2. Introduction

The ability of pathogens to infect, feed and ultimately proliferate on their host/s determines their host range and pathogenicity, which is dependent on interactions that occur at different times and places during the infection process. To characterize these interactions between a broad taxa of fungi and plants requires many tools and histological examination during the infection process is an important one. Remel lactophenol aniline blue (Bhadauria et al., 2010) was the most widely used stain for presumptive microscopic observation of fungi in laboratories, although it is not effective for visualization of internal fungal structures that grow inside multiple layers of host tissue. The recent advent of molecular tagging with fluorescent dyes provided an excellent tool for fungal visualization, especially when growing inside host tissue. Although obligate biotrophic fungal pathogens such as *Puccinia graminis* f. sp *tritici*, the causal agent of the disease wheat stem rust, require intimate host association for their survival, establishment, and colonization, thus, transformation using fluorescently tagged proteins is not possible with the current technologies.

Many fluorescent dyes are amiable for histochemical staining of fungi in planta (Coleman et al., 1989) such as those that bind chitin which is abundantly found in fungal cell walls, but is not a molecule present in plants. Yet, the efficacy and effectiveness of these dyes to stain fungal

structures inside the host tissue is limited mainly due to penetration, which is mainly due to the physiology of host cuticle and cell walls. Calcofluor white and Uvitex 2B are commonly used fluorescein in clinical and plant studies although Calcofluor white fades quickly and is not very efficient after counterstaining (Bonifaz et al., 2013). Solophenyl flavine will stain fungal cell wall and fades slowly compare to calcofluor white (Hoch et al., 2005), yet requires a safranin counterstain of the plant tissues for differentiation while imaging (Knight and Sutherland, 2011). Uvitex 2B provides an alternate solution (Diagne et al., 2011; Dugyala et al., 2015), but use of formalin as a fixative for specimens drastically reduces the fluorescent intensity of Uvitex 2B (van Gool et al., 1993). Further, the corrosive and irritant nature of these chemicals make sample handling hazardous.

The protocol developed and reported here is very efficient and effective in fungal structure staining and visualization inside layers of host tissue. This effective visualization using Wheat Germ Agglutinin (WGA) conjugated dyes (Kobae and Ohtomo, 2016) by autoclaving the samples on slides overcomes the fragility of samples. This was a major obstacle with the previous protocols for preparing representative sample slides for robust visualization of fungal structures *in planta*. The quality of the images generated allows for fungal volume analysis using Bitplane-Imaris software which is an excellent tool for fungal total growth volume quantification and surface creation for complete fungal structure visualization, even deep host leaf cell layers.

3.3. Material and methods

3.3.1. Plant material, pathogen, inoculations procedure and sample collection

For inoculation and visualization *in planta* we utilized *Puccinia graminis* f. sp. *tritici* (*Pgt*) the biotrophic fungal pathogen that causes the disease stem rust on barley and wheat and the necrotrophic pathogen *Bipolaris sorokiniana,* which causes the leaf spot disease spot blotch

on barley and wheat. *P. graminis* f. sp. *tritici*, race QCCJ was used for inoculations which is a surrogate race for the highly virulent race *P. graminis* f. sp. *tritici* race TTKSK (Brueggeman et al., 2008). Stem rust inoculations were performed on the resistant barley cultivar Q21861, known to carry the *rpg4*/*Rpg5*-mediated resistance locus (*RMRL*), effective against *Pgt* races QCCJ and TTKSK (Wang et al., 3014; Steffenson et al., 2016). For the *Pgt* compatible interaction the universal susceptible barley cultivar (cv) Steptoe was inoculated. The susceptible wheat cv Morocco was also inoculated and used to determine if the protocol works with the same efficiency for wheat. The necrotrophic pathogen *Bipolaris sorokiniana* was used to determine if staining and visualization of fungal structure inside host leaves associated with dying and dead tissue is also efficient using these methodologies. The spot blotch resistant barley cultivar Bowman and the γ-irradiation induced spot blotch susceptible mutant in the cv Bowman background, *nec3,* were inoculated with *B. sorokiniana* isolate ND85F.

P. graminis f. sp. *tritici* inoculations were carried out according to previously published methods (Steffenson et al., 2016). In brief, nine-day old barley and wheat plants were inoculated with stem rust urediniospores on fully expanded primary leaves. 10mg/ml of urediniospores mixed in soltrol oil was used to inoculate each 96-cone rack having one seed per cone. ~ 800 µl spore mixture was sprayed in form of fine mist for uniform inoculations. Plants were kept in the dark humidity chamber at 100% humidity immediately after drying surface oil at 20°C. After 18 hours of darkness at 100% humidity the inoculated seedlings were transferred to a growth chamber with a 16-hour light cycle starting at 7:00 AM till 10:59 PM and an 8-hour dark cycle starting at 11:00 PM till 6:59 AM while maintained at 21°C. A 3-cm cutting from the center of primary inoculated leaves were collected. For the necrotrophic pathogen infected barley samples, 15-day old barley seedlings of cv Bowman and the *nec3* mutant were inoculated with *Bipolaris*

sorokiniana isolate ND85F (pathotype 1). This isolate has been a common isolate used for resistance screening over the past 20 years (Zhou and Steffenson, 2013). The inoculation procedure utilized was as previously described by Fetch and Steffenson (1999). In short *Bipolaris sorokiniana* isolate ND85F was grown on V8-PDA at 21℃ under a 12-hour photoperiod. Conidia were collected by gently scrapping five days old growing mycelial culture on V8 PDA plates and a suspension of ~2,000 conidia/ml in distilled water amended with 10µl/100ml of Tween-20 to facilitate distribution and adherence. The plants were inoculated using a fine mist generated by spray inoculators. The inoculated barley plants were placed in a humidity chambers with 100% humidity for 16-hours and then moved to growth chambers with a 16h light and 8 h dark photoperiod at 21℃. The leaf tissue was collected at 24 hours post inoculation. The inoculated leaves on intact seedlings were evaluated 10 days post inoculation according to the spot blotch rating scale (Fetch and Steffenson, 1999).

3.3.2. Fixation and clearing of leaf samples

Anhydrous Farmers Fixative (FF), 3 EtOH : 1 Glacial acidic acid, was used to fix and clear the infected leaf samples. The fresh leaf samples (~ 3 cm) were placed in 50 mL polypropylene tubes with 40 mL FF and rotated at ~25^{o} C for 6 hours at 130 rpm in an orbital shaker. The cleared and fixed leaf samples were stored in fresh FF until staining.

3.3.3. Heat treatment of cleared samples for efficient stain penetration

A major hurdle to visualize pathogen structures developed inside the plant tissue is the penetration of fluorescence dyes due to presence of the cuticle waxy layers on the leaf surface. To facilitate the penetration of dyes through leaf epidermis, previously published protocols (Ayliffe et al., 2011) suggested autoclaving the leaf samples for 15 minutes at 121℃ in 1M KOH supplemented with a wetting agents such as Silwet-L77. However, this process leads to very

fragile leaf tissue samples after autoclaving (Fig. 3.1.A). These fragile leaf samples result in a high proportion of sample disruption during the staining and microscopic slides transfer process which results in wasted consumables and time.

The method described here enables the user to process fixed and cleared leaf samples for autoclaving, washing, staining, and mounting on the microscope slides, thus avoiding all possible sample disruption during handling prior to visualization under the microscope.

First, samples were removed from FF and washed in 30 ml 1x PBS (Phosphate Buffer Saline - 0.256 g NaH_2PO_4, 1,194 g Na_2HPO_4 and 10.2 g NaCl mixed in one liter, solution adjusted at pH 7.4) supplemented with 0.05% Tween 20, twice for five minutes at 60 rpm. Again, sample were washed two times for five minutes at 60 rpm with Tris HCl pH 7.4+ 0.05% Tween-20 to remove residual farmer's fixative from the tissues which is critical before the staining process. Alternate washing with PBS and Tris HCl helps in proper washing and pH maintenance of samples.

Before transferring the samples to the slides, a hydrophobic oval boundary is applied using ImmeEdge hydrophobic barrier PAP pen (Fig. 3.1.C). The slide is then placed on a autoclavable empty pipette tip tray to allow for ease of handling. The washed leaf samples were carefully transferred to the glass slide inside the hydrophobic boundaries, keeping the adaxial surface of leaf sample facing up. 350µl 1M KOH + 0.05 % Tween-20 solution was carefully pipetted onto the leaf sample keeping the sample and solution inside the hydrophobic barrier. The hydrophobic barrier helps to maintain the liquid solution on the glass slide covering the leaf sample and keeping it hydrated and submerged (Fig. 3.1.C). The tray with the slide on top was kept on a plate shaker at 50 rpm for three minutes then the solution was replaced with fresh 1M KOH + 0.05 % Tween-20 solution using a 1 ml pipette. The sample-slides were then autoclaved

on top of the tip box on the liquid cycle for 15 minutes, 121℃ at 15 PSI. After autoclaving, the remaining KOH buffer was pipetted off the slide and the slides were cleaned with a Kim wipe to remove the distorted hydrophobic boundary (Fig. 3.1.D) without disturbing the autoclaved leaf sample. Then a new hydrophobic boundary was made encircling the sample. This slide autoclaving procedure avoids sample disruption mainly due to fragility as a result of sample boiling in excess KOH solution and subsequent sample transfer and handling. After applying the new hydrophobic barrier, the samples were washed twice with 1x PBS pH 7.4 + 0.05 % Tween-20 solution for 5 minutes at 50 rpms and the buffer solution was pipetted off.

Fig. 3.1.A Fig. 3.1.B Fig. 3.1.C Fig. 3.1.D

Fig. 3.1. Sample processing on the glass slide. **(A)** Fragile leaf bits due to autoclaving in 1M KOH. **(B)** Hydrophobic barrier made by ImmeEdge PAP pen on the glass slide. **(C)** Hydrophobic barrier containing the leaf sample, buffer and staining solution inside the boundaries thus leaf remain submerged. **(D)** distorted hydrophobic boundary due to autoclaving and KOH.

3.3.4. Sample staining and mounting

Samples were stained with a final concentration of WGA-Alexa Fluor 488 dye (20µg/ml) dissolved in PBS buffer (pH 7.5) supplemented with 0.05% Tween 20. For immediate staining 350µl of dye was pipetted onto the samples inside the hydrophobic boundary after removal of the

PBS buffer. This procedure allows for the use of a small amount of staining solution (350µl) for each sample, which greatly reduces the cost of the experiment as staining in tubes or small glass petri plates required at least 15-20 mL of staining solution. Samples were stained for one hour at 50 rpm rotation at room temperature. However, 10-15 minutes of staining worked equally as well. Longer staining must be avoided as evaporation of buffer staining molecules remain tightly bound to the leaf surface resulting in high background fluorescence.

After staining, the samples were washed thrice with Tris HCl pH 7.4 for 5 minutes at 60 rpm to remove the excess dye on the leaf surface. 200 µl of 20 % glycerol was pipetted onto the leaf sample and left for five minutes. Finally, the glycerol was pipetted off, the hydrophobic barrier was removed and the glass around the sample was cleaned using Kim wipe. To prepare slides for confocal microscopy, enough 40% glycerol was pipetted onto the sample to cover thoroughly and a coverslip was carefully placed on the samples starting from one end of the glass slide to avoid trapping air bubbles. The slides were sealed with quick dry Sally Henson double duty nail paint top coat and stored in dark at 4℃ until visualized under the microscope. We observed that properly stored slides retain fluorescence for more than 2 months without losing emittance efficiency. Prepared slides were visualized by Zeiss Observer Z1 microscope equipped with LSM 700 laser scanning confocal head using Plan-Apochromat 40x/1.3 oil immersion lens and 10x/0.45 NA (Zeiss, Thornwood, NY). Green channel 488 was assigned for WGA-Alexa fluor staining and red channel 555 was used for auto fluorescence detection. For inner structure visualization Z-stack images were taken depending upon the depth of stem rust structures developed inside the plant system (100-300 images per infection site20 to 100 microns thick). Images were analyzed using the Imaris (9.0.1) software (Bitplane, South Windsor, CT) by reconstructing the pathogen and the leaf structures for volume and interaction analyses.

3.3.5. Image capturing and analysis

Images were processed in Imaris 9.0.1 software. Imported pictures were subjected to channel correction for red and green channel. Image processing was performed using attenuation correction for the green channel using intensity front 256 and intensity back 128 values. Smoothing for channel green was performed using median filter size 5x5x5. Processed images were subjected to contrast change using normalized layers to remove the background. This process enabled the visualization and 3D reconstruction of pathogen growth inside the plant cells while removing the background plant noise as recorded in the red channel. Once pathogen growth volume area was determined, using the surface creation function, the surface area of pathogen growth was created specifically for the green channel using surface detail value 0.491 at absolute thresholding. All nonspecific signals were removed using volume filtering. All the artifact surface creation was removed manually, and statistical analysis was run for surface volume assessment using the total volume of fungal structures present from appressoria to in planta growth. It is important to create the surface avoiding overexposure which facilitates the loss of poorly stained pathogen, yet causes inclusion of plant structures and underestimates the computed volume of pathogen structures, thus it is important to calculate volume as a function of average value for all the constructed surfaces.

3.4. Results

3.4.1. Visualization of fungal structures

Upon fungal staining and microscopy, we were able to visualize pathogen structures growing inside and outside the leaf surface in resistance and susceptible barley lines and susceptible wheat line. For each fungal infection spot Z stacked were used for analysis. For *P. graminis* f. sp. *tritici* visualization of germ tubes, appressoria, sub-stomatal vesicles, primary

infection hyphae, and haustoria were clear (Fig. 3.2.A, 3.2.B, 3.2.C) enabling the determination of pathogen growth.

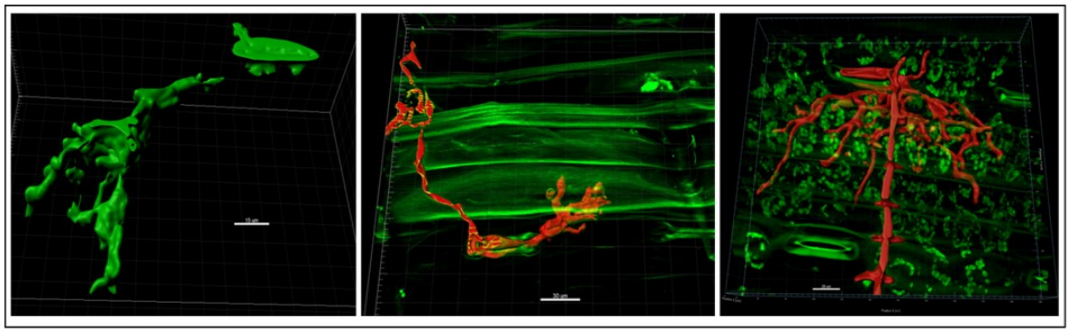

Fig. 3.2.A Fig. 3.2.B Fig. 3.2.C

Fig. 3.2. *Puccinia graminis* growth captured using surface creation in barley and wheat genotypes at 48 hours post inoculation. Images of pathogen structures were captured starting from spore germination, germ tube growth, appressoria formation, sub stomatal vesicle development, intercellular hyphae growth and haustoria formation. **(A)** Pathogen growth showing appressoria and intercellular hyphae on resistant barley line Q21861 without the background plant surface. **(B)** The wheat susceptible genotype Morocco inoculated with *Puccinia graminis* and images taken at 48 HPI showing *Puccinia graminis* growth red and background plant tissue green. **(C)** The susceptible barley cv Steptoe showing *Puccinia graminis* growth red and background plant tissue green.

High quality images were also produced during the infection process with the necrotrophic pathogen *Bipolaris sorokiniana* on the susceptible barley mutant line *nec3* and resistant cultivar Bowman, which produces germ tubes from both ends of the conidia and directly penetrate a single epidermal cell with infection hyphae where it forms a haustoria-like structures (Carlson et al., 1991) and later continue to invade neighboring epidermal cells and mesophyll cells (Fig. 3.3.A). After the initial colonization the necrotroph induces cell death supporting its lifestyle. A dark background was observed depicting the area of cell death requirement for the establishment of pathogen (Fig. 3.3.A). Thus, this protocol is also able to detect cell death due to the detection of the pathogen resulting in incompatible (resistant) or compatible (susceptible) reactions depending on the lifestyle of pathogen, biotroph or necrotroph, respectively (Fig. 3.3.B).

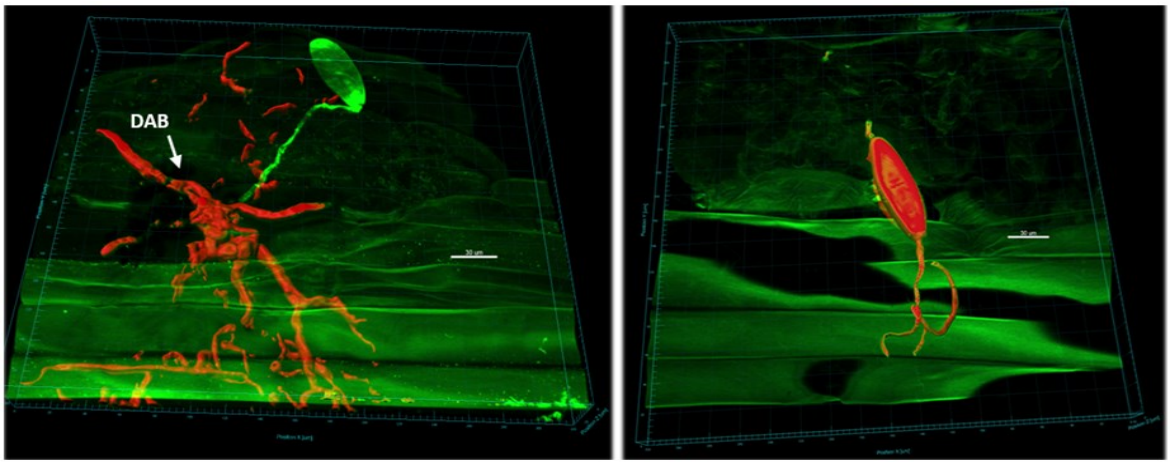

Fig. 3.3.A Fig. 3.3.B

Fig. 3.3. Visualization of necrotrophic pathogen structures. *Bipolaris Sorokiniana* growth captured at 24-hour post pathogen inoculation using surface creation in susceptible and resistant barley genotypes. Pathogen structures were captured starting from conidia, bipolar germ tube, penetration, and intercellular hyphae growth. **(A)** Pathogen growth from conidia to inter cellular hyphae on the susceptible *nec3* mutant in the cv Bowman background. Surface growth was rendered in green. The black area surrounding the penetration site indicates cell death and absence of autofluorescence from plant tissues. **(B)** Resistant barley Bowman with *Bipolaris* growth red and background plant tissue green.

3.4.2. Surface creation and fungal surface calculation

Using the surface creation function specifically for the fungal structures stained with AF-488 (green) and avoiding background autofluorescence (red) of plant structures we calculated the volume of pathogen growth for both necrotrophic and biotrophic pathogens in planta for a representative infection site (Fig. 3.4.A, 3.4.B). For *Pgt* and *B. sorokiniana* one fungal infection site was analyzed in resistant and susceptible hosts. *Pgt* biovolume at 48 HPI in susceptible barley line Steptoe was 37205.9 μm^3 whereas in resistant Q21861 was 12342.7 μm^3. In Morocco wheat *Pgt* biovolume was recorded 6473.27 μm^3 at 48 HPI. *Bipolaris sorokiniana* biovolume was recorded in barley resistant Bowman and susceptible *Nec3* 32907.1 μm^3 and 55484.3 μm^3 respectively.

The data clearly showed differential pathogen growth between the resistance and susceptible barley lines during the early infection process, a critical determinant of pathogen virulence on adapted host.

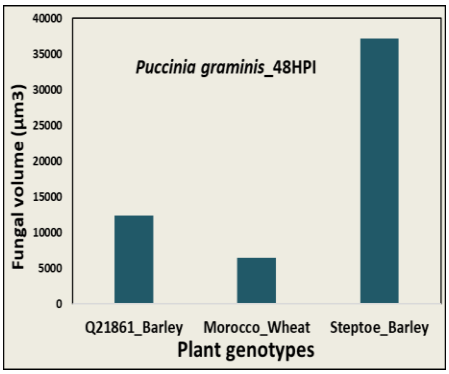

Fig. 3.4.A

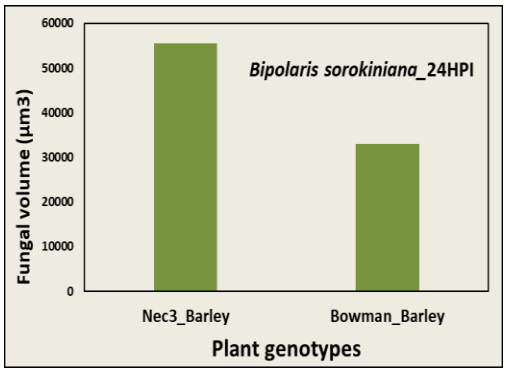

Fig. 3.4.B

Fig. 3.4. Fungal biovolume analysis on biotroph (*Pgt*) and necrotroph pathogen (*B. sorokiniana*) on host plants. Y axis represents the fungal biovolume in μm^3 and X axis represents the different plant hosts. **(A)** *Pgt* biovolume calculation at 48 HPI on barley (resistant- Q21861 and susceptible- Steptoe) and wheat (susceptible- Morocco) host **(B)** *B. sorokiniana* biovolume calculation at 48 HPI on barley (resistant- Bowman and susceptible – Bowman gamma mutant *Nec3*).

3.4.3. Cost comparison

An advantage of the method described is the overall reduction in use of chemicals. Cost of WGA-AF488 is a major consideration when designing experiments as it is a relatively expensing fluorescent stain. In conventional methods, at least 15-20 mL of staining solution (20µg AF/mL) is required for proper submerging of samples stained in small petri plates or 50 mL polypropylene tubes. Thus, only thirteen different sample types can be processed possibly having three biological replicates and totaling 39 individual samples, with five gm of AF constituting 250 mL of staining solution (20µg/ml). Our new method uses only 350µl of staining solution for each sample slide, thus 715 individual slides can be processed using 5 gm of WGA-AF-488 (Fig. 3.5). However, processing multiple samples together using the conventional methods can reduce the use of staining solution yet the difference remains remarkable.

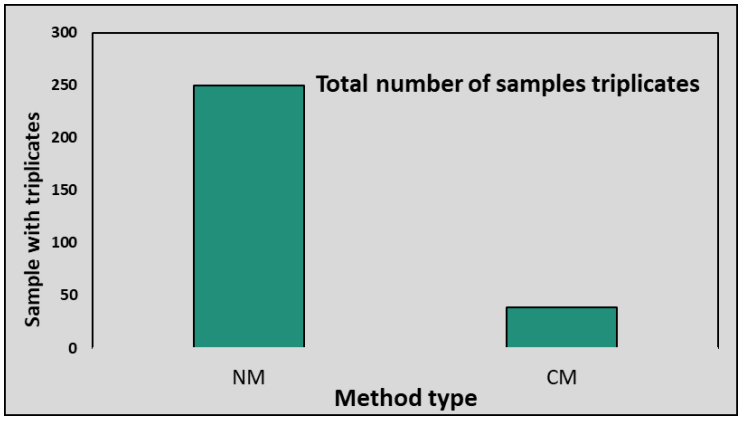

Fig. 3.5. A comparison of new method (NM) with conventional methods (CM) for total number of sample slides using 20µg/ml WGA-AF488 stain. More than six times number of samples can be processed using equal amount of stain.

3.5. Discussion and conclusions

The protocol developed and described here significantly enhances the current methodology for staining, visualization and biovolume analysis of fungal pathogens in-planta, an important tool in the study host-pathogen interactions irrespective of their life style i.e. biotrophy or necrotrophy in diverse hosts. The unique sample preparation method on glass slides using hydrophobic barriers to retain buffers and stains avoids all possible mishandling during autoclaving, sample transfer and staining procedure, thus enabling more robust sample preparation reducing the time spent preparing and analyzing samples, significantly lowering the amount of expensive reagents consumed, and facilitating the generation of high quality images and accurate pathogen volume analysis. Further, a method for biovolume calculation was developed and described which can be very useful to understand the progression of pathogen colonization and growth inside the host. Presented method works equally well to stain and visualize biotrophic or necrotrophic fungal pathogens and their intercellular structures in different cereal host species and their biovolume calculation. Biovolume calculation for *Pgt* a biotroph fungal pathogen on barley at 48 HPI reveals presence of approximately three times

more fungal volume in the susceptible host Steptoe (37205.9 μm^3) comparing with resistant host Q21861 (12342.7 μm^3). In susceptible wheat cultivar Morocco *Pgt* biovolume was 6473.27 μm^3, less than resistant barley Q21861. However, a definite conclusion cannot be made with only one fungal infection site biovolume calculation and a detailed study to explore this perspective will be required. For necrotroph growth analysis, in resistant barley cv. Bowman, *Bipolaris sorokiniana* biovolume was 32907.1 μm^3, 1.69-fold less than susceptible Bowman gamma ray induced mutant *Nec3* (55484.3 μm^3) at 24 HPI. Thus, comparison of fungal growth can be analyzed at different time points during infection process for resistant or susceptibility response of host. Further, use of very less reagents and fungal cell wall specific WGA-Alexa Fluor-488 dye significantly reduces the cost of experiment. This method is easy to use, effectively visualize fungal structures inside the plant tissues, reproducible and saves in reagent costs thus will provide a valuable tool to study host pathogen interaction avoiding the requirement of fungal transformation to efficiently visualize pathogen internal growth structures.

3.6. Literature cited

Ayliffe, M., Devilla, R., Mago, R., White, R., Talbot, M., Pryor, A., and Leung, H. (2011). Nonhost resistance of rice to rust pathogens. *Mol Plant Microbe Interact* 24, 1143–1155. doi:10.1094/MPMI-04-11-0100.

Bhadauria, V., Miraz, P., Kennedy, R., Banniza, S., and Wei, Y. (2010). Dual trypan-aniline blue fluorescence staining methods for studying fungus-plant interactions. *Biotech Histochem* 85, 99–105. doi:10.1080/10520290903132196.

Bonifaz, A., Rios-Yuil, J. M., Arenas, R., Araiza, J., Fernández, R., Mercadillo-Pérez, P., and Ponce-Olivera, R. M. (2013). Comparison of direct microscopy, culture and calcofluor white for the diagnosis of onychomycosis. *Rev Iberoam Micol* 30, 109–111. doi:10.1016/j.riam.2012.07.001.

Coleman, T., Madassery, J. V., Kobayashi, G. S., Nahm, M. H., and Little, J. R. (1989). New fluorescence assay for the quantitation of fungi. *J Clin Microbiol* 27, 2003–2007.

Deshmukh, S., Hückelhoven, R., Schäfer, P., Imani, J., Sharma, M., Weiss, M., Waller, F., and Kogel, K.-H. (2006). The root endophytic fungus Piriformospora indica requires host cell

death for proliferation during mutualistic symbiosis with barley. *Proc Natl Acad Sci U S A* 103, 18450–18457. doi:10.1073/pnas.0605697103.

Diagne, N., Escoute, J., Lartaud, M., Verdeil, J. L., Franche, C., Kane, A., Bogusz, D., Diouf, D., Duponnois, R., and Svistoonoff, S. (2011). Uvitex2B: a rapid and efficient stain for detection of arbuscular mycorrhizal fungi within plant roots. *Mycorrhiza* 21, 315–321. doi:10.1007/s00572-010-0357-8.

Dugyala, S., Borowicz, P., and Acevedo, M. (2015). Rapid protocol for visualization of rust fungi structures using fluorochrome Uvitex 2B. *Plant Methods* 11, 54. doi:10.1186/s13007-015-0096-0.

Van Gool, T., Snijders, F., Reiss, P., Eeftinck Schattenkerk, J. K., van den Bergh Weerman, M. A., Bartelsman, J. F., Bruins, J. J., Canning, E. U., and Dankert, J. (1993). Diagnosis of intestinal and disseminated microsporidial infections in patients with HIV by a new rapid fluorescence technique. *J Clin Pathol* 46, 694–699.

Hoch, H. C., Galvani, C. D., Szarowski, D. H., and Turner, J. N. (2005). Two new fluorescent dyes applicable for visualization of fungal cell walls. *Mycologia* 97, 580–588.

Knight, N. L., and Sutherland, M. W. (2011). A rapid differential staining technique for Fusarium pseudograminearum in cereal tissues during crown rot infections. *Plant pathology* 60, 1140–1143. doi:10.1111/j.1365-3059.2011.02462.x.

Kobae, Y., and Ohtomo, R. (2016). An improved method for bright-field imaging of arbuscular mycorrhizal fungi in plant roots. *Soil science and plant nutrition* 62, 27–30. doi:10.1080/00380768.2015.1106923.

Meyberg, M. (1988). Selective staining of fungal hyphae in parasitic and symbiotic plant-fungus associations. *Histochemistry* 88, 197–199.

CHAPTER 4. EVADING THROUGH DARK: ENTRY OF WHEAT STEM RUST IN BARLEY DOES NOT REQUIRE LIGHT INDUCED STOMATAL OPENING

4.1. Abstract

Puccinia graminis asexual urediniospore infection of host plants is considered biphasic. The first phase, spore germination, requires a dark period with high moisture and the second phase, stomatal penetration, occurs via appressorium formation over the guard cells and was hypothesized to require the morning light to induce stomate opening. The requirement of light for pathogen penetration through the stomatal pore was considered absolutely required, as it was shown that an extended dark period extending past the required time for germination inhibited colonization due to the inability of stomatal penetration through closed stomates in the dark. In the present study, we have challenged this long-held paradigm by showing *Puccinia graminis* f. sp. *tritici* (*Pgt*) race QCCJ and HKHJ penetration during extended dark period in both resistant (Q21861 and HQ18) or susceptible (Steptoe and Harrington) barley lines along with the susceptible wheat line Morocco. Detailed microscopic visualization and fungal biovolume analysis for QCCJ shows fungal intercellular infection hyphae below the guard cells indicating successful penetration in extened dark period in both resistsnt and suceptible plants. However, branching and haustoria development were reduced showing significantly lower fungal biovolume *in planta* in the susceptible cultivar Steptoe under continuous dark compared to the normal light/dark cycle indicating that light induces developmental changes in the pathogen and plays a critical role in the pathogen establishment and colonization. We have concluded that *Pgt* penetration through stomata does not require the light and major differences in the pathogen growth dynamics in resistant and susceptible genotypes takes place for 62-86 hours post pathogen inoculation in the normal dark and light treated plants.

4.2. Introduction

The biotrophic fungal pathogen *Puccinia graminis* (*Pg*) causes "Stem Rust", one of the most devastating disease of the cereal hosts including wheat and barley that are important crops produced in the grain baskets of the world (Leonard and Szabo, 2005; Brueggeman and Solanki, 2017; Solanki et al., 2016; Steffenson et al., 2016). The mechanisms of *Puccinia graminis* f. sp. *tritici* (*Pgt*) infection on their primary grass hosts requires asexual urediniospores landing on the host, its germination in the dark with extension of germ tubes within 3-5 hours after contacting the leaf surface (Leonard and Szabo, 2005). This process evolved to occur during the night when high humidity allows for dew formation on the stem and leaf sheath to avoid germ tube and appressoria desiccation during the heat of the day. Germ tubes grow perpendicular to leaf veins until they encounter stomata. The topology of host guard cells plays an important role in stomata identification and formation of appressorium around 4 -16 hours post inoculation (Figueroa et al., 2016). The appressoria forms a penetration peg and substomatal tube between the two guard cells and initiate substomatal growth. This is shortly followed by formation of primary infection hyphae (PIH) that grow intracellularly until encounters the mesophyll cells. Contact with the mesophyll cells induces differentiation and the formation of the haustorial mother cells. From the haustorial mother cells located at the outside of the mesophyll cells degradation of the cell wall occurs followed by invagination of the host cell plasma membrane leading to the formation of haustoria. The haustoria is the pathogen's feeding structure acting as powerhouse of pathogen colony growth. The haustoria also facilitates pathogen manipulation of the host as the pathogen hijacks host cell physiology utilizing an effector repertoire that establishes an artificial nutrient sink that leads to pathogen feeding and profuse growth. In a short period of time, ~7-10 days, a life cycle shift results in the formation of Uredinium and millions of Urediniospores erupting

from the epidermis of the stem and leaf surface ~10-14 days after infection fulfilling the pathogen's main goal of reproduction (Leonard and Szabo, 2005). The urediniospores act as secondary inoculum continuing the cyclic disease which rapidly develops into an epidemic when conducive environmental conditions and susceptible hosts are available.

Pathogen signs occur primarily on the stem and leaf sheaths but may also be found on leaves and glumes. Typical signs of *Pgt* are characterized by small chlorotic flecks 4-5 days after inoculation, progressing into round to elongated diamond shaped brick red lesions on its cereal host ~8-10 days post inoculation (Roelfs, 1985; Roelfs and Bushnell, 1985). Successful colonization from asexual *Pgt* urediniospores requires high humidity and an initial dark period after landing on the leaf surface (Givan and Bromfield, 1964, 1963; Yirgou and Caldwell, 1968). The dark period is shown to absolutely required for spore germination and high humidity favors germination, thus is also critical for early establishment. Temperature also plays a crucial role in germination efficiency and low temperature (15℃-23℃) is required for effective germination (Givan and Bromfield, 1963; Burrage, 1970). This initial dark, cool and humid period is required for early establishment, which involves spore attachment, germination, and the formation of specialized appressoria on top of host stomatal guard cells that is the only mechanism of *Pgt* penetration. An early study by Helen Hart (Hart, 1929) using the wheat variety Webster and Little club inoculated with *Pgt* with extended dark periods post inoculation showed that the majority of spores failed to penetrate wheat. However, the appearance of few, very minute pustules were attributed to infection near to leaf tip possibly entering through hydathodes or due to forced entry via a single germ tube. Inoculations made away from leaf tips and given extended dark period for 9 days did not resulted in any sporulation in these wheat lines except one case that was attributed to the possibility of a random open stomata. Thus, it was concluded that *Pgt*

entry into wheat and barley requires opening of stomata due to light stimulus rather than pathogen induced stomatal aperture opening. Henceforth the penetration through the stomatal guard cells is considered to be light dependent for stem rust and it was concluded that appressoria remain quiescent on top of stomata until light induced stomatal opening facilitate pathogen penetration (Yirgou and Caldwell, 1963, 1968; Figueroa et al., 2016; Wu et al., 2015; Garnica et al., 2014).

In the present study, we demonstrated the ability of wheat stem rust *P. graminis* f. sp. *tritici* race QCCJ to penetrate the stomatal guard cells gaining entry to the barley and wheat hosts in the absence of light during the dark period, a sharp contrast to previous interpretation of the stem rust infection process. Given extend periods of continuous dark treatment 48 Hours Post Inoculations (HPI), 62 HPI and 86 HPI after inoculation of barley and wheat plants, we observed phenotypic differences on the leaf for disease progression and pustule development after 6-day post pathogen inoculation, indicating a slow and latent intercellular growth in the dark after successful initial penetration. Microscopic observations confirmed the penetration of QCCJ during dark period, yet the branching of PIH in the normally dark-light cycle treated plant were profuse and tend to have more intercellular volume. Our study presents a new paradigm in the understanding of the penetration and colonization processes in the *P. graminis*-cereal host pathosystems.

4.3. Material and methods

4.3.1. Plant maintenance and pathogen inoculations

Five plant genotypes including two *P. graminis* f. sp. *tritici* susceptible and two resistant barley lines and the susceptible wheat line Morocco, were used in the study. The barley line utilized were the universally susceptible lines Steptoe (*RMRL-/Rpg1-*) and Harrington (*RMRL-*

/Rpg1-) and the highly resistant line Q21861 (*RMRL+/Rpg1+*). The *RMRL+/Rpg1+* genotype is resistant to all known stem rust pathotypes. A resistant Near Isogenic Line (NIL) HQ18 (*RMRL+/Rpg1*-) was created by transferring the *RMRL* into the Harrington genetic background (Harrington x Q21861) by repetitive backcrossing to the BC_6 generation. Two different *P. graminis* f. sp. *tritici* races, QQCJ (virulent on *Rpg1*) and HKHJ (virulent on *RMRL*), were used. The *RMRL* provide effective resistance against *Pgt* race QCCJ, and *Rpg1* provide resistance for *Pgt* race HKHJ.

Nine days old plants were used for stem rust urediniospores inoculation on fully expanded primary leaves. A 10 mg/ml inoculation mixture in lightweight mineral oil (Soltrol 170 isoparaffinic oil, Chevron Phillips chemical company) of freshly collected urediniospores was used to inoculate each 96-cone rack having one plant per cone. ~ 700 µl spore mixture was sprayed in form of fine mist with specialized rust inoculators (Browder, 1971) at 20kPa pressure using an air pump for uniform inoculations. Plants were kept in dark humidity chamber immediately after the drying of the surface oil at 20°C.

4.3.2. Controlling of dark period time points after inoculation and sample collections

Growth chambers for plant maintenance were set to provide 16 hours of light starting from 7 A.M. - to 11 P.M. and 8 hours of dark from 11 P.M. to 7 A.M at 21°C (Fig. 4.1). Plants were inoculated at 12:30 A.M. night, after shutting down of growth chamber lights providing 1.5 hours of dark period before pathogen inoculation to ensure closer of leaf stomata. After the initial incubation period of 18 hours dark and 100% humidity required for germination, one rack of inoculated seedlings containing the five barley and wheat genotypes described above were transferred into growth chambers providing normal growth conditions for plants i.e. 16 hours of light starting from 7 A.M. - to 11 P.M. and 8 hours of dark from 11 P.M. to 7 A.M. The second

rack of inoculated barley seedlings were given extended dark period treatment. After removing the rack from the humidity chamber, they were placed into a dark growth chamber without exposing them to any light (Fig. 4.1). We assayed plants exposed to continuous dark periods of 48 Hours Post Inoculation (HPI), 62 HPI and 86 HPI before moving them to a growth chamber with the normal light cycle and growth conditions. Through the experiment temperature was maintained at ~20-21℃.

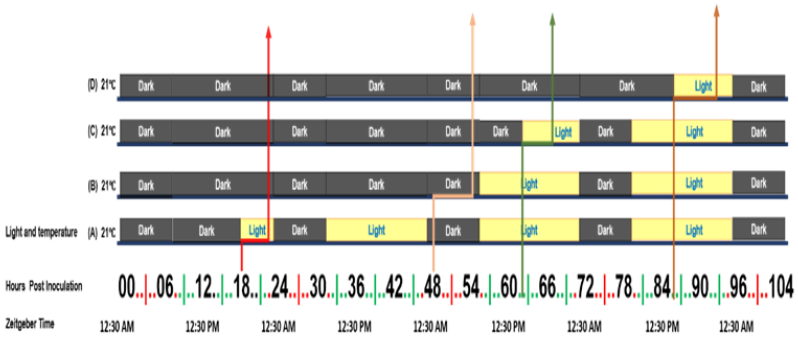

Fig. 4.1. Growth chamber light conditions at different leaf sample collection time after *P. graminis* f. sp. *tritici* races QCCJ and HKHJ inoculations on host plants. Arrows indicate sample collection times i.e. (A) 18 HPI, (B) 48 HPI, (C) 62 HPI and (D) 86 HPI at different light conditions represented by horizontal bars applied to seedlings used for phenotyping at ~6.5 and 14 days post inoculation. The later three-time points (B, C, D) were used for sample collection for confocal microscopy.

4.3.3. Disease phenotyping

Phenotyping for pathogen signs and plant symptoms was performed at 6.5th days after pathogen inoculation (DPI) for 18 HPI, 48 HPI, 62 HPI and 86 HPI dark treated plants for presence of spore pustules and chlorotic spots on leaf. Later at 14th DPI disease phenotyping was carried out using modified Stakman IT (Infection Type) scale used for barley (Steffenson et al., 2009; Stakman et al., 1962).

4.3.4. Fixing, clearing, and staining of the leaf samples

2.5-centimeter long cuttings from the middle portion of primary leaves was collected at each time point and immediately stained for six hours in freshly made DAB (3,3′-Diaminobenzidine) solution. Leaf samples were washed with sterilized water twice for five minutes before transferring into anhydrous farmers fixative (Ethanol 3 parts: Glacial acidic acid 1 part) for fixing as well as leaf clearing. Samples were stored in fresh farmer's fixative until processed for microscopy staining purposes. For staining, samples were removed from farmers fixative and washed in PBS buffer supplemented with 0.05% Tween-20 twice at 60 rpm. Again, the samples were washed twice with Tris HCl pH 7.5 + 0.05% Tween-20. Later, the samples were transferred to a corning glass slide on which hydrophobic boundaries were made using a ImmeEdge hydrophobic barrier PAP pen. Then, 350 µl 1M KOH supplemented with 0.05 % Tween-20 solution was pipetted onto the leaf inside the hydrophobic barrier. Thus, the hydrophobic barrier helped to maintain the liquid solution covering the leaf sample on the slide. Sample was incubated for five minutes and then replaced with fresh KOH + 0.05 % Tween-20 solution. These slides were autoclaved on top of a mini bench in a liquid cycle autoclave for 15-minutes (121℃at 15 PSI). After autoclaving samples, a fresh hydrophobic boundary was applied, and the samples were washed twice with Tris HCl pH 7.5 solution. Finally, the samples were stained with WGA-Alexa Fluor 488 dye (20 µg/ml) dissolved in 1x PBS buffer supplemented with 0.05% Tween-20. 350 µl dye solution was pipetted on the samples inside the hydrophobic boundary. The samples were stained for one hour at 50 rpm rotation at room temperature. After staining samples were washed twice with Tris HCl pH 7.5 to remove the excess dye on the leaf surface. 200 µl 20% glycerol was pipetted onto the leaf sample and left for 5 minutes. Finally, the glycerol was pipetted out, hydrophobic barrier was removed and glass

around the sample was cleaned using Kim-wipes. To prepare slides for confocal microscopy, enough 40 % glycerol was pipetted to cover the sample and a coverslip was carefully placed on top of sample starting from one end of glass slide, so no air bubbles were trapped. Slides were sealed with quick dry Sally Henson double duty nail paint top coat to avoid escape of moisture. Slides were stored in the dark at 4^0C until used for microscopy. All the washing steps were performed for five minutes if not mention in the method specifically.

4.3.5. Microscopic observations and processing

Prepared slides were visualized by Zeiss Observer Z1 microscope equipped with LSM 700 laser scanning confocal head using Plan-Apochromat 40x/1.3 oil immersion lens and 10x/0.45 NA (Zeiss, Thornwood, NY). Green channel 488 was assigned for WGA-Alexa-Fluor fungal staining and red channel 555 was used for autofluorescence detection. For inner structure visualization Z-stack images were taken depending upon the depth of stem rust structures developed inside the plant system (100-300 images per infection site 20 to 100 microns thick). At least fifteen infection sites were visualized, and three sites were chosen for imaging and biovolume analysis.

4.3.6. Analysis of pathogen volume present inside the plant system

Images were processed in Imaris 9.0.1 software. Imported pictures were subjected to channel correction for red and green channel. Image processing was performed using attenuation correction for the green channel using intensity front 256 and intensity back 128 values. Smoothing for channel green was performed using median filter size 5x5x5. Processed images were subjected to contrast change using normalized layer to remove the background noise. This process enabled the visualization of the volume of pathogen growth inside the plant cells while removing the background plant noise recorded in the red channel. Once pathogen growth area

was determined, using the surface creation function the surface area of pathogen growth was created only for the green channel using surface detail value 0.491 at absolute thresholding. All nonspecific signals were removed using manual curation and volume filtering. All the nonspecific surface creation was removed manually, and fungal surface volume was computed for fungal structures present from appressoria to secondary infection hyphae and haustoria. An average volume was calculated for all the recorded structures starting from Appressoria until the last recorded structures.

4.4. Results

4.4.1. Phenotypic variations among the susceptible genotypes for variable early dark periods

Upon inoculations with *P. graminis* f. sp. *tritici* races QCCJ and HKHJ phenotypic variations were accessed at the 3rd, 6.5th and 14th DPI. After 3.5-day post stem rust inoculations no visible leaf symptoms were observed on any of tested genotypes (barley lines HQ18, Q21861, Harrington, and Steptoe, and the wheat line Morocco). On 4.5th day onward small pinpoint chlorotic spots were observed on the leaf surface of susceptible genotypes (Steptoe, Harrington and Morocco for QCCJ; Steptoe, Harrington, HQ18 and Morocco for HKHJ), that were limited to the normal light cycle treated plants and no visible leaf symptoms were observed in any of extended dark periods (i.e. 48 HPI, 62 HPI and 86 HPI) treated plants. Although interesting observations were made on the dark treated plants from 6.5th day onwards. At the 6.5th day post inoculation rust pustule formation was started in the susceptible genotypes inoculated with *P. graminis* f. sp. *tritici* races QCCJ or HKHJ treated seedlings for both the normal light cycle or the extended 48 hours dark period post inoculations (Fig. 4.2-4.7). However, the overall size of pustules was smaller and the yellow chlorotic halos surrounding the pustules for the 48-hour dark

treated plants (Fig. 4.2-4.7). Adding to our interest 62-hour and 86-hour dark treated susceptible plants started showing large diffused chlorotic spots on leaf surface without the formation of pustules at this time point of observations, thus indicating intercellular pathogen growth and colonization. Due to extended period of darkness, an overall light green paleness on primary and newly emerging secondary leaves was observed in 62-hour and 86-hour dark treated plants. 86 hours dark treated plants showed drying of leaf tips and a slight reduction in vigor too. Resistant genotypes (Q21861, HQ18 for QCCJ; Steptoe, Q21861 for HKHJ) showed no visible difference for pathogen symptoms at any time points.

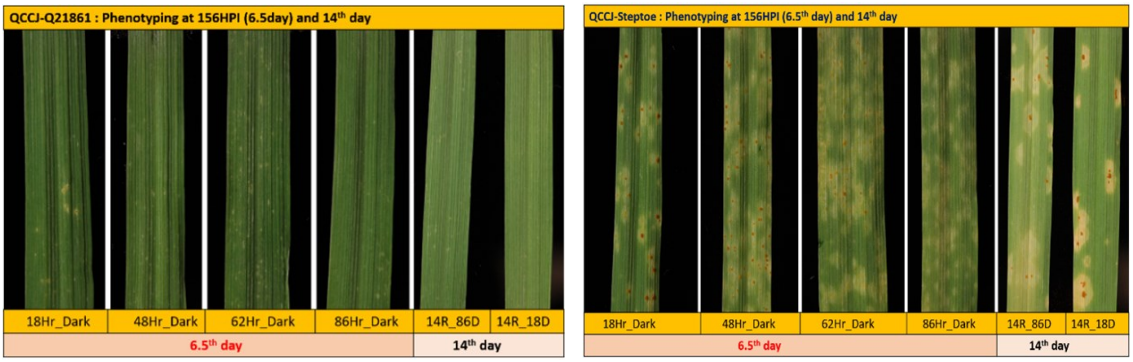

Fig. 4.2.A **Fig. 4.2.B**

Fig. 4.2. Disease phenotyping in barley genotypes, resistant Q21861 (*RMRL+/Rpg1+*) and susceptible Steptoe (*RMRL-/Rpg1-*) barley lines after inoculation with *P. graminis* f. sp. *tritici* (*Pgt*) race QCCJ (avirulent on *RMRL* but virulent on *Rpg1* containing barley genotypes). Four different sets of inoculated plants were given 18, 48, 62 and 86 hour of dark period post inoculation with stem rust race QCCJ followed by resuming the normal light cycle of 16 hours light and 8 hours of dark in a growth chamber. To underline the difference in disease progression phenotyping was done at 156 hours post pathogen inoculation. Disease was further evaluated on the 14th day post inoculation between normal 18-hour and extended 86-hour dark period treated genotypes. **(A)** Resistant genotype Q21861 showed no differences in pustule and chlorosis size and shape. **(B)** The susceptible genotype Steptoe showing difference in pustule and chlorosis size and shape.

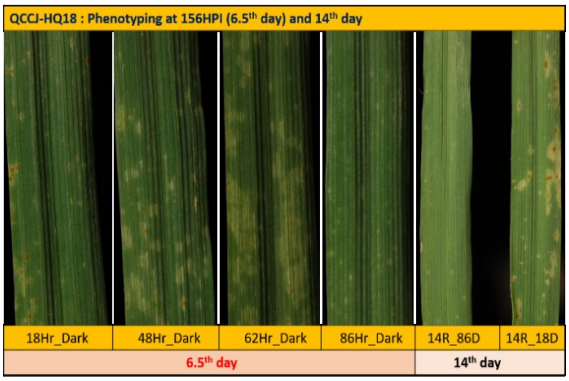

Fig. 4.3.A

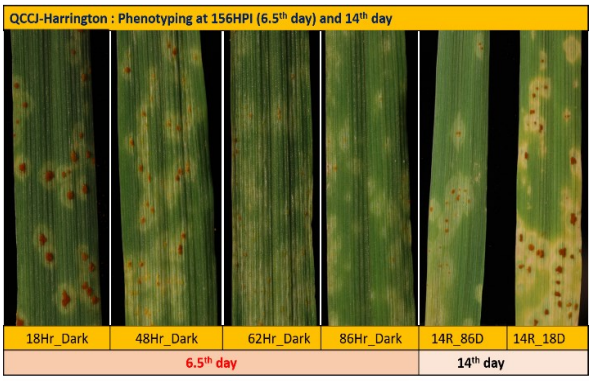

Fig. 4.3.B

Fig. 4.3. Disease phenotyping in barley genotypes, resistant near isogenic line HQ18 (Q21861x Harrington - *RMRL+/Rpg1*-) and susceptible Harrington (*RMRL-/Rpg1*-) after inoculation with wheat stem rust race QCCJ (avirulent race on *RMRL* but virulent on *Rpg1* containing barley genotypes). Four different sets of inoculated plants were given 18, 48, 62 and 86 hour of dark period post inoculation with *P. graminis* f. sp. *tritici* race QCCJ followed by resuming the normal light cycle of 16 hours light and 8 hours of dark in a growth chamber. To assay the progression of colonization and disease, phenotyping was performed at 156-hour and the 14th day post pathogen inoculation with both the normal 18-hour and extended 86-hour dark period treated genotypes**. (A)** Resistant genotype HQ18 showing difference in pustule and chlorosis size and shape. **(B)** The susceptible genotype Harrington showing difference in pustule and chlorosis size and shape.

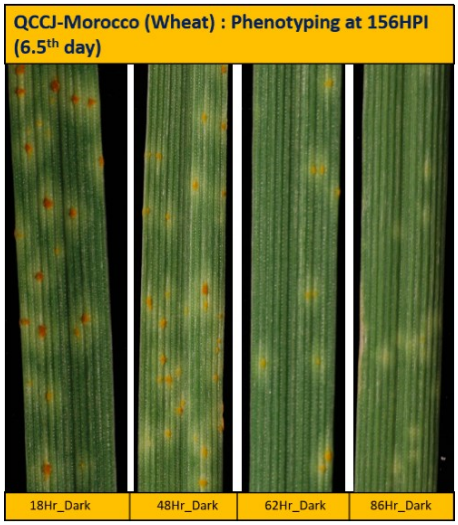

Fig. 4.4. Disease phenotypes of the susceptible wheat line Morocco inoculated with *P. graminis* f. sp. *tritici* (*Pgt*) race QCCJ. Four different sets of inoculated plants were given 18, 48, 62 and 86 hour of dark period post inoculation with *Pgt* race QCCJ followed by resuming the normal light cycle of 16 hours light and 8 hours of dark in a growth chamber. To assay the progression of colonization and disease, phenotyping was performed at 156 hours and on the 14th day post pathogen inoculation.

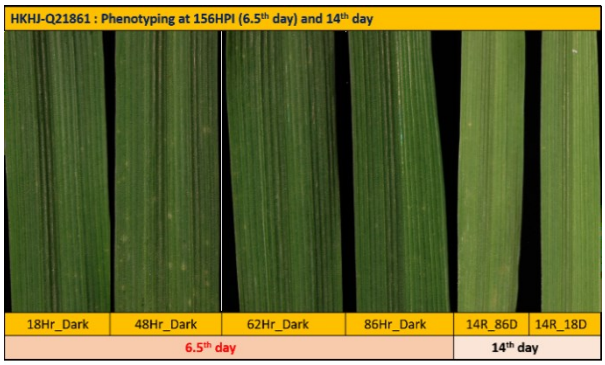

Fig. 4.5.A

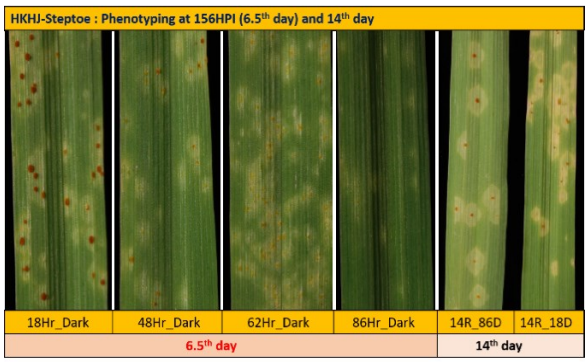

Fig. 4.5.B

Fig. 4.5. Disease phenotyping in barley genotypes, resistant Q21861 (*RMRL+/Rpg1+*) and susceptible Steptoe (*RMRL-/Rpg1-*) after inoculation with *P. graminis* f. sp. *tritici* (*Pgt*) race HKHJ (avirulent race on *Rpg1* but virulent on *RMRL* containing barley genotypes). Four different sets of inoculated plants were given 18, 48, 62 and 86 hours of dark period post inoculation with *P. graminis* f. sp. *tritici* race HKHJ followed by resuming the normal light cycle of 16 hours light and 8 hours of dark in a growth chamber. To assay the progression of colonization and disease, phenotyping was performed at 156-hour and the 14th day post pathogen inoculation with both the normal 18-hour and extended 86-hour dark period treated genotypes. **(A)** Resistant line Q21861 shows no differences with very small chlorotic flecks. **(B)** The susceptible line Steptoe shows difference in pustule and chlorosis size and shape.

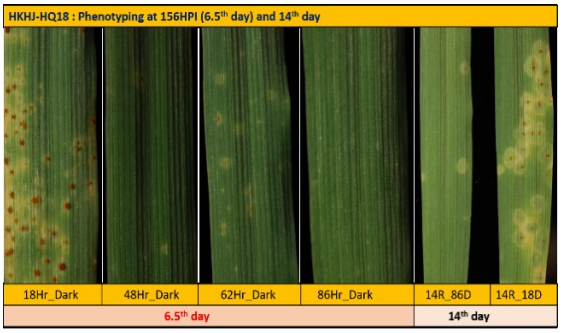

Fig. 4.6.A

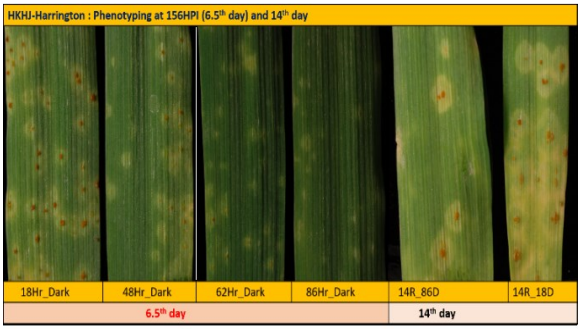

Fig. 4.6.B

Fig. 4.6. Disease phenotyping of the barley recombinant inbred line, HQ18 (*RMRL+/Rpg1-*) and the susceptible line Harrington (*RMRL-/Rpg1-*) into which the Q21861 *RMRL* locus was introgressed. Both HQ18 and Harrington are susceptible *P. graminis* f. sp. *tritici* race HKHJ (avirulent on *Rpg1* but virulent on *RMRL*). Four different sets of inoculated plants were given 18, 48, 62 and 86 hour of dark period post inoculation with *P. graminis* f. sp. *tritici* race HKHJ followed by resuming the normal light cycle of 16 hours of light and 8 hours of dark in a growth chamber. To assay the progression of colonization and disease, phenotyping was performed at 156 hours and the 14th day post pathogen inoculation with both the normal 18-hour and extended 86-hour dark period treated genotypes. **(A)** HQ18 showed difference in pustule and chlorosis size and shape **(B)** Harrington showing difference in pustule and chlorosis size and shape.

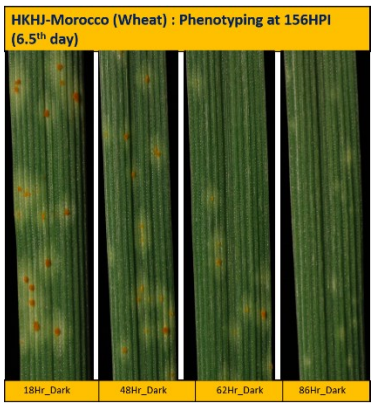

Fig. 4.7. Disease phenotypes of the susceptible wheat line Morocco inoculated with *P. graminis* f. sp. *tritici* (*Pgt*) race HKHJ. Four different sets of inoculated plants were given 18, 48, 62 and 86 hour of dark period post inoculation with *Pgt* race QCCJ followed by resuming the normal light cycle of 16 hours light and 8 hours of dark in a growth chamber. The phenotyping and photos were taken at 156 post pathogen inoculation with both the normal 18-hour and extended 86-hour dark period treated genotypes.

At the 14th day post pathogen inoculation susceptible wheat and barley lines inoculated with *Pgt* races QCCJ and HKHJ exhibit similar disease phenotypes and lesion progression when the time points were compared between the two isolates. However, the chlorotic halos were typically larger in the size for the dark treated plants, and more pronounced for the extended dark treated seedlings when assayed at 14 days post inoculation.

4.4.2. Confocal microscopy to visualize pathogen growth in the plant system

Microscopic observations were made to determine if *Pgt* penetration through the stomata is light dependent or if the pathogen can effectively penetrate in presence of continuous dark. *Pgt* race QCCJ inoculated resistant barley line Q21861 and susceptible line Steptoe leaf samples were collected 48, 62 and 86 HPI with both normal and extended dark periods were visualized and data was analyzed. For the resistant line Q21861, treated with the normal 18-hour dark period after pathogen inoculation followed by 16/8-hour light/dark period, *Pgt* structures (i.e. spores, germ tube and appressoria) were clearly observed at all the tested time-points. For the 48-hour samples, sub-stomatal vesicles, primary infection hyphae and hyphal branching was

observed clearly. However, the overall branching and haustoria formation was contained to cells adjacent to the breached stomata and did not significantly spread at the later time points (Fig. 4.8). In the samples with extended continuous dark period substomatal vesicle and primary infection hyphae were also observed at all the time points (i.e. 48, 62 and 86 hours) indicating that penetration of the pathogen is light independent. Yet, hyphal branching and pathogen growth past the sub-stomatal vesicles formation was greatly reduced with minimal haustoria formation comparing with the normal samples, indicating a role of light in the induction of pathogen growth, branching and haustoria formation after the initial penetration.

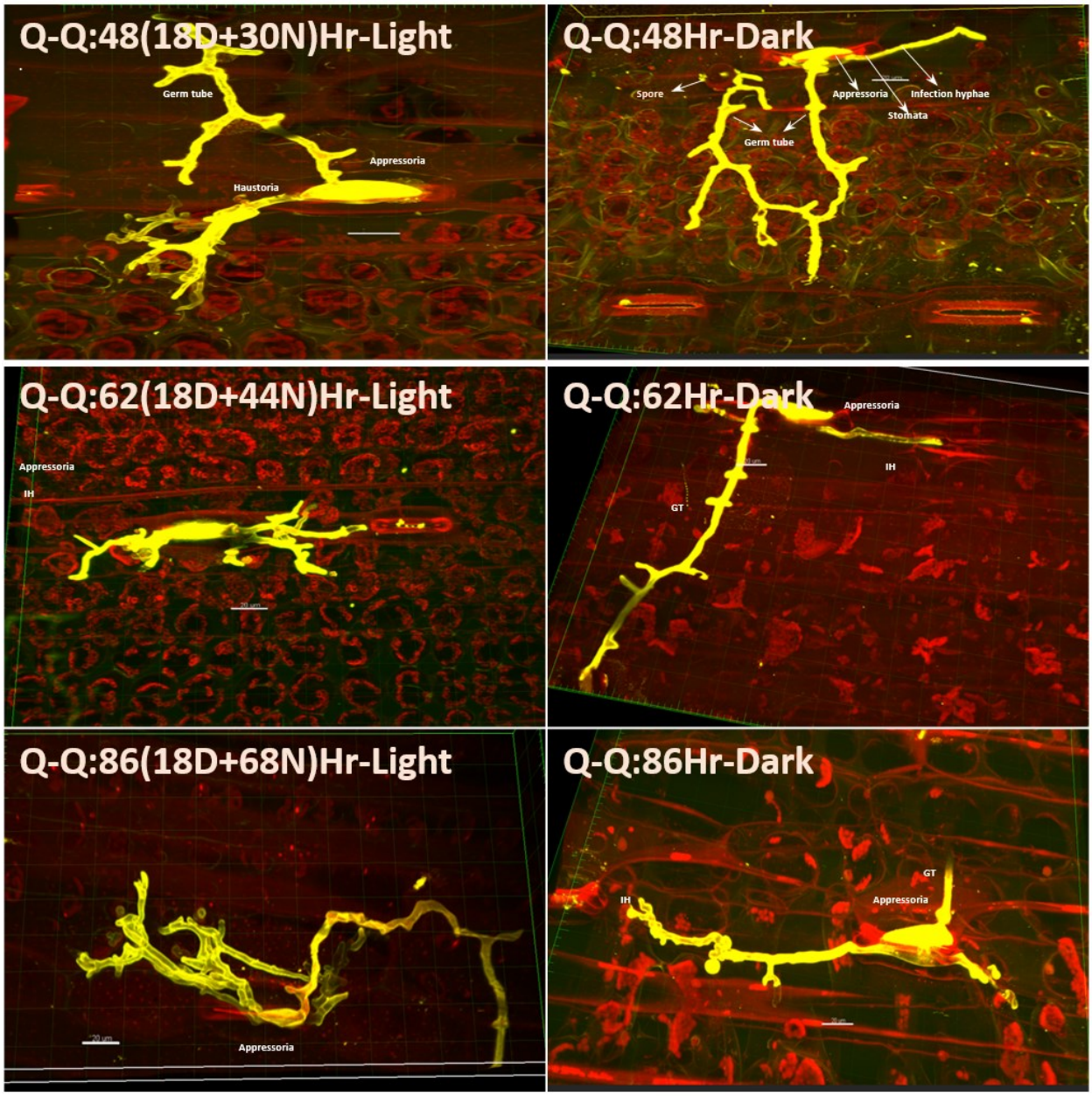

Fig. 4.8. Microscopic visualization of *P. graminis* f. sp. *tritici* (*Pgt*) race QCCJ structures inside the resistant barley line Q21861 (*RMRL+/Rpg1+*) at 48, 62 and 86 hours post inoculation (HPI). Inoculated plants were treated with normal (18-hour initial dark period followed by 16/8-hour light/dark cycle) and constant dark period (48, 62, 86 HPI). *Pgt* structures were visualized using Alexa Fluor-488-WGA dye shown here with yellow color, whereas background plant structures were shown with red color. *Pgt* race QCCJ was able to penetrate inside the plant irrespective of the presence or absence of light at 48 HPI and later time points. However, a reduction in branching and haustoria formation was observed if continuous dark period was provided to the infected plants.

In the susceptible barley line Steptoe, profuse branching of ICH was observed with extensive haustoria formation that spread deep into the mesophyll cell layers in the 48-hour sample for the normal 18-hour initial dark period followed by the 16/8-hour light/dark cycle. At the later stages (62 and 86 HPI) the overall growth of the pathogen was found to increase rapidly. For the samples with the extend dark periods a great reduction of ICH branching and haustoria formation was observed, however the pathogen was still able to penetrate during the dark period.

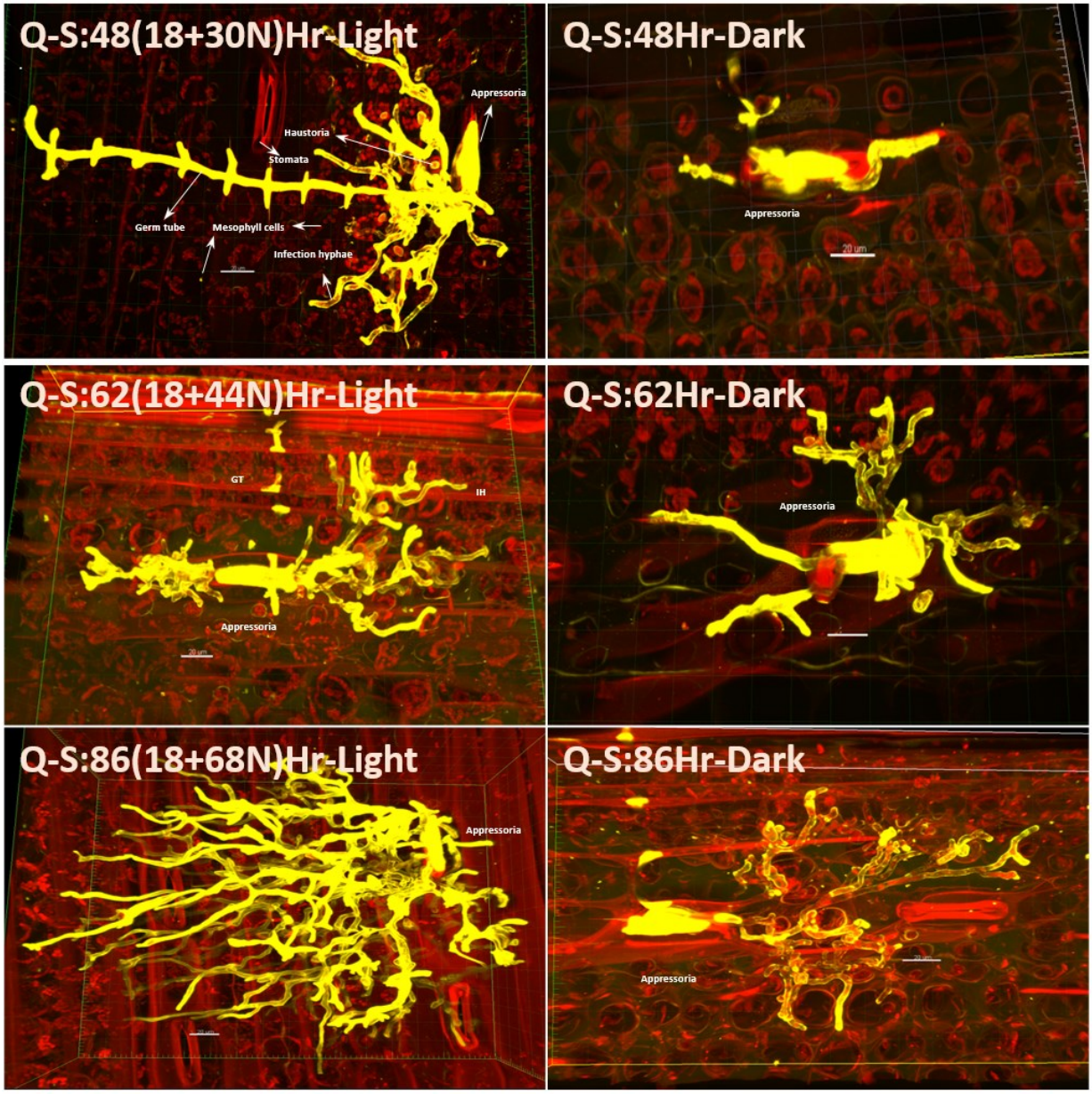

Fig. 4.9. Microscopic visualization of *P. graminis* f. sp. *tritici* (*Pgt*) race QCCJ structures in the susceptible barley line Steptoe (*RMRL-/Rpg1-*) at 48, 62 and 86 hours post inoculation (HPI). Inoculated plants were given normal (18-hour initial dark period followed by a 16/8-hour light/dark cycle) and constant dark period (48, 62, 86 HPI) treatment. *Pgt* structures were visualized using Alexa Fluor-488-WGA dye and shown with yellow color, whereas plant structures were shown with red color. *Pgt* race QCCJ was able to penetrate inside the plant irrespective of presence of absence of light at 48 HPI. Profuse *Pgt* inter cellular hyphae (ICH) was observed in normal dark period treated plants (48 HPI), greatly increasing at time points 62, and 86 HPI. Drastic reduction in branching and haustoria formation was observed if continuous dark periods were used with pathogen growth limited to cells adjacent or near to breached stomata.

4.4.3. Volume analysis

Fungal biovolume for *Pgt* race QCCJ was recorded in infected barley resistant line Q21861 and susceptible line Steptoe using samples collected at three differ time points 48, 62 and 86 HPI. These samples were treated with normal (18-hour initial dark period followed by 16/8-hour light/dark treatment; 48L, 62L and 86L) and continuous extended dark (48D, 62D, and 86D) period. Average pathogen area was calculated for three different *Pgt* race QCCJ infection sites exhibiting a general growth pattern observed across 15 infection sites (Table 4.1). For the resistant line Q21861, the average pathogen biovolume was computed 12,445.30 μm^3, 33,590.23 μm^3 and 37,975.33 μm^3 for 48L, 62L and 86L HPI time-points respectively. For the 48D, 62D and 86D HPI extended dark periods, the average biovolumes were computed as 8,233.77 μm^3, 7,912.84 μm^3 and 10,031.58 μm^3, respectively. For Steptoe, recorded *Pgt* race QCCJ biovolume for the normal light period was greater than Q21861, as expected due to its compatible interaction (susceptibility), with the average pathogen biovolumes were recorded as 29,197.93 μm^3, 61,412.30 μm^3 and 42,2619.30 μm^3 for 48L, 62L and 86L HPI time-points, respectively. For the 48D, 62D and 86D HPI extended dark period samples the average biovolumes were recorded as 7,824.15 μm^3, 16,409.39 μm^3 and 14,306.56 μm^3, respectively. Means and standard-errors were calculated at each time points for three observed infection sites (Table 4.1).

Table 4.1. Biovolume analysis of *P. graminis* f. sp. *tritici* (*Pgt*) race QCCJ growth in resistant (Q21861) and susceptible (Steptoe) barley lines at three different time points, 48, 62 and 86 hours post inoculation (HPI).

Time points	Q21861 (μm^3)	Biovolume Mean (μm^3)	Std Dev	Std Error	Steptoe (μm^3)	Biovolume Mean (μm^3)	Std Dev	Std Error
48L	12342.70				37205.90			
48L	13805.00	12445.30	1070.76	618.21	27774.40	29197.93	6041.76	3488.21
48L	11188.20				22613.50			
62L	22555.50				26880.10			
62L	19809.40	33590.23	17583.03	10151.57	53188.80	61412.30	32084.00	18523.70
62L	58405.80				104168.00			
86L	19765.80				490278.00			
86L	80443.70	37975.33	30131.05	17396.17	658212.00	422619.30	225124.40	129975.60
86L	13716.50				119368.00			
48D	9870.44				6784.30			
48D	7869.83	8233.77	1215.32	701.66	8100.72	7824.15	761.66	439.74
48D	6961.04				8587.42			
62D	9146.70				32906.30			
62D	8673.86	7912.84	1423.74	822.00	9168.83	16409.39	11694.07	6751.57
62D	5917.95				7153.04			
86D	11423.90				8100.72			
86D	11238.90	10031.58	1839.77	1062.20	26103.80	14306.56	8345.68	4818.38
86D	7431.94				8715.17			

L- Normal 18-hour dark period followed by 16-hour light and 8-hour dark period. D- Continuous dark period. Mean value was calculated taking the average of three individual colonies which were representing a general growth pattern for 15 visualized infection sites.

4.5. Discussion and conclusions

The biotrophic fungal pathogen *Puccinia graminis* (*Pg*) spore germination is greatly impacted by the initial period of darkness after providing the favorable germination conditions

such as high humidity and ambient temperature (Givan and Bromfield, 1964; Leonard and Szabo, 2005). However, light does not cause absolute inhibition of spore germination, rather causes reduction in germination rate. Studies pointed out that inhibition in the spore germination due to light is readily reversible since spores incubated in one hour of light period followed by one hour of dark period showed significantly better germination than spores incubated in two hours of continuous darkness (Givan and Bromfield, 1964). Interestingly, contrasting findings were reported for *Puccinia recondita* (*P. recondita*) spore germination with respect to light. Stock et al. (Stock, 1931) reported no effect of light on *P. recondita* uredospore germination whereas Weston et al. (Dillon Weston, 1932) noted light inhibition. Similarly, the effect of light and CO_2 concentration on stomatal penetration by *Pgt* substomatal vesicle was studied in wheat by Yirgou and Caldwell (Yirgou and Caldwell, 1963) and they have found that if 9-10 hours of dark period was provided after an initial 10 hour of dark-moist incubation period, then only 2-5% penetration was observed. Upon providing CO_2 free 10-hour dark environment after incubation, stem rust penetration greatly increased up to 24.6-28.4%, whereas in presence of 5% CO_2 for 10 hours in light after dark incubation greatly reduced stomatal penetration from ~60% to ~2.4%. This study concluded plant stomatal opening and stimulation by *Pgt* in daylight is not the limiting factor for stem rust penetration, instead CO_2 concentration also plays a major role. Yirgou and Caldwell (Yirgou and Caldwell, 1963) further speculated that in darkness due to respiration and absence of photosynthesis, increased intercellular CO_2 level negatively impacts *Pgt* penetration through stomata. However, light induced photosynthetic reduction of intercellular CO_2 level increases the stomatal penetration. In a later study Yirgou and Caldwell (Yirgou and Caldwell, 1968) suggested that *P. graminis* appressoria do not penetrate the stomata until exposer of the plant to the light, findings consistent with study by Hart (Hart, 1929). In

another study Burrage (Burrage, 1970) subjected wheat plants to different degrees of water stress in the presence of light after the initial dark and moist incubation period and showed that infection percentage reduced to a level at par with dark treated plants. These findings suggest stomatal manipulation during *Puccinia graminis* penetration plays a key role and possibly not always solely depends on light, demanding more thorough retrospection of these findings (Royle, 1976).

RMRL mediated resistance requires the *Rpg5* NLR with an unusual C-terminal kinase domain (Brueggeman et al., 2008; Wang et al., 2013; Arora et al., 2013). The *Rpg5-kinase* domain shows high homology with the barley *Gak1* kinase which is predicted to encode a guard cell expressed stomatal aperture controlling protein based on its close homologs AtApk1b in *Arabidopsis* (dissertation chapter 2). Thus, it is possible that stomatal manipulation by the pathogen possibly plays a role in stomatal opening and entry into the plant. Our attempt to investigate effect of extended initial period of darkness after pathogen (*Pgt* race QCCJ) inoculation leads to interesting observations. Susceptible plants given 16-18 hours of dark period after stem rust inoculation usually develop light yellow colored specks of chlorosis by the fourth to fifth day post inoculation (100-110 HPI) which leads to development of small spore pustules 5.5^{th} to 6^{th} (130-140 HPI) day after inoculations that progress to fully developed spore pustules by the 11^{th} to 14^{th} day post inoculations. This observation helped in estimation of time-line required for visible spore production on leaf surface, taking approximately 118-130 hours after initial 18 hours of dark humid period, followed by exposure to light. Investigation to explore the effect of extended dark period on the stomatal penetration using two different *P. graminis* f. sp. races QCCJ and HKHJ lead to the interesting findings, in sharp contrast with previously published results. Firstly, we determined that upon inoculation using either of *Pgt* races QCCJ

and HKHJ with extended dark period of 30 hours or 36 hours, phenotypically observation of pathogen growth follows a normal pattern of colonization and infection type progression without any difference in visual symptoms. This phenotypic observation indicates that initial phase of pathogen growth is slow, and effect of extended dark period is not much pronounced initially. Secondly, Extended dark period (48, 62, 86 HPI) resulted in large and diffuse chlorotic spots appeared on the leaf lagging with normally treated plants. Plants given 62 hours of continuous dark period showed large chlorotic halo at 115-120 HPI and started sporulation at 140-145 hours post inoculation. This observation was much clearer with 86-hour continuous dark period treated susceptible genotype and they developed very large coalesced yellow chlorotic island, after 110-120 hours of inoculation and developed very minute light brown colored spore pustules at 145-150 HPI. These observations were remarkable, since visible sporulation took only 83-88 hours in sixty-two hour extended dark period treated susceptible genotypes and 59-64 hours in 86 hours extended dark period treated susceptible plant genotypes after exposing them to the normal light period (16/8-hours light/dark period). According to previous literatures (Yirgou and Caldwell, 1968; Hart, 1929; Givan and Bromfield, 1964; Leonard and Szabo, 2005; Figueroa et al., 2016), *Pgt* spores after forming appressoria on top of stomata should remain quiescent in dark, waiting for light induced stomatal opening facilitating penetration. In this condition extended dark period should have an inhibitory effect on *Pgt* growth at appressoria stage and after exposure to normal light/dark period it should take 118-130 hours for visible spore production. However, our phenotypic observations clearly concluded that spore production in extend dark period treated plants is earlier (59-88 hours) than normal (118-130 hours) after exposure to light, indicating presence of light independent Pgt penetration, and initial growth of pathogen, yet unable to attain minimum vigor required for sporulation.

Microscopic observations clearly show that irrespective of the extended periods of dark treatment most of the fungal appressoria are able to produce substomatal vesicles and gain entry through the stomata (Fig. 4.8 and Fig. 4.9). We have completed the microscopic observations with the barley lines Q21861, HQ18, Steptoe, and Harrington and the wheat line Morocco inoculated with *Pgt* race QCCJ showing the penetration of substomatal vesicle and intercellular hyphal growth during the dark period irrespective of compatibility or incompatibility. Observations with susceptible and resistant barley lines inoculated with *Pgt* race HKHJ is still underway and initial observations indicate the similar conclusions.

In resistant barley line Q21861 we have observed *Pgt* race QCCJ able to penetrate effectively but the overall branching and formation of haustoria was suppressed compared to the susceptible barley line Steptoe at each tested time points (48, 62, 86 HPI), if the normal dark/light treatment was used. At 62 and 86 hours post pathogen inoculation the intercellular infection hyphae branching and haustoria formation in Steptoe was increased rapidly, whereas in Q21861 pathogen growth was contained and limited to adjacent mesophyll cells near to the breached stomata without any substantial branching. Thus, we can conclude that resistance mechanism effectively takes place post pathogen penetration of the stomatal aperture and suppress the pathogen growth both pre and post haustoria formation. These results are consistent with the barley dual kinase *Rpg1* R-gene (Brueggeman et al., 2002) mediated resistance mechanism. Rpg1 has been shown to be phosphorylate within five minutes once avirulent *Pgt* race MCCF lands on the leaf surface (Nirmala et al., 2010). Rpg1 phosphorylation is required for its subsequent degradation at 24 HPI (Nirmala et al., 2007) which is indispensable for the resistance response, indicating early pre-haustorial pathogen induced protein modification of Rpg1 may prime the mechanism for a later post-haustorial resistance response.

The *RMRL*-mediated resistance response was previously reported to initiate a HR (Brueggeman and Solanki, 2017) based on a small sample size without correlating presence of DAB stain with spore germination and fungal appressoria formation, however this detailed study established that *RMRL*-mediated resistance does not follow the typical R-gene mediated HR response (dissertation chapter 2) and cell death. We can conclude that the reduction of fungal intercellular hyphal branching and reduced number of fungal haustoria results in the inability of avirulent races to establish itself on resistant genotype and effectively colonize and sporulate. Studies showed that non host resistance in *Zea mays* (corn) , *Vigna sinensis*, *Helianthus annus* (sunflower) and *Phaseolus vulgaris* toward three rust pathogens, *Puccinia sorghi*, *Uromyces phaseoli* var. *vignae* and *Puccinia helianthin* can be attributed to limited haustoria formation (Heath, 1977). In the nonhost plant rice, *Pgt* and four other cereal rust species i.e. *Puccinia hordei*, *Puccinia sorghi*, *Puccinia triticina* and *Puccinia striformis* f. sp. *tritici* were shown to produce all the infection structures required for the colonization and ability to uptake limited amount of nutrients leading to establishment of moderate infection sites, although infection did not resulting in sporulation (Ayliffe et al., 2011).

Irrespective of resistant or susceptible plant genotype (barley and wheat) or virulent or avirulent stem rust race, in our study the *Pgt* pathogen is shown to gain entry inside the plant system suggesting that the resistance is post penetration. Interestingly in the extended dark period the length and branching of primary infection hyphae diminished irrespective of resistant or susceptible barley genotypes. Stark contrast was observed for *Pgt* race QCCJ growth on the susceptible barley line Steptoe compared to the normal 18 hours and extended dark period (48, 62, 86 HPI) treated plants after inoculations. Plants with continuous 48-hour dark treatment, QCCJ intercellular growth was contained for 3-4 laterally adjacent cells to stomata, whereas a

large intercellular pathogen growth was observed in the normal dark/light (initial 18-hour continuous dark period) treated plants. Visual differences in QCCJ branching and haustoria formation were more pronounced if extended dark period (62 and 86 HPI) was given and compared with samples collected at the same time point but with normal light/dark cycle. At later time points rapid visual growth and branching was observed for QCCJ covering almost the whole visual area under microscope. On the other hand, continuous dark treated plants after inoculations had very contained intercellular pathogen growth with few PIH branching points and haustoria, and primarily resided in the upper mesophyll cell layers. Microscopic visualization helped to conclusively say that the stem rust pathogen can penetrate inside barley and wheat successfully in the dark period and do not required light induced stomatal opening.

Analysis of the biovolume of stem rust intercellular growth further supported our findings and for each tested sample we were able to quantify intercellular pathogen growth. However, if continuous dark treatment was given then not much difference in terms of overall pathogen volume was recorded between Q21861 and Steptoe (Table 4.1, Fig. 4.10). In the normal dark/light treated plants the volume of pathogen growth between Q21861 and Steptoe was significantly different at 48 HPI and 86 HPI ($P<0.05$). However, at 62 HPI the difference in pathogen volume was not significant. At 48-hour pathogen growth was 2.4-fold more in the susceptible line but at 62 hours the fold difference was only 1.8 (Fig. 4.10). This suggest an inhibition of QCCJ growth in the Steptoe at early stage which was not observed in the Q21861. However, at 86 hours the fold difference was 11.12, indicating enormous growth of pathogen in susceptible barley line Steptoe. Interestingly a very small insignificant change in the pathogen growth between 62 HPI (33590 μm^3) and 86 HPI (37975 μm^3) in the Q21861 barley line was noted indicating a stagnation in the growth due to the non-HR resistance response (Table 4.1,

Fig. 4.10). In the susceptible line Steptoe, 7.9-fold change in the growth was noted between 62 HPI (61412 μm^3) and 86 HPI (422619 μm^3), confirming that this is a rapid stage of pathogen growth (Table 4.1, Fig. 4.10). It is possible that in Steptoe initially pathogen growth is slow, and the rapid phase of pathogen growth takes place after 62 hours, an observation consistent with Zurn et al. (Zurn et al., 2015). We can speculate that due to multiple branching of intercellular hyphae and rapid haustoria formation the pathogen is able to support its further growth in the susceptible cultivars. However, in resistant cultivars the presence of the *Rpg5* resistance gene initiated a non-HR defense response (dissertation chapter 2) containing the branching of ICH and haustoria formation, thus, the pathogen unable to support rapid growth and sporulation. This suggests that *RMRL* represents a basal non-host type of rust resistance, commonly referred to as durable slow rusting resistance.

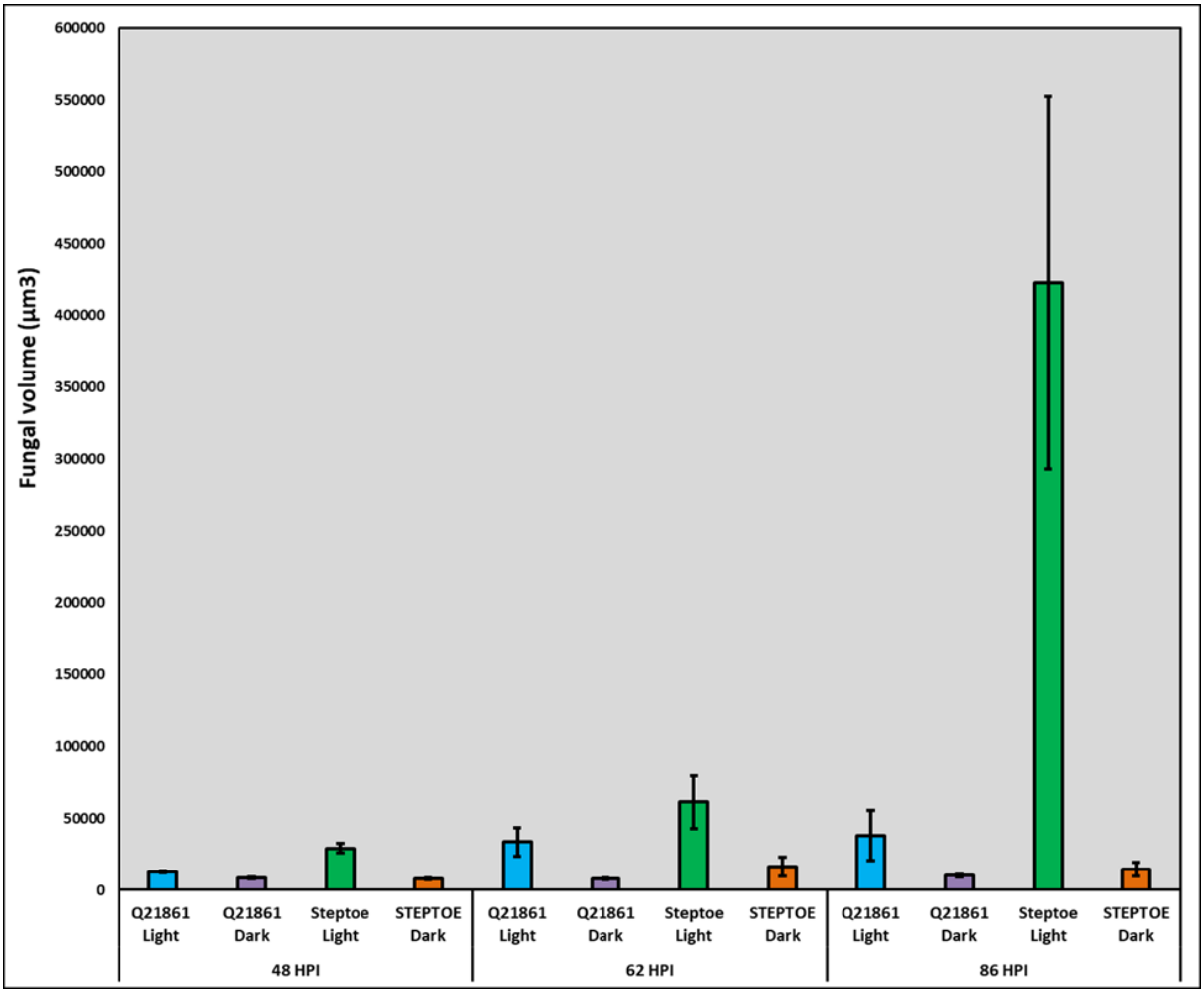

Fig. 4.10. *Pgt* race QCCJ biovolume calculation at different time points (48, 62 and 86 hours post inoculation) in normal and extended dark period treated resistant barley line Q21861 and susceptible barley line Steptoe. The X-axis represents timing of different barley cultivar leaf samples collection with normal initial 18-hour dark moist period followed by 16/8-hour light/dark cycle after pathogen inoculation and extended continuous dark period (48, 62, 86 hours) followed by 18 hours of initial moist dark period after pathogen inoculation. The Y-axis represents average biovolume of QCCJ computed for three infection sites in μm^3.

Previous publications suggested that the stem rust pathogen forms appressoria on top of stomata and waits until light induced stomatal guard cells opening before entry occurs followed by formation of the sub stomatal tube (Hart, 1929; Yirgou and Caldwell, 1968, 1963; Givan and Bromfield, 1964; Garnica et al., 2014; Figueroa et al., 2016). Nonetheless with the experimental evidences provided here we are able to show that *Pgt* races QCCJ and HKHJ can penetrate

through stomata during the dark period, although ICH branching and haustoria formations are drastically suppressed. Future studies will characterize if this reduction is due to effects of light on the plant biological process or on the pathogen physiology.

4.6. Literature cited

Arora, D., Gross, T., and Brueggeman, R. (2013). Allele characterization of genes required for rpg4-mediated wheat stem rust resistance identifies Rpg5 as the R gene. *Phytopathology* 103, 1153–1161. doi:10.1094/PHYTO-01-13-0030-R.

Ayliffe, M., Devilla, R., Mago, R., White, R., Talbot, M., Pryor, A., and Leung, H. (2011). Nonhost resistance of rice to rust pathogens. *Mol Plant Microbe Interact* 24, 1143–1155. doi:10.1094/MPMI-04-11-0100.

Browder, L. E. (1971). *Pathogenic specialization in cereal rust fungi, especially Puccinia recondita f. sp. tritici: Concepts, methods of study, and application*. US Agricultural Research Service.

Brueggeman, R., Druka, A., Nirmala, J., Cavileer, T., Drader, T., Rostoks, N., Mirlohi, A., Bennypaul, H., Gill, U., Kudrna, D., et al. (2008). The stem rust resistance gene Rpg5 encodes a protein with nucleotide-binding-site, leucine-rich, and protein kinase domains. *Proc Natl Acad Sci U S A* 105, 14970–14975. doi:10.1073/pnas.0807270105.

Brueggeman, R., Rostoks, N., Kudrna, D., Kilian, A., Han, F., Chen, J., Druka, A., Steffenson, B., and Kleinhofs, A. (2002). The barley stem rust-resistance gene Rpg1 is a novel disease-resistance gene with homology to receptor kinases. *Proc Natl Acad Sci U S A* 99, 9328–9333. doi:10.1073/pnas.142284999.

Brueggeman, R. S., and Solanki, S. (2017). " Barley Stem Rust Resistance Mechanisms: Diversity, Genestructure, and Function Suggest a Recently Evolved Host-Pathogen Relationship," in *Management of wheat and barley diseases*, ed. D. P. Singh (6000 Broken Sound Parkway NW, Suite 300 Boca Raton, FL 33487-2742: CRC Press), 579–604. doi:10.1201/9781315207537-26.

Burrage, S. W. (1970). Environmental factors influencing the infection of wheat by Puccinia graminis. *Annals of Applied Biology* 66, 429–440. doi:10.1111/j.1744-7348.1970.tb04622.x.

Dillon Weston, W. A. R. (1932). The reaction of disease organisms to certain wave lengths in the visible and invisible spectrum. *Phytopathology*.

Figueroa, M., Upadhyaya, N. M., Sperschneider, J., Park, R. F., Szabo, L. J., Steffenson, B., Ellis, J. G., and Dodds, P. N. (2016). Changing the Game: Using Integrative Genomics to Probe Virulence Mechanisms of the Stem Rust Pathogen Puccinia graminis f. sp. tritici. *Front Plant Sci* 7, 205. doi:10.3389/fpls.2016.00205.

Garnica, D. P., Nemri, A., Upadhyaya, N. M., Rathjen, J. P., and Dodds, P. N. (2014). The ins and outs of rust haustoria. *PLoS Pathog* 10, e1004329. doi:10.1371/journal.ppat.1004329.

Givan, C., and Bromfield, K. (1963). Light inhibition of uredospore germination in Puccinia graminis var. tritici. *Light inhibition of uredospore germination in Puccinia graminis var. tritici*. Available at: http://www.dtic.mil/docs/citations/AD0410395.

Givan, C. V., and Bromfield, K. (1964). Light inhibition of uredospore germination in Puccinia graminis var. tritici. *Phytopatholo* 54, 382–384. Available at: http://oai.dtic.mil/oai/oai?verb=getRecord&metadataPrefix=html&identifier=AD0410395.

Hart, H. (1929). Relation of stomatal behavior to stem-rust resistance in wheat. *J. agric. Res* 39, 929–48. Available at: https://naldc.nal.usda.gov/download/IND43967653/PDF.

Heath, M. C. (1977). A comparative study of non-host interactions with rust fungi. *Physiological Plant Pathology* 10, 73–88. doi:10.1016/0048-4059(77)90009-1.

Leonard, K. J., and Szabo, L. J. (2005). Stem rust of small grains and grasses caused by Puccinia graminis. *Mol Plant Pathol* 6, 99–111. doi:10.1111/j.1364-3703.2005.00273.x.

Nirmala, J., Dahl, S., Steffenson, B. J., Kannangara, C. G., von Wettstein, D., Chen, X., and Kleinhofs, A. (2007). Proteolysis of the barley receptor-like protein kinase RPG1 by a proteasome pathway is correlated with Rpg1-mediated stem rust resistance. *Proc Natl Acad Sci U S A* 104, 10276–10281. doi:10.1073/pnas.0703758104.

Nirmala, J., Drader, T., Chen, X., Steffenson, B., and Kleinhofs, A. (2010). Stem rust spores elicit rapid RPG1 phosphorylation. *Mol Plant Microbe Interact* 23, 1635–1642. doi:10.1094/MPMI-06-10-0136.

Roelfs, A. (1985). Epidemiology in North America. *The cereal rusts* 2, 403–434. Available at: http://www.globalrust.org/sites/default/files/cereal-rusts/volume2.pdf#page=395.

Roelfs, A., and Bushnell, W. (1985). The Cereal Rusts. Vol. 2. Diseases, Distribution. *Epidemiology, and Control. Academic Press, Orlando*.

Royle, D. (1976). "Structural Features of Resistance to Plant Diseases," in *Biochemical Aspects of Plant–Parasite Relationships* (Proceedings of The Phytochemical Society Symposium, University of Hull), 161–193. Available at: http://www.sciencedirect.com/science/article/pii/B9780122679506500144.

Steffenson, B. J., Jin, Y., Brueggeman, R. S., Kleinhofs, A., and Sun, Y. (2009). Resistance to stem rust race TTKSK maps to the rpg4/Rpg5 complex of chromosome 5H of barley. *Phytopathology* 99, 1135–1141. doi:10.1094/PHYTO-99-10-1135.

Stock, F. (1931). Untersuchungen über Keimung und Keimschlauchwachstum der Uredosporen einiger Getreideroste. Available at: http://publikationen.ub.uni-frankfurt.de/frontdoor/index/index/docId/15674.

Wang, X., Richards, J., Gross, T., Druka, A., Kleinhofs, A., Steffenson, B., Acevedo, M., and Brueggeman, R. (2013). The rpg4-mediated resistance to wheat stem rust (Puccinia graminis) in barley (Hordeum vulgare) requires Rpg5, a second NBS-LRR gene, and an actin depolymerization factor. *Mol Plant Microbe Interact* 26, 407–418. doi:10.1094/MPMI-06-12-0146-R.

Yirgou, D., and Caldwell, R. (1968). Stomatal penetration of wheat seedlings by stem and leaf rusts in relation to effects of carbon dioxide light and stomatal aperture. *Phytopathology* 58.

Yirgou, D., and Caldwell, R. M. (1963). Stomatal penetration of wheat seedlings by stem and leaf rust: effect of light and carbon dioxide. *Science* 141, 272–273. doi:10.1126/science.141.3577.272.

Zurn, J. D., Dugyala, S., Borowicz, P., Brueggeman, R., and Acevedo, M. (2015). Unraveling the Wheat Stem Rust Infection Process on Barley Genotypes Through Relative qPCR and Fluorescence Microscopy. *Phytopathology* 105, 707–712. doi:10.1094/PHYTO-09-14-0251-R.

CHAPTER 5. TOWARDS IDENTIFICATION OF THE *RPR9* GENE REQUIRED FOR *RPG1* AND *RPG4* MEDIATED WHEAT STEM RUST RESISTANCE IN BARLEY

5.1. Abstract

In the wake of the threat that *Puccinia graminis* f. sp. *tritici* (*Pgt*) race TTKSK and its lineage present to barley production extensive research was conducted to identify, clone and characterize the *rpg4*/*Rpg5*-mediated resistance locus (*RMRL*) that was initially identified providing effective resistance to *Pgt* races QCCJ and TTKSK in the unimproved barley line Q21861. The *RMRL* providing resistance against a broad spectrum of stem rust races contains two nucleotide binding site-leucine rich repeat (NLR) R-genes, *Rpg5* and *HvRga1,* that are required together for stem rust resistance. Fast neutron mutagenesis of Q21861 was utilized in a forward genetics approach to identify other components that function in this atypical broad spectrum, non-hypersensitive resistance that follows the dual NLR integrated sensory domain resistance mechanism model. A mutant was identified that compromised the *RMRL* and it was designated *rpr9* (Required for *P. graminis* Resistance 9). The *rpr9* mutant was crossed with the Swiss landrace line *Hv*584, which was shown to carry *RMRL* but is polymorphic with Q21861. A recombinant inbred population was developed containing 95 individuals and was phenotyped with *Pgt* race QCCJ (a surrogate race for TTKSK) at the seedling stage and with *Pgt* race TTKSK at the adult plant stage in the field. The RIL population was genotyped with the Illumina iSelect 9k marker panel, and the phenotype and genotype data were used to map the *rpr9* mutant to a 7.1 cM region on barley chromosome 3H, delimited by the SNP markers SCRI_RS_164675 and SCRI_RS_146347. The nimble gene barley exome capture array was utilized on *rpr9* and wt Q21861, followed by Illumina sequencing, which resulted in the identification of 0.841 Mbp deletion harboring eleven high confidence annotated deleted genes. The best candidate *rpr9*

genes in the region are SKP1-like 9 protein and F-box family protein annotated based on similarity with the model plant *Arabidopsis thaliana*. We will utilize post-transcriptional gene silencing via BSMV-VIGS and *Agrobacterium*-mediated transient expression of gene specific double stranded RNA to further functionally characterized the mutant genes responsible for the *rpr9* susceptible stem rust phenotype.

5.2. Introduction

The obligate biotrophic fungal pathogen, *Puccinia graminis,* causes the disease stem rust on a broad range of primary hosts including more than 365 species of cereals and grasses. However, *formae specialis* that commonly infect cereal crops are subdivided into: wheat stem rust, *P. graminis* f. sp. *tritici* infecting wheat and barley; rye stem rust, *P. graminis* f. sp. *secalis* infecting rye and barley; and oat stem rust, *P. graminis* f. sp. *avenae* infecting oat and some barley lines (Leonard, 2001). While all three *forma specialis* cause disease on barley, wheat stem rust is considered as one of the most serious disease of wheat and barley, and historically caused devastating epidemics especially in the Upper Midwestern US in the early to mid-20th century. However, in the mid-20th century wheat breeders began pyramiding several resistance genes into varieties providing durable resistance ending the occurrence of major epidemics on wheat. Stem rust was also managed by genetic resistance in barley, but only a single resistance gene, *Rpg1*, was deployed in the Midwestern US, protecting barley cultivars since 1942 (Steffenson, 1992). The *Rpg1* gene was identified in 2002 by a positional cloning effort and was predicted to encode a protein with two serine/threonine protein kinase domains designated pK1 and pK2 (Brueggeman et al., 2002). The pK2 domain was characterized as an active kinase and the pK1 domain appeared to be a pseudokinase lacking phosphorylation activity. However, both domains were shown to function in stem rust resistance as demonstrated by *in vitro* generated mutants

transformed into the susceptible cultivar Golden Promise lacking an *Rpg1* allele (Nirmala et al., 2006). Interestingly, it was also shown that the RPG1 protein was systemically phosphorylated *in vivo,* within five minutes post inoculation with avirulent stem rust urediniospores (Nirmala et al., 2010), but did not respond to virulent races. The RPG1 protein is degraded between 20-24 HPI (Hour Post Inoculation) with avirulent isolates (Nirmala et al., 2007) and both the phosphorylation and ubiquitin ligase mediated degradation are required to elicit the resistance response/s. Two unique effector proteins putatively present at the surface of avirulent stem rust spores were identified by affinity chromatography using a RGD (arginine-glutamic acid-aspartic acid) coupled sepharose column (Nirmala et al., 2011). Affinity chromatography utilizing the RGD peptides were utilized to isolate interacting RGD binding and VPS9 effector proteins that induce RPG1 dependent HR and protein degradation. This approach was adopted as it was shown that spores treated with RGD peptide, did not induce RPG1 phosphorylation and failed to infect the susceptible cultivar Steptoe (*rpg1*) despite retaining their viability to germinate on 2% water agar. RGD peptides are known to mask the RGD binding domains of certain proteins and prevent cell attachment and thereby disrupt vital functions.

A new pathotype of *Pgt*, designated race QCCJ, virulent on barley containing *Rpg1* was identified in North Dakota in 1989 (Roelfs, 1989). QCCJ increased in prevalence and became one of the most common virulence types in North America causing disease epidemics (Roelfs et al., 1993). The threat to barley production by this new stem rust race virulent on *Rpg1* prompted the evaluation of over 18,000 barley accessions from the USDA National Small Grains collection with the best source of *Pgt* race QCCJ resistance discovered in the unimproved barley line Q21861 from Queensland, Australia via CMMYT (Jin et al., 1994a). Genetic studies revealed that the resistance was conferred by the single recessive gene designated *rpg4*. The *rpg4* gene

was also shown to be temperature sensitive providing resistance at lower (17-22°C) temperatures (Jin et al., 1994b), but completely ineffective at temperatures above 27°C. The *rpg4* gene was genetically mapped to the long arm of barley chromosome 5H (Borovkova et al., 1995).

A highly virulent strain of stem rust, race TTKSK (A.K.A. Ug99) emerged in Uganda, Africa in 1999 (Pretorius et al., 2000) and is considered highly virulent because it carries a unique combination of virulence genes and is capable of infecting more than 80% of the wheat grown worldwide (Jin et al., 2007, 2008) and more than 97% of barley cultivars, including those having *Rpg1* (Steffenson et al., 2013). The threat posed by Ug99 has raised concerns over world food security (Stokstad, 2007). Fortunately, the *RMRL* (*rpg4/Rpg5*-mediated resistance locus) in the barley line Q21861 has been shown to confer effective resistance against race TTKSK (Steffenson et al., 2009).

Line Q21861 also contains resistance to isolates of rye stem rust, including *Pgs* isolate 92-MN-90, which was designated the *Rpg5* gene. The single dominant resistant gene was shown to be tightly linked to *rpg4* (Druka et al., 2000) and it was initially reported that *rpg4* and *Rpg5* could be the same gene despite the different inheritance, recessive vs. dominant. When *Rpg5* was cloned (Brueggeman et al., 2008) it was reported distinct from *rpg4* based on high-resolution mapping and recombinant progeny segregating for wheat and rye stem rust resistance with an actin depolymerization factor, *HvAdf2*, reported as the best *rpg4* candidate gene (Kleinhofs et al., 2009). However, further high-resolution analysis utilizing SNP markers identified by genomic sequence comparison determined that *HvAdf2* was not *rpg4.* Also, the *Rpg5* gene is required for *rpg4*-mediated wheat stem rust resistance (Wang et al., 2013) and was shown to be the functionally polymorphic *R*-gene at the *RMRL* (Arora et al., 2013). The cloning and characterization of *RMRL* determined that the two resistances, *rpg4*-mediated wheat stem rust

and *Rpg5*-mediated rye stem rust resistance mechanisms although somewhat distinct in their mode of action and resistance (Brueggeman et al., 2008) both depend on *Rpg5* as the *R*-gene component (Brueggeman and Solanki, 2017) however there are still some modifiers of the resistance mechanisms tightly linked to the locus that give a somewhat different interaction with the rye stem rust and wheat stem rust when crosses are made with genotypes such as cv Steptoe (Wang et al., 2013). Thus, *rpg4* and *Rpg5* cannot be considered distinct *R*-genes because *rpg4*-mediated resistance against wheat stem rust still requires resistance components in common with *Rpg5*-mediated rye-stem rust resistance in barley.

The *rpg4*-mediated wheat stem rust resistance in barley (*Hordeum vulgare*) is conferred by the complex *RMRL*. The *RMRL* has been cloned (Brueggeman et al., 2008) and shown to harbor three tightly linked genes required for resistance including the dominant NBS-LRR R gene (NLR) rye stem rust resistance gene *Rpg5*, a second NLR resistance gene *Hv*Rga1, and the actin depolymerization factor, *HvAdf3* (Wang et al., 2013). Transcript analysis of the barley line Q21861 suggests that *HvAdf3* is differentially regulated 6 hours post inoculation with avirulent *Pgt* pathotypes, suggesting early prehaustorial recognition and resistance responses similar to what has been shown for *Rpg1* (Solanki et al., 2016). The very early *Rpg1* resistance response is triggered by the recognition of effector proteins located on the surface of the spore and occurs almost immediately after the spore contacts the leaf surface (Nirmala et al., 2010). Thus, the timing of the *RMRL* resistance responses also indicates pathogen detection occurring early at the leaf surface similar to *Rpg1*. This suggests that the early detection of *Pgt* may be dependent on a PAMP-like plasma membrane localized receptor located at the cell periphery. In our pursuit to identify this putative receptor we generated two distinct Q21861 mutants of the *RMRL* stem rust resistance pathway, *rpr8* and *rpr9*, and *rpr9*, represses both the *Rpg1*- and *RMRL* resistance

pathways indicating that the two pathways overlap. Although the *Rpg1* and *RMRL* confer some differential specificity (Sun and Steffenson, 2005; Steffenson et al., 2013), the *rpr9* mutant suggests the two mechanisms contain common resistance component/s either downstream in a converging resistance pathway or possibly rely on a common extracellular receptor. We hypothesis that the only two effective stem rust resistance genes characterized in barley to date, the *Rpg1* and *RMRL*, conferring broad spectrum resistance, mediate early response mechanisms showing spatial, temporal and functional hallmarks that suggest non-host resistance mechanisms possibly pathogen associated molecular pattern (PAMP) triggered immunity (PTI)-like responses. However, interestingly *RMRL*-mediated resistance is a non-HR resistance mechanism (dissertation chapter 2) indicative of a PTI –like response whereas *Rpg1*-mediated resistance is an HR dependent resistance mechanism more indicative of an ETI response.

The plant innate immunity system has been separated into distinct layers with the first line of defense known as pathogen associated molecular patterns (PAMP) triggered immunity (PTI) which has been classified as an active form of non-host resistance. This early defense mechanism triggered at the cell surface by extracellular pathogen effectors, induce responses including H_2O_2 accumulation, pathogen related (PR) gene expression, callose deposition at the point of ingress, and sometimes a low amplitude PCD response that is typically limited to a small number of cells surrounding the infection site (Orozco-Cárdenas et al., 2001). These general PTI responses are induced through conserved transmembrane cell surface receptor complexes known to contain pattern recognition receptors (PRRs). The PRRs fall into the transmembrane domain proteins class that typically contain an intracellular kinase signaling domain known as the receptor-like kinases (RLKs). RLKs are separated into three classes based on their differential extracellular domains; 1) LRRs, 2) LysM domain, and 3) Ca^{2+} binding and GUB domains. PRRs

identify PAMPs, which are conserved molecules of microbial origin present in broad genera or species that are indispensable for pathogen fitness such as flg22 the subunit of bacterial flagella required for motility of many bacterial species or chitin a major component of fungal cell walls. PTI responses can also be elicited by damage associated molecular patterns (DAMPs), which are host cell extracellular matrix subunits such as oligogalacturonides residues released from plant cell walls upon partial degradation by microbial pathogens whose detection by the Wall associated kinases (WAKs) alert the host of its own compromised cell integrity indicating pathogen ingress or challenge (Ferrari et al., 2013).

Host specific pathogens counter evolved virulence effectors to evade these PTI responses by masking their PAMPs from detection, as is the case with chitin binding effector proteins (van Esse et al., 2007; Sánchez-Vallet et al., 2013) or by blocking the signaling pathways as is seen with effectors that inhibit FLS2 PRR-mediated signaling following flg22 perception (Bigeard et al., 2015). These virulence effectors, i.e. the fungal chitin binding effectors, are secreted into the apoplast or into the host cells via the TTSS (Type Three Secretion System) for bacteria such as *Xanthomonas translucens* or *Psuedomonas syringae* and yet to be identified and characterized secretion mechanisms for fungal pathogens. However, as postulated in the zig-zag model (Jones and Dangl, 2006) plants counter-evolved cytoplasmic localized immunity receptors, typically with NLR protein domain architecture, that recognize the presence of these effectors and elicit the hallmark higher amplitude PCD immunity response in plants, referred to as the hypersensitive response (HR). Once an effector is recognized by a cognate NLR immunity receptor then it becomes an avirulence protein. For biotrophic pathogens that require living host cells to feed these effectors no longer facilitates disease but hinders the pathogen by eliciting PCD which kills the cells they are feeding from. Thus, the HR or strong PCD response is critical

to plant innate immunity against biotrophic plant pathogens including viruses, bacteria, fungi, oomycetes, and invertebrates (Glazebrook, 2005).

Fast neutron bombardment mutagenesis can induce DNA deletions from 1 bp (base pair) to several Megabase (Li et al., 2002, 2001; Koornneef et al., 1982). A fast neutron (FN) irradiation induced mutant in the Q21861 background compromised for stem rust race QCCJ resistance was identified (Zhang et al., 2006) and designated as the *rpr9* mutant. This mutant still retains the *RMRL* locus yet is compromised for the QCCJ resistance response indicating importance of the *Rpr9* gene in the *RMRL*-mediated resistance pathway. To our interest these mutants also have a stunted root phenotype, short roots at early growth stages, thus, we attempted to identify the mutant gene/s responsible for the stunted root phenotype as well.

Here we report on the identification of eleven candidate *rpr9* genes via genetic mapping and exome capture. QTL mapping delimits the *rpr9* gene to a genetic interval of 7.1 cM containing 365 high confidence and 266 low confidence genes. Our attempt to identify the mutations responsible for the stunted root phenotype resulted in the identification of a region overlapping with the *rpr9* gene region. To identify the deletion within or containing the *Rpr9* gene the barley Nimblgen (Roche) exome capture array was utilized on the *rpr9* mutant and wildtype Q21861 identifying a gene rich deletion block inside the *rpr9* delimited region covering 1.167 Mbp of physical sequence on chromosome 3H based on barley POPSEQ positions for the flanking intact genes and the region characterized from the barley genome sequence. This deletion contains eleven high confidence genes classified into a family of four peroxidases, two NAD(P)H-quinone oxidoreductases, a SKP1- like 9 protein, a F-box family protein, a L-tyrosine decarboxylase and a Octicosapeptide/Phox/Bem1p family protein. We posit that our top candidates encode the *SKP1*-like 9 and F-box proteins which were shown to work together as a

component of SCF (SKP/Cullin/F-box and ring finger protein Rbx1) E3 ubiquitin ligase complex which have a role in stomatal opening and early plant immunity pathways. The genetic analyses and tools developed here will facilitate the identification and functional validation of the *rpr9* gene and the gene responsible for the stunted root phenotype.

5.3. Materials and methods

5.3.1. Mutant screens

The barley line Q21861 was utilized for the forward genetics screen because it carries *RMRL* as well as the *Rpg1* stem rust resistance gene and to clone the *Rpg5* gene (Brueggeman et al., 2008) and identify *RMRL* (Wang et al., 2014, Arora et al., 2014). The genetic quality Q21861 seed was the original source used to develop the Steptoe x Q21861, Harrington x Q21861 and MD2 x Q21861 high resolution mapping population (Brueggeman et al., 2008) that were used for the positional cloning of the *Rpg5* and *RMRL* (Brueggeman et al., 2008; Wang et al., 2014). After three generations of single seed descent and seed increase the genetic quality Q21861 seed (~3 kg) was irradiated with fast neutrons (3.5 or 4.0 Gy using protocol 563) at the FAO/IAEA Seibersdof SNIF facility near Vienna, Austria. Q21861 $M1$ seed was planted and allowed to self and ~6,000 spikes containing M_2 seed were harvested from individual plants. In the greenhouse, 20–30 M_2 seed from individual spikes were planted in cones filled with a peat moss:perlite (3:1 v/v) potting mix (#1 Sunshine Mix, Fisons, Vancouver, Canada). Plants were inoculated with pathotype *Pgt*-QCCJ when the first leaves were fully expanded and assessed for their infection types 12–14 days post inoculation using the protocols developed by Steffenson et al. (1993). Infection type (IT) were based on a 0-4 scale (defined by Stackman et al. US Dept. Agric. Serv. E-617, 705-712, 1962) where 0 is highly resistant and 4 is highly susceptible with the in between numbers representing intermediate reactions which are further modified by + or – and a fleck (;)

which indicates a small necrotic area. IT1 indicates minute uredinia; IT2 small uredinia with chlorosis; IT3 medium uredinia often with chlorosis; and IT4 indicates large uredinia with chlorosis. Barley often exhibits mesothetic reactions with two or more ITs on a single leaf therefore ITs observed are recorded in order of their prevalence and this categorical disease rating converted to a single numerical value as described in Zhou et al. (Zhou et al., 2014). When segregation for stem rust reactions were observed within an individual M_2 spike, single heads were harvested and phenotyped with pathotype *Pgt*-QCCJ at the M_3 generation (Appendix Table A4). Two consistent mutants were identified and designated as *rpr8* and *rpr9*. However only *rpr9* mutant charcteriation will be discussed here.

5.3.2. Segregation analysis and RIL population development

The *rpr9* mutant generated in the Q21861 background was backcrossed to Q21861 for four generations and 15 BCF_2 individuals were phenotyped at each back cross (BC) generation to identify homozygous *rpr9* mutant individuals. Pollen from the *rpr9* mutant with the background mutations cleaned up with four generations of backcrossing was crossed with the Swiss landrace Hv584 as the female parent to generate the Hv584/*rpr9* population. For inheritance studies Hv584/*rpr9* F_2 individuals were phenotyped at the seedling stage with *Pgt* race QCCJ in the growth chamber as described in Mirlohi et al., 2008. The single gene segregation analysis was calculated utilizing a χ^2 test with the null hypothesis that the *rpr9* phenotype was contributed by a single recessive gene. A Hv584/*rpr9* RIL population consisting of 95 individuals was developed through single seed decent till the $F_{5:6}$ generation.

5.3.3. Rag-Doll test for root growth analysis

Germination of *rpr9* mutants and wildtype Q21861 parents lead to the observation that the mutants had a stunted root phenotype during the early germination process. After four rounds

of backcrossing the mutant to wildtype Q21861 to clean up background mutations it was observed that the stunted root phenotype was still present. Two seed germination papers/brown paper towels were placed together, and a horizontal line was drawn using a pencil at the center of the paper. The paper towels were moistened with H_2O. Twenty *rpr9* and wt Q21861 seed were selected randomly and placed separately on one half of the moist germination papers keeping them on the drawn horizontal line. The germination paper was carefully rolled vertically from the drawn line avoiding seed movement into a moderately tight tube and secured with duct tape. All the tubes were labelled and kept in a warm place at ~25ºC for four days before taking the root length readings in mm from seed base to the end of the longest root. A similar method was followed using the 95 individual Hv584/*rpr9* RILs, Q21861, Hv584 and the *rpr9* mutant and root length was recorded for 3 germinated seeds and data was used for QTL mapping (Table 5.1).

Table 5.1. Root length phenotype in Hv584/rpr9 $F_{2:6}$ RIL population with parents (Hv584, rpr9) and wild type Q21861.

Genotype	Root Length 1 (mm)	Root Length 2 (mm)	Root Length 3 (mm)	Average Root Length (mm)
Hv584/rpr9 F2:6 -RIL-1	36	-	-	36
Hv584/rpr9 F2:6 -RIL-2	14	14	11	13
Hv584/rpr9 F2:6 -RIL-3	14	-	-	14
Hv584/rpr9 F2:6 -RIL-4	23	14	-	18.5
Hv584/rpr9 F2:6 -RIL-5	15	13	8	12
Hv584/rpr9 F2:6 -RIL-6	30	9	17	18.6
Hv584/rpr9 F2:6 -RIL-7	25	19	-	22
Hv584/rpr9 F2:6 -RIL-8	13	13	14	13.3
Hv584/rpr9 F2:6 -RIL-9	23	10	18	17
Hv584/rpr9 F2:6 -RIL-10	14	25	-	19.5
Hv584/rpr9 F2:6 -RIL-11	27	23	-	25
Hv584/rpr9 F2:6 -RIL-12	20	13	8	13.7
Hv584/rpr9 F2:6 -RIL-13	6	13	11	10
Hv584/rpr9 F2:6 -RIL-14	19	17	16	17.3
Hv584/rpr9 F2:6 -RIL-15	15	24	18	19
Hv584/rpr9 F2:6 -RIL-16	16	10	-	13
Hv584/rpr9 F2:6 -RIL-17	12	19	-	15.5
Hv584/rpr9 F2:6 -RIL-18	4	20	13	12.3
Hv584/rpr9 F2:6 -RIL-19	15	5	-	10
Hv584/rpr9 F2:6 -RIL-20	31	29	24	28

Table 5.1. Root length phenotype in Hv584/rpr9 F2:6 RIL population with parents (Hv584, rpr9) and wild type Q21861 (continued).

Genotype	Root Length 1 (mm)	Root Length 2 (mm)	Root Length 3 (mm)	Average Root Length (mm)
Hv584/rpr9 F2:6 -RIL-21	-	-	-	-
Hv584/rpr9 F2:6 -RIL-22	12	-	-	12
Hv584/rpr9 F2:6 -RIL-23	3	6	15	8
Hv584/rpr9 F2:6 -RIL-24	22	-	-	22
Hv584/rpr9 F2:6 -RIL-25	17	19	9	15
Hv584/rpr9 F2:6 -RIL-26	26	17	21	21.3
Hv584/rpr9 F2:6 -RIL-27	10	15	-	12.5
Hv584/rpr9 F2:6 -RIL-28	31	6	12	16.3
Hv584/rpr9 F2:6 -RIL-29	11	4	-	7.5
Hv584/rpr9 F2:6 -RIL-30	16	9	11	12
Hv584/rpr9 F2:6 -RIL-31	13	9	-	11
Hv584/rpr9 F2:6 -RIL-32	20	11	9	13.3
Hv584/rpr9 F2:6 -RIL-33	10	28	23	20.3
Hv584/rpr9 F2:6 -RIL-34	26	-	-	26
Hv584/rpr9 F2:6 -RIL-35	19	9	11	13
Hv584/rpr9 F2:6 -RIL-36	24	16	-	20
Hv584/rpr9 F2:6 -RIL-37	27	28	-	27.5
Hv584/rpr9 F2:6 -RIL-38	13	18	8	13
Hv584/rpr9 F2:6 -RIL-39	17	-	-	17
Hv584/rpr9 F2:6 -RIL-40	9	19	18	15.3
Hv584/rpr9 F2:6 -RIL-41	30	17	22	23
Hv584/rpr9 F2:6 -RIL-42	24	-	-	24
Hv584/rpr9 F2:6 -RIL-43	16	13	13	14
Hv584/rpr9 F2:6 -RIL-44	17	13	18	16
Hv584/rpr9 F2:6 -RIL-45	32	29	19	26.7
Hv584/rpr9 F2:6 -RIL-46	22	26	-	24
Hv584/rpr9 F2:6 -RIL-47	22	28	15	21.7
Hv584/rpr9 F2:6 -RIL-48	10	22	28	20
Hv584/rpr9 F2:6 -RIL-49	19	18	-	18.5
Hv584/rpr9 F2:6 -RIL-50	22	17	11	16.7
Hv584/rpr9 F2:6 -RIL-51	23	21	19	21
Hv584/rpr9 F2:6 -RIL-52	21	27	30	26
Hv584/rpr9 F2:6 -RIL-53	7	-	-	7
Hv584/rpr9 F2:6 -RIL-54	10	-	-	10
Hv584/rpr9 F2:6 -RIL-55	-	-	-	-
Hv584/rpr9 F2:6 -RIL-56	15	10	5	10
Hv584/rpr9 F2:6 -RIL-57	18	24	22	21.3
Hv584/rpr9 F2:6 -RIL-58	16	11	-	13.5
Hv584/rpr9 F2:6 -RIL-59	-	-	-	-
Hv584/rpr9 F2:6 -RIL-60	16	11	-	13.5
Hv584/rpr9 F2:6 -RIL-61	29	13	21	21
Hv584/rpr9 F2:6 -RIL-62	21	-	-	21
Hv584/rpr9 F2:6 -RIL-63	21	14	14	16.3
Hv584/rpr9 F2:6 -RIL-64	8	5	-	6.5
Hv584/rpr9 F2:6 -RIL-65	13	-	-	13
Hv584/rpr9 F2:6 -RIL-66	-	-	-	-

Table 5.1. Root length phenotype in Hv584/rpr9 F2:6 RIL population with parents (Hv584, rpr9) and wild type Q21861 (continued).

Genotype	Root Length 1 (mm)	Root Length 2 (mm)	Root Length 3 (mm)	Average Root Length (mm)
Hv584/rpr9 F2:6 -RIL-67	14	13	22	16.3
Hv584/rpr9 F2:6 -RIL-68	6	3	5	4.7
Hv584/rpr9 F2:6 -RIL-69	6	11	-	8.5
Hv584/rpr9 F2:6 -RIL-70	12	13	19	14.7
Hv584/rpr9 F2:6 -RIL-71	10	10	-	10
Hv584/rpr9 F2:6 -RIL-72	19	15	20	18
Hv584/rpr9 F2:6 -RIL-73	16	15	16	15.7
Hv584/rpr9 F2:6 -RIL-74	10	8	-	9
Hv584/rpr9 F2:6 -RIL-75	21	20	-	20.5
Hv584/rpr9 F2:6 -RIL-76	21	33	23	25.7
Hv584/rpr9 F2:6 -RIL-77	29	21	18	22.7
Hv584/rpr9 F2:6 -RIL-78	23	27	22	24
Hv584/rpr9 F2:6 -RIL-79	19	22	-	20.5
Hv584/rpr9 F2:6 -RIL-80	10	-	-	10
Hv584/rpr9 F2:6 -RIL-81	10	-	-	10
Hv584/rpr9 F2:6 -RIL-82	9	-	-	9
Hv584/rpr9 F2:6 -RIL-83	10	8	-	9
Hv584/rpr9 F2:6 -RIL-84	17	21	-	19
Hv584/rpr9 F2:6 -RIL-85	5	24	-	14.5
Hv584/rpr9 F2:6 -RIL-86	15	14	14	14.7
Hv584/rpr9 F2:6 -RIL-87	12	16	4	10.7
Hv584/rpr9 F2:6 -RIL-88	16	15	-	15.5
Hv584/rpr9 F2:6 -RIL-89	10	8	7	8.3
Hv584/rpr9 F2:6 -RIL-90	10	13	8	10.3
Hv584/rpr9 F2:6 -RIL-91	10	17	19	15.3
Hv584/rpr9 F2:6 -RIL-92	7	5	-	6
Hv584/rpr9 F2:6 -RIL-93	4	12	-	8
Hv584/rpr9 F2:6 -RIL-94	8	12	-	10
Hv584/rpr9 F2:6 -RIL-95	9	9	5	7.7
Hv584	40	24	-	32
Q21861	21	20	20	20.3
rpr9	10	6	11	9

5.3.4. Genotyping and QTL analysis

The Hv584/*rpr9* RIL population was genotyped using the 9k Illumina Infinium iSelect assay (Muñoz-Amatriaín et al. 2014) at the USDA cereal genotyping lab, Fargo ND. Markers containing greater than 30% missing data were removed from the data set. The linkage map for the Hv584/*rpr9* RIL population was generated using MapDisto 2.0 (Lorieux, 2012). The command ‘find groups’ was used to make markers linkage group with a logarithm of the odds

(LOD) value of 3.0 and rmax of 0.3. The 'AutoOrder', 'AutoCheckInversions', and 'AutoRipple' commands were utilized to generate the linkage map at a LOD of 3.0 and Kosambi mapping function was used to calculate the genetic distances. The final linkage map was developed using 'Automap' command for QTL analysis. The resulting map were then utilized in QGene 4.0 (Johanes and Nelson 2008) using composite interval mapping (CIM) to identify resistance/ susceptibility QTL to SFNB. A permutation test with 1,000 iterations was performed to find LOD threshold at a significance level p=0.05 and 0.01. Cosegregating markers were removed, leaving the marker with the least amount of missing data at each position. Quantitative trait locus (QTL) analysis was conducted in Qgene 4.4 (Joehanes and Nelson 2008) using the single-trait multiple interval mapping (MIM) algorithm. A permutation test consisting of 1000 iterations was used to determine a LOD threshold at the p = 0.05 significance level. Genetic positions based on POPSEQ (Mascher et al. 2013) were also obtained for each iSelect marker using IPK barley BLAST server (http://webblast.ipk-gatersleben.de/barley_ibsc/) and aligning with the draft sequence assembly of barley cultivar Morex (International Barley Genome Sequencing Consortium et al., 2012). Physical positions of the markers flanking the identified QTL were obtained from aligning the sequence of flanking markers of QTL with the recently available barley physical map (Mascher et al. 2017) using IPK barley BLAST sever. Gene content in the deleted region between the obtained physical position for flanking markers was determined based on the annotated genes at chromosome 3H publicly available at IPK BLAST server (http://webblast.ipk-gatersleben.de/barley_ibsc/) and used to identify the region targeted for putative deletions from the exom capture data.

5.3.5. DNA extraction, fragmentation, exome capture library preparation, and sequencing

Eleven seed of wt Q21861, and the *rpr9* mutants were placed on water-soaked Whatman filter paper in a disposable petri dish for 24 hours. Embryos were excised using a sterilized DNase free scalpel and a total of five excised embryos were used for DNA extraction using the PowerPlant Pro DNA isolation kit (MoBIO Laboratories Inc., QIAGEN Carlsbad CA). Mechanical lysis of samples was done using a mechanical bead beater at 2000 rpm for 2 cycles of 3 minutes each and the manufacturer's protocol was followed for DNA isolation. The quality of extracted DNA was checked by running an aliquot of 1 µL of gDNA on a 1% agarose gel supplemented with GelRED (Biotium) fluorescent nucleic acid dye. The DNA was determined to have good integrity when it showed a high molecular weight band ~15-20 kb with minimal low molecular weight smearing indicative of DNA degradation. The gDNA was quantified using the Qubit Broad Range DNA Quantification kit (Thermo Scientific). Enzymatic DNA shearing was optimized to generate desired fragment sizes of 250-450 bp by conducting a time course experiment with digestion reactions consisting of 1.5 µg of gDNA in a 20 µl reaction with NEB dsDNA Fragmentase enzyme, 1x Fragmentase reaction buffer and 10mM $MgCl_2$ (New England Biolabs, Ipswich MA). Digestion reactions were incubated at 37°C for 10, 15, 20, 25 and 30 minutes and then inactivated by adding 5 µl of 0.5 M EDTA, followed by AMPure XP magnetic bead DNA purification (Agencourt). DNA size distribution was analyzed on the Agilent 2100 Bioanalyzer (Agilent Technologies) using a DNA 1000 kit following the manufacturer protocol for chip loading and data analysis. The 25-minute enzymatic digestion was found to produce the optimal fragment size distribution ranging between 250-450 base pairs (Fig. 5.1) and was used to produce fragmented DNA libraries of Q21861, and *rpr9*.

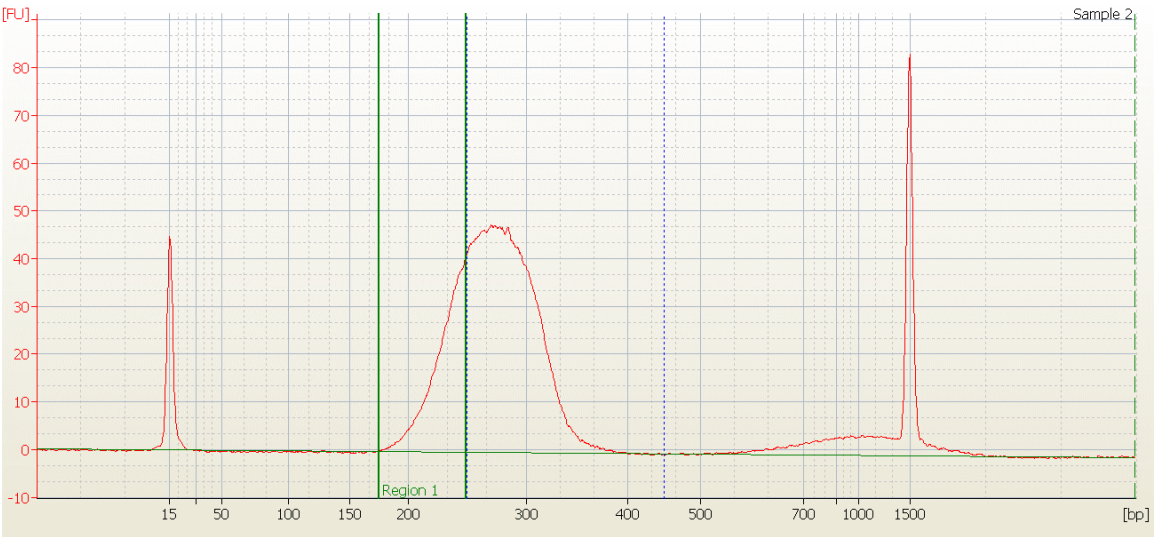

Fig. 5.1. Size determination of fractionated DNA after 25 minutes of barley DNA digestion with NEB DNA fragmentize enzyme on Bioanalyzer 1000 DNA chip. A 25-minute enzymatic digestion produced DNA fragments in the size range of 250-450 base pairs, which was required for exome capture library preparation. The X-axis represents the fluorescence units and Y-axis represents the size of DNA fragments. The two terminal peaks represent the DNA ladder peaks with the lower marker at 25 base pairs (left) and the upper marker 1000 base pairs (right).

Fragmented gDNA samples were utilized with the KAPA HTP library preparation kit for gDNA library preparation for Illumina sequencing after whole exome capture using the Roche NimbleGen SeqCap EZ Developer probe pool barley exome design 120426_Barley_BEC_D04 with a total capture design size of 88.6 Mb. The standard manufacturer protocol was followed for library preparation using the KAPA HTP kit, except for size selection being performed on a Pippin Prep gel purification system (Sage Science) with a target of 250-450 bp size selection. The gDNA used to prepare the barcoded barley whole exome capture multiplexed library was developed according to seqCAP EZ Library SR user guide 4.1 protocol. Quality and size distribution of the final capture library was determined using a bioanalyzer as previously described. A Qubit fluorometer was used to quantify the library for final dilution and sequencing on an Illumina NextSeq flow cell generating 150 base pair single end reads. Qubit readings were used since bioanalyzer tends to underestimate the quantity for size selected libraries due to

presence of DNA fragments not falling within the desired range (150-450). Thus, posing a possible chance of over-flooding of the flow cells due to the under-diluted library.

5.3.6. Data analysis and bioinformatics

The *rpr9* mutant and wildtype Q21861 sequencing reads were parsed by their specific barcodes added during library preparation. A total of 115,741,280 base reads for Q21861 and 104,846,733 base reads for *rpr9* were obtained averaging 151 bases per read count. Quality score of the raw reads sequencing reads were determined by using FQC dashboard (Brown et al., 2017). Sequencing reads were imported into CLC Genomics Workbench v8.0 and trimmed for the presence of adapter sequences. Mutant and wildtype reads were then aligned to the barley reference genome (IBGSC 2012) using the BWA 'mem' algorithm (Li and Durbin 2010) with default settings. Aligned reads were used to identify deleted region utilizing two separate pipelines. (1) Small deletions (less than 100 bp) were identified using SAMtools 'mpileup' with default settings (Li et al. 2009). The identified variants were filtered for a minimum read depth of 3 and a minimum individual genotype quality of 10 using VCFtools (Danacek et al. 2011). (2) As fast neutron mutagenesis may induce large chromosomal deletions, sequencing coverage was calculated across all exome capture targets using BEDTools 'genomecov' (Quinlan and Hall 2010) to identify full gene deletions. Physical positions of fully deleted exome capture targets were obtained from the barley physical map (Mascher et al. 2017), allowing for the identification of candidate genes within the delimited region and characterization of the larger chromosomal deletions containing multiple genes.

5.4. Results

5.4.1. Identification of mutants compromised for RMRL mediated restance responces

The phenotyping of the Q21861 fast neutron (FN) irradiated M_2 generation with Pgt race QCCJB identified two putative mutants that compromised RMRL-mediated resistance designated *rpr8* and *rpr9*. Eleven *rpr9* individuals were phenotyped with *Pgt* race QCCJB and exhibited ITs ranging from 2-3 to 3- with a mode of 3-,2 compared to the highly resistant wild type line Q21861, which showed ITs ranging from 0; to 0;12 with a mode of 0; (Table 1). The line Q21861 is resistant to QCCJ due to the RMRL and is also resistant to *Pgt* race HKHJ due to *Rpg1* specific resistance. Interestingly, *rpr9* also exhibited susceptible ITs to *Pgt* race HKHJ ranging from 2,1 to 3- with a mode of 3-,21 compared to the resistant wild type line Q21861 which shows ITs ranging from 0;1 to 0;12 with a mode of 0; (Table 5.2). Thus, the *rpr9* mutant generated in the wheat stem rust resistant barley line Q21861 background, which carries both the *Rpg1* and *RMRL* is compromised for resistance (Table 5.2) to both *Pgt* race QCCJ that is specifically avirulent on *RMRL* and HKHJ that is specifically avirulent on *Rpg1*.

It was determined that the *rpr9* mutant generated in the wheat stem rust resistant barley line Q21861 background, which carries both the *Rpg1* and *RMRL* (Brueggeman et al., 2002; Mirlohi et al., 2008; Brueggeman et al., 2008; Wang et al., 2013) is compromised for resistance (Table 5.2) to both *P. graminis* f. sp. *tritici* race QCCJ that is avirulent on *RMRL* (Steffenson et al., 2009) and HKHJ that is avirulent on *Rpg1* (Brueggeman et al., 2002; Kleinhofs et al., 2009).

Table 5.2. Stem rust *Puccinia graminis* f. sp. *tiritici* race QCCJ, and HKHJ were used for disease phenotyping on Q21861 and mutant *rpr9*. Q21861 is resistant for QCCJ race and *rpr9* mutation compromise the disease resistance response. Race HKHJ is virulent on *Rpg5* but not on *Rpg1* R gene thus Q21861 (*RMRL+/Rpg1+*) remains resistant. However, *rpr9* mutation abolish the *Rpg1* resistance with *RMRL* resistance.

	Rust race			Rust race	
Genotype	***QCCJ***	***HKHJ***	**Genotype**	***QCCJ***	***HKHJ***
rpr9	213-	3-,21	Q21861	0;1	0;1
rpr9	3-,2	3-,21	Q21861	0;1	2,1
rpr9	3-,2	3-,2	Q21861	0;	;12
rpr9	2	33-2	Q21861	0;1	1;2
rpr9	23-	23-1	Q21861	0;	;1
rpr9	2	3-,2	Q21861	0;	0;1
rpr9	2	2,1	Q21861	0;	;1
rpr9	2	3-,2	Q21861	0;1	1;
rpr9	2	3-,21	Q21861	0;12	1;
rpr9	3-,2	3-,21	Q21861	0;12	;1
rpr9	3-,2		Q21861	0;1	0;1
			Q21861	0;1	
			Q21861	0;	

5.4.2. Identification of stuntd root phenotype associated with *rpr9*

Upon root length measurements between the *rpr9* mutant and wt Q21861 genotypes, we observed that *rpr9* had a stunted root length that was measured at the 4th day of germination compared to Q21861. A ragdoll test was conducted using 20 randomly selected seed for *rpr9* and wild type Q21861 and the root length of 14 germinated seed was measured at 4 days of germination and an unpaired *t* test was run to determine if the differences were statistically different. The calculated mean value for root length of total of fourteen germinated seed of the *rpr9* mutants was 16.5 mm whereas for wt Q21861 it was 25.64 mm. The difference in root length was found to be statistically significant (two tailed $P<0.05$) among *rpr9* and wt Q21861. After four rounds of backcrossing the mutant to wildtype Q21861 to clean up background mutations the stunted root phenotype was still present suggesting that it could be determined by

the same mutation that compromised RMRL-mediated resistanc. Thus, the mutation events present in the *rpr9* mutant not only compromise stem rust resistance but also cause the stunted root phenotype.

Fig. 5.2. A representative picture of three germinated seed and their root length determination by the Ragdoll test. A constant small root length phenotype was found to be associated with *rpr9* mutants comparing to wild type genotype Q21861. Difference between the root length was statistically significant (two tailed P value =0.0065).

Table 5.3. The unpaired *t* test to determine if difference of the root length taken at 4th day of germination is significantly different between the *rpr9* mutant and wildtype Q21861. A total of 14 germinated seeds were analyzed for each genotype.

Group	Q21861	*rpr9*
N (Sample size)	14	14
Mean	16.5	25.64
SD	1.65	1.82
SEM	0.44	.49

5.4.3. Linkage mapping and QTL analysis for *rpr9* and stunted root phenotype

The mapping of the *rpr9* stem rust susceptibility and stunted root growth phenotype was performed utilizing the 9k Infinium chip genotyping data of the Hv584/*rpr9* F_6 RIL population. A robust linkage map with 2,647 polymorphic markers distributed across the seven-barley

chromosome representing ~35% polymorphism for the 9000 iSelect markers on the 9k Infinium chip (Fig. 5.3.).

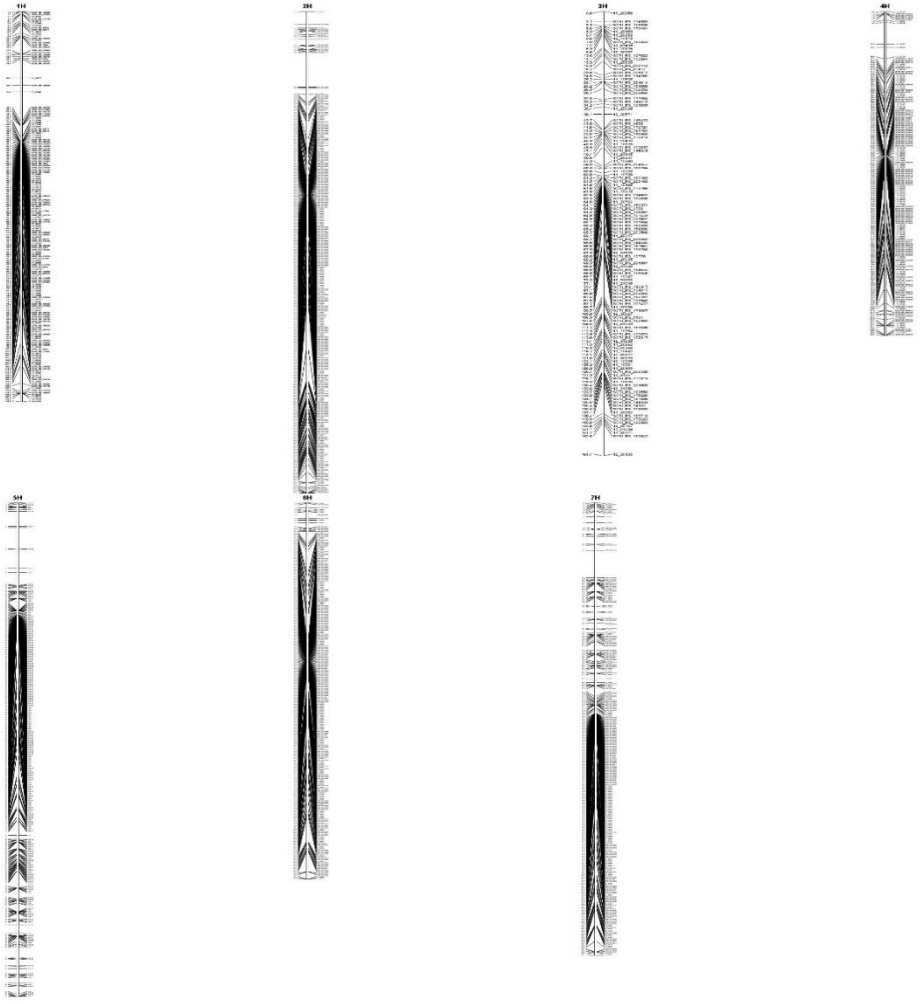

Fig. 5.3. Linkage map of Hv584*/rpr9* F_6 recombinant inbred line population spanning the 7 barley chromosomes containing 2,647 polymorphic SNP markers, created using QGene software.

QTL analysis identified an ~7.1 cM region harboring the *Rpr9* gene as well as the mutations resulting in the stunted root phenotype. A total of 1,957 SNP markers were anchored to POPSEQ positions in the barley genome and following removal of co-segregating markers, the final linkage map consisted of 812 SNPs to be used for QTL analysis. The analysis identified a significant QTL delimited by the flanking markers SCRI_RS_164675 and SCRI_RS_146347

covering POPSEQ positions from 68.6 cM -75.7 cM representing the physical region from 550,216,233 - 582,491,575 bp on chromosome 3H (Fig. 5.4). This physical region was region harbors a total of 365 high confidence genes (Appendix Table A5) and 266 low confidence genes (Appendix Table A6) identified in the barley reference genome assembly (Mascher et al., 2017)

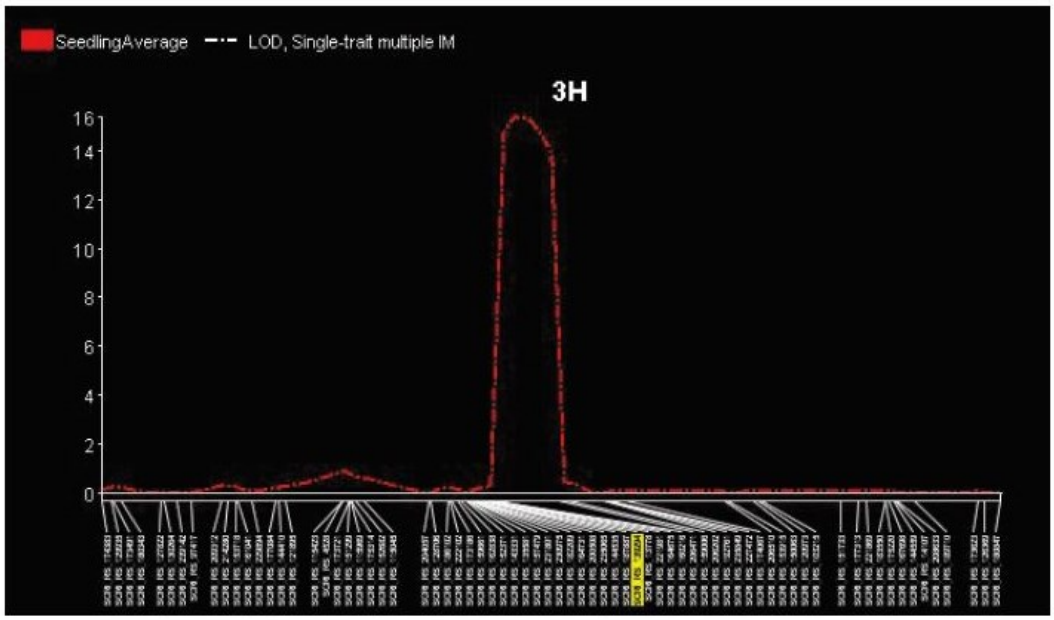

Fig. 5.4. QTL map for *Rp9* region required for *RMRL* mediated stem rust race QCCJ resistance mapped in Hv584 x *rpr9* F_6 RIL population. The vertical Y-axis represents LOD values and X-bar represents the 9K iSelect SNP markers on barley chromosome 3H.

5.4.4. Identification of candidate deleted genes using exome capture

A total of 115,741,280 exome capture sequence reads were generated for wt Q21861 and 104,846,733 reads were generated for the *rpr9* mutant. Alignment of the reads to the Morex draft genome sequence resulted in 88.79% of wt Q21861 and 82.60% of the *rpr9* reads aligning to the reference.

The analysis identified a large block of deleted genes within the *rpr9* region delimited by the genetic map which spanned a physical region from 560,447,102 to 561,614,572 bp based on the position of two genes, HORVU3Hr1G074910.1 (position on the barley physical map ch. 3H

– 560,447,102) and HORVU3Hr1G075070.1 (position on the barley physical map ch. 3H – 561,614,572) that flank the deletion yet are are present in the *rpr9* mutant with tweleve annotated deleted HC genes falling in between. The region presents between the most proximal and distal deleted genes, HORVU3Hr1G074920.1 (start position on the barley physical map ch. 3H – 560,659,267) and HORVU3Hr1G075060.1 (end position on the barley physical map ch. 3H – 561,501,311), respectively, on the barley physical map (Masher et al., 2017), show a minimum deletion of 840,985 base pairs. However, based on the physical position of the flanking genes present in the mutant the maximum deletion range is 1,167,470 base pairs from 560,447,102 to 561,614,572 bp on the barley physical map (Fig. 5.5). Within this ~1.17 Mb deletion there were originally tweleve annotated deleted HC genes.

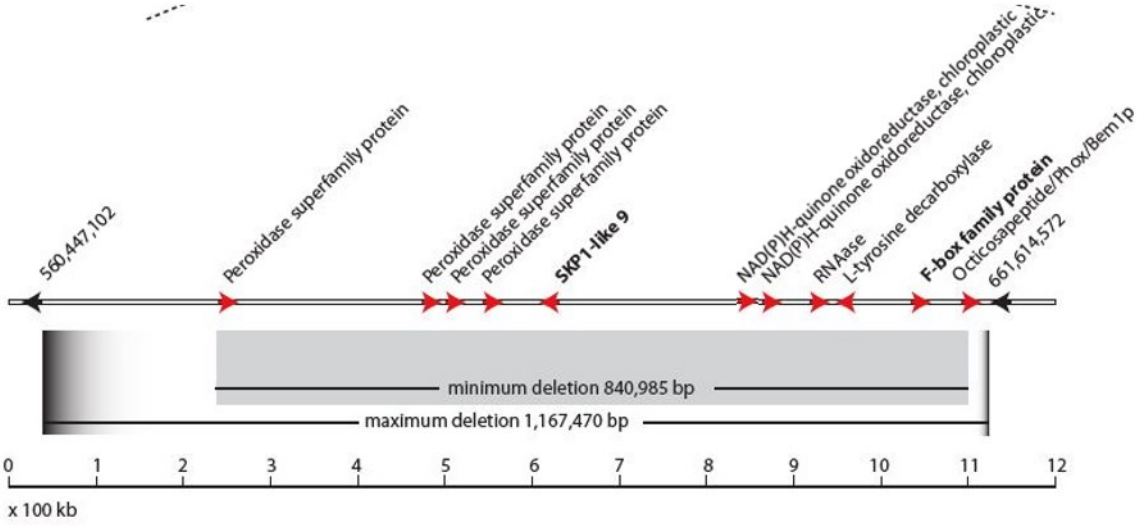

Fig. 5.5. The deletion detected by exome capture sequencing in the region delimiting *rpr9* and the stunted root phenotype QTL on barley chromosome 3H. The deletion covers a block of eleven high confidence and three low confidence annotated genes in the *rpr9* mutant. The horizontal grey bar represents the genome sequence of cv Morex with red arrows represent the relative positions and directionality of annotated genes. Black arrows represent the position and direction of the flanking genes that were present in both wildtype Q21861 and the *rpr9* mutant. The black lines below denote the minimum (0.841 Mbp) and maximum (1.167 Mbp) deletion size. The 100 kilobase scale is shown below.

This block of tweleve HC genes were annotated in barley genome as present within the deletion including a leucine-rich repeat receptor-like protein kinase which was not deleted based on a significant number of reads mapping to the gene. Upon manual curation and comparison of barely genome data we found that this gene is mis-annotated twice in baley genome and actually presnt on chr3H between the physical sequence postion of 509,350,259-509,352,312, outside the *rpr9* QTL region. Thus, *rpr9* deletion region originally had a SKP1-like 9 protein, a NAD(P)H-quinone oxidoreductase subunit H, a NAD(P)H-quinone oxidoreductase subunit 1, a RNAase protein, one L-tryrosine decarboxylase, an F-box family protein and Oticosapeptide/Phox/Bem1p family protein. Four peroxidase superfamily proteins are also present in the deletion block thus representing a total of eleven deleted HC genes (Table 5.4).

Table 5.4. List of twelve high confidence genes present in *rpr9* deletion region on barley chromosome 3H contain the gene name and chromosome number along with the annotated physical sequence position for start and end position for coding determining region (CDS) and Pfam protein ID.

Gene Name	Barley Chr.	Start	End	Annotation	Pfam Terms
HORVU3Hr1G074920.1	chr3H	560659267	560660724	Peroxidase superfamily protein	PF00141
*HORVU3Hr1G074930.1	chr3H	560737798	560739850	Leucine-rich repeat receptor-like protein kinase family protein	PF07714
HORVU3Hr1G074940.1	chr3H	560884155	560885580	Peroxidase superfamily protein	PF00141
HORVU3Hr1G074950.3	chr3H	560902589	560904079	Peroxidase superfamily protein	PF00141
HORVU3Hr1G074960.1	chr3H	560934358	560935865	Peroxidase superfamily protein	PF00141
HORVU3Hr1G074970.1	chr3H	561006112	561007794	SKP1-like 9	PF01466
HORVU3Hr1G075000.1	chr3H	561254447	561255632	NAD(P)H-quinone oxidoreductase subunit H, chloroplastic	PF00346
HORVU3Hr1G075010.1	chr3H	561255634	561256481	NAD(P)H-quinone oxidoreductase subunit 1, chloroplastic	PF00146
HORVU3Hr1G075030.1	chr3H	561299425	561299615	RNAase	none
HORVU3Hr1G075040.1	chr3H	561302733	561304797	L-tyrosine decarboxylase	PF00282
HORVU3Hr1G075050.2	chr3H	561432288	561438786	F-box family protein	PF12937
HORVU3Hr1G075060.1	chr3H	561500252	561501311	Octicosapeptide/Phox/Bem1p family protein	PF00564

* denotes the mis-annotated LRK gene present in *rpr9* QTL.

5.5. Discussion and conclusions

In wheat, nearly 80 stem rust resistance genes have been identified and hundreds of different races have been typed using single R-gene differentials. However, in barley only 5 stem rust resistance genes have been identified and of these only two, *Rpg1* and the *rpg4*/*Rpg5* complex or *RMRL* have been shown to be effective. However, recent association mapping using landraces and wild barley populations (Sallam et al., 2017) have identified novel stem rust resistances in barley. The *Rpg1* and *RMRL* genes/loci confer broad-spectrum resistance and when combined currently provide resistance to all known races of wheat stem rust. Recent functional characterization of the *Rpg1* and *RMRL* mechanisms have shown that both may be forms of early pre-haustorial resistance (Brueggeman et al., unpublished). We speculate that barley is a recent non-host to wheat stem rust and has not undergone a prolonged molecular arms race with the adapted pathogen leading to a large number of race specific *R*-genes and multiple pathogen races according to these specific resistances as is seen in wheat. We hypothesize that the *Rpg1* and *RMRL*-mediated resistance mechanisms may be forms of non-host resistance that do not fall into the usual class of typical NLR rust R-genes which are post-haustorial resistance mechanisms as characterized in the classic flax-flax rust model system (Dodds et al., 2006) and the majority of stem rust resistance genes characterized in wheat.

Forward genetics approaches such as mutagenesis are considered an efficient method to identify nonpolymorphic genes that function in conserved signaling pathways. In barley, the *RMRL* provide resistance against a broad spectrum of stem rust races including the highly virulent race TTKSK. To identify conserved genes that function in RMRL or *Rpg1* resistance, FN irradiation of barley line Q21861 (*Rpg1*+ *and RMRL*+) was used to induce the deletion mutant *rpr9* that is susceptible to *Pgt* race QCCJB which is specifically avirulent on RMRL and

also susceptible to *Pgt* race HKHJ which is specifically avirulent on *Rpg1* containing barley lines. The *rpr9* mutant was utilized for genetic mapping via a *rpr9* x Hv584 cross followed by exome capture and mapping-by-sequencing to rapidly identify candidate *Rpr9* genes that underlie the mutant phenotypes. Genetic mapping using the 9k iSelect marker panel delimited *rpr9 to* a ~32.27 Mbp region on chromosome 5H between the SNP markers SCRI_RS_164675 and SCRI_RS_146347 located at physical map positions from 550,216,233 - 582,491,515, respectively. This relatively small region of the barley genome harbors 365 high confidence and 266 low confidence genes. We also determined that the *rpr9* mutant also retained a stunted root phenotype after cleaning the genetic background of *rpr9* with four rounds of backcrossing suggesting that *rpr9* and the stunted root mutation may not be distinct. Mapping of the stunted root phenotype in the Hv584/*rpr9* RIL population utilizing QTL mapping identified the most significant QTL delimited to the same interval as *rpr9* on ch. 3H (Fig. 5.6), thus indicating that the same mutation event may be pleiotropic and inducing both the loss of *RMRL*- and *Rpg1*-mediated resistance responses as well as the stunted root phenotype.

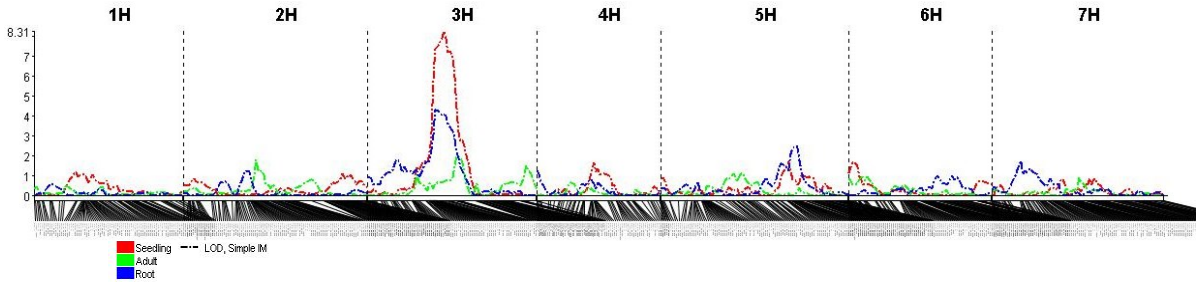

Fig. 5.6. The stunted root phenotype and *rpr9* QTL overlapped with each other. The red line represents growth chamber seedling assays with *Puccinia graminis* f. sp. *tritici* (Pgt) race QCCJ. The red line represents QTL mapping using two replications of field trials inoculated with Pgt race TTKSK in Njoro, Kenya. The blue line represents the root length QTL analyses**.** The genetic map below was generated using a 9k iSelect marker panel generated with a 2647 polymorphic SNPs.

The distribution of root length in the RIL population was found to have a continuous distribution rather than following a bimodal distribution (Fig. 5.7) suggesting that although the major QTL maps to the *rpr9* locus the natural polymorphism present between Q21861and Hv584 contributes to the segregating and continuous distribution of the root lengths within the RIL population.

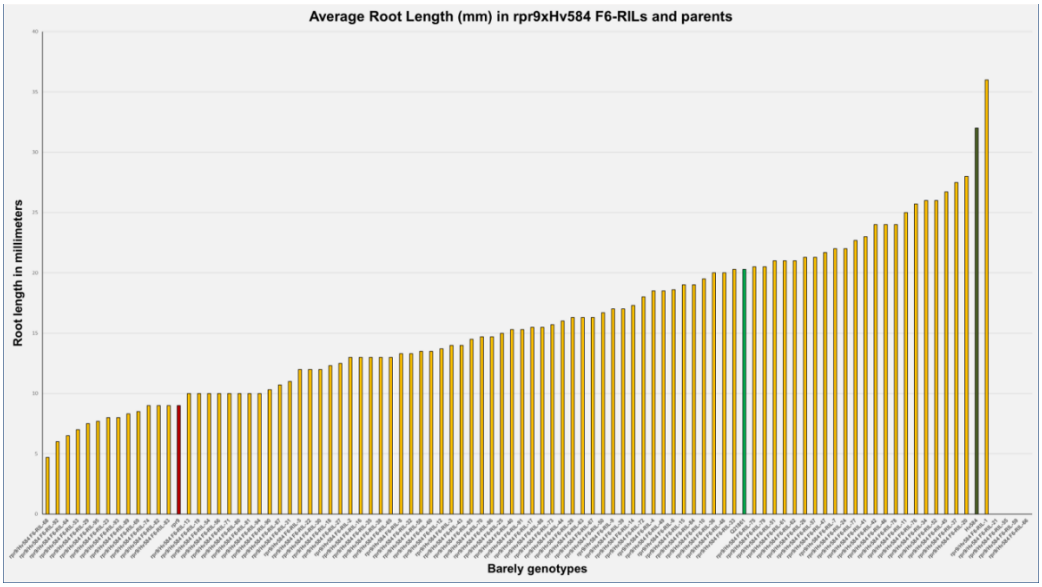

Fig. 5.7. Average root length distribution for 95 individuals from the *rpr9* x Hv584 F6 RIL population (yellow bars) along with wild type Q21861 (green bar), mutant *rpr9* (red bar) and Hv584 (blue bar) in increasing order. The Y-axis represents root length in millimeters and x-axis denotes all the barley genotypes tested. A continuous distribution was observed indicating the effect of multiple genes on the root length phenotype.

Using the recently developed barley exome capture array followed by Illumina sequencing of the *rpr9* mutant compared with the wt Q21861 a deletion with a maximum length of 1.167 Mbp was identified on chromosome 3H underlying the *rpr9* delimited region. The deletion falls at the physical position 560447102 to 561614572 based on the presence of the two flanking genes HORVU3Hr1G074910.1 and HORVU3Hr1G075070.1 in both wild type Q21861 and *rpr9* mutant. The deleted region contains eleven high confidence and three low confidence genes along with a mis-annotated LRK. The eleven high confidence genes are classified as a

block of four peroxidases, two NAD(P)H-quinone oxidoreductases and one each of SKP1- like 9, a F-box family protein, a L-tyrosine decarboxylase, a RNase, and an octicosapeptide/Phox/Bem1p family protein.

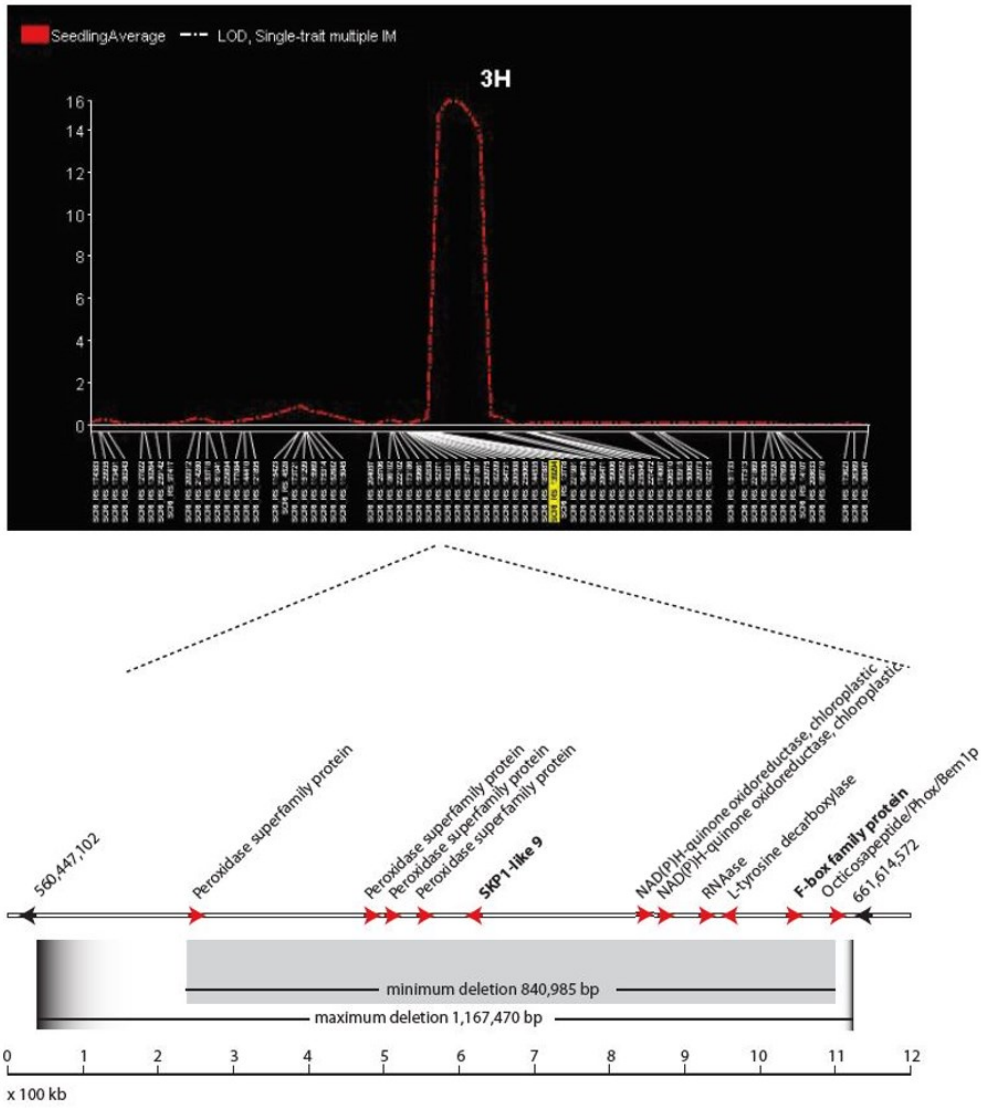

Fig. 5.8. Representation of the ch. 3H *rpr9* region utilizing the 9k Illumina Infinium iSelect genotyping data for seedling QTL mapping. The original analysis contained a misannotated receptor-like kinase gene that was removed leaving ten high confidence genes as *rpr9* candidates. The horizontal grey bar represents the genome sequence of cv Morex with red arrows represent the relative positions and directionality of annotated genes. Black arrows represent the position and direction of the flanking genes that were present in both wildtype Q21861 and the *rpr9* mutant. The black lines below denote the minimum (0.841 Mbp) and maximum (1.167 Mbp) deletion size. The 100 kilobase scale is shown below.

The genetic mapping and exome capture data suggest that the stunted root phenotype and *rpr9* disease susceptibility phenotype are possibly governed by two different genes present in the deletion block or a single gene within the deletion is responsible for both mutant phenotypes. If a single gene controls both phenotypes, then it represents an interesting example of a pleiotropic effect. However, there are many examples of pleiotropic genes effecting both abiotic and biotic resistances as well as developmental processes (Parker, 1990; Burstin et al., 2007).

It has been hypothesized that since the *rpr9* mutant compromises both the very early *Rpg1*-mediated stem rust resistance mechanisms (Nirmala et al., 2010) as well as the early responses induced by *RMRL* that there may be a cell surface receptor responsible for the early perception of the pathogen to get responses within minutes of the pathogen contacting the leaf surface. Therefore, upon our initial characterization of the deletion region the receptor-like kinase gene present in the region was of great interest and our initial top candidate gene. However, in recently released IPK barley high confidence gene list utilized for exome data analysis, this receptor like kinase gene is annotated twice on chromosome 3H as HORVU3Hr1G074930.1 (560,737,798-560,739,850) and HORVU3Hr1G067050.1 (509,350,259-509,352,312) and both gene annotations are identical. Interestingly in draft genome sequence of Morex published in 2012 this gene was annotated only once at 57.08 cM on chromosome 3H. We further manually checked the exome data and found sequencing reads aligning to both positions (HORVU3Hr1G074930.1 and HORVU3Hr1G067050.1) in the reference sequence and concluded a mis-annotation at position 560737798-560739850. Thus, we focused on the other candidate genes within the deleted region (Fig. 5.8). Interestingly two of the candidate genes are predicted to encode *SKP1* (S-phase kinase- associated protein) and F-box proteins, known to be part of functional component of the multiprotein E3 ubiquitin ligase

complex known as SCF (SKP/Cullin/F-box and ring finger protein Rbx1). In *Arabidopsis* 21 *SKP* genes (ASK) were predicted (Farrás et al., 2001), however in yeast and human only one functional *SKP1* gene is present (Yu et al., 1998). We found that in barley 16 high confidence SKP genes were predicted upon genome search.

Proteasomal protein degradation is an ATP dependent process controlling important functions and regulatory processes and consists of highly concerted molecular operations. The sequential action of three enzymes are required for the ubiquitination process which tags multiple ubiquitin molecule to target proteins resulting in their recognition by the 26S proteasome and subsequent degradation (Baumeister et al., 1998; Hellmann and Estelle, 2002). E1 (ubiquitin-activating) and E2 (Ubiquitin-conjugating enzyme) are required for activation of ubiquitin molecules. E3 (ubiquitin ligase) recognizes specific target proteins and attached $glycine_{76}$ of ubiquitin to a lysine amino acid of the targeted substrate protein destined for ubiquitination (Hellmann and Estelle, 2002; d Azzo et al., 2005; Sadowski et al., 2010). SCF type E3 ubiquitin ligases are well characterized (Willems et al., 2004) and in SCF complexes the Cullin and Rbx1 proteins constitutes a scaffold core which is connected to F-box proteins through SKP1 (Zheng et al., 2002). In the SCF complex F box proteins determine the specificity for ubiquitination thus are considered substrate recognition components (Xu et al., 2009).

Many evidences suggested the role of SCF complex in regulation of plant immunity. In tobacco it has been reported that *NbSGT1* (Nicotiana benthamiana suppressor of G2 allele of SKP1) a highly conserved cochaperone component of the SCF complex, interacts directly with *NbSKP1* (a component of the SCF ubiquitin ligase complex) and NbRar1 (Liu et al., 2002a, 2002b). *Rar1* is required for TNL (Toll/interlukin 1 receptor-Nucleotide binding-Lucine rich repeats) *N* gene mediated resistance in tobacco and also has been shown to function downstream

of powdery mildew recognition and upstream of plant hypersensitive cell death responses upon H_2O_2 accumulation via several CNLs (CC-NB-LRR) including *Mla* mediated resistance in barley (Shirasu et al., 1999). TNL and CNL proteins are involved in pathogen recognition and defense mechanisms yet diverse signaling pathways. TNLs are rare in monocots and absent in cereals whereas CNLs are found in dicots. Thus, *Rar1* represents a signaling factor functioning in common pathways evoked by TNL and CNL resistance genes. In tobacco upon *SKP1* or *SGT1* silencing, *N* gene mediated resistance have been shown to be compromised for TMV resistance. *Triticum aestivum SKP1* (*TSK1*) was found to be expressed in young root and spikes and a low-level expression was detected in leaves. *TSK1* overexpression in *Arabidopsis* was shown to increases abscisic acid (ABA) responsive phenotypes such as stomatal closure, root growth and seed germination and enhanced drought tolerance (Li et al., 2012), thus possibly functioning as a positive regulator of ABA signaling .

In barley five high confidence (HORVU3Hr1G075050.2, HORVU1Hr1G077600.2, HORVU4Hr1G052070.1, HORVU0Hr1G030450.1, HORVU1Hr1G068570.1) and one low confidence (HORVU3Hr1G079580.6) *F-box* genes were mined from the IPK database. In *Arabidopsis* 694 *F-BOX* genes were predicted (Xu et al., 2009) making it one of the largest protein families. F-box proteins show high functional diversity and are involve in many functions including pathogen perception and circadian rhythm. *Arabidopsis* DOR (DrOught tolerance Repressor) is a SFL (S-locus F box like) family protein and is expressed in the stomatal guard cells and shown to control the ABA biosynthetic pathway and negatively controls ABA induced stomatal closure under drought stress (Zhang et al., 2008). In another study the *Arabidopsis F-box-Nictaba* was shown to be a pathogen inducible gene and overexpression in plants showed resulted in reduced infection by *Pseudomonas syringae* pv. *tomato* strain DC3000 (Stefanowicz

et al., 2016). It was also shown that the F-box protein ACIF1 (Avr9/Cf-9–Induced F-BOX1) silencing suppressed the hypersensitive response triggered by a diversity of pathogen elicitors such as Avr9, AvrPto and the P50 helicase of TMV (van den Burg et al., 2008). Thus, the E3 ubiquitin ligase SCF complex components identified within the deletion in the *rpr9* mutant region are certainly strong *rpr9* candidate genes. This is also supported by the data showing that the *rpr9* mutant also compromised *Rpg1*-mediated resistance mechanisms. It has been determined that *Rpg1*-mediated resistance is dependent upon RPG1 ubiquitination and subsequent E3-mediated degradation, thus the deleted SCF complex proteins may be responsible for the loss of *Rpg1* specific stem rust resistance.

Although the SCF complex proteins are considered our best candidates there are other deleted genes in the region that are associated with biotic stress responses. Two other candidates are the NQO (NAD(P)H-quinone oxidoreductase) subunit H and subunit 1 that were previously show to be involved in electron transport in photosystem II and quinone detoxification (Chesis et al., 1984; Hurley et al., 2014). Also, the *Arabidopsis* L-tyrosine decarboxylase (TyrDC) was shown to be induced by wounding, drought stress and fungal effector perception (Kawalleck et al., 1993; Guillet and De Luca, 2005; Lehmann and Pollmann, 2009) and is known as the first enzyme in the benzylisoquinoline alkaloids pathway. These metabolites act as antimicrobial compounds and cell wall reinforcement agent to provide immune function (Yogendra et al., 2017). Peroxidases are well characterized in plant defense responses and have been shown to be involved in removal of hydrogen peroxide at the cell wall and initiate the wounding defense responses (Orozco-Cárdenas et al., 2001; Bindschedler et al., 2006; Kimura and Kawano, 2015; Chasov et al., 2002). Thus, future functional studies are warranted to validate the *rpr9* gene among the list of the eleven candidate genes identified.

5.6. Literature cited

Arora, D., Gross, T., and Brueggeman, R. (2013). Allele characterization of genes required for rpg4-mediated wheat stem rust resistance identifies Rpg5 as the R gene. *Phytopathology* 103, 1153–1161. doi:10.1094/PHYTO-01-13-0030-R.

D Azzo, A., Bongiovanni, A., and Nastasi, T. (2005). E3 ubiquitin ligases as regulators of membrane protein trafficking and degradation. *Traffic* 6, 429–441. doi:10.1111/j.1600-0854.2005.00294.x.

Baumeister, W., Walz, J., Zühl, F., and Seemüller, E. (1998). The proteasome: paradigm of a self-compartmentalizing protease. *Cell* 92, 367–380.

Bigeard, J., Colcombet, J., and Hirt, H. (2015). Signaling mechanisms in pattern-triggered immunity (PTI). *Mol Plant* 8, 521–539. doi:10.1016/j.molp.2014.12.022.

Bindschedler, L. V., Dewdney, J., Blee, K. A., Stone, J. M., Asai, T., Plotnikov, J., Denoux, C., Hayes, T., Gerrish, C., Davies, D. R., et al. (2006). Peroxidase-dependent apoplastic oxidative burst in *Arabidopsis* required for pathogen resistance. *Plant J* 47, 851–863. doi:10.1111/j.1365-313X.2006.02837.x.

Borovkova, I., Steffenson, B., Jin, Y., Rasmussen, J., Kilian, A., Kleinhofs, A., Rossnagel, B., and Kao, K. (1995). Identification of molecular markers linked to the stem rust resistance gene rpg4 in barley. *Phytopathology (USA)*, 4. Available at: http://agris.fao.org/agris-search/search.do?recordID=US9564992.

Brown, J., Pirrung, M., and McCue, L. A. (2017). FQC Dashboard: integrates FastQC results into a web-based, interactive, and extensible FASTQ quality control tool. *Bioinformatics*. doi:10.1093/bioinformatics/btx373.

Brueggeman, R., Druka, A., Nirmala, J., Cavileer, T., Drader, T., Rostoks, N., Mirlohi, A., Bennypaul, H., Gill, U., Kudrna, D., et al. (2008). The stem rust resistance gene Rpg5 encodes a protein with nucleotide-binding-site, leucine-rich, and protein kinase domains. *Proc Natl Acad Sci U S A* 105, 14970–14975. doi:10.1073/pnas.0807270105.

Brueggeman, R., Rostoks, N., Kudrna, D., Kilian, A., Han, F., Chen, J., Druka, A., Steffenson, B., and Kleinhofs, A. (2002). The barley stem rust-resistance gene Rpg1 is a novel disease-resistance gene with homology to receptor kinases. *Proc Natl Acad Sci U S A* 99, 9328–9333. doi:10.1073/pnas.142284999.

Brueggeman, R. S., and Solanki, S. (2017). " Barley Stem Rust Resistance Mechanisms: Diversity, Genestructure, and Function Suggest a Recently Evolved Host-Pathogen Relationship," in *Management of wheat and barley diseases*, ed. D. P. Singh (6000 Broken Sound Parkway NW, Suite 300 Boca Raton, FL 33487-2742: CRC Press), 579–604. doi:10.1201/9781315207537-26.

Van den Burg, H. A., Tsitsigiannis, D. I., Rowland, O., Lo, J., Rallapalli, G., Maclean, D., Takken, F. L. W., and Jones, J. D. G. (2008). The F-box protein ACRE189/ACIF1 regulates cell death and defense responses activated during pathogen recognition in tobacco and tomato. *Plant Cell* 20, 697–719. doi:10.1105/tpc.107.056978.

Burstin, J., Marget, P., Huart, M., Moessner, A., Mangin, B., Duchene, C., Desprez, B., Munier-Jolain, N., and Duc, G. (2007). Developmental genes have pleiotropic effects on plant morphology and source capacity, eventually impacting on seed protein content and productivity in pea. *Plant Physiol* 144, 768–781. doi:10.1104/pp.107.096966.

Chasov, A. V., Gordon, L. K., Kolesnikov, O. P., and Minibaeva, F. V. (2002). [Cell surface peroxidase--generator of superoxide anion in wheat root cells under wound stress]. *Tsitologiia* 44, 691–696.

Chesis, P. L., Levin, D. E., Smith, M. T., Ernster, L., and Ames, B. N. (1984). Mutagenicity of quinones: pathways of metabolic activation and detoxification. *Proc Natl Acad Sci U S A* 81, 1696–1700.

Druka, A., Kudrna, D., Han, F., Kilian, A., Steffenson, B., Frisch, D., Tomkins, J., and Wing, R. (2000). Physical mapping of the barley stem rust resistance gene rpg4. *Molecular and General Genetics MGG* 264, 283–290. doi:10.1007/s004380000320.

Van Esse, H. P., Bolton, M. D., Stergiopoulos, I., de Wit, P. J. G. M., and Thomma, B. P. H. J. (2007). The chitin-binding Cladosporium fulvum effector protein Avr4 is a virulence factor. *Mol Plant Microbe Interact* 20, 1092–1101. doi:10.1094/MPMI-20-9-1092.

Farrás, R., Ferrando, A., Jásik, J., Kleinow, T., Okrész, L., Tiburcio, A., Salchert, K., del Pozo, C., Schell, J., and Koncz, C. (2001). SKP1-SnRK protein kinase interactions mediate proteasomal binding of a plant SCF ubiquitin ligase. *EMBO J* 20, 2742–2756. doi:10.1093/emboj/20.11.2742.

Ferrari, S., Savatin, D. V., Sicilia, F., Gramegna, G., Cervone, F., and Lorenzo, G. D. (2013). Oligogalacturonides: plant damage-associated molecular patterns and regulators of growth and development. *Front Plant Sci* 4, 49. doi:10.3389/fpls.2013.00049.

Glazebrook, J. (2005). Contrasting mechanisms of defense against biotrophic and necrotrophic pathogens. *Annu Rev Phytopathol* 43, 205–227. doi:10.1146/annurev.phyto.43.040204.135923.

Guillet, G., and De Luca, V. (2005). Wound-inducible biosynthesis of phytoalexin hydroxycinnamic acid amides of tyramine in tryptophan and tyrosine decarboxylase transgenic tobacco lines. *Plant Physiol* 137, 692–699. doi:10.1104/pp.104.050294.

Hellmann, H., and Estelle, M. (2002). Plant development: regulation by protein degradation. *Science* 297, 793–797. doi:10.1126/science.1072831.

Hurley, B., Subramaniam, R., Guttman, D. S., and Desveaux, D. (2014). Proteomics of effector-triggered immunity (ETI) in plants. *Virulence* 5, 752–760. doi:10.4161/viru.36329.

International Barley Genome Sequencing Consortium, Mayer, K. F. X., Waugh, R., Brown, J. W. S., Schulman, A., Langridge, P., Platzer, M., Fincher, G. B., Muehlbauer, G. J., Sato, K., et al. (2012). A physical, genetic and functional sequence assembly of the barley genome. *Nature* 491, 711–716. doi:10.1038/nature11543.

Jin, Y., Singh, R., Ward, R., Wanyera, R., Kinyua, M., Njau, P., Fetch, T., Pretorius, Z., and Yahyaoui, A. (2007). Characterization of seedling infection types and adult plant infection responses of monogenic Sr gene lines to race TTKS of Puccinia graminis f. sp. tritici. *Plant Disease* 91, 1096–1099. Available at: http://apsjournals.apsnet.org/doi/abs/10.1094/PDIS-91-9-1096.

Jin, Y., Steffenson, B., and Fetch, T. (1994a). Sources of resistance to pathotype QCC of Puccinia graminis f. sp. tritici in barley. *Crop Sci* 34, 285–288. Available at: https://dl.sciencesocieties.org/publications/cs/abstracts/34/1/CS0340010285.

Jin, Y., Steffenson, B., and Miller, J. (1994b). Inheritance of resistance to pathotypes QCC and MCC of Puccinia graminis f. sp. tritici in barley line Q21861 and temperature effects on the expression of resistance. *pathology* 84, 452–455. Available at: http://admin.apsnet.org/publications/phytopathology/backissues/Documents/1994Articles/Phyto84n05_452.PDF.

Jin, Y., Szabo, L., Pretorius, Z., Singh, R., Ward, R., and Jr, T. (2008). Detection of virulence to resistance gene Sr24 within race TTKS of Puccinia graminis f. sp. tritici. *Plant Disease* 92, 923–926. Available at: http://apsjournals.apsnet.org/doi/abs/10.1094/PDIS-92-6-0923.

Jones, J. D. G., and Dangl, J. L. (2006). The plant immune system. *Nature* 444, 323–329. doi:10.1038/nature05286.

Kawalleck, P., Keller, H., Hahlbrock, K., Scheel, D., and Somssich, I. E. (1993). A pathogen-responsive gene of parsley encodes tyrosine decarboxylase. *J Biol Chem* 268, 2189–2194.

Kimura, M., and Kawano, T. (2015). Salicylic acid-induced superoxide generation catalyzed by plant peroxidase in hydrogen peroxide-independent manner. *Plant Signal Behav* 10, e1000145. doi:10.1080/15592324.2014.1000145.

Kleinhofs, A., Brueggeman, R., Nirmala, J., Zhang, L., Mirlohi, A., Druka, A., Rostoks, N., and Steffenson, B. (2009). Barley stem rust resistance genes: structure and function. *The plant genome* 2, 109–120. Available at: https://dl.sciencesocieties.org/publications/tpg/abstracts/2/2/109.

Koornneef, M., Dellaert, L. W., and van der Veen, J. H. (1982). EMS- and radiation-induced mutation frequencies at individual loci in *Arabidopsis* thaliana (L.) Heynh. *Mutat Res* 93, 109–123.

Lehmann, T., and Pollmann, S. (2009). Gene expression and characterization of a stress-induced tyrosine decarboxylase from *Arabidopsis* thaliana. *FEBS Lett* 583, 1895–1900. doi:10.1016/j.febslet.2009.05.017.

Leonard, K. (2001). Stem rust–future enemy. *Stem rust of wheat: from ancient enemy to modern foe. American Phytopathological Society, St Paul Minnesota*. Available at: https://www.ars.usda.gov/research/publications/publication/?seqNo115=100512.

Li, C., Liu, Z., Zhang, Q., Wang, R., Xiao, L., Ma, H., Chong, K., and Xu, Y. (2012). SKP1 is involved in abscisic acid signalling to regulate seed germination, stomatal opening and root growth in *Arabidopsis* thaliana. *Plant Cell Environ* 35, 952–965. doi:10.1111/j.1365-3040.2011.02464.x.

Li, X., Lassner, M., and Zhang, Y. (2002). Deleteagene: a fast neutron deletion mutagenesis-based gene knockout system for plants. *Comp Funct Genomics* 3, 158–160. doi:10.1002/cfg.148.

Li, X., Song, Y., Century, K., Straight, S., Ronald, P., Dong, X., Lassner, M., and Zhang, Y. (2001). A fast neutron deletion mutagenesis-based reverse genetics system for plants. *Plant J* 27, 235–242.

Liu, Y., Schiff, M., Marathe, R., and Dinesh-Kumar, S. P. (2002a). Tobacco Rar1, EDS1 and NPR1/NIM1 like genes are required for N-mediated resistance to tobacco mosaic virus. *Plant J* 30, 415–429.

Liu, Y., Schiff, M., Serino, G., Deng, X.-W., and Dinesh-Kumar, S. P. (2002b). Role of SCF ubiquitin-ligase and the COP9 signalosome in the N gene-mediated resistance response to Tobacco mosaic virus. *Plant Cell* 14, 1483–1496.

Mascher, M., Gundlach, H., Himmelbach, A., Beier, S., Twardziok, S. O., Wicker, T., Radchuk, V., Dockter, C., Hedley, P. E., Russell, J., et al. (2017). A chromosome conformation capture ordered sequence of the barley genome. *Nature* 544, 427–433. doi:10.1038/nature22043.

Mirlohi, A., Brueggeman, R., Drader, T., Nirmala, J., Steffenson, B. J., and Kleinhofs, A. (2008). Allele sequencing of the barley stem rust resistance gene Rpg1 identifies regions relevant to disease resistance. *Phytopathology* 98, 910–918. doi:10.1094/PHYTO-98-8-0910.

Nirmala, J., Brueggeman, R., Maier, C., Clay, C., Rostoks, N., Kannangara, C. G., von Wettstein, D., Steffenson, B. J., and Kleinhofs, A. (2006). Subcellular localization and functions of the barley stem rust resistance receptor-like serine/threonine-specific protein kinase Rpg1. *Proc Natl Acad Sci U S A* 103, 7518–7523. doi:10.1073/pnas.0602379103.

Nirmala, J., Dahl, S., Steffenson, B. J., Kannangara, C. G., von Wettstein, D., Chen, X., and Kleinhofs, A. (2007). Proteolysis of the barley receptor-like protein kinase RPG1 by a proteasome pathway is correlated with Rpg1-mediated stem rust resistance. *Proc Natl Acad Sci U S A* 104, 10276–10281. doi:10.1073/pnas.0703758104.

Nirmala, J., Drader, T., Chen, X., Steffenson, B., and Kleinhofs, A. (2010). Stem rust spores elicit rapid RPG1 phosphorylation. *Mol Plant Microbe Interact* 23, 1635–1642. doi:10.1094/MPMI-06-10-0136.

Nirmala, J., Drader, T., Lawrence, P. K., Yin, C., Hulbert, S., Steber, C. M., Steffenson, B. J., Szabo, L. J., von Wettstein, D., and Kleinhofs, A. (2011). Concerted action of two avirulent spore effectors activates Reaction to Puccinia graminis 1 (Rpg1)-mediated cereal stem rust resistance. *Proc Natl Acad Sci U S A* 108, 14676–14681. doi:10.1073/pnas.1111771108.

Orozco-Cárdenas, M. L., Narváez-Vásquez, J., and Ryan, C. A. (2001). Hydrogen peroxide acts as a second messenger for the induction of defense genes in tomato plants in response to wounding, systemin, and methyl jasmonate. *Plant Cell* 13, 179–191.

Parker, M. A. (1990). The pleiotropy theory for polymorphism of disease resistance genes in plants. *Evolution* 44, 1872–1875. doi:10.1111/j.1558-5646.1990.tb05257.x.

Pretorius, Z., Singh, R., Wagoire, W., and Payne, T. (2000). Detection of virulence to wheat stem rust resistance gene Sr31 in Puccinia graminis. f. sp. tritici in Uganda. *Plant Disease* 84, 203–203. Available at: http://apsjournals.apsnet.org/doi/abs/10.1094/pdis.2000.84.2.203b.

Roelfs, A. (1989). Epidemiology of the cereal rusts in North America. *Canadian Journal of Plant Pathology* 11, 86–90. Available at: http://www.tandfonline.com/doi/pdf/10.1080/07060668909501153.

Roelfs, A., Long, D., and Roberts, J. (1993). Races of Puccinia graminis in the United States during 1991. *Plant Dis* 77, 129–132. Available at: https://www.ars.usda.gov/research/publications/publication/?seqNo115=42377.

Sadowski, M., Suryadinata, R., Lai, X., Heierhorst, J., and Sarcevic, B. (2010). Molecular basis for lysine specificity in the yeast ubiquitin-conjugating enzyme Cdc34. *Mol Cell Biol* 30, 2316–2329. doi:10.1128/MCB.01094-09.

Sánchez-Vallet, A., Saleem-Batcha, R., Kombrink, A., Hansen, G., Valkenburg, D.-J., Thomma, B. P. H. J., and Mesters, J. R. (2013). Fungal effector Ecp6 outcompetes host immune receptor for chitin binding through intrachain LysM dimerization. *elife* 2, e00790. doi:10.7554/eLife.00790.

Shirasu, K., Lahaye, T., Tan, M. W., Zhou, F., Azevedo, C., and Schulze-Lefert, P. (1999). A novel class of eukaryotic zinc-binding proteins is required for disease resistance signaling in barley and development in C. elegans. *Cell* 99, 355–366.

Solanki, S., Ameen, G., Richards, J., and S. Brueggeman, R. (2016). Modulation of integrated decoy R-genes/transcription factor assembly elicits wheat stem rust resistance responses in barley: rpg4/Rpg5-mediated Ug99 resistance. in *International Barley Genetics Symposium* Biotic Stresses., eds. K. Smith and R. Dill-Macky (Minneapolis-St. Paul, Minnesota, USA: IBGS). Available at: http://ibgs2016.org/.

Stefanowicz, K., Lannoo, N., Zhao, Y., Eggermont, L., Van Hove, J., Al Atalah, B., and Van Damme, E. J. M. (2016). Glycan-binding F-box protein from *Arabidopsis* thaliana protects plants from Pseudomonas syringae infection. *BMC Plant Biol* 16, 213. doi:10.1186/s12870-016-0905-2.

Steffenson, B. (1992). Analysis of durable resistance to stem rust in barley. *Breeding for Disease Resistance*, 153–167. Available at: http://link.springer.com/chapter/10.1007/978-94-017-0954-5_13.

Steffenson, B. J., Jin, Y., Brueggeman, R. S., Kleinhofs, A., and Sun, Y. (2009). Resistance to stem rust race TTKSK maps to the rpg4/Rpg5 complex of chromosome 5H of barley. *Phytopathology* 99, 1135–1141. doi:10.1094/PHYTO-99-10-1135.

Steffenson, B. J., Zhou, H., Chai, Y., and Grando, S. (2013). "Vulnerability of cultivated and wild barley to african stem rust race TTKSK," in *Advance in barley sciences*, eds. G. Zhang, C. Li, and X. Liu (Dordrecht: Springer Netherlands), 243–255. doi:10.1007/978-94-007-4682-4_21.

Stokstad, E. (2007). Deadly wheat fungus threatens world's breadbaskets. *Science* 315, 1786–1787. Available at: http://science.sciencemag.org/content/315/5820/1786.short.

Sun, Y., and Steffenson, B. J. (2005). Reaction of barley seedlings with different stem rust resistance genes to*Puccinia graminis* f. sp.*tritici* and*Puccinia graminis* f. sp.*secalis*. *Canadian Journal of Plant Pathology* 27, 80–89. doi:10.1080/07060660509507198.

Tarr, D. E. K., and Alexander, H. M. (2009). TIR-NBS-LRR genes are rare in monocots: evidence from diverse monocot orders. *BMC Res Notes* 2, 197. doi:10.1186/1756-0500-2-197.

Wang, X., Richards, J., Gross, T., Druka, A., Kleinhofs, A., Steffenson, B., Acevedo, M., and Brueggeman, R. (2013). The rpg4-mediated resistance to wheat stem rust (Puccinia graminis) in barley (Hordeum vulgare) requires Rpg5, a second NBS-LRR gene, and an actin depolymerization factor. *Mol Plant Microbe Interact* 26, 407–418. doi:10.1094/MPMI-06-12-0146-R.

Willems, A. R., Schwab, M., and Tyers, M. (2004). A hitchhiker's guide to the cullin ubiquitin ligases: SCF and its kin. *Biochim Biophys Acta* 1695, 133–170. doi:10.1016/j.bbamcr.2004.09.027.

Xu, G., Ma, H., Nei, M., and Kong, H. (2009). Evolution of F-box genes in plants: different modes of sequence divergence and their relationships with functional diversification. *Proc Natl Acad Sci U S A* 106, 835–840. doi:10.1073/pnas.0812043106.

Yogendra, K. N., Dhokane, D., Kushalappa, A. C., Sarmiento, F., Rodriguez, E., and Mosquera, T. (2017). StWRKY8 transcription factor regulates benzylisoquinoline alkaloid pathway in potato conferring resistance to late blight. *Plant Sci* 256, 208–216. doi:10.1016/j.plantsci.2016.12.014.

Yu, Z. K., Gervais, J. L., and Zhang, H. (1998). Human CUL-1 associates with the SKP1/SKP2 complex and regulates p21(CIP1/WAF1) and cyclin D proteins. *Proc Natl Acad Sci U S A* 95, 11324–11329.

Zhang, L., Fetch, T., Nirmala, J., Schmierer, D., Brueggeman, R., Steffenson, B., and Kleinhofs, A. (2006). Rpr1, a gene required for Rpg1-dependent resistance to stem rust in barley. *Theor Appl Genet* 113, 847–855. doi:10.1007/s00122-006-0342-y.

Zhang, Y., Xu, W., Li, Z., Deng, X. W., Wu, W., and Xue, Y. (2008). F-box protein DOR functions as a novel inhibitory factor for abscisic acid-induced stomatal closure under drought stress in *Arabidopsis*,. *Plant Physiol* 148, 2121–2133. doi:10.1104/pp.108.126912.

Zheng, N., Schulman, B. A., Song, L., Miller, J. J., Jeffrey, P. D., Wang, P., Chu, C., Koepp, D. M., Elledge, S. J., Pagano, M., et al. (2002). Structure of the Cul1-Rbx1-Skp1-F boxSkp2 SCF ubiquitin ligase complex. *Nature* 416, 703–709. doi:10.1038/416703a.

CHAPTER 6. SUMMARY

The "integrated decoy hypothesis" outlines the role of dual NLR genes and why one typically contains a fused mimic of a protein that was originally a host protein targeted by a pathogen virulence effector to facilitate disease. Yet, once fused to a NLR immunity receptor acts as an integrated sensory domains (ISD) to trap the pathogen and initiate defense. *rpg4/Rpg5* mediated resistance against many *forma specialis* of *Puccinia graminis* require two NLRs at this locus, *Rga1* and *Rpg5*. Concerted action of the barley NLRs, *Rpg5* and *HvRga1,* is required for resistance to *Puccinia graminis (Pg)*, the stem rust pathogen. Resistance *Rpg5* alleles have a serine threonine protein kinase (PK) ISD and the progenitor ISD PK gene was identified and designated as the guard cell associated kinase 1 (*Gak1*). Alleles of *Rpg5* contain functionally diverse C-terminal ISDs, resistance alleles have a serine threonine protein kinase (PK) ISD whereas the major class of *rpg5* susceptible alleles contain a protein phosphatase 2C (PP2C) ISD. Here in Fig. 6.1 and Fig. 6.2 we briefly describe the functional model for *rpg4/Rpg5* resistance based on our previous scientific knowledge and generated data in the dissertation chapters in pictorial and schematic form.

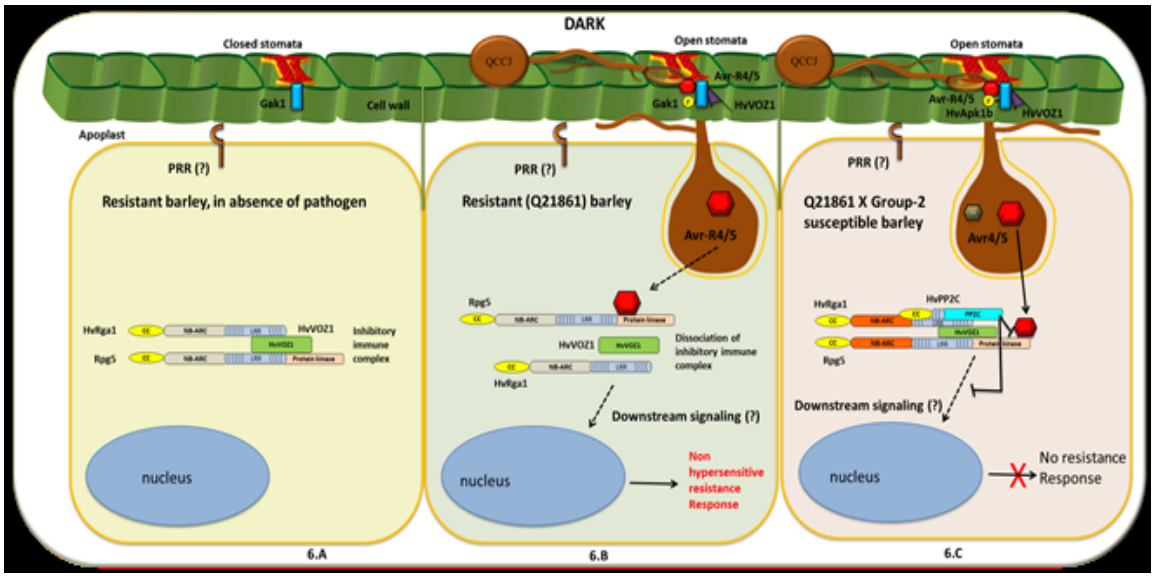

Fig. 6.1. Our model for molecular mechanism taking place during *rpg4/Rpg5* mediated stem rust resistance. Upon pathogen (*Puccinia graminis* - *Pg*) arrival in the dark, stomata's on the barley leaf surface are closed (Fig. 6.A) but stem rust elicitor Avr4/5 mimics the daylight and induces guard cells opening in the dark period upon interacting and manipulating the Gak1, a guard cell kinase responsible for stomatal opening in light. Phytochrome-B (far red-light receptor in plants) and HvVoz1 possibly plays a direct role in the Gak1 regulation at the stomata. Mimicking light helps pathogen to enter inside the plant system using substomatal vesicle, making intercellular hyphae and subsequently penetration of host cells by fungal haustoria to release the effectors required for the inhibition of early PTI responses. In resistant barley lines, HvVOZ1 act as scaffold protein and hold Rpg5 and HvRga1 in a complex intracellularly, thus this immune complex remains in an inhibited state (Fig. 6.A). At later stages of intercellular growth of *Pg*, secreted effector Avr-R4/5 get trapped by Rpg5-PK-ISD bait domain present in the resistant barley lines (Q21861). This effector trapping releases the inhibition of inactive immune complex to initiate downstream signaling cascade to regulate defense related genes resulting in non-hypersensitive resistance (non-HR) responses takes place to provide effective resistance (Fig. 6.B). In susceptible barley lines (Group 2 susceptibles – Steptoe) rpg5-PP2C also become part of complex and inhibit either Rpg5-PK manipulation by Avr 4/5 or suppress downstream signaling, thus no resistance response was observed (Fig. 6.C). However, the many upstream (such as cell surface pattern recognition receptors -PRRs) or downstream signaling components of *rpg4/Rpg5* mediated resistance are largely unknown and we have utilized the fast neutron mutagenesis approach to identify these signaling components. One such mutant is *rpr9,* compromised for *Pgt* resistance and out top candidates are SCF complex proteins, shown to take part in the stomatal manipulation.

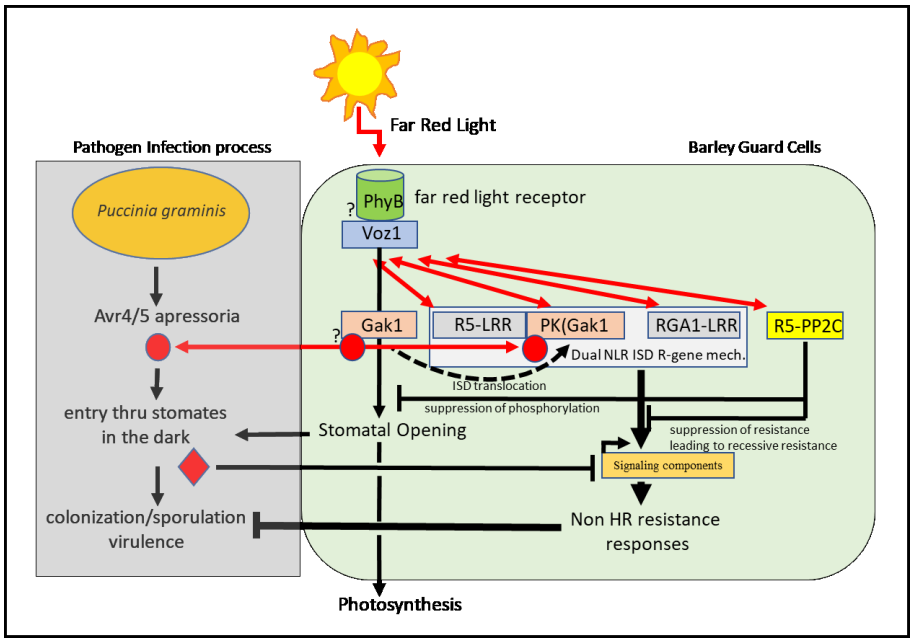

Fig. 6.2. A schematic model describing the mechanism underlying rpg4/Rpg5 locus mediated resistance (*RMRL*). Phytochrome B interacts with HvVoz1 upon far red-light sensing, this interaction modifies HvGak1 to open the stomatal pores, constituting a vital plant physiological process involved in light induced photosynthesis. However, on the resistant barley line Q21861, upon arrival of Pgt avirulent races (such as QCCJ containing Avr 4/5 effector) which manipulates the Gak1 in the dark, stomata open inappropriately to provide pathogen entry inside the host system. Since Rpg5 protein kinase domain is a fusion paralog of Gak1, thus kinase domain act as an integrated sensory domain (ISD) bait to trap the Avr4/5 elicitor to initiate the downstream defense signaling via non-hypersensitive resistance responses. In the susceptible barley varieties (Group-2 susceptibles) with PP2C ISD, rpg5-PP2C suppress the Rpg5-PK mediated resistance response and act as a dominant susceptibility factor. Thus, Rpg5 represents a unique NLR (NBS-LRR) protein with two different diverse ISDs. Upon infection with virulent races of Pgt on *RMRL* locus, producing haustorial virulence effectors efficiently inhibiting the downstream components of *RMRL* resistance, the non-HR defense signaling gets suppressed, enabling successful pathogen establishment and sporulation.

APPENDIX A. PRIMER NAME, PRIMER SEQUENCE, AMPLICON SIZE AND PCR CONDITIONS

Table A1. Primers used in experiments described in dissertation chapter 2, their name, sequence, amplicon size with PCR reaction conditions. Type of DNA polymerase used for PCR (Q5 hot start or Taq DNA polymerase) and qPCR SYBR Green mastermix (EvaGreen or SsoAdvance Universal) are also indicated.

Amplicon Name	Primer name	Primer Sequence	Amplicon size	PCR reaction parameters	Type of DNA polymerase or SYBRmastermix
Rpg5-Full (4137)	SS_Rpg5 FP1 SS_Rpg5 RP1	CACCTCGCAGAGTAGCATGGAGG CTATGGCTGTTCCTGCCATTCA	4172	98℃-1', (98℃-10", 63.1℃-20",72℃-2.3") x35,72℃-5',4℃_ON	Q5 Hot Start DNA polymersae (NEB)
Rpg5-NBS_domain (874-1530)	SS_Rpg5-NBS-FP SS_Rpg5-NBS-RP	CACCAACACCGCTGGCTGTAG TCAGAGCAACAGGCTTGCTAT	664	98℃-2', (98℃-10", 62℃-45",72℃-1") x35,72℃-15',4℃_ON	Q5 Hot Start DNA polymersae (NEB)
Rpg5-LRR_domain (1537-3114)	SS_Rpg5-LRR-FP-N RPG-LRR-RP-N	CACCAAGTGGAACCCTGCAATGTG TCATCCAGCTTTAGATGCTAATGTCGAG	1585	98℃-2', (98℃-10", 62℃-45",72℃-1") x35,72℃-15',4℃_ON	Q5 Hot Start DNA polymersae (NEB)
Rpg5-PK_domain (3172-4137)	SS_Rpg5-PK-FP SS_Rpg5 RP1	CACCGCCACACGGAACTTCAG CTATGGCTGTTCCTGCCATTCA	989	98℃-2', (98℃-10", 62℃-45",72℃-1") x35,72℃-15',4℃_ON	Q5 Hot Start DNA polymersae (NEB)
Rpg5_qPCR	RPGQF6 RPGQR6	AGATGCACCTATCTGCATCGAGCAC ATGTCGAGCCTGAGACTACTGACAC	191	95℃-30", (95℃-5", 60℃-5") x40, (65℃-95℃ for 5" at 0.5℃ increment)	SsoFast Evagreen supermix (BioRad)
rpg5-pp2c_domain	PP2C-PE-FP PP2C-PE-RP	CACCATCAGGATTTCTATGCTGCCG TTACGACCAGGCCAGATCG	1188	98℃-2', (98℃-10", 61℃-45",72℃-1") x35,72℃-15',4℃_ON	Q5 Hot Start DNA polymersae (NEB)
rpg5-pp2c_KD	SS-PP2CKD1-5'-FP SS-PP2CKD1-5'-RP	AGTTTAATTAAATGGCTTATGTCCAGGCTA AGTGCGGCCGCTTGGAGATTAGGGAAGAGAT	172	98℃-2', (98℃-10", 64℃-45",72℃-1") x35,72℃-15',4℃_ON	Q5 Hot Start DNA polymersae (NEB)

Table A1. Primers used in experiments described in dissertation chapter 2, their name, sequence, amplicon size with PCR reaction conditions. Type of DNA polymerase used for PCR (Q5 hot start or Taq DNA polymerase) and qPCR SYBR Green mastermix (EvaGreen or SsoAdvance Universal) are also indicated (continued).

Amplicon Name	Primer name	Primer Sequence	Amplicon size	PCR reaction parameters	Type of DNA polymerase or SYBRmastermix
Rga1-Full (2688)	SS_Rga1FP SS_Rga1RP	CACCATGGAGGTTGCGGTGGTCGTC TCATGCTTGTGCACGGCCAAGATCC	2688	98°C-2', (98°C-10", 62°C-30",72°C-2") x35,72°C-10',4°C_ON	Q5 Hot Start DNA polymersae (NEB)
Rga1-LRR (1324-2688)	SS_Rga1-LRR_FP SS_Rga1-LRR_RP	CACCATGTTGTGTGCCGGCCAG TCAGCGCATCAGGATCTTGGCCGTG	1365	98°C-2', (98°C-10", 62°C-45",72°C-2") x35,72°C-10',4°C_ON	Q5 Hot Start DNA polymersae (NEB)
Rga1QPCR	R4-JR-F8 R4-JR-R8	TTATGCCTTGTGGGCAGCAAAGGA TCTTGGCCGTGCACAAGCAAAGATG	372	95°C-30", (95°C-5", 60°C-5") x40, (65°C-95°C for 5" at 0.5°C increment)	SsoFast Evagreen supermix (BioRad)
rpg5-PP2C allele specific	Rpg5-LRKF1 PP2C-R1	CTGCTGGCACAGAGTCTGCCTTGAG ACATAAGCCATGGAGAGCTCACCAG	512	94°C-5', (94°C-45", 60.5°C-45",72°C-1.5") x35,72°C-5',4°C_ON	GoTaq DNA polymerase (Promega)
Rpg5-STPK allele specific	Rpg5-LRKF1 Rpg5-LRKR1	CTGCTGGCACAGAGTCTGCCTTGAG ACTCTCGGGTCTGAAGTTCCGTGTG	221	94°C-5', (94°C-45", 60.5°C-45",72°C-1.5") x35,72°C-5',4°C_ON	GoTaq DNA polymerase (Promega)
GAPDH	HvGAPDH ccw1 HvGAPDH cw1	CAGCCTTGTCCTTGTCAGTG CGTTCATCACCACCGACTAC	225	94°C-5', (94°C-60", 60°C-60",72°C-1.5") x35,72°C-5',4°C_ON 95°C-30", (95°C-5", 60°C-5") x40, (65°C-95°C for 5" at 0.5°C increment)	GoTaq DNA polymerase (Promega) SsoFast Evagreen supermix (BioRad)
Gak1 qCR primer	SS_GAK1_qF1 SS_GAK1_qR1	AGATCGCCGATGCACGAA GTCATCTTCAACACAATATCC	512	95°C-30", (95°C-5", 60°C-5") x40, (65°C-95°C for 5" at 0.5°C increment)	SsoAdvance Universal SYBR Green (BioRad)

APPENDIX B. DISEASE PHENOTYPIC CONVERSION NUMBERIC SCALE FOR STEM RUST

Table B1. Table describing formulae used to transform seedling categorical infection type (it) data for stem rust (ttksk) disease ratings into numerical data for statistical analysis (Zhou et al., 2014).

No. of ITs on leaves	Multiplier for respective ITs			Formulae for numeric score
	Most prevalent IT	Second most prevalent IT	Next most prevalent IT	
One	A[a]x100%[b]	-[c]	-	A
Two	Ax75%	Bx25%	-	0.75A+0.25B
Three	Ax60%	Bx30%	Cx10%	0.6A+0.3B+0.1C

[a]A, B or C represent numeric values from 0.0 to 4.5 for the most prevalent IT, second most prevalent IT, and next most prevalent IT, respectively. For the calculation of numeric data categoncal IT “0" was coded as 0.0; IT “;” as 0.5, IT"1"as 2.0, IT “2” as 3, IT “3-” as 3.5, IT “3" as 4.0, and IT “3+" as 4.5.

[b]Barley commonly exhibits mesothetic reactions, i.e. a mixture of different infection types on the same leaf. The multiplier after A, B, and C reflects the generalized proportions of the most prevalent IT, second most prevalent IT and next most prevalent IT observed on leaves. The final numeric disease score for the line was calculated from the transformed IT values after the multiplier was applied. Multipliers were based on generalized IT proportions assessed from many infected leaf samples.

APPENDIX C. RPG5-PP2C KNOCKDOWN DISEASE PHENOTYPING

Table C1. Wheat stem rust race QCCJ disease ratings on tertiary leaf of BSMV_rpg5-PP2C, BSMV_MCS and non-BSMV inoculated plants. Mesothetic categorical disease ratings were converted to a single numerical value according to conversion method described in Zhou et al (Zhou et al., 2014).

Treatment	Reading	Genotype	QCCJ Response
BSMV_rpg5-PP2C-KD_QCCJ	2	Rpg5_PK+/rpg5_PP2C-	R
BSMV_rpg5-PP2C-KD_QCCJ	2.15	Rpg5_PK+/rpg5_PP2C-	R
BSMV_rpg5-PP2C-KD_QCCJ	1.625	Rpg5_PK+/rpg5_PP2C-	R
BSMV_rpg5-PP2C-KD_QCCJ	0.125	Rpg5_PK+/rpg5_PP2C-	R
BSMV_rpg5-PP2C-KD_QCCJ	0	Rpg5_PK+/rpg5_PP2C-	R
BSMV_rpg5-PP2C-KD_QCCJ	1.2	Rpg5_PK+/rpg5_PP2C-	R
BSMV_rpg5-PP2C-KD_QCCJ	0.5	Rpg5_PK+/rpg5_PP2C-	R
BSMV_rpg5-PP2C-KD_QCCJ	0.875	Rpg5_PK+/rpg5_PP2C-	R
BSMV_rpg5-PP2C-KD_QCCJ	0.35	Rpg5_PK+/rpg5_PP2C-	R
BSMV_rpg5-PP2C-KD_QCCJ	1.625	Rpg5_PK+/rpg5_PP2C-	R
BSMV_rpg5-PP2C-KD_QCCJ	2.15	Rpg5_PK+/rpg5_PP2C-	R
BSMV_rpg5-PP2C-KD_QCCJ	0.35	Rpg5_PK+/rpg5_PP2C+	R
BSMV_rpg5-PP2C-KD_QCCJ	0.875	Rpg5_PK+/rpg5_PP2C+	R
BSMV_rpg5-PP2C-KD_QCCJ	2.25	Rpg5_PK+/rpg5_PP2C+	R
BSMV_rpg5-PP2C-KD_QCCJ	1.625	Rpg5_PK+/rpg5_PP2C+	R
BSMV_rpg5-PP2C-KD_QCCJ	1.625	Rpg5_PK+/rpg5_PP2C+	R
BSMV_rpg5-PP2C-KD_QCCJ	0.35	Rpg5_PK+/rpg5_PP2C+	R
BSMV_rpg5-PP2C-KD_QCCJ	1.625	Rpg5_PK+/rpg5_PP2C+	R
BSMV_rpg5-PP2C-KD_QCCJ	2.25	Rpg5_PK+/rpg5_PP2C+	R
BSMV_rpg5-PP2C-KD_QCCJ	0.125	Rpg5_PK+/rpg5_PP2C+	R
BSMV_rpg5-PP2C-KD_QCCJ	0.35	Rpg5_PK+/rpg5_PP2C+	R
BSMV_rpg5-PP2C-KD_QCCJ	3.375	Rpg5_PK+/rpg5_PP2C+	S
BSMV_rpg5-PP2C-KD_QCCJ	1.25	Rpg5_PK+/rpg5_PP2C+	R
BSMV_rpg5-PP2C-KD_QCCJ	1.125	Rpg5_PK+/rpg5_PP2C+	R
BSMV_rpg5-PP2C-KD_QCCJ	1.6	Rpg5_PK+/rpg5_PP2C+	R
BSMV_rpg5-PP2C-KD_QCCJ	3.75	Rpg5_PK+/rpg5_PP2C+	S
BSMV_rpg5-PP2C-KD_QCCJ	0.35	Rpg5_PK+/rpg5_PP2C+	R
BSMV_rpg5-PP2C-KD_QCCJ	1.625	Rpg5_PK+/rpg5_PP2C+	R
BSMV_rpg5-PP2C-KD_QCCJ	0.875	Rpg5_PK+/rpg5_PP2C+	R
BSMV_rpg5-PP2C-KD_QCCJ	2.15	Rpg5_PK+/rpg5_PP2C+	R
BSMV_rpg5-PP2C-KD_QCCJ	0.125	Rpg5_PK+/rpg5_PP2C+	R
BSMV_rpg5-PP2C-KD_QCCJ	3.875	Rpg5_PK-/rpg5_PP2C+	S
BSMV_rpg5-PP2C-KD_QCCJ	3.875	Rpg5_PK-/rpg5_PP2C+	S
BSMV_rpg5-PP2C-KD_QCCJ	0.35	Rpg5_PK-/rpg5_PP2C+	R

Table C1. Wheat stem rust race QCCJ disease ratings on tertiary leaf of BSMV_rpg5-PP2C, BSMV_MCS and non-BSMV inoculated plants. Mesothetic categorical disease ratings were converted to a single numerical value according to conversion method described in Zhou et al (Zhou et al., 2014) (continued).

Treatment	Reading	Genotype	QCCJ Response
BSMV_rpg5-PP2C-KD_QCCJ	3.125	Rpg5_PK-/rpg5_PP2C+	S
BSMV_rpg5-PP2C-KD_QCCJ	2.45	Rpg5_PK-/rpg5_PP2C+	S
BSMV_rpg5-PP2C-KD_QCCJ	3.875	Rpg5_PK-/rpg5_PP2C+	S
BSMV_rpg5-PP2C-KD_QCCJ	1.2	Rpg5_PK-/rpg5_PP2C+	R
BSMV_rpg5-PP2C-KD_QCCJ	0.125	Rpg5_PK-/rpg5_PP2C+	R
BSMV_rpg5-PP2C-KD_QCCJ	3.625	Rpg5_PK-/rpg5_PP2C+	S
BSMV_rpg5-PP2C-KD_QCCJ	3.125	Rpg5_PK-/rpg5_PP2C+	S
BSMV_rpg5-PP2C-KD_QCCJ	3.625	Rpg5_PK-/rpg5_PP2C+	S
BSMV_rpg5-PP2C-KD_QCCJ	3.625	Rpg5_PK-/rpg5_PP2C+	S
BSMV_MCS_QCCJ	3.875	Rpg5_PK+/rpg5_PP2C+	S
BSMV_MCS_QCCJ	2	Rpg5_PK-/rpg5_PP2C+	R
BSMV_MCS_QCCJ	3.875	Rpg5_PK+/rpg5_PP2C+	S
BSMV_MCS_QCCJ	0.75	Rpg5_PK+/rpg5_PP2C+	R
BSMV_MCS_QCCJ	3.875	Rpg5_PK+/rpg5_PP2C-	S
BSMV_MCS_QCCJ	3.375	Rpg5_PK+/rpg5_PP2C+	S
BSMV_MCS_QCCJ	0.125	Rpg5_PK-/rpg5_PP2C+	R
BSMV_MCS_QCCJ	2.75	Rpg5_PK+/rpg5_PP2C+	R
BSMV_MCS_QCCJ	0.125	Rpg5_PK+/rpg5_PP2C+	R
BSMV_MCS_QCCJ	2.25	Rpg5_PK+/rpg5_PP2C-	R
QCCJ	4.125	Rpg5_PK-/rpg5_PP2C+	S
QCCJ	3.375	Rpg5_PK-/rpg5_PP2C+	S
QCCJ	3.875	Rpg5_PK-/rpg5_PP2C+	S
QCCJ	3.625	Rpg5_PK-/rpg5_PP2C+	S
QCCJ	3.875	Rpg5_PK-/rpg5_PP2C+	S
QCCJ	3.875	Rpg5_PK-/rpg5_PP2C+	S
QCCJ	4	Rpg5_PK-/rpg5_PP2C+	S
QCCJ	3.75	Rpg5_PK-/rpg5_PP2C+	S
QCCJ	3	Rpg5_PK+/rpg5_PP2C-	S
QCCJ	2.15	Rpg5_PK+/rpg5_PP2C-	R
QCCJ	2.45	Rpg5_PK+/rpg5_PP2C-	R
QCCJ	0.875	Rpg5_PK+/rpg5_PP2C-	R
QCCJ	1.2	Rpg5_PK+/rpg5_PP2C-	R
QCCJ	0.35	Rpg5_PK+/rpg5_PP2C-	R
QCCJ	1.65	Rpg5_PK+/rpg5_PP2C-	R
QCCJ	0.875	Rpg5_PK+/rpg5_PP2C-	R
QCCJ	3.875	Rpg5_PK+/rpg5_PP2C+	S
QCCJ	3.625	Rpg5_PK+/rpg5_PP2C+	S

Table C1. Wheat stem rust race QCCJ disease ratings on tertiary leaf of BSMV_rpg5-PP2C, BSMV_MCS and non-BSMV inoculated plants. Mesothetic categorical disease ratings were converted to a single numerical value according to conversion method described in Zhou et al (Zhou et al., 2014) (continued).

Treatment	Reading	Genotype	QCCJ Response
QCCJ	3.375	Rpg5_PK+/rpg5_PP2C+	S
QCCJ	3.125	Rpg5_PK+/rpg5_PP2C+	S
QCCJ	3.875	Rpg5_PK+/rpg5_PP2C+	S
QCCJ	3	Rpg5_PK+/rpg5_PP2C+	S
QCCJ	3.375	Rpg5_PK+/rpg5_PP2C+	S
QCCJ	3.5	Rpg5_PK+/rpg5_PP2C+	S
QCCJ	4.125	Rpg5_PK+/rpg5_PP2C+	S
QCCJ	3.875	Rpg5_PK+/rpg5_PP2C+	S
QCCJ	3.4	Rpg5_PK+/rpg5_PP2C+	S

APPENDIX D. DISEASE PHENOTYPING OF HV584 X Q21861 RIL POPULATION

Table D1. Hv584 x *rpr9* RIL population of 95 individuals along with the parents phenotyped for QCCJ disease response at seedling and adult plant stage. Stunted root phenotype was also recorded. Data was used for genetic mapping of *rpr9* mutation and stunted root QTL.

Genotype	Seedling- QCCJ disease rating average	Adult plant- QCCJ disease rating average	Root legth average
Hv584/rpr9 F2:6 -RIL- 13	2	2	10
Hv584/rpr9 F2:6 -RIL- 25	1	4	15
Hv584/rpr9 F2:6 -RIL- 38	2	-	13
Hv584/rpr9 F2:6 -RIL- 50	3	13.5	16.7
Hv584/rpr9 F2:6 -RIL- 62	1	3	21
Hv584/rpr9 F2:6 -RIL- 74	1	0	9
Hv584/rpr9 F2:6 -RIL- 86	3	4.5	14.7
Hv584/rpr9 F2:6 -RIL- 14	2	-	17.3
Hv584/rpr9 F2:6 -RIL- 26	1	3	21.3
Hv584/rpr9 F2:6 -RIL- 39	3	4.5	17
Hv584/rpr9 F2:6 -RIL- 63	3	4.5	16.3
Hv584/rpr9 F2:6 -RIL- 75	1	4.5	20.5
Hv584/rpr9 F2:6 -RIL- 87	2	3	10.7
Hv584/rpr9 F2:6 -RIL- 15	1	4	19
Hv584/rpr9 F2:6 -RIL- 27	1	0.4	12.5
Hv584/rpr9 F2:6 -RIL- 52	3	2	26
Hv584/rpr9 F2:6 -RIL- 64	2	0.4	6.5
Hv584/rpr9 F2:6 -RIL- 76	1	4.5	25.7
Hv584/rpr9 F2:6 -RIL- 88	1	9	15.5
Hv584/rpr9 F2:6 -RIL- 4	2	3	18.5
Hv584/rpr9 F2:6 -RIL- 16	3	3	13
Hv584/rpr9 F2:6 -RIL- 28	2	13.5	16.3
Hv584/rpr9 F2:6 -RIL- 41	1	0.8	23
Hv584/rpr9 F2:6 -RIL- 53	3	0.8	7
Hv584/rpr9 F2:6 -RIL- 53	3	0.8	7
Hv584/rpr9 F2:6 -RIL- 65	1	-	13
Hv584/rpr9 F2:6 -RIL- 77	3	4.5	22.7
Hv584/rpr9 F2:6 -RIL- 89	1	4.5	8.3
Hv584/rpr9 F2:6 -RIL- 5	3	4	12
Hv584/rpr9 F2:6 -RIL- 17	1	0.8	15.5

Table D1. Hv584 x *rpr9* RIL population of 95 individuals along with the parents phenotyped for QCCJ disease response at seedling and adult plant stage. Stunted root phenotype was also recorded. Data was used for genetic mapping of *rpr9* mutation and stunted root QTL (continued).

Genotype	Seedling- QCCJ disease rating average	Adult plant- QCCJ disease rating average	Root legth average
Hv584/rpr9 F2:6 -RIL- 29	3	4.5	7.5
Hv584/rpr9 F2:6 -RIL- 42	2	0.4	24
Hv584/rpr9 F2:6 -RIL- 54	1	0.8	10
Hv584/rpr9 F2:6 -RIL- 66	2	2	-
Hv584/rpr9 F2:6 -RIL- 78	1	4.5	24
Hv584/rpr9 F2:6 -RIL- 90	1	4	10.3
Hv584/rpr9 F2:6 -RIL- 6	2	0.4	18.6
Hv584/rpr9 F2:6 -RIL- 18	3	13.5	12.3
Hv584/rpr9 F2:6 -RIL- 30	1	0.8	12
Hv584/rpr9 F2:6 -RIL- 43	1	0	14
Hv584/rpr9 F2:6 -RIL- 55	2	4.5	-
Hv584/rpr9 F2:6 -RIL- 67	1	0.8	16.3
Hv584/rpr9 F2:6 -RIL- 79	2	3	20.5
Hv584/rpr9 F2:6 -RIL- 91	1	4.5	15.3
Hv584/rpr9 F2:6 -RIL- 19	1	2	10
Hv584/rpr9 F2:6 -RIL- 32	3	0.9	13.3
Hv584/rpr9 F2:6 -RIL- 44	3	0.9	16
Hv584/rpr9 F2:6 -RIL- 56	1	4	10
Hv584/rpr9 F2:6 -RIL- 68	1	0.6	4.7
Hv584/rpr9 F2:6 -RIL- 80	3	4.5	10
Hv584/rpr9 F2:6 -RIL- 92	3	4.5	6
Hv584/rpr9 F2:6 -RIL- 8	1	0.4	13.3
Hv584/rpr9 F2:6 -RIL- 20	1	4	28
Hv584/rpr9 F2:6 -RIL- 33	2	4.5	20.3
Hv584/rpr9 F2:6 -RIL- 45	1	4.5	26.7
Hv584/rpr9 F2:6 -RIL- 57	1	0	21.3
Hv584/rpr9 F2:6 -RIL- 81	1	3	10
Hv584/rpr9 F2:6 -RIL- 93	1	0.9	8
Hv584/rpr9 F2:6 -RIL- 9	1	6	17
Hv584/rpr9 F2:6 -RIL- 21	1	4.5	-
Hv584/rpr9 F2:6 -RIL- 34	1	0	26
Hv584/rpr9 F2:6 -RIL- 46	1	0.4	24
Hv584/rpr9 F2:6 -RIL- 70	2	0.6	14.7

Table D1. Hv584 x *rpr9* RIL population of 95 individuals along with the parents phenotyped for QCCJ disease response at seedling and adult plant stage. Stunted root phenotype was also recorded. Data was used for genetic mapping of *rpr9* mutation and stunted root QTL (continued).

Genotype	Seedling- QCCJ disease rating average	Adult plant- QCCJ disease rating average	Root legth average
Hv584/rpr9 F2:6 -RIL- 82	3	4.5	9
Hv584/rpr9 F2:6 -RIL- 10	3	2	19.5
Hv584/rpr9 F2:6 -RIL- 22	3	4.5	12
Hv584/rpr9 F2:6 -RIL- 35	1	0	13
Hv584/rpr9 F2:6 -RIL- 47	2	0	21.7
Hv584/rpr9 F2:6 -RIL- 59	3	4.5	-
Hv584/rpr9 F2:6 -RIL- 71	3	0.9	10
Hv584/rpr9 F2:6 -RIL- 83	1	0.4	9
Hv584/rpr9 F2:6 -RIL- 11	1	8	25
Hv584/rpr9 F2:6 -RIL- 23	1	4	8
Hv584/rpr9 F2:6 -RIL- 36	1	2	20
Hv584/rpr9 F2:6 -RIL- 48	1	0.9	20
Hv584/rpr9 F2:6 -RIL- 60	1	4	13.5
Hv584/rpr9 F2:6 -RIL- 72	1	4	18
Hv584/rpr9 F2:6 -RIL- 84	2	4	19
Hv584/rpr9 F2:6 -RIL- 12	2	3	13.7
Hv584/rpr9 F2:6 -RIL- 37	1	0.4	27.5
Hv584/rpr9 F2:6 -RIL- 49	1	0.8	18.5
Hv584/rpr9 F2:6 -RIL- 61	1	4.5	21
Hv584/rpr9 F2:6 -RIL- 73	3	9	15.7
Hv584/rpr9 F2:6 -RIL- 85	3	0.4	14.5

APPENDIX E. LIST OF HIGH CONFIDENCE GENES UNDER THE *RPR9* LOCUS

Table E1. List of high confidence genes under the *rpr9* gentic map.

Chromosome	Gene ID	Start	Stop
chr3H	HORVU3Hr1G072930	550217065	550217640
chr3H	HORVU3Hr1G072940	550356010	550356903
chr3H	HORVU3Hr1G072950	550415075	550418932
chr3H	HORVU3Hr1G072960	550470506	550471320
chr3H	HORVU3Hr1G072970	550537437	550539346
chr3H	HORVU3Hr1G073020	551155550	551159338
chr3H	HORVU3Hr1G073030	551262457	551262955
chr3H	HORVU3Hr1G073040	551495692	551502968
chr3H	HORVU3Hr1G073050	551757646	551760662
chr3H	HORVU3Hr1G073090	552038070	552038979
chr3H	HORVU3Hr1G073100	552233064	552237117
chr3H	HORVU3Hr1G073110	552240818	552242796
chr3H	HORVU3Hr1G073120	552516379	552517392
chr3H	HORVU3Hr1G073140	552518239	552519222
chr3H	HORVU3Hr1G073150	552521082	552522200
chr3H	HORVU3Hr1G073160	552624371	552624760
chr3H	HORVU3Hr1G073170	552625009	552634592
chr3H	HORVU3Hr1G073180	552636388	552639762
chr3H	HORVU3Hr1G073190	552681371	552682259
chr3H	HORVU3Hr1G073200	552704092	552706819
chr3H	HORVU3Hr1G073220	552738456	552743697
chr3H	HORVU3Hr1G073230	552863869	552903482
chr3H	HORVU3Hr1G073240	552892014	552894544
chr3H	HORVU3Hr1G073280	552906682	552907580
chr3H	HORVU3Hr1G073290	552910072	552913299
chr3H	HORVU3Hr1G073300	553037292	553038573
chr3H	HORVU3Hr1G073340	553073323	553074692
chr3H	HORVU3Hr1G073350	553094872	553096429
chr3H	HORVU3Hr1G073360	553109601	553114267
chr3H	HORVU3Hr1G073450	553189017	553192768
chr3H	HORVU3Hr1G073460	553194902	553196035
chr3H	HORVU3Hr1G073470	553609683	553622869
chr3H	HORVU3Hr1G073500	553697277	553698132
chr3H	HORVU3Hr1G073520	553834059	553834824
chr3H	HORVU3Hr1G073540	553877313	553880397
chr3H	HORVU3Hr1G073560	553888432	553897295
chr3H	HORVU3Hr1G073580	553939881	553941957

Table E1. List of high confidence genes under the *rpr9* gentic map (continued).

Chromosome	Gene ID	Start	Stop
chr3H	HORVU3Hr1G073600	554175342	554175617
chr3H	HORVU3Hr1G073630	554364480	554385487
chr3H	HORVU3Hr1G073650	554545342	554545674
chr3H	HORVU3Hr1G073660	554564871	554565894
chr3H	HORVU3Hr1G073670	554566694	554588777
chr3H	HORVU3Hr1G073680	554600431	554600637
chr3H	HORVU3Hr1G073690	554695372	554700257
chr3H	HORVU3Hr1G073700	554811268	554811723
chr3H	HORVU3Hr1G073710	554893597	554894281
chr3H	HORVU3Hr1G073730	554900388	554901447
chr3H	HORVU3Hr1G073740	554954898	554956056
chr3H	HORVU3Hr1G073750	554962112	554970626
chr3H	HORVU3Hr1G073770	555183451	555185118
chr3H	HORVU3Hr1G073780	555352769	555355130
chr3H	HORVU3Hr1G073790	555470279	555480793
chr3H	HORVU3Hr1G073800	555555698	555558354
chr3H	HORVU3Hr1G073830	555807762	555810453
chr3H	HORVU3Hr1G073840	556194513	556199229
chr3H	HORVU3Hr1G073850	556294872	556298196
chr3H	HORVU3Hr1G073860	556298730	556300410
chr3H	HORVU3Hr1G073870	556300751	556311627
chr3H	HORVU3Hr1G073910	556371583	556374944
chr3H	HORVU3Hr1G073930	556478848	556482474
chr3H	HORVU3Hr1G073940	556524795	556527065
chr3H	HORVU3Hr1G073950	556527373	556527651
chr3H	HORVU3Hr1G073960	556559699	556568621
chr3H	HORVU3Hr1G074000	556576675	556578906
chr3H	HORVU3Hr1G074010	556604714	556606322
chr3H	HORVU3Hr1G074020	556622089	556624360
chr3H	HORVU3Hr1G074040	556701538	556705081
chr3H	HORVU3Hr1G074070	556752825	556754421
chr3H	HORVU3Hr1G074090	556826163	556826473
chr3H	HORVU3Hr1G074100	557074771	557076003
chr3H	HORVU3Hr1G074120	557078570	557082058
chr3H	HORVU3Hr1G074130	557216044	557217104
chr3H	HORVU3Hr1G074160	557341645	557342419
chr3H	HORVU3Hr1G074180	557357652	557358891
chr3H	HORVU3Hr1G074190	557359236	557365104
chr3H	HORVU3Hr1G074210	557364161	557374353
chr3H	HORVU3Hr1G074220	557381815	557384921

Table E1. List of high confidence genes under the *rpr9* gentic map (continued).

Chromosome	Gene ID	Start	Stop
chr3H	HORVU3Hr1G074230	557551444	557555429
chr3H	HORVU3Hr1G074250	557560214	557573028
chr3H	HORVU3Hr1G074270	557571407	557571975
chr3H	HORVU3Hr1G074280	557603531	557607104
chr3H	HORVU3Hr1G074290	557949641	557950774
chr3H	HORVU3Hr1G074300	557962590	557963481
chr3H	HORVU3Hr1G074310	557989135	557992211
chr3H	HORVU3Hr1G074320	558020676	558022073
chr3H	HORVU3Hr1G074330	558033886	558047668
chr3H	HORVU3Hr1G074340	558037984	558038259
chr3H	HORVU3Hr1G074350	558242665	558243949
chr3H	HORVU3Hr1G074360	558275983	558278629
chr3H	HORVU3Hr1G074370	558414166	558417096
chr3H	HORVU3Hr1G074380	558528449	558529558
chr3H	HORVU3Hr1G074390	558694151	558694943
chr3H	HORVU3Hr1G074430	558709024	558710357
chr3H	HORVU3Hr1G074470	558737483	558738122
chr3H	HORVU3Hr1G074480	558777508	558783519
chr3H	HORVU3Hr1G074490	558787640	558791251
chr3H	HORVU3Hr1G074510	558847394	558847689
chr3H	HORVU3Hr1G074570	558854506	558859311
chr3H	HORVU3Hr1G074600	558927771	558929085
chr3H	HORVU3Hr1G074620	558954084	558956582
chr3H	HORVU3Hr1G074640	559036774	559041226
chr3H	HORVU3Hr1G074660	559095266	559105577
chr3H	HORVU3Hr1G074670	559136249	559136491
chr3H	HORVU3Hr1G074680	559145074	559148627
chr3H	HORVU3Hr1G074720	559499433	559501360
chr3H	HORVU3Hr1G074730	559501224	559506647
chr3H	HORVU3Hr1G074770	559794503	559801078
chr3H	HORVU3Hr1G074780	559801203	559801937
chr3H	HORVU3Hr1G074790	559868237	559870255
chr3H	HORVU3Hr1G074800	559879827	559884313
chr3H	HORVU3Hr1G074820	560185568	560248301
chr3H	HORVU3Hr1G074840	560315309	560320649
chr3H	HORVU3Hr1G074850	560316839	560326306

Table E1. List of high confidence genes under the *rpr9* gentic map (continued).

Chromosome	Gene ID	Start	Stop
chr3H	HORVU3Hr1G074860	560328216	560328492
chr3H	HORVU3Hr1G074870	560328716	560328829
chr3H	HORVU3Hr1G074880	560329502	560329998
chr3H	HORVU3Hr1G074890	560330015	560330262
chr3H	HORVU3Hr1G074900	560330324	560330539
chr3H	HORVU3Hr1G074910	560447102	560448070
chr3H	HORVU3Hr1G074920	560659267	560660724
chr3H	HORVU3Hr1G074930	560737798	560739850
chr3H	HORVU3Hr1G074940	560884155	560885580
chr3H	HORVU3Hr1G074950	560902498	560904068
chr3H	HORVU3Hr1G074960	560934358	560935865
chr3H	HORVU3Hr1G074970	561006112	561007794
chr3H	HORVU3Hr1G075000	561254447	561255632
chr3H	HORVU3Hr1G075010	561255634	561256481
chr3H	HORVU3Hr1G075030	561299425	561299615
chr3H	HORVU3Hr1G075040	561302733	561304797
chr3H	HORVU3Hr1G075050	561431835	561432766
chr3H	HORVU3Hr1G075060	561500252	561501311
chr3H	HORVU3Hr1G075070	561614572	561615955
chr3H	HORVU3Hr1G075090	561675424	561676036
chr3H	HORVU3Hr1G075100	561676680	561680004
chr3H	HORVU3Hr1G075110	561739412	561739823
chr3H	HORVU3Hr1G075120	561789245	561791158
chr3H	HORVU3Hr1G075130	561836214	561836624
chr3H	HORVU3Hr1G075150	561960823	561962277
chr3H	HORVU3Hr1G075160	562125392	562128780
chr3H	HORVU3Hr1G075180	562163595	562168459
chr3H	HORVU3Hr1G075200	562221199	562221736
chr3H	HORVU3Hr1G075210	562235077	562236462
chr3H	HORVU3Hr1G075220	562266303	562282240
chr3H	HORVU3Hr1G075250	562433367	562437543
chr3H	HORVU3Hr1G075260	562580077	562580445
chr3H	HORVU3Hr1G075270	562581386	562581601
chr3H	HORVU3Hr1G075280	562583065	562583686
chr3H	HORVU3Hr1G075290	562588201	562592499
chr3H	HORVU3Hr1G075310	562950891	562955901

Table E1. List of high confidence genes under the *rpr9* gentic map (continued).

Chromosome	Gene ID	Start	Stop
chr3H	HORVU3Hr1G075330	563007569	563010030
chr3H	HORVU3Hr1G075340	563053326	563061402
chr3H	HORVU3Hr1G075350	563157025	563157721
chr3H	HORVU3Hr1G075370	563330849	563331404
chr3H	HORVU3Hr1G075380	563332489	563335510
chr3H	HORVU3Hr1G075400	563530557	563530721
chr3H	HORVU3Hr1G075410	563902083	563902944
chr3H	HORVU3Hr1G075460	564048946	564049422
chr3H	HORVU3Hr1G075470	564049319	564051839
chr3H	HORVU3Hr1G075480	564145211	564147096
chr3H	HORVU3Hr1G075500	564177356	564180335
chr3H	HORVU3Hr1G075510	564196345	564197248
chr3H	HORVU3Hr1G075540	564770923	564779282
chr3H	HORVU3Hr1G075550	564802693	564803023
chr3H	HORVU3Hr1G075560	564857855	564858055
chr3H	HORVU3Hr1G075580	565093670	565096205
chr3H	HORVU3Hr1G075590	565117159	565125452
chr3H	HORVU3Hr1G075600	565141151	565142513
chr3H	HORVU3Hr1G075610	565144426	565145791
chr3H	HORVU3Hr1G075620	565395906	565422259
chr3H	HORVU3Hr1G075690	565423550	565424698
chr3H	HORVU3Hr1G075710	565652663	565661139
chr3H	HORVU3Hr1G075730	565663700	565665620
chr3H	HORVU3Hr1G075750	565667900	565670340
chr3H	HORVU3Hr1G075770	565783316	565784434
chr3H	HORVU3Hr1G075780	565937201	565939308
chr3H	HORVU3Hr1G075790	566000361	566004889
chr3H	HORVU3Hr1G075800	566000418	566008651
chr3H	HORVU3Hr1G075820	566281456	566287193
chr3H	HORVU3Hr1G075830	566356674	566361686
chr3H	HORVU3Hr1G075840	566406716	566409738
chr3H	HORVU3Hr1G075850	566524751	566533154
chr3H	HORVU3Hr1G075870	566531044	566534084
chr3H	HORVU3Hr1G075890	566693885	566702925
chr3H	HORVU3Hr1G075900	566697230	566698772
chr3H	HORVU3Hr1G075910	566984724	566989254

Table E1. List of high confidence genes under the *rpr9* gentic map (continued).

Chromosome	Gene ID	Start	Stop
chr3H	HORVU3Hr1G075920	567046660	567052004
chr3H	HORVU3Hr1G075960	567163924	567166836
chr3H	HORVU3Hr1G075970	567169189	567169393
chr3H	HORVU3Hr1G075990	567387812	567397405
chr3H	HORVU3Hr1G076000	567419572	567421491
chr3H	HORVU3Hr1G076010	567475580	567476160
chr3H	HORVU3Hr1G076030	567513840	567518550
chr3H	HORVU3Hr1G076060	567578333	567582963
chr3H	HORVU3Hr1G076080	567671564	567673945
chr3H	HORVU3Hr1G076110	567759134	567759940
chr3H	HORVU3Hr1G076120	567762104	567764519
chr3H	HORVU3Hr1G076160	567940390	567941190
chr3H	HORVU3Hr1G076190	567955174	567960157
chr3H	HORVU3Hr1G076220	567973945	567981653
chr3H	HORVU3Hr1G076230	567977456	567977724
chr3H	HORVU3Hr1G076250	568011982	568012499
chr3H	HORVU3Hr1G076270	568080762	568081071
chr3H	HORVU3Hr1G076300	568105163	568106220
chr3H	HORVU3Hr1G076310	568143147	568143499
chr3H	HORVU3Hr1G076320	568150537	568174714
chr3H	HORVU3Hr1G076370	568174871	568177483
chr3H	HORVU3Hr1G076400	568354400	568355245
chr3H	HORVU3Hr1G076430	568581093	568582221
chr3H	HORVU3Hr1G076480	568830688	568848448
chr3H	HORVU3Hr1G076490	568831240	568831452
chr3H	HORVU3Hr1G076520	568849153	568855449
chr3H	HORVU3Hr1G076530	568901752	568902006
chr3H	HORVU3Hr1G076550	568915332	568916269
chr3H	HORVU3Hr1G076560	568917990	568918218
chr3H	HORVU3Hr1G076620	568990465	569002821
chr3H	HORVU3Hr1G076630	569014663	569015522
chr3H	HORVU3Hr1G076640	569034122	569035435
chr3H	HORVU3Hr1G076650	569133776	569134417
chr3H	HORVU3Hr1G076660	569204602	569206050
chr3H	HORVU3Hr1G076670	569329075	569330103
chr3H	HORVU3Hr1G076680	569417183	569429535

Table E1. List of high confidence genes under the *rpr9* gentic map (continued).

Chromosome	Gene ID	Start	Stop
chr3H	HORVU3Hr1G076710	569508359	569509168
chr3H	HORVU3Hr1G076740	569992909	569995187
chr3H	HORVU3Hr1G076750	569995433	570001063
chr3H	HORVU3Hr1G076760	570001436	570005650
chr3H	HORVU3Hr1G076790	570093778	570095731
chr3H	HORVU3Hr1G076800	570174983	570175673
chr3H	HORVU3Hr1G076840	570437056	570446342
chr3H	HORVU3Hr1G076880	570788593	570797369
chr3H	HORVU3Hr1G076890	570851038	570854298
chr3H	HORVU3Hr1G076910	570857092	570866043
chr3H	HORVU3Hr1G076920	570908294	570912853
chr3H	HORVU3Hr1G076940	570945947	570947527
chr3H	HORVU3Hr1G076960	570984470	570989561
chr3H	HORVU3Hr1G076970	571065105	571065614
chr3H	HORVU3Hr1G077000	571141113	571146034
chr3H	HORVU3Hr1G077010	571148748	571149005
chr3H	HORVU3Hr1G077020	571152216	571156063
chr3H	HORVU3Hr1G077030	571154180	571156268
chr3H	HORVU3Hr1G077040	571156523	571166687
chr3H	HORVU3Hr1G077050	571168129	571168842
chr3H	HORVU3Hr1G077070	571301429	571301922
chr3H	HORVU3Hr1G077080	571303082	571306176
chr3H	HORVU3Hr1G077110	571493242	571497775
chr3H	HORVU3Hr1G077130	571554417	571565073
chr3H	HORVU3Hr1G077160	571626961	571627583
chr3H	HORVU3Hr1G077170	571729835	571730292
chr3H	HORVU3Hr1G077180	571798518	571799625
chr3H	HORVU3Hr1G077200	571935852	571936809
chr3H	HORVU3Hr1G077210	571942935	571946234
chr3H	HORVU3Hr1G077220	571947091	571953876
chr3H	HORVU3Hr1G077230	572075755	572076237
chr3H	HORVU3Hr1G077250	572137417	572141337
chr3H	HORVU3Hr1G077260	572188126	572190245
chr3H	HORVU3Hr1G077280	572394611	572396747
chr3H	HORVU3Hr1G077290	572480924	572483060
chr3H	HORVU3Hr1G077330	572501586	572502496

Table E1. List of high confidence genes under the *rpr9* gentic map (continued).

Chromosome	Gene ID	Start	Stop
chr3H	HORVU3Hr1G077340	572504371	572504706
chr3H	HORVU3Hr1G077360	572642818	572645451
chr3H	HORVU3Hr1G077380	572883434	572883838
chr3H	HORVU3Hr1G077390	572923082	572924959
chr3H	HORVU3Hr1G077400	572947680	572949672
chr3H	HORVU3Hr1G077430	573114377	573115153
chr3H	HORVU3Hr1G077440	573114391	573117095
chr3H	HORVU3Hr1G077450	573126424	573129415
chr3H	HORVU3Hr1G077490	573264220	573266921
chr3H	HORVU3Hr1G077500	573268831	573269508
chr3H	HORVU3Hr1G077530	573456662	573461907
chr3H	HORVU3Hr1G077540	573469652	573474878
chr3H	HORVU3Hr1G077560	573564340	573565143
chr3H	HORVU3Hr1G077570	573572730	573573719
chr3H	HORVU3Hr1G077580	573806875	573808911
chr3H	HORVU3Hr1G077610	574097510	574098766
chr3H	HORVU3Hr1G077630	574209536	574212012
chr3H	HORVU3Hr1G077640	574212208	574212769
chr3H	HORVU3Hr1G077660	574246394	574247520
chr3H	HORVU3Hr1G077670	574276620	574280017
chr3H	HORVU3Hr1G077680	574429621	574431416
chr3H	HORVU3Hr1G077690	574433359	574438442
chr3H	HORVU3Hr1G077700	574438512	574442454
chr3H	HORVU3Hr1G077710	574617934	574618257
chr3H	HORVU3Hr1G077730	574655663	574660346
chr3H	HORVU3Hr1G077740	574664766	574669907
chr3H	HORVU3Hr1G077770	574833337	574835529
chr3H	HORVU3Hr1G077780	574886154	574890042
chr3H	HORVU3Hr1G077790	574906584	574908486
chr3H	HORVU3Hr1G077800	574922799	574929689
chr3H	HORVU3Hr1G077830	574978971	574979118
chr3H	HORVU3Hr1G077850	574993077	575018281
chr3H	HORVU3Hr1G077880	575124231	575125296
chr3H	HORVU3Hr1G077890	575137842	575138829
chr3H	HORVU3Hr1G077920	575185667	575186229
chr3H	HORVU3Hr1G077930	575246061	575254865

Table E1. List of high confidence genes under the *rpr9* gentic map (continued).

Chromosome	Gene ID	Start	Stop
chr3H	HORVU3Hr1G077950	575344241	575348963
chr3H	HORVU3Hr1G077960	575421996	575424645
chr3H	HORVU3Hr1G077980	575567037	575569143
chr3H	HORVU3Hr1G078030	575736925	575741318
chr3H	HORVU3Hr1G078090	576142004	576149293
chr3H	HORVU3Hr1G078100	576142353	576146580
chr3H	HORVU3Hr1G078110	576162439	576164429
chr3H	HORVU3Hr1G078140	576638043	576640726
chr3H	HORVU3Hr1G078150	576753889	576754856
chr3H	HORVU3Hr1G078190	577012931	577013857
chr3H	HORVU3Hr1G078200	577046942	577255364
chr3H	HORVU3Hr1G078210	577073218	577077259
chr3H	HORVU3Hr1G078220	577142016	577142826
chr3H	HORVU3Hr1G078230	577183965	577185588
chr3H	HORVU3Hr1G078260	577355113	577357894
chr3H	HORVU3Hr1G078270	577392564	577394768
chr3H	HORVU3Hr1G078300	577640392	577644084
chr3H	HORVU3Hr1G078330	577713922	577718141
chr3H	HORVU3Hr1G078350	577726585	577727831
chr3H	HORVU3Hr1G078360	577862446	577867238
chr3H	HORVU3Hr1G078370	578003070	578003806
chr3H	HORVU3Hr1G078380	578007471	578008278
chr3H	HORVU3Hr1G078390	578100274	578101175
chr3H	HORVU3Hr1G078420	578142357	578143348
chr3H	HORVU3Hr1G078430	578385543	578385952
chr3H	HORVU3Hr1G078450	578419716	578420079
chr3H	HORVU3Hr1G078460	578420236	578421303
chr3H	HORVU3Hr1G078470	578424002	578433823
chr3H	HORVU3Hr1G078480	578424357	578424662
chr3H	HORVU3Hr1G078490	578461509	578465298
chr3H	HORVU3Hr1G078520	578602529	578603623
chr3H	HORVU3Hr1G078530	578730032	578734028
chr3H	HORVU3Hr1G078540	579031627	579034954
chr3H	HORVU3Hr1G078550	579045376	579047319
chr3H	HORVU3Hr1G078560	579189854	579190529
chr3H	HORVU3Hr1G078590	579242314	579250436

Table E1. List of high confidence genes under the *rpr9* gentic map (continued).

Chromosome	Gene ID	Start	Stop
chr3H	HORVU3Hr1G078620	579384034	579387081
chr3H	HORVU3Hr1G078650	579541238	579543344
chr3H	HORVU3Hr1G078660	579747332	579753561
chr3H	HORVU3Hr1G078670	579747432	579749278
chr3H	HORVU3Hr1G078680	579791316	579792117
chr3H	HORVU3Hr1G078710	579993767	579995615
chr3H	HORVU3Hr1G078720	579997522	579997716
chr3H	HORVU3Hr1G078760	580163039	580165168
chr3H	HORVU3Hr1G078780	580242083	580244212
chr3H	HORVU3Hr1G078790	580244775	580246395
chr3H	HORVU3Hr1G078800	580262340	580262670
chr3H	HORVU3Hr1G078810	580342487	580344228
chr3H	HORVU3Hr1G078820	580440661	580443718
chr3H	HORVU3Hr1G078830	580440772	580441469
chr3H	HORVU3Hr1G078840	580479631	580482592
chr3H	HORVU3Hr1G078850	580626749	580628694
chr3H	HORVU3Hr1G078860	580633265	580636504
chr3H	HORVU3Hr1G078880	580637849	580640885
chr3H	HORVU3Hr1G078900	580703158	580708235
chr3H	HORVU3Hr1G078920	580972110	580974506
chr3H	HORVU3Hr1G078930	581047343	581049277
chr3H	HORVU3Hr1G078940	581094773	581098244
chr3H	HORVU3Hr1G078950	581098605	581102982
chr3H	HORVU3Hr1G078960	581129340	581131317
chr3H	HORVU3Hr1G078980	581197066	581197768
chr3H	HORVU3Hr1G078990	581274857	581279240
chr3H	HORVU3Hr1G079000	581279340	581290246
chr3H	HORVU3Hr1G079010	581291047	581293931
chr3H	HORVU3Hr1G079040	581515108	581517964
chr3H	HORVU3Hr1G079050	581638333	581645407
chr3H	HORVU3Hr1G079060	581747398	581747630
chr3H	HORVU3Hr1G079180	582301713	582303766
chr3H	HORVU3Hr1G079210	582465119	582484395
chr3H	HORVU3Hr1G079230	582468363	582484516
chr3H	HORVU3Hr1G079260	582491401	582498825

APPENDIX F. LIST OF LOW CONFIDENCE GENES UNDER THE *RPR9* QTL

Table F1. List of low confidence genes under the *rpr9* QTL.

Chromosome	Gene ID	Start	Stop
chr3H	HORVU3Hr1G072980	550974460	550975635
chr3H	HORVU3Hr1G072990	550975893	550976330
chr3H	HORVU3Hr1G073000	551017855	551021814
chr3H	HORVU3Hr1G073010	551022002	551024699
chr3H	HORVU3Hr1G073060	551763308	551763853
chr3H	HORVU3Hr1G073070	552001142	552002592
chr3H	HORVU3Hr1G073080	552008305	552013642
chr3H	HORVU3Hr1G073130	552518199	552519460
chr3H	HORVU3Hr1G073210	552725970	552726463
chr3H	HORVU3Hr1G073250	552892719	552893303
chr3H	HORVU3Hr1G073260	552895697	552895987
chr3H	HORVU3Hr1G073270	552905841	552906407
chr3H	HORVU3Hr1G073310	553046991	553047315
chr3H	HORVU3Hr1G073320	553057634	553057804
chr3H	HORVU3Hr1G073330	553058522	553058888
chr3H	HORVU3Hr1G073370	553143148	553145952
chr3H	HORVU3Hr1G073380	553143211	553145619
chr3H	HORVU3Hr1G073390	553146664	553147603
chr3H	HORVU3Hr1G073400	553148235	553149291
chr3H	HORVU3Hr1G073410	553150692	553151113
chr3H	HORVU3Hr1G073420	553184270	553195750
chr3H	HORVU3Hr1G073430	553186742	553187414
chr3H	HORVU3Hr1G073440	553188628	553188864
chr3H	HORVU3Hr1G073480	553609695	553613683
chr3H	HORVU3Hr1G073490	553623099	553623371
chr3H	HORVU3Hr1G073510	553770464	553770925
chr3H	HORVU3Hr1G073530	553859388	553860703
chr3H	HORVU3Hr1G073550	553882127	553882249
chr3H	HORVU3Hr1G073610	554178522	554178711
chr3H	HORVU3Hr1G073620	554364480	554365149
chr3H	HORVU3Hr1G073640	554365297	554367092
chr3H	HORVU3Hr1G073720	554895933	554896342
chr3H	HORVU3Hr1G073760	555068107	555068338
chr3H	HORVU3Hr1G073810	555784440	555788596
chr3H	HORVU3Hr1G073820	555793001	555793309
chr3H	HORVU3Hr1G073890	556308068	556308193
chr3H	HORVU3Hr1G073900	556323120	556323455

Table F1. List of low confidence genes under the *rpr9* QTL (continued).

Chromosome	Gene ID	Start	Stop
chr3H	HORVU3Hr1G073920	556449162	556449287
chr3H	HORVU3Hr1G073970	556569257	556569628
chr3H	HORVU3Hr1G073980	556572652	556573977
chr3H	HORVU3Hr1G073990	556574125	556576071
chr3H	HORVU3Hr1G074030	556632951	556633474
chr3H	HORVU3Hr1G074050	556745837	556746160
chr3H	HORVU3Hr1G074060	556747360	556747814
chr3H	HORVU3Hr1G074080	556825264	556825403
chr3H	HORVU3Hr1G074110	557076558	557077185
chr3H	HORVU3Hr1G074150	557340257	557340544
chr3H	HORVU3Hr1G074170	557352225	557353486
chr3H	HORVU3Hr1G074200	557361657	557362824
chr3H	HORVU3Hr1G074240	557558623	557559839
chr3H	HORVU3Hr1G074260	557564084	557564587
chr3H	HORVU3Hr1G074400	558695610	558696494
chr3H	HORVU3Hr1G074410	558696789	558705129
chr3H	HORVU3Hr1G074420	558703000	558715724
chr3H	HORVU3Hr1G074440	558711591	558714028
chr3H	HORVU3Hr1G074450	558720215	558721424
chr3H	HORVU3Hr1G074460	558730444	558731745
chr3H	HORVU3Hr1G074500	558791686	558792230
chr3H	HORVU3Hr1G074520	558848478	558849172
chr3H	HORVU3Hr1G074530	558849174	558849461
chr3H	HORVU3Hr1G074540	558850043	558850549
chr3H	HORVU3Hr1G074550	558851235	558851630
chr3H	HORVU3Hr1G074560	558852241	558852501
chr3H	HORVU3Hr1G074580	558857663	558857923
chr3H	HORVU3Hr1G074590	558858062	558858222
chr3H	HORVU3Hr1G074610	558953956	558954467
chr3H	HORVU3Hr1G074630	559016410	559016768
chr3H	HORVU3Hr1G074650	559092801	559093467
chr3H	HORVU3Hr1G074690	559150275	559150627
chr3H	HORVU3Hr1G074700	559173384	559173743
chr3H	HORVU3Hr1G074710	559186502	559186900
chr3H	HORVU3Hr1G074740	559685956	559698070
chr3H	HORVU3Hr1G074750	559686043	559687258
chr3H	HORVU3Hr1G074760	559687976	559691046
chr3H	HORVU3Hr1G074810	560164661	560164768
chr3H	HORVU3Hr1G073890	556308068	556308193
chr3H	HORVU3Hr1G073900	556323120	556323455

Table F1. List of low confidence genes under the *rpr9* QTL (continued).

Chromosome	Gene ID	Start	Stop
chr3H	HORVU3Hr1G073920	556449162	556449287
chr3H	HORVU3Hr1G073970	556569257	556569628
chr3H	HORVU3Hr1G073980	556572652	556573977
chr3H	HORVU3Hr1G073990	556574125	556576071
chr3H	HORVU3Hr1G074030	556632951	556633474
chr3H	HORVU3Hr1G074050	556745837	556746160
chr3H	HORVU3Hr1G074060	556747360	556747814
chr3H	HORVU3Hr1G074080	556825264	556825403
chr3H	HORVU3Hr1G074110	557076558	557077185
chr3H	HORVU3Hr1G074150	557340257	557340544
chr3H	HORVU3Hr1G074170	557352225	557353486
chr3H	HORVU3Hr1G074200	557361657	557362824
chr3H	HORVU3Hr1G074240	557558623	557559839
chr3H	HORVU3Hr1G074260	557564084	557564587
chr3H	HORVU3Hr1G074400	558695610	558696494
chr3H	HORVU3Hr1G074410	558696789	558705129
chr3H	HORVU3Hr1G074420	558703000	558715724
chr3H	HORVU3Hr1G074440	558711591	558714028
chr3H	HORVU3Hr1G074450	558720215	558721424
chr3H	HORVU3Hr1G074460	558730444	558731745
chr3H	HORVU3Hr1G074500	558791686	558792230
chr3H	HORVU3Hr1G074520	558848478	558849172
chr3H	HORVU3Hr1G074530	558849174	558849461
chr3H	HORVU3Hr1G074540	558850043	558850549
chr3H	HORVU3Hr1G074550	558851235	558851630
chr3H	HORVU3Hr1G074560	558852241	558852501
chr3H	HORVU3Hr1G074580	558857663	558857923
chr3H	HORVU3Hr1G074590	558858062	558858222
chr3H	HORVU3Hr1G074610	558953956	558954467
chr3H	HORVU3Hr1G074630	559016410	559016768
chr3H	HORVU3Hr1G074650	559092801	559093467
chr3H	HORVU3Hr1G074690	559150275	559150627
chr3H	HORVU3Hr1G074700	559173384	559173743
chr3H	HORVU3Hr1G074710	559186502	559186900
chr3H	HORVU3Hr1G074740	559685956	559698070
chr3H	HORVU3Hr1G074750	559686043	559687258
chr3H	HORVU3Hr1G074760	559687976	559691046
chr3H	HORVU3Hr1G074810	560164661	560164768
chr3H	HORVU3Hr1G074830	560295121	560295775
chr3H	HORVU3Hr1G074980	561007945	561008151

Table F1. List of low confidence genes under the *rpr9* QTL (continued).

Chromosome	Gene ID	Start	Stop
chr3H	HORVU3Hr1G074990	561077596	561078171
chr3H	HORVU3Hr1G075020	561296852	561297044
chr3H	HORVU3Hr1G075080	561655427	561655712
chr3H	HORVU3Hr1G075140	561913106	561917752
chr3H	HORVU3Hr1G075170	562125469	562127926
chr3H	HORVU3Hr1G075190	562166879	562167418
chr3H	HORVU3Hr1G075230	562267372	562267545
chr3H	HORVU3Hr1G075240	562332148	562332558
chr3H	HORVU3Hr1G075300	562916044	562916614
chr3H	HORVU3Hr1G075320	562961227	562961769
chr3H	HORVU3Hr1G075360	563195014	563199952
chr3H	HORVU3Hr1G075390	563528732	563529468
chr3H	HORVU3Hr1G075420	563903676	563904820
chr3H	HORVU3Hr1G075430	563906920	563908116
chr3H	HORVU3Hr1G075440	563908336	563908810
chr3H	HORVU3Hr1G075450	563912594	563913671
chr3H	HORVU3Hr1G075490	564168097	564168500
chr3H	HORVU3Hr1G075520	564197904	564198306
chr3H	HORVU3Hr1G075530	564769238	564770442
chr3H	HORVU3Hr1G075570	564858373	564858519
chr3H	HORVU3Hr1G075630	565398197	565410883
chr3H	HORVU3Hr1G075640	565400612	565401098
chr3H	HORVU3Hr1G075650	565410649	565411629
chr3H	HORVU3Hr1G075660	565412049	565416912
chr3H	HORVU3Hr1G075670	565417753	565419381
chr3H	HORVU3Hr1G075680	565421643	565422481
chr3H	HORVU3Hr1G075700	565519237	565520174
chr3H	HORVU3Hr1G075720	565653726	565653944
chr3H	HORVU3Hr1G075740	565667422	565667766
chr3H	HORVU3Hr1G075760	565783088	565790047
chr3H	HORVU3Hr1G075810	566010123	566010563
chr3H	HORVU3Hr1G075860	566527327	566527536
chr3H	HORVU3Hr1G075880	566618325	566625377
chr3H	HORVU3Hr1G075930	567050816	567052103
chr3H	HORVU3Hr1G075940	567156483	567157475
chr3H	HORVU3Hr1G075950	567156663	567157486
chr3H	HORVU3Hr1G075980	567344339	567345039
chr3H	HORVU3Hr1G076040	567561921	567562226
chr3H	HORVU3Hr1G076050	567578207	567578737
chr3H	HORVU3Hr1G076070	567588119	567588441

Table F1. List of low confidence genes under the *rpr9* QTL (continued).

Chromosome	Gene ID	Start	Stop
chr3H	HORVU3Hr1G076090	567674234	567674355
chr3H	HORVU3Hr1G076100	567758656	567759037
chr3H	HORVU3Hr1G076130	567936815	567937314
chr3H	HORVU3Hr1G076140	567937354	567937682
chr3H	HORVU3Hr1G076150	567937881	567938150
chr3H	HORVU3Hr1G076170	567948965	567949864
chr3H	HORVU3Hr1G076180	567952304	567954221
chr3H	HORVU3Hr1G076200	567960282	567960610
chr3H	HORVU3Hr1G076210	567964844	567964966
chr3H	HORVU3Hr1G076240	567984020	567985047
chr3H	HORVU3Hr1G076260	568023894	568024451
chr3H	HORVU3Hr1G076280	568084416	568085126
chr3H	HORVU3Hr1G076290	568088133	568088715
chr3H	HORVU3Hr1G076330	568163709	568166591
chr3H	HORVU3Hr1G076340	568166952	568167385
chr3H	HORVU3Hr1G076350	568167573	568167988
chr3H	HORVU3Hr1G076360	568174871	568177442
chr3H	HORVU3Hr1G076380	568215182	568215983
chr3H	HORVU3Hr1G076390	568348264	568349522
chr3H	HORVU3Hr1G076410	568529535	568530182
chr3H	HORVU3Hr1G076420	568575958	568576617
chr3H	HORVU3Hr1G076440	568702090	568702453
chr3H	HORVU3Hr1G076450	568712212	568712985
chr3H	HORVU3Hr1G076460	568791928	568793426
chr3H	HORVU3Hr1G076470	568830633	568831104
chr3H	HORVU3Hr1G076500	568836382	568836726
chr3H	HORVU3Hr1G076510	568841357	568841895
chr3H	HORVU3Hr1G076540	568914342	568914731
chr3H	HORVU3Hr1G076570	568959671	568960891
chr3H	HORVU3Hr1G076580	568965559	568966044
chr3H	HORVU3Hr1G076590	568969231	568969796
chr3H	HORVU3Hr1G076600	568969487	568970152
chr3H	HORVU3Hr1G076610	568972016	568972528
chr3H	HORVU3Hr1G076690	569417183	569422983
chr3H	HORVU3Hr1G076700	569481700	569482501
chr3H	HORVU3Hr1G076720	569588683	569589282
chr3H	HORVU3Hr1G076730	569675716	569676509
chr3H	HORVU3Hr1G076770	570003622	570003755
chr3H	HORVU3Hr1G076780	570004081	570004302
chr3H	HORVU3Hr1G076810	570384205	570384342

Table F1. List of low confidence genes under the *rpr9* QTL (continued).

Chromosome	Gene ID	Start	Stop
chr3H	HORVU3Hr1G076820	570384374	570384556
chr3H	HORVU3Hr1G076830	570386599	570386911
chr3H	HORVU3Hr1G076850	570441003	570441507
chr3H	HORVU3Hr1G076860	570498047	570498563
chr3H	HORVU3Hr1G076870	570758853	570759633
chr3H	HORVU3Hr1G076900	570854276	570854785
chr3H	HORVU3Hr1G076930	570938917	570940146
chr3H	HORVU3Hr1G076950	570957286	570958909
chr3H	HORVU3Hr1G076980	571078115	571078348
chr3H	HORVU3Hr1G076990	571128465	571128865
chr3H	HORVU3Hr1G077060	571298978	571302132
chr3H	HORVU3Hr1G077090	571415329	571415475
chr3H	HORVU3Hr1G077100	571476070	571476352
chr3H	HORVU3Hr1G077120	571498182	571499586
chr3H	HORVU3Hr1G077140	571559298	571559735
chr3H	HORVU3Hr1G077150	571560035	571560271
chr3H	HORVU3Hr1G077190	571934139	571934845
chr3H	HORVU3Hr1G077240	572135288	572135742
chr3H	HORVU3Hr1G077270	572188173	572189008
chr3H	HORVU3Hr1G077300	572495294	572495710
chr3H	HORVU3Hr1G077310	572497850	572498196
chr3H	HORVU3Hr1G077320	572498621	572498943
chr3H	HORVU3Hr1G077350	572640126	572641251
chr3H	HORVU3Hr1G077370	572872790	572873620
chr3H	HORVU3Hr1G077410	572953266	572956684
chr3H	HORVU3Hr1G077420	572957507	572958449
chr3H	HORVU3Hr1G077460	573130238	573132234
chr3H	HORVU3Hr1G077470	573130473	573131275
chr3H	HORVU3Hr1G077480	573134025	573135026
chr3H	HORVU3Hr1G077510	573270947	573271132
chr3H	HORVU3Hr1G077520	573442442	573443027
chr3H	HORVU3Hr1G077550	573476481	573476862
chr3H	HORVU3Hr1G077590	573892899	573894217
chr3H	HORVU3Hr1G077600	573909888	573910229
chr3H	HORVU3Hr1G077620	574203492	574203881
chr3H	HORVU3Hr1G077650	574245124	574245643
chr3H	HORVU3Hr1G077720	574620185	574621849
chr3H	HORVU3Hr1G077750	574667055	574667511
chr3H	HORVU3Hr1G077760	574689044	574690196
chr3H	HORVU3Hr1G077810	574925112	574925281

Table F1. List of low confidence genes under the *rpr9* QTL (continued).

Chromosome	Gene ID	Start	Stop
chr3H	HORVU3Hr1G077820	574929306	574929791
chr3H	HORVU3Hr1G077840	574993032	574993566
chr3H	HORVU3Hr1G077860	575016002	575016782
chr3H	HORVU3Hr1G077870	575031387	575033413
chr3H	HORVU3Hr1G077900	575138073	575138826
chr3H	HORVU3Hr1G077910	575157425	575157639
chr3H	HORVU3Hr1G077940	575247080	575247718
chr3H	HORVU3Hr1G077970	575422404	575422634
chr3H	HORVU3Hr1G077990	575688293	575689539
chr3H	HORVU3Hr1G078000	575689776	575690665
chr3H	HORVU3Hr1G078010	575693695	575694362
chr3H	HORVU3Hr1G078020	575727216	575727557
chr3H	HORVU3Hr1G078040	575767245	575767541
chr3H	HORVU3Hr1G078050	575773500	575774897
chr3H	HORVU3Hr1G078060	575816964	575818691
chr3H	HORVU3Hr1G078070	576076225	576076876
chr3H	HORVU3Hr1G078080	576081122	576082519
chr3H	HORVU3Hr1G078120	576162527	576163597
chr3H	HORVU3Hr1G078130	576625323	576626028
chr3H	HORVU3Hr1G078160	576755597	576755997
chr3H	HORVU3Hr1G078170	576956282	576959831
chr3H	HORVU3Hr1G078180	577012902	577013023
chr3H	HORVU3Hr1G078240	577220342	577221523
chr3H	HORVU3Hr1G078250	577334122	577335340
chr3H	HORVU3Hr1G078280	577504342	577504843
chr3H	HORVU3Hr1G078290	577566776	577567066
chr3H	HORVU3Hr1G078310	577645597	577646234
chr3H	HORVU3Hr1G078320	577647139	577649228
chr3H	HORVU3Hr1G078340	577719075	577720442
chr3H	HORVU3Hr1G078400	578102133	578110671
chr3H	HORVU3Hr1G078410	578111924	578112169
chr3H	HORVU3Hr1G078440	578418929	578419234
chr3H	HORVU3Hr1G078500	578466065	578468894
chr3H	HORVU3Hr1G078510	578600764	578601251
chr3H	HORVU3Hr1G078570	579207848	579208247
chr3H	HORVU3Hr1G078580	579241483	579241948
chr3H	HORVU3Hr1G078600	579278066	579279098
chr3H	HORVU3Hr1G078610	579283368	579283709
chr3H	HORVU3Hr1G078630	579386643	579387199
chr3H	HORVU3Hr1G078640	579432997	579448113

Table F1. List of low confidence genes under the *rpr9* QTL (continued).

Chromosome	Gene ID	Start	Stop
chr3H	HORVU3Hr1G078690	579946605	579947650
chr3H	HORVU3Hr1G078700	579986885	579987507
chr3H	HORVU3Hr1G078730	580039176	580039687
chr3H	HORVU3Hr1G078740	580078197	580078548
chr3H	HORVU3Hr1G078750	580097420	580097653
chr3H	HORVU3Hr1G078770	580239204	580239508
chr3H	HORVU3Hr1G078870	580633903	580634331
chr3H	HORVU3Hr1G078890	580644247	580644670
chr3H	HORVU3Hr1G078910	580715468	580716724
chr3H	HORVU3Hr1G078970	581178029	581178585
chr3H	HORVU3Hr1G079020	581297232	581320083
chr3H	HORVU3Hr1G079030	581320783	581320998
chr3H	HORVU3Hr1G079070	581796633	581796850
chr3H	HORVU3Hr1G079080	582026492	582027091
chr3H	HORVU3Hr1G079090	582168872	582170923
chr3H	HORVU3Hr1G079100	582266529	582267491
chr3H	HORVU3Hr1G079110	582267100	582268979
chr3H	HORVU3Hr1G079120	582269058	582272847
chr3H	HORVU3Hr1G079130	582273137	582275423
chr3H	HORVU3Hr1G079140	582277349	582286488
chr3H	HORVU3Hr1G079150	582287668	582290124
chr3H	HORVU3Hr1G079160	582291080	582296443
chr3H	HORVU3Hr1G079170	582296511	582300522
chr3H	HORVU3Hr1G079190	582461913	582462450
chr3H	HORVU3Hr1G079200	582463687	582464106
chr3H	HORVU3Hr1G079220	582468362	582468871
chr3H	HORVU3Hr1G079240	582471629	582473536
chr3H	HORVU3Hr1G079250	582491127	582492459